Lecture Notes in Electrical Engineering 975

Krishna Murari
Narayana Prasad Padhy
Sukumar Kamalasadan *Editors*

Soft Computing Applications in Modern Power and Energy Systems

Select Proceedings of EPREC 2022

Springer

Lecture Notes in Electrical Engineering

Volume 975

Series Editors

Leopoldo Angrisani, Department of Electrical and Information Technologies Engineering, University of Napoli Federico II, Naples, Italy
Marco Arteaga, Departament de Control y Robótica, Universidad Nacional Autónoma de México, Coyoacán, Mexico
Bijaya Ketan Panigrahi, Electrical Engineering, Indian Institute of Technology Delhi, New Delhi, Delhi, India
Samarjit Chakraborty, Fakultät für Elektrotechnik und Informationstechnik, TU München, Munich, Germany
Jiming Chen, Zhejiang University, Hangzhou, Zhejiang, China
Shanben Chen, Materials Science and Engineering, Shanghai Jiao Tong University, Shanghai, China
Tan Kay Chen, Department of Electrical and Computer Engineering, National University of Singapore, Singapore, Singapore
Rüdiger Dillmann, Humanoids and Intelligent Systems Laboratory, Karlsruhe Institute for Technology, Karlsruhe, Germany
Haibin Duan, Beijing University of Aeronautics and Astronautics, Beijing, China
Gianluigi Ferrari, Università di Parma, Parma, Italy
Manuel Ferre, Centre for Automation and Robotics CAR (UPM-CSIC), Universidad Politécnica de Madrid, Madrid, Spain
Sandra Hirche, Department of Electrical Engineering and Information Science, Technische Universität München, Munich, Germany
Faryar Jabbari, Department of Mechanical and Aerospace Engineering, University of California, Irvine, CA, USA
Limin Jia, State Key Laboratory of Rail Traffic Control and Safety, Beijing Jiaotong University, Beijing, China
Janusz Kacprzyk, Systems Research Institute, Polish Academy of Sciences, Warsaw, Poland
Alaa Khamis, German University in Egypt El Tagamoa El Khames, New Cairo City, Egypt
Torsten Kroeger, Stanford University, Stanford, CA, USA
Yong Li, Hunan University, Changsha, Hunan, China
Qilian Liang, Department of Electrical Engineering, University of Texas at Arlington, Arlington, TX, USA
Ferran Martín, Departament d'Enginyeria Electrònica, Universitat Autònoma de Barcelona, Bellaterra, Barcelona, Spain
Tan Cher Ming, College of Engineering, Nanyang Technological University, Singapore, Singapore
Wolfgang Minker, Institute of Information Technology, University of Ulm, Ulm, Germany
Pradeep Misra, Department of Electrical Engineering, Wright State University, Dayton, OH, USA
Sebastian Möller, Quality and Usability Laboratory, TU Berlin, Berlin, Germany
Subhas Mukhopadhyay, School of Engineering and Advanced Technology, Massey University, Palmerston North, Manawatu-Wanganui, New Zealand
Cun-Zheng Ning, Electrical Engineering, Arizona State University, Tempe, AZ, USA
Toyoaki Nishida, Graduate School of Informatics, Kyoto University, Kyoto, Japan
Luca Oneto, Department of Informatics, BioEngineering, Robotics and Systems Engineering, University of Genova, Genova, Genova, Italy
Federica Pascucci, Dipartimento di Ingegneria, Università degli Studi "Roma Tre", Rome, Italy
Yong Qin, State Key Laboratory of Rail Traffic Control and Safety, Beijing Jiaotong University, Beijing, China
Gan Woon Seng, School of Electrical and Electronic Engineering, Nanyang Technological University, Singapore, Singapore
Joachim Speidel, Institute of Telecommunications, Universität Stuttgart, Stuttgart, Germany
Germano Veiga, Campus da FEUP, INESC Porto, Porto, Portugal
Haitao Wu, Academy of Opto-electronics, Chinese Academy of Sciences, Beijing, China
Walter Zamboni, DIEM—Università degli studi di Salerno, Fisciano, Salerno, Italy
Junjie James Zhang, Charlotte, NC, USA

The book series *Lecture Notes in Electrical Engineering* (LNEE) publishes the latest developments in Electrical Engineering—quickly, informally and in high quality. While original research reported in proceedings and monographs has traditionally formed the core of LNEE, we also encourage authors to submit books devoted to supporting student education and professional training in the various fields and applications areas of electrical engineering. The series cover classical and emerging topics concerning:

- Communication Engineering, Information Theory and Networks
- Electronics Engineering and Microelectronics
- Signal, Image and Speech Processing
- Wireless and Mobile Communication
- Circuits and Systems
- Energy Systems, Power Electronics and Electrical Machines
- Electro-optical Engineering
- Instrumentation Engineering
- Avionics Engineering
- Control Systems
- Internet-of-Things and Cybersecurity
- Biomedical Devices, MEMS and NEMS

For general information about this book series, comments or suggestions, please contact leontina.dicecco@springer.com.

To submit a proposal or request further information, please contact the Publishing Editor in your country:

China

Jasmine Dou, Editor (jasmine.dou@springer.com)

India, Japan, Rest of Asia

Swati Meherishi, Editorial Director (Swati.Meherishi@springer.com)

Southeast Asia, Australia, New Zealand

Ramesh Nath Premnath, Editor (ramesh.premnath@springernature.com)

USA, Canada

Michael Luby, Senior Editor (michael.luby@springer.com)

All other Countries

Leontina Di Cecco, Senior Editor (leontina.dicecco@springer.com)

**** This series is indexed by EI Compendex and Scopus databases. ****

Krishna Murari · Narayana Prasad Padhy ·
Sukumar Kamalasadan
Editors

Soft Computing Applications in Modern Power and Energy Systems

Select Proceedings of EPREC 2022

Springer

Editors
Krishna Murari
Department of Electrical and Computer Engineering
Clarkson University
Potsdam, NY, USA

Narayana Prasad Padhy
Department of Electrical Engineering
Indian Institute of Technology Roorkee
Roorkee, India

Sukumar Kamalasadan
Department of Electrical and Computer Engineering
The University of North Carolina at Charlotte
Charlotte, NC, USA

ISSN 1876-1100 ISSN 1876-1119 (electronic)
Lecture Notes in Electrical Engineering
ISBN 978-981-19-8352-8 ISBN 978-981-19-8353-5 (eBook)
https://doi.org/10.1007/978-981-19-8353-5

© The Editor(s) (if applicable) and The Author(s), under exclusive license to Springer Nature Singapore Pte Ltd. 2023
This work is subject to copyright. All rights are solely and exclusively licensed by the Publisher, whether the whole or part of the material is concerned, specifically the rights of translation, reprinting, reuse of illustrations, recitation, broadcasting, reproduction on microfilms or in any other physical way, and transmission or information storage and retrieval, electronic adaptation, computer software, or by similar or dissimilar methodology now known or hereafter developed.
The use of general descriptive names, registered names, trademarks, service marks, etc. in this publication does not imply, even in the absence of a specific statement, that such names are exempt from the relevant protective laws and regulations and therefore free for general use.
The publisher, the authors, and the editors are safe to assume that the advice and information in this book are believed to be true and accurate at the date of publication. Neither the publisher nor the authors or the editors give a warranty, expressed or implied, with respect to the material contained herein or for any errors or omissions that may have been made. The publisher remains neutral with regard to jurisdictional claims in published maps and institutional affiliations.

This Springer imprint is published by the registered company Springer Nature Singapore Pte Ltd.
The registered company address is: 152 Beach Road, #21-01/04 Gateway East, Singapore 189721, Singapore

Contents

About the Editors

Krishna Murari received the B.Tech. degree in electrical engineering from WBUT, India, in 2010, the M.E. degree in power systems from Thapar University, India in 2014, and the Ph.D. degree in electrical engineering from the Indian Institute of Technology Roorkee, India in 2019. He is currently a Postdoctoral Research Associate with the Electrical and Computer Engineering Department, Clarkson University, Potsdam, New York, USA. Previously, he was a Postdoctoral Fellow with the Energy Production, and Infrastructure Center (EPIC), University of North Carolina at Charlotte, North Carolina, USA. He is a member of IEEE and has published several papers in journals and conference proceedings. His current research areas are AC-DC load flow, distribution network pricing, demand-side management, distribution system modeling and analysis, power system computing, soft computing, and its application to power system problems and smart grid. He has some significant research outcomes in the field of AC-DC distribution system analysis and planning.

Narayana Prasad Padhy received a Ph.D. degree in power systems engineering from Anna University, Chennai, India, in 1997. He is an institute chair professor with the Department of Electrical Engineering, at the Indian Institute of Technology Roorkee, India. He is heading many national and international projects, such as DSIDES, ID-EDGe, and HEAPD. He is also part of other international projects, namely Indo–US UI-ASSIST and Indo UK ZED-I. His research interests include power system analysis, optimization, demand-side management, and smart grids. Dr. Padhy is also a fellow of the Indian National Academy of Engineers, Institution of Engineering and Technology, and Institution of Engineers India.

Sukumar Kamalasadan received his B.Tech. degree in electrical and electronics engineering from the University of Calicut, in 1991, an M.E. degree in electrical power systems management from the Asian Institute of Technology, Thailand, in 1999, and a Ph.D. degree in electrical engineering from The University of Toledo, USA, in 2004. He is currently a professor with the Department of Electrical and Computer Engineering, the University of North Carolina at Charlotte, USA. His research interests include intelligent and autonomous control, power systems

dynamics, stability and control, smart grid, microgrid, and real-time optimization and control of power systems. Dr. Kamalasadan was the recipient of several awards, including the NSF CAREER Award and IEEE Best Paper Award.

Optimal Placement of IPFC Device for Enhancing Transmission System Performance Using WIPSO

Kiran Kumar Kuthadi, ND. Sridhar, and CH. Ravi Kumar

Abstract The Interline Power Flow Controller (IPFC) is an important component in order to enhance both the static and dynamic performance of a power system network. In order to regulate power flow, automated generation control, oscillation damping, congestion management, power system status estimation and power system protection, the Interline Power Flow Controller (IPFC) is a set of Flexible AC Transmission Systems (FACTS). The placement of the IPFC in the power system affects its performance, so there is a need to choose the best place for the device. In addition, the best location for one application may not be the best location for other applications. The weighted PSO is used to optimally place the device in the power system to reduce power loss. MATLAB was used to simulate IEEE 5, 9 and 30 bus systems. Finally, the WIPSO findings were compared to the PSO and genetic algorithm results produced.

Keywords GA-Genetic Algorithm · PSO-Particle Swarm Optimization · WIPSO-Weight-Improved PSO · IPFC-Interline Power Flow Controller · VSI-Voltage Stability Index

1 Introduction

Energy is a vital sector in any economy. There are various forms and sources of energy. Coal, water, wind and sunlight are various sources through which electric energy can be generated. Electric power is today used more importantly as source of green energy. The future of world economies is heavily dependent of electric power after the exhaust of fossil fuels. Electric vehicles, appliances and industrialization and household needs are all dependent on uninterrupted supply of electricity. A

K. K. Kuthadi (✉) · ND. Sridhar
Department of Electrical Engineering, Annamalai University, Chidambaram, Tamil Nadu, India
e-mail: kiran9949610070@gmail.com; eeehod@sreevahini.edu.in

CH. Ravi Kumar
Department of Electrical Engineering, Acharya Nagarjuna University, Guntur, Andhra Pradesh, India

© The Author(s), under exclusive license to Springer Nature Singapore Pte Ltd. 2023

K. Murari et al. (eds.), *Soft Computing Applications in Modern Power and Energy Systems*, Lecture Notes in Electrical Engineering 975,
https://doi.org/10.1007/978-981-19-8353-5_1

blackout or collapse of grid would the functioning of industries, communication sector, and transport, banking, and medical care, supply of water, policing and even online businesses and education sector as well. Failures in power supply are also due to high levels of pressure on the transmission lines. This has necessitated the need for an effective power supply management system to avert blackouts and collapse of grids [1]. The most versatile and contemporary devices in the process of enhancing transfer capacity of transmission lines are IPFC, voltage sources converter and UPFC [2]. One shunt converter is used in IPFC to control the costs in power flow control. Ensuring active and reactive power balance across multiple lines is the main objective of using IPFC. Besides, it makes up for the reactive power relating to the line and builds the effect of the compensation system for disturbance transient and dynamic [3]. In addition to improving the power handling capacity or new generation plant installation, the use of IPFC in the power system helps in lowering the generation costs by using the available excess power [4–6].

How IPFC performs in a power system is investigated in this research paper. IPFC power injection model which is an elaborated mathematical model is presented in this research article [7]. The effect of Interline Power Flow Controller on the power system can be understood with the help of this model. The IPFC injection model can without problems be integrated into the constant-state power flow model. Demonstration of the features of IPFC is the objective of proposed model. In the present paper indicates IPFC possess capacity of controlling bus voltages, active power flow, reactive power flow and reducing electricity losses concurrently. Reduction in loss of power using the PSO algorithm is the main purpose of optimization explained in this paper. IPFC cost, VSI and power loss are the three terms of objective function formulation MATLAB software simulation.

2 Mathematical Modelling of IPFC

To facilitate series compensation for different lines, DC-to-AC converters are employed in IPFC. The converters in IPFC are connected to transmission lines in series format. IPFC comprises various SSSC. IPFC uses series coupling transformers. The two back-to-back DC-to-AC converters are connected in series with two lines of transmission. As depicted in Fig. 1, a common DC link connects DC connections of converters. Besides facilitating series reactive compensation, IPFC will also be used to control any converter in the process of supplying active power to DC link extracted from power transmission line [8].

Figure 2 shows the steady state model derived using the corresponding circuit of an Interline Power Flow Controller. This model of IPFC comprises two controllable voltage sources. These voltage sources are connected in series VcR and ZcR-series-coupling transformer impedances. Moreover, a dynamic power control equation, connecting two voltage sources in series, is required.

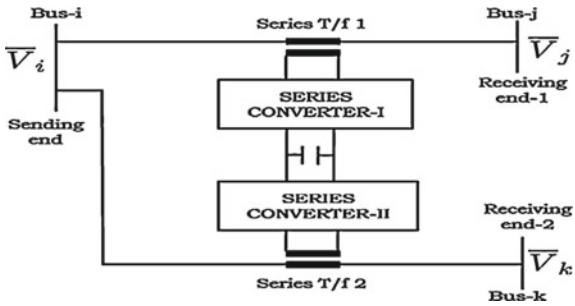

Fig. 1 IPFC—schematic representation

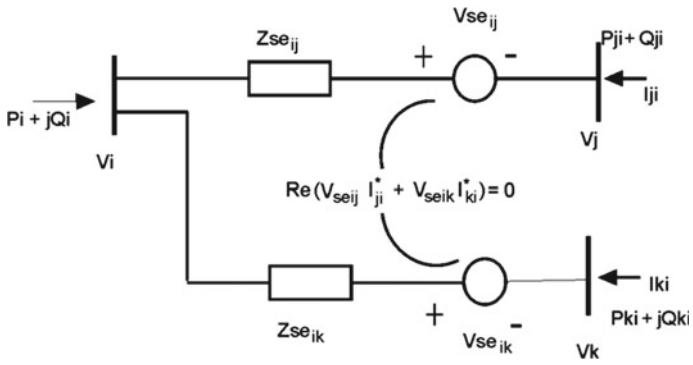

Fig. 2 Representation of IPFC—identical circuit

The configurable series injected voltage sources are represented as:

$$V_{\mathrm{cR1}} = V_{\mathrm{cR1}} e^{j\theta_{cR1}} \text{ and } V_{\mathrm{cR2}} = V_{\mathrm{cR2}} e^{j\theta 2} (\because V_{\mathrm{seik}} = V_{\mathrm{CR1}} \text{ and } V_{\mathrm{seij}} = V_{\mathrm{CR2}}) \quad (1)$$

It should be carried out by the limitations of inequality imposed by the admissible limits of the corresponding angle and series-injected voltage magnitude:

$$V_{\mathrm{cR1\,min}} \leq V_{\mathrm{cR1}} \leq V_{\mathrm{cR1\,max}} \text{ and } 0 \leq \theta_{\mathrm{cR1}} \leq 2\Pi \quad (2)$$

$$V_{cR2\,\mathrm{min}} \leq V_{cR2} \leq V_{cR2\,\mathrm{max}} \text{ and } 0 \leq \theta_{cR2} \leq 2\Pi \quad (3)$$

The current source is given as [3]

$$I_{\mathrm{se,in}} = -\mathrm{jb}_{\mathrm{se,in}} V_{\mathrm{se,in}} \quad (4)$$

The active power (inject a current in phase with the grid voltage) and reactive power (to phase shift the injected current with respect to the grid voltage) injections at *i*th bus are

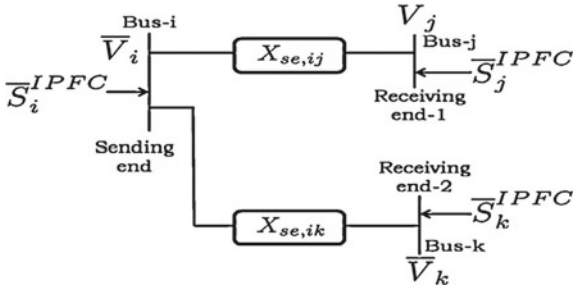

Fig. 3 Power injection method of two converters

$$P_{\text{inj},i} = \text{Real}(S_{\text{inj},i}) = \sum_{n=j,k} (V_i V_{\text{se,in}} b_{\text{se,in}} \text{Sin}(\theta_i - \theta_{\text{se,in}})) \tag{5}$$

$$Q_{\text{inj},i} = \text{Imag}(S_{\text{inj},i}) = \sum_{n=j,k} (V_i V_{\text{se,in}} b_{\text{se,in}} \text{Cos}(\theta_i - \theta_{\text{se,in}})) \tag{6}$$

At nth bus, the active power and reactive power injection after simplification are

$$P_{\text{inj},i} = \text{Real}(S_{\text{inj},i}) = -V_n V_{\text{se,in}} b_{\text{se,in}} \text{Sin}(\theta_i - \theta_{\text{se,in}}) \tag{7}$$

$$Q_{\text{inj},i} = \text{Imag}(S_{\text{inj},i}) = -V_n V_{\text{se,in}} b_{\text{se,in}} \text{Cos}(\theta_i - \theta_{\text{se,in}}) \tag{8}$$

From Eqs. (5–8), three-phase power injection across buses i, j and k of power injection method of IPFC will be depicted in Fig. 3.

NR power flow algorithm is implemented with IPFC power injection model wherein the power mismatch equations are added with power injections. The power balance equations will be given below

$$\Delta P_j = \Delta P_j^0 + P_{\text{inj},j} \tag{9}$$

$$\Delta Q_j = \Delta Q_j^0 + Q_{\text{inj},j} \tag{10}$$

$$\Delta P_n = \Delta P_n^0 + P_{\text{inj},n} \tag{11}$$

$$\Delta Q_n = \Delta Q_n^0 + Q_{\text{inj},n} \tag{12}$$

3 Weight-Improved Particle Swarm Optimization

The similarity of swarm of bird flocking and fish schooling is the basis for the PSO suggested by Eberhart and Kennedy in the process of development of AI techniques. In comparison to other mathematical models, it is easy to implement and compute the efficiency with the simple concept proposed under PSO model which became popular in recent times. Reactive power and voltage control, economic dispatch, transient stability optimal power transmission and several applications are the various optimization problems where the PSO techniques have been successfully tested [9–12].

The weight parameter is very significant in PSO method. Weight is one such parameter which influences speed of convergence and accuracy of solution. Weight-improved particle swarm optimization is an alternative put forward by researchers in the recent past. In WIPSO, the problem of maximization is addressed by swarm particles. The own experience of swarm particles along with the experience of its participating particles helps the swarm to adjust their position. The location and speed of *i*th molecule in *N*-dimensional search area are shown in the below representation. The velocity theory represents modification done. Velocity of individual unit can be modified by the given expression:

$$V_i^{k+1} = WV_i^k + C_1 \times r_1 \times (P_{\text{besti}} - S_i^k) + C_2 \times r_2 \times (G_{\text{besti}} - S_i^k) \tag{13}$$

$$W = W_{\max} - \frac{W_{\max} - W_{\min}}{\text{iter}_{\max}} \times \text{iter} \tag{14}$$

The above expression represents inertia weights approach (IWA) equation. The diversification trait is gradually reduced by using the above equation. Then velocity which slowly passes through the present search area near P_{best} and G_{best} is calculated. The present location (search point the solution space) can be altered by the below expression:

$$S_i^{k+1} = S_i^k + V_i^{k+1} \tag{15}$$

WIPSO method is the source for improved weight parameter function. Changes are made to inertia weight, social and cognitive factors to obtain a better acceptable solution by using the PSO traditional algorithm. The velocity of a single agent of WIPSO is calculated by

$$V_i^{k+1} = W_{\text{new}} V_i^k + C_1 \times r_1 \times (P_{\text{besti}} - S_i^k) + C_2 \times r_2 \times (G_{\text{besti}} - S_i^k) \tag{16}$$

$$W_{\text{new}} = W_{\min} + W \times r_3 \tag{17}$$

$$W = W_{\max} - \frac{W_{\max} - W_{\min}}{\text{iter}_{\max}} \times \text{iter} \tag{18}$$

$$C_1 = C_{1,\max} - \frac{C_{1\max} - C_{1\min}}{\text{iter}_{\max}} \times \text{iter} \tag{19}$$

$$C_2 = C_{2,\max} - \frac{C_{2\max} - C_{2\min}}{\text{iter}_{\max}} \times \text{iter} \tag{20}$$

4 Cost of IPFC and Fitness Function *(K)*

Considering that, there is not much variation in the development of IPFC and UPFC (i.e. we consider that UPFC and IPFC along with control circuit have two inverters and two transformers); the same cost function can be used for obtaining the cost function for Interline Power Flow Controller [13]. The cost function of unified power flow controller can be altered as

$$C_{\text{IPFC},A} = 0.00015S_i^2 - 0.01345S_i + 94.11,\ \text{US\$/kVAR} \tag{21}$$

$$C_{IPFC,B} = 0.00015S_j^2 - 0.01345S_j + 94.11,\ \text{US\$/kVAR} \tag{22}$$

$$C_{\text{IPFC}} = C_{\text{IPFC},A} + C_{\text{IPFC},B} \tag{23}$$

where the corresponding cost function for converters connected to bus i and j is $S_i = |Q_{i2}| - |Q_{i1}|$, $S_j = \left|Q_{j2}\right| - \left|Q_{j1}\right|$, S_i, S_j. The reactive power flows in ith line prior to and later positioning of Interline Power Flow Controller are Q_{i1} and Q_{i2}. The reactive power flows in jth line prior to and later positioning of Interline Power Flow Controller are Q_{j1} and Q_{j2}.

$$\text{Function} = K_1(L_{j,\max}) + K_2(C_{\text{IPFC}}) + K_3(\text{PowerLoss}) \tag{24}$$

The Voltage Stability Index (L-reference) equation utilized to indicate jth node could be implemented as below [10–12, 14],

$$L_{j,\max} = \left|1 - \sum_{i=1}^{i=g} \left|F_{ji}\right| \frac{|V_{i|}|}{|V_j|}(F_{ji}^r + jF_{ji}^m)1 - \sum_{i=1}^{i=g} \left|F_{ji}\right| \frac{|V_i|}{|V_j|} \angle(\theta_{ij} + \delta_i - \delta_j)\right|$$

$$L_{j,\max} = \left|1 - \sum_{i=1}^{i=g} \left|F_{ji}\right| \frac{|V_{i|}|}{|V_j|}(F_{ji}^r + jF_{ji}^m)\right|$$

5 Simulated Results

In this proposed simulation, MATLAB simulation for WIPSO, GA and PSO, a modified power flow algorithm was developed and integrated to include IPFC. The authentication of applied techniques WIPSO, GA and PSO algorithms were put to test on the IEEE 5, 9 and 30-Bus test systems for installation. The magnitude of maximum number of generation for all GA, PSO and WIPSO value is 100. A design parameter is 2, and population size is 20 which are listed in Table 1.

5.1 Location of IPFC

To identify whether a bus is weak or critical, electric voltage stability reference (*L*-index) approach was utilized. The bus possess the highest *L*-reference magnitude will be considered as weak bus. Weak or critical bus impacts first disruption in the system. Across the load bus, only this *L*-reference finds out utilizing Eq. (17). For IEEE 5, 9 and 30 Bus Test System, the *L*-index values are calculated. In IEEE 5 Bus Test System, that was analysed that fifth bus possesses the highest *L*-reference magnitude, i.e. 0.0391, that was contemplated as weak or critical bus. The greatest value, 0.0483, is found on the fourth bus in the IEEE 9 Bus test system, while the highest *L*-index value, 0.0636, is found on the 24th bus in the IEEE 30 Bus test system, indicating that these are the places for IPFC. *L*-index values for IEEE 5, 9 and 30 Bus Test System are as given in Table 2, respectively.

Table 1 Parameter values for GA, PSO and WIPSO

GA parameters		PSO parameters		WIPSO parameters	
Parameters	Values	Parameters	Values	Parameters	Values
Max number of generation	100	Max number of population	100	Max number of population	100
Number of design variable	2	Number of design variable	2	Number of design variable	2
Population size	20	Population size	20	Population size	20
Crossover probability	80%	Inertial weights Wmax and Wmin	0.9–0.2	Inertial weights Wmax and Wmin	0.9–0.2
Mutation probability	10%	Constant C1max and C1min	2 and 0	Constant C1max and C1min	2 and 0
Rand	0–1	Constant C1max and C1min	2 and 0	Constant C2max and C2min	2 and 0
Crossover	Single point	Rand1	0–1	Rand1, 2	0–1
		Rand2	0–1	Rand3	0–1

Table 2 *L*-index for IEEE 5, 9, and 30 bus test system

Load bus no.	*L*-index	Rank
IEEE 5 bus test system		
5	0.0391	1
4	0.0358	2
3	0.0354	3
IEEE 9 bus test system		
4	0.0483	1
5	0.0425	2
3	0.0328	3
9	0.0309	4
8	0.0282	5
6	0.0178	6
IEEE 30 bus test system		
24	0.0636	1
7	0.0571	2
29	0.0566	3
26	0.0555	4
10	0.0538	5
20	0.0489	6
21	0.0484	7
18	0.0474	8
19	0.0449	9
23	0.0438	10
30	0.0406	11
17	0.0402	12
16	0.0353	13
5	0.0342	14
14	0.0226	15
15	0.0184	16
12	0.014	17
4	0.0018	18
2	0.0092	19
8	0.0056	20
3	0.0008	21

5.2 IPFC Bus Voltage Results

For the IEEE 5 Bus System, two generators (bus 1 and bus 2), three electric buses (from bus 3 to bus 5) and seven power transmission lines are introduced. Similarly, the IEEE 9-Bus System includes three generators (buses 1, 2 and 7) besides six electric buses (electric buses 3, 4, 5, 6, 8 and 9) and eleven transmission lines. For the IEEE 30-Bus System, there are six generators (bus 1, 2, 5, 8, 11, 13), 21 load buses (bus 2, 3, 4, 5, 7, 8, 20, 12, 14, 15, 16, 17, 18, 19, 20, 21, 23, 24, 26, 29, 30) and 41 transmission lines. Tables 3, 4, and 5 show the bus voltage for the IEEE 5, IEEE 9 and IEEE 30 Bus systems with GA, PSO and WIPSO.

For the IEEE 5-Bus System, the bus voltage is 0.959 per unit (p.u.) in the absence of GA, PSO and WIPSO, but 0.970 p.u. in the presence of GA, 0.984 p.u. in the presence of PSO and 1.000 p.u. in the presence of WIPSO. Table 3 exemplifies how IPFC improves bus voltage.

The bus voltage for the IEEE 9-Bus System across electric bus number 8 is 0.9898 per unit (p.u.) without GA, PSO or WIPSO, i.e. 0.9899 p.u. besides GA, 0.9990 p.u. with PSO and 1.000 p.u. with WIPSO. Table 4 shows the IPFC-enhanced bus voltage.

Table 3 Electric bus voltage utilized for IEEE 5 bus systems in p.u with GA, PSO and WIPSO

Bus numbers	With IPFC		
	GA	PSO	WIPSO
1	1.060	1.060	1.060
2	1.000	1.000	1.000
3	0.987	0.988	0.999
4	0.984	0.997	1.001
5	0.970	0.984	1.000

Table 4 Electric bus voltage utilized for IEEE 9 bus systems in p.u with GA, PSO and WIPSO

Bus numbers	With IPFC		
	GA	PSO	WIPSO
1	1.0600	1.0600	1.0600
2	1.0400	1.0411	1.0420
3	0.9893	0.9893	1.0000
4	0.9828	0.9900	1.0000
5	0.9936	0.9946	0.9947
6	0.9990	1.0000	1.0000
7	1.0000	1.0200	1.0200
8	0.9899	0.9990	1.0000
9	0.9990	1.0000	1.0000

Table 5 Bus voltage with GA, PSO and WIPSO used in IEEE-30 bus systems in p.u

Bus numbers	With IPFC		
	GA	PSO	WIPSO
1	1.0600	1.0600	1.0600
2	1.0433	1.0430	1.0430
3	0.9990	1.0000	1.0000
4	0.9770	0.9770	0.9960
5	1.0100	1.0100	1.0100
6	0.9999	0.9990	1.0000
7	0.9980	0.9990	1.0000
8	1.0100	1.0100	1.0210
9	0.9990	1.0000	1.0000
10	0.9770	0.9770	0.9960
11	1.0222	1.0222	1.0300
12	1.0000	1.0000	1.0000
13	1.0211	1.0200	1.0240
14	0.9999	0.9990	1.0130
15	0.9900	0.9900	1.0000
16	0.9944	0.9940	1.0000
17	0.9761	0.9760	0.9940
18	0.9731	0.9730	0.9910
19	0.9666	0.9660	0.9840
20	0.9688	0.9680	0.9860
21	0.9640	0.9640	0.9890
22	0.9700	0.9640	0.9910
23	0.9510	0.9700	1.0000
24	0.9510	0.9582	1.0000
25	0.9392	0.9580	0.9820
26	0.9722	0.9390	0.9640
27	0.9990	0.9720	1.0000
28	0.9512	1.0000	1.0000
29	0.9399	0.9510	0.9670
30	0.9850	0.9900	1.000

For the IEEE-30 Bus System, for the bus voltage at bus number 24 with absence of GA, PSO and WIPSO was 0.9490 p.u, though we are utilizing GA, the value of 0.9510 p.u, besides PSO that was 0.9582 p.u and in the case of WIPSO, it is determined to be 1.000 p.u. Table 5 represents the bus voltage enhances with IPFC. Tables 3, 4, and 5 show a positive change in load bus voltage.

From Tables 3, 4, and 5, it is evident that the results from PSO and GA are outperformed by those attained with WIPSO. Figures 4, 5, and 6 show the graphical representation of voltage for the IEEE 5, 9-bus, and IEEE-30 Bus test systems, respectively.

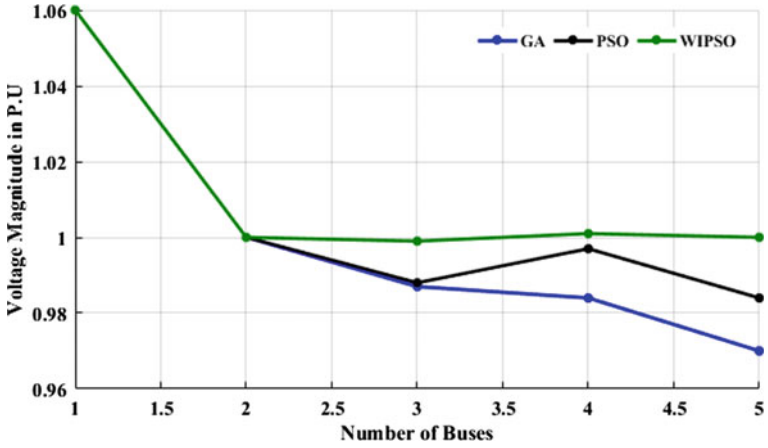

Fig. 4 Using GA, PSO and WIPSO to simulate the IEEE 5 bus system voltage magnitude in a P.U

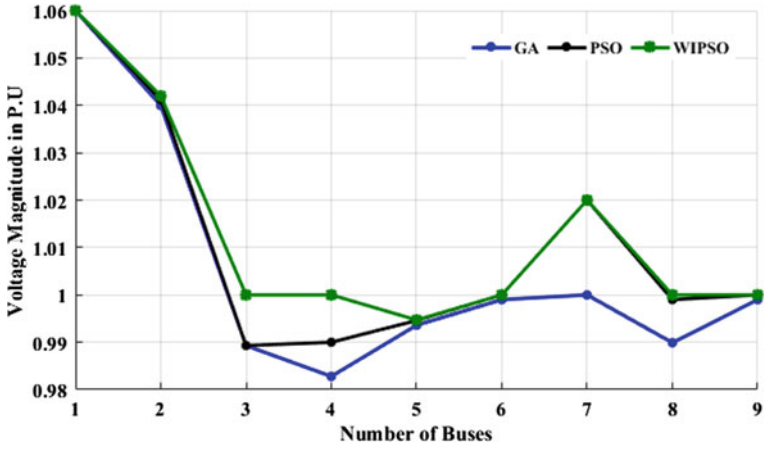

Fig. 5 Using GA, PSO and WIPSO to simulate the IEEE 9 bus system voltage magnitude in a P.U

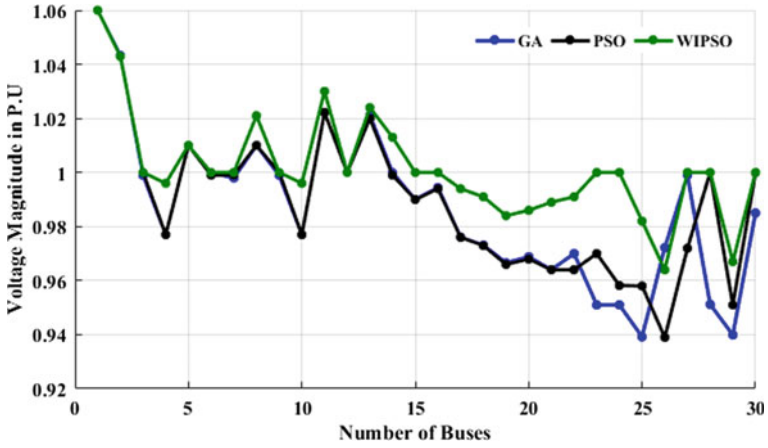

Fig. 6 Using GA, PSO and WIPSO to simulate the IEEE 30 bus system voltage magnitude in a P.U

5.3 The Best Fitness Function of IPFC Outcomes

It was discovered that in the IEEE 5 Bus system, bus 4 is extremely sensitive to security. Therefore, to improve electric power system security/stability, Bus 5 possesses maximum economical situation for IPFC. The fitness function (K) of the IPFC via WIPSO for IEEE 5 Bus System was 42.206 and PSO, GA is 43.100 and 43.309, and the graphical simulate of fitness function (K) with GA, PSO and WIPSO for IEEE 5 bus System is shown in Fig. 7. Comparison of fitness function (K) using optimization techniques is shown in Table 6.

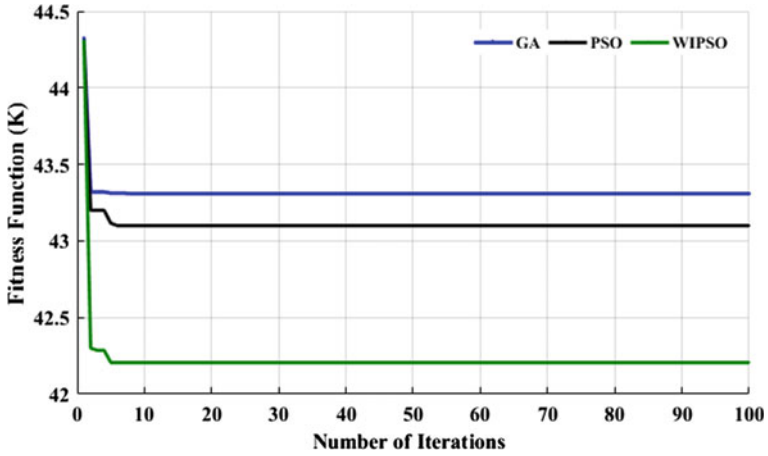

Fig. 7 IEEE 5 bus system fitness function (K) using GA, PSO and WIPSO

Table 6 Using optimization techniques for comparison of fitness function *(K)*

Fitness function *(K)* with IPFC			
Bus system/optimization techniques	GA	PSO	WIPSO
IEEE 5 bus system	43.309	43.1	42.206
IEEE 9 bus system	55.20	51.21	50.80
IEEE 30 bus system	128.00	127.77	127.683

For IEEE 9 Bus system, it is evident the bus 4 is more sensitive across security. So, in order to improve electric power system security/stability, Bus 4 is high optimal location for IPFC. For IEEE 9 Bus System, the fitness function *(K)* of the IPFC via WIPSO was 50.800, and PSO and GA are 51.210 and 55.200. Figure 8 presents the graphical representation of fitness function *(K)* for IEEE 9 bus system with GA, PSO and WIPSO. In Table 6, fitness function *(K)* is compared using optimization techniques.

Bus 24 is observed to be highly sensitive towards security for IEEE 30 Bus system. Therefore, electric Bus 24 possesses more minimal situation for IPFC to improve electric power system security/stability. For IEEE 30 Bus System, the fitness function *(K)* of the IPFC via WIPSO was 127.683, and PSO and GA are 127.77 and 128.00. For IEEE 30 bus system, the graphical representation of fitness function *(K)* with GA, PSO and WIPSO is shown in Fig. 9. Comparison of fitness function *(K)* using optimization techniques is shown in Table 6.

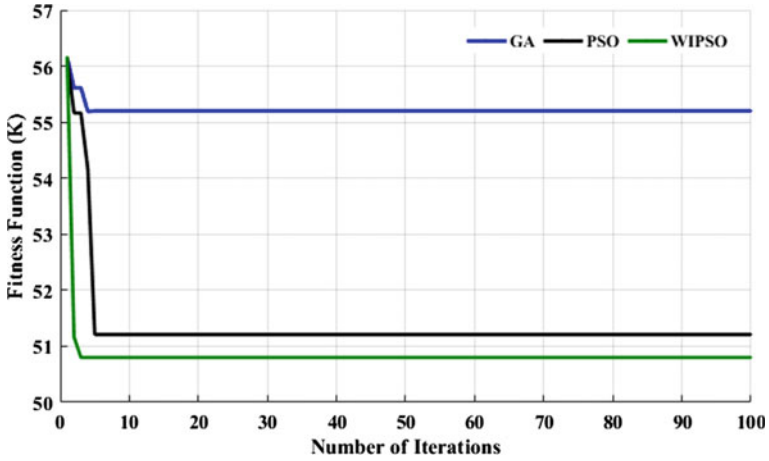

Fig. 8 Fitness function *(K)* using GA, PSO and WIPSO for IEEE 9 bus system

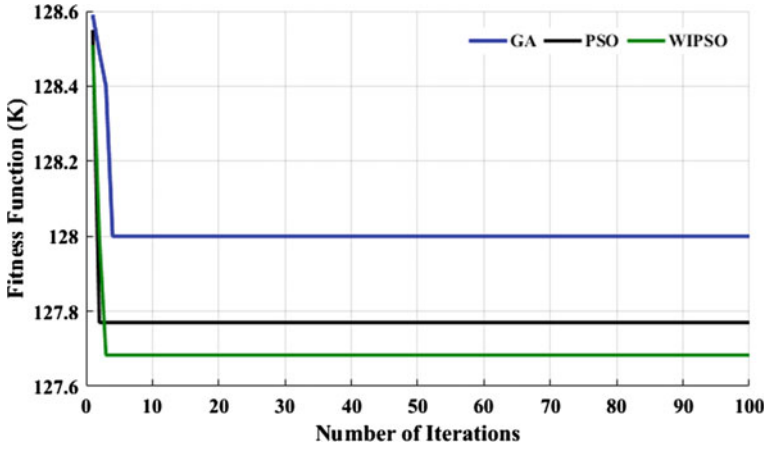

Fig. 9 Fitness function *(K)* for IEEE 30 bus system using GA, PSO and WIPSO

6 Conclusions

Voltage Stability Index is used for identification of economical situation of IPFC electric power system network. Minimization in FACTS device cost of installation, power loss reduction, enhancement in voltage profile in the power system network is the objective of both GA, PSO and WIPSO methods. The present cost function of UPFC is used to obtain the cost function for IPFC. IEEE 5 bus, IEEE 9 bus and IEEE 30 bus test systems are the standard platforms on which the proposed methods are tested. Considerable reduction in loss of power, improvement in voltage profile and increase in power flow are the result of proposed methodology for research. For all the test cases, illustration of the optimal location for the induction of IPFC is clearly shown. The convergence rate and complexities involved in calculation for both WIPSO and GA and PSO methods are explained. The outcomes of this method are a testimony that the proposed WIPSO methodology is effective in getting both an acceptable solution and good convergence rate when compared to the results of GA and PSO methods.

References

1. A. Mishra, V.N.K. Gundavarapu, Contingency management of power system with interline power flow controller using real power performance index and line stability index. Ain Shams Eng. J. **7**(1), 209–222 (2016)
2. N.M.R. Santosab, O.P. Diasa, V.F. Pires, Use of an interline power flow controller model for power flow analysis. Energy Procedia **14**, 2096–2101 (2012)
3. M.A. Kamarposhti, The optimal location of interline power flow controller in the transmission lines for reduction losses using the particle swarm optimization algorithm. Majlesi J. Electr. Eng. **12**(2) (2018)

4. S. Kamel, F. Jurado, Power flow analysis with easy modelling of interline power flow controller. Electr. Power Syst. Res. **108**, 234–244 (2014)
5. A.S. Siddiqui, M. Rani, Enhancing power system loadability using IPFC device. Int. J. Syst. Assur. Eng. Manag. **8**, 154–159 (2017)
6. N.A. Hussein, A.A. Eisa, E.E.M. Rashad, Analyzing the interline power flow controller (IPFC) steady state performance in power systems, in *Proceedings of the 15th International Middle East Power Systems Conference (MEPCONâ•Ž12)*, Alexandria University, Egypt, pp. 23–25 (2012)
7. A.V. Naresh Babu, S. Sivanagaraju, Mathematical modelling, analysis and effects of interline power flow controller (IPFC) parameters in power flow studies, in *India International Conference on Power Electronics 2010 (IICPE2010)*, New Delhi, pp. 1–7 (2011). https://doi.org/10.1109/IICPE.2011.5728060
8. A.V. Naresh Babu, S. Sivanagaraju, C. Padmanabharaju, T. Ramana, Multi-line power flow control using interline power flow controller (IPFC) in power transmission systems. Int. J. Electr. Comput. Eng. **4**(3) (2010)
9. P. Vu, D. Le, N. Vo, J. Tlusty, A novel weight-improved particle swarm optimization algorithm for optimal power flow and economic load dispatch problems, in *IEEE PES T&D 2010*, New Orleans, pp. 1–7 (2010). https://doi.org/10.1109/TDC.2010.5484396
10. K.K. Kuthadi, N.D. Sridhar, C.H. Ravi Kumar, WIPSO, PSO and GA techniques to locate UPFC effectively in power system to improve voltage stability and reduce losses. Int. J. Recent Technol. Eng. (IJRTE) **8**(2) (2019). https://doi.org/10.35940/ijrte.B2048.078219
11. K.K. Kuthadi, N.D. Sridhar, C.H. Ravi Kumar, Voltage stability index based optimal placement of SVC in power system network using weight improved PSO. J. Adv. Res. Dyn. Control Syst. **12**(02) (2020). https://doi.org/10.5373/JARDCS/V12I2/S20201248
12. K.K. Kuthadi, N.D. Sridhar, C.H. Ravi Kumar, Application of optimization algorithms to enhance the transmission system performance using thyristor controlled series capacitor. J. Inst. Eng. India Ser. B (2021). https://doi.org/10.1007/s40031-021-00650-1
13. S. Sreejith, S.P. Simon, M.P. Selvan, Optimal location of interline power flow controller in a power system network using ABC algorithm. Arch. Electr. Eng. **62**(1), 91–110 (2013)
14. D. Sarkar, M. Chakrabarty, R. Ghosh et al., An offline strategic planning for service restoration using multi-constraints priority-based Dijkstra's algorithm. J. Inst. Eng. India Ser. B **101**, 309–320 (2020). https://doi.org/10.1007/s40031-020-00469-2

IoT-Based Kalman Filtering and Particle Swarm Optimization for Detecting Skin Lesion

J. Ramkumar, S. Samson Dinakaran, M. Lingaraj, S. Boopalan, and B. Narasimhan

Abstract In the current world, IoT has started providing multiple services that exploit the computing power of numerous devices. IoT-based healthcare applications are observed as a benchmark development for diagnosing a disease. Synchronization of data collection and its monitoring becomes more accessible because of IoT. Most of the data collected will be vast and unstructured, and more chances are there for the presence of redundant data. Hence, a significant task arises to identify a unique way to perform mining in a massive dataset with the available computing resources. Various sensors are used to collect real-time data because detecting skin lesion images plays a significant role. This paper proposes IoT-based Kalman filtering and Particle Swarm Optimization to detect skin lesions more accurately. Particle swarm optimization is applied to detect skin lesions in an optimized manner with less time and modified Kalman filtering is used for classification. The proposed classifier is evaluated using the HAM10000 benchmark dataset, and standard metrics are utilized to assess the proposed classifier. It seems the suggested classifier outperforms the current classifier in terms of performance.

Keywords Skin · Lesion · Kalman · Particle swarm · Optimization

J. Ramkumar (✉)
Department of Computer Science, Dr. N.G.P. Arts and Science College, Coimbatore, India
e-mail: jramkumar1986@gmail.com

S. Samson Dinakaran
Department of Computer Science, VLB Janakiammal College of Arts and Science, Coimbatore, India

M. Lingaraj
Department of Computer Science, Sankara College of Science and Commerce, Coimbatore, India

S. Boopalan
Department of Computer Technology, KGiSL Institute of Information Management, Coimbatore, India

B. Narasimhan
Department of Computer Technology, Dr. N.G.P. Arts and Science College, Coimbatore, India

© The Author(s), under exclusive license to Springer Nature Singapore Pte Ltd. 2023

K. Murari et al. (eds.), *Soft Computing Applications in Modern Power and Energy Systems*,
Lecture Notes in Electrical Engineering 975,
https://doi.org/10.1007/978-981-19-8353-5_2

1 Introduction

Technology development in the recent years has started providing enhanced solutions for multiple problems. Because of the advanced developments in wearable sensor devices, data gathering and monitoring are reliable and accessible. Tracking of patient health status can be achieved lively, and it becomes economical. Also, it assists in routinely monitoring health. Infrastructures that are based on IoT will provide betterment in collecting the data from patients geographically, which provides a way for analyzing the real-time data [1]. It helps doctors at a high level because it can collect and store data dynamically where it never depends on statistical results from the laboratory. IoT-based data collection does not only provide an effective mechanism for gathering data, but it helps in mining and analyzing the essential data in health care. Doctors will get a chance to give better advice to patients by using the real-time data gathered; also, doctors can recommend daily routine activities that exactly match certain patients. Customized medicines can be designed by doctors that depend on the patient's lifestyle for a speedy recovery. Effective utilization of the healthcare system based on IoT can surely enhance the healthcare industry's advancement even more. The significant level of time spent and expenses can be greatly reduced with high accuracy and trust [2].

In the upcoming days, science and technology fields can face a great revolution because of IoT. Various sensors are currently available to capture the different physical parameters. The two main issues present in IoT-based systems are (i) redundant data and (ii) unstructured data. These two things result in (i) making the system consume more energy, (ii) complexity in processing a vast quantity of data, and (iii) low accuracy in results. Enhancements in technology are possible only if algorithms make efficient processing with minimum utilization of resources to provide more accuracy in results with reduced time [3]. There should not be any way present in IoT-based systems wasting energy. Sophisticated methods are necessary to mine the gathered information that is collected via sensors. In biomedical image data, efficient algorithms are essential to process data to get maximum accuracy in results in minimum duration. It ends with low consumption of energy; else, there is no use in implementing such large-scale systems [4]. Optimization has placed its impression in all domains [5–19], and currently, it entered medical and healthcare professions.

This paper exploits image analysis on biomedical data with the machine learning algorithm to meet the current healthcare industry and the advantages of computer-aided diagnosis. The proposed work of this paper blends the machine learning algorithm and IoT for the effective processing of gathered data in the biomedical field. Generally, in IoT environments, the magnitude of the image is always very enormous, and it is always a challenge. This work attempts to minimize the redundancy of data by proposing an optimized classifier that performs the task by utilizing the minimum infrastructure of the IoT environment. Its inherent capabilities optimize

the features and help get results quickly with enhanced accuracy. Metaheuristic optimization methodology is applied for enhanced convergence. Further, it will assist in implementing the large-scale IoT healthcare system to find results more accurately in minimum time with affordable cost.

2 Literature Review

IoT lifestyle disease management [20] proposes different critical factors that potentially influence users' acceptance. Additional significant attributes are identified from the information gathered from service providers, devices, task scope, and experts. The conjoint analysis was applied to calculate the significance level attributes. Cloud-centric diagnosing framework [21] is proposed to predict the severity level of potential disease. Computational science concepts are explored to measure student health based on different prototypes. An energy-efficient diagnosis model [22] is proposed to perform clustering in the sensed data in the healthcare world. It performs cluster based on the patient's age, and the cluster head is selected to perform the transmission of data to the cloud server. The categorization is done in the cloud using a neural network-based classifier. An IoT-based pandemic illness detection system has been suggested using a tiny polymerase sequence reaction instrument, and an IoT-based pandemic illness detection system [23] has been proposed. When the dengue fever virus is amplified using complementary deoxyribonucleic acid (CDNA), it exhibits the system's capabilities. The gathered data is delivered to a centralized network using Bluetooth, available on Android devices.

Cloud and IoT-based disease prediction [24] is proposed to predict diabetes disease among patients. Medical sensors are utilized to gather medical data. A fuzzy logic-based rule classifier is used to identify the patients with high diabetes. IoT-based heart disease prediction [25] is proposed to collect heart-related details before and after heart disease. The collected data is sent to a central server and processed using a deep neural network. Previous data analysis is used to identify cardiac problems and present the findings. The compressive IoT-based healthcare system (CIoTHCS) [26] is proposed for Parkinson's disease patients who cannot communicate with others. They can't send commands to the brain to act accordingly. Several chips are developed to send different signals to the brain to do work to overcome this issue. IoT for predicting age-related macular degeneration disease [27] is proposed to predict individual patients' problems present in vision. Patient retina fundus images are initially gathered and stored in the cloud to identify the severity and progression. A convolution neural network with 152 layers is utilized to predict disease. Fog-assisted IoT system (FIoTS) [28] is proposed to monitor health remotely and detect falls. It makes use of e-health signals for monitoring. By applying fog computing at the end, it provides advanced services cum distributed storage with minimum energy consumption.

3 IoT-Based Kalman Filtering and Particle Swarm Optimization

To estimate the state of the system, the Kalman filter is utilized. Eqs. (1) and (2) applied for processing and measuring the linear dynamic system.

$$\mathrm{ssv}_{k+1} = \mathrm{tm}_k\ \mathrm{ssv}_k + \mathrm{rel}_k \mathrm{ivf}_k + \mathrm{pnv}_k \tag{1}$$

$$\mathrm{mv}_k = \mathrm{mm}_k \mathrm{ssv}_k + \mathrm{mnv}_k \tag{2}$$

where ssv_k indicates system-state-vector, tm_k indicates the matrix of transition, which is interrelated with ssv_k and ssv_{k+1}. ivf_k represents the input vector function, rel_k is the relationship matrix of ssv_{k+1} and ivf_k. pnv_k is the process-noise-vector, mv_k indicates the measuring vector, mm_k indicates the matrix that is related to mv_k. ssv_k and mnv_k indicate the noise vector used for measuring. pnv_k and mnv_k vectors are uncorrelated.

$$\mathrm{EV}\left[\mathrm{pnv}_k \mathrm{pnv}_c^{\mathrm{TP}}\right] = \begin{cases} \mathrm{PNC}; k = c \\ 0; k \neq c \end{cases} \tag{3}$$

$$\mathrm{EV}\left[\mathrm{mnv}_k \mathrm{mnv}_c^{\mathrm{TP}}\right] = \begin{cases} \mathrm{MNC}; k = c \\ 0; k \neq c \end{cases} \tag{4}$$

$$\mathrm{EV}\left[\mathrm{pnv}_k \mathrm{mnv}_c^{\mathrm{TP}}\right] = 0 \text{ for all } k \text{ and } c \tag{5}$$

where PNC indicates the process-noise-covariance, MNC indicates the measuring-noise-covariance, TP indicates the transpose matrix, $E[]$ indicates the expected value. Significant equations of Kalman filtering are segregated into two categories, which are:

(a) Timing Update

$$\mathrm{ssv}_{k+1}^{-} = \mathrm{tm}_k \mathrm{ssv}_k + \mathrm{TP}_k \mathrm{ivf}_k \tag{6}$$

$$\mathrm{cm}_{k+1}^{-} = \mathrm{tm}_k \mathrm{cm}_k \mathrm{tm}_k^{\mathrm{TP}} \tag{7}$$

(b) Measuring Update

$$\mathrm{kg}_k = \mathrm{cm}_k^{-} \mathrm{mm}_k^{\mathrm{TP}} \left[\mathrm{mm}_k \mathrm{cm}_k^{-} \mathrm{mm}_k^{\mathrm{TP}} + \mathrm{mvc}_k\right]^{-1} \tag{8}$$

$$\mathrm{ssv}_k = \mathrm{ssv}_{k^-} + \mathrm{kg}_k [\mathrm{mv}_k - \mathrm{mm}_k \mathrm{ssv}_{k^-}] \tag{9}$$

$$\mathrm{cm}_k = \left[1 - \mathrm{kg}_k \mathrm{mm}_k\right] \mathrm{cm}_k^- \tag{10}$$

where ssv_k is the system state estimation, kg_k indicates the Kalman-gain, $\mathrm{mm}_k \mathrm{ssv}_k$ represents the predicted output, cm_k indicates the covariance matrix related to an error in state estimation, and it can define as Eq. (11).

$$\mathrm{cm}_k = E\left[\mathrm{ssv}_k^{\mathrm{TP}}\right] \tag{11}$$

The sequence of innovation is described in Eq. (12)

$$h_k = \mathrm{mv}_k - \mathrm{mm}_k \mathrm{ssv}_k \tag{12}$$

Equation (13) defines the weighted innovation

$$\mathrm{WI} = \mathrm{kg}_k [\mathrm{mv}_k - \mathrm{mm}_k \mathrm{ssv}_k] \tag{13}$$

The swarm intelligence of flocking birds inspires Kalman filtering using Particle Swarm Optimization. This research work assumes a constant speed at which particles move. If it is an n-dimension optimization problem, then the position of the particle is $p_1, p_2, p_3, \ldots, p_{n-1}, p_n$ and speed of movement is termed as $v_1, v_2, v_3, \ldots, v_{n-1}, v_n$. For the particle j, it has the position vector as p_i, speed-vector as v_i, and a fitness value.

The position and speed of vectors are initialized randomly. Fitness value calculation is performed for each particle. Specific measures are done to find the local-best and global-best, i.e., $p_{\mathrm{lbest}}(t)$ and $p_{\mathrm{gbest}}(t)$. The speed of the particle in which it moves is updated based on Eq. (14).

$$v^i(t+1) \leftarrow v^i(t) + c_1 r(p(t) - p_{\mathrm{lbest}}(t)) + c_2 r\left(p(t) - p_{\mathrm{gbest}}(t)\right) \tag{14}$$

The position of the particles is updated using Eq. (15)

$$p(t+1) \leftarrow p(t) + v(t+1) \tag{15}$$

where $p(t)$ indicates the position vector, c_1 and c_2 are the constants lies in [0, 1, 2]. It is utilized to control the variations that arise in speed at a certain level, r is a variable used to explore the randomization. The procedure mentioned above is repeated until the expected fitness value is achieved or the highest iteration count is met.

4 Results and Discussion

4.1 Evaluation Metrics

KF-PSO's performance was examined using the following conventional performance measures established in Eqs. (16–21). The four measures used to measure performance include:

- True Positive (TP): Correctly determining the presence of a skin lesion
- True Negative (TN): Correctly determining the absence of a skin lesion
- False Positive (FP): Wrongly determining the presence of a skin lesion
- False Negative (FN): Wrongly determining the absence of a skin lesion.

$$\text{PSNR} = \log_{10}\left(\frac{255*255}{\text{Mean Squarrred Error}}\right) \tag{16}$$

$$\text{Sensitivity} = \frac{\text{TP}}{(\text{TP} + \text{FN})} \tag{17}$$

$$\text{Specificity} = \frac{\text{TP}}{(\text{TP} + \text{FN})} \tag{18}$$

$$\text{Precision} = \frac{\text{TP}}{\text{TP} + \text{FP}} \tag{19}$$

$$F\text{ - Measure} = \frac{2 \times \text{Precision} \times \text{Sensitivity}}{\text{Precision} + \text{Sensitivity}} \tag{20}$$

$$\text{Classification Accuracy} = \frac{\text{TP} + \text{TN}}{\text{TP} + \text{FP} + \text{TN} + \text{FN}} \tag{21}$$

4.2 About HAM10000 Dataset

To test the proposed IoT-based classifier, the HAM10000 dataset is utilized. It contains 10015 dermoscopic skin lesion pictures (i.e., 600 × 450 pixel images). The dataset is separated into two halves, one for training and the other for testing, including 9514 and 501 photos. Images with a resolution of 600 × 450 pixels are first reduced to 450 × 450 pixels, then downsampled to 256 × 256 pixels. Table 1 gives the distribution of the dataset's classes concerning each other.

Table 1 Seven types of skin lesion in HAM10000 dataset

Skin lesion	HAM	Training	Testing
Melanoma	1113	1058	55
Melanocytic nevus	6705	6366	339
Basal cell carcinoma	514	485	29
Actinic keratosis	327	314	13
Benign keratosis	1099	1046	53
Dermatofibroma	115	110	5
Vascular	142	135	7

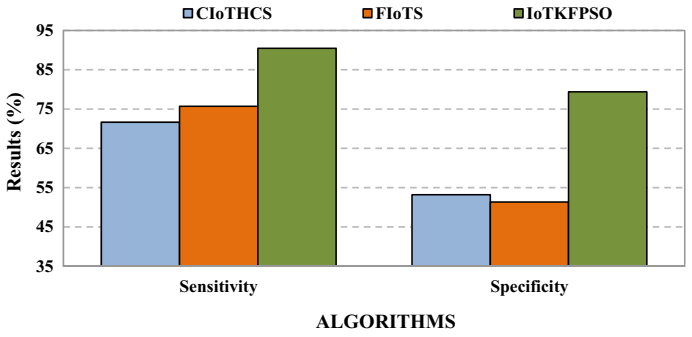

Fig. 1 Sensitivity and specificity—analysis

4.3 Performance Evaluation

The current section compares the performance of proposed classifier IOTKFPSO against the current classifiers CIOTHCS and FIOTS.

4.3.1 Sensitivity and Specificity Analysis

In Fig. 1, the *x*-axis depicts the sensitivity and specificity metrics, while the *y*-axis represents the percentage values for the associated metrics. Figure 1 clearly shows that the proposed IOTKFPSO outperforms the CIOTHCS and FIOTS. Optimization plays a major role in obtaining the better results.

4.3.2 Classification Accuracy and Precision Analysis

In Fig. 2, classification accuracy and precision are shown on the *x*-axis and percentage results for each parameter. From Fig. 2, it was identified that the proposed classifier

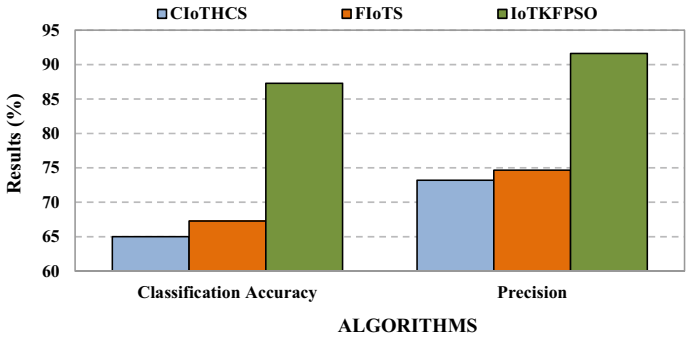

Fig. 2 Classification accuracy and precision—analysis

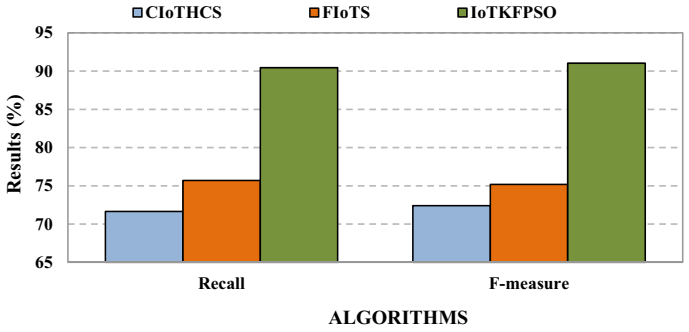

Fig. 3 Recall and *F*-measure—analysis

IOTKFPSO outperformed the current classifiers and FIOTS in classifying pictures of skin lesions. Precision was a good indicator of categorization quality.

4.3.3 Recall and F-Measure Analysis

Recall and F-measure are noted on the *x*-axis of Fig. 3, and the appropriate percentage values are shown on the *y*-axis. It is clear from Fig. 3 that IOTKFPSO has outperformed previous algorithms CIOTHCS and FIOTS in detecting relevant skin lesions. IOTKFPSO has a superior weighted harmonic mean regarding the accuracy and recall of the existing classifiers.

4.3.4 PSNR Analysis

In Fig. 4, algorithms are shown on the *x*-axis, while PSNR % results are shown on the *y*-axis. The proposed classifier IOTKFPSO has a better PSNR than existing

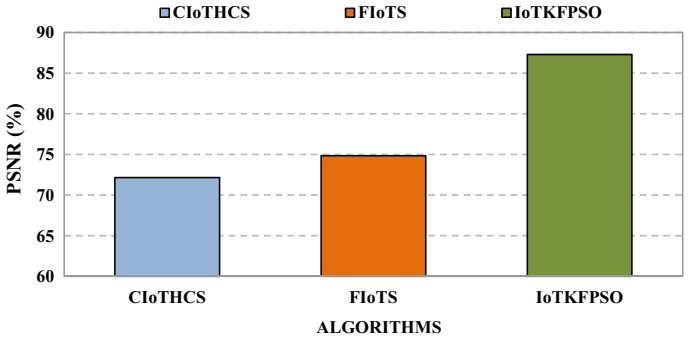

Fig. 4 PSNR—analysis

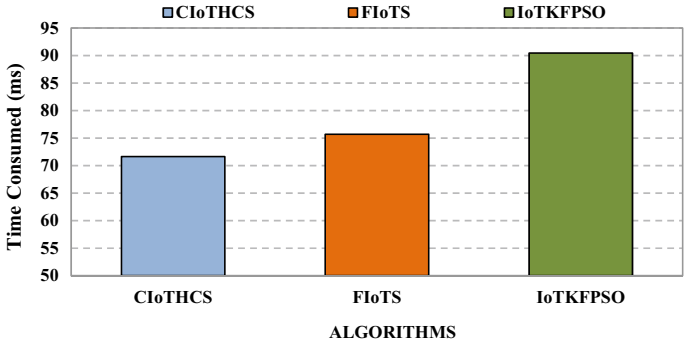

Fig. 5 Time consumption—analysis

CIOTHCS and FIOTS methods, as shown in Fig. 4. Skin lesions may be detected more precisely if optimization is present.

4.3.5 Time Consumption Analysis

It is possible to see how much time is spent on each algorithm in Fig. 5, which shows the *x*- and *y*-axis. Figure 5 shows that the proposed IOTKFPSO classifier consumes less time than CIOTHCS and FIOTS methods to categorize the skin lesions.

5 Conclusion

In this Paper, IoT-based Kalman filtering and Particle Swarm Optimization are proposed to achieve high benefits in exploring and utilizing the efficiency of IoT in the healthcare industry. Its framework is based on IoT to diagnose skin lesions

with the assistance of computer-aided systems automatically. Kalman filtering is modified to minimize the burdens faced in classification. Particle Swarm Optimization is applied to classify more efficiently, resulting in minimum power consumption. Results confirm that the proposed classifier has better performance when compared with existing classifiers.

References

1. G. Xing, Y. Chen, L. He, W. Su, R. Hou, W. Li, C. Zhang, X. Chen, Energy consumption in relay underwater acoustic sensor networks for NDN. IEEE Access **7**, 42694–42702 (2019). https://doi.org/10.1109/ACCESS.2019.2907693
2. M. Faheem, R.A. Butt, R. Ali, B. Raza, M.A. Ngadi, V.C. Gungor, CBI4.0: a cross-layer approach for big data gathering for active monitoring and maintenance in the manufacturing industry 4.0. J. Ind. Inf. Integr. 100236 (2021). https://doi.org/10.1016/j.jii.2021.100236
3. G. Chen, J. Tang, J.P. Coon, Optimal routing for multihop social-based D2D communications in the internet of things. IEEE Internet Things J. **5**, 1880–1889 (2018). https://doi.org/10.1109/JIOT.2018.2817024
4. M.A. Khan, F. Algarni, A healthcare monitoring system for the diagnosis of heart disease in the IoMT cloud environment using MSSO-ANFIS. IEEE Access **8**, 122259–122269 (2020). https://doi.org/10.1109/ACCESS.2020.3006424
5. J. Ramkumar, R. Vadivel, Performance modeling of bio-inspired routing protocols in cognitive radio ad hoc network to reduce end-to-end delay. Int. J. Intell. Eng. Syst. **12**, 221–231 (2019). https://doi.org/10.22266/ijies2019.0228.22
6. J. Ramkumar, R. Vadivel, Bee inspired secured protocol for routing in cognitive radio ad hoc networks. Indian J. Sci. Technol. **13**, 3059–3069 (2020). https://doi.org/10.17485/IJST/v13i30.1152
7. J. Ramkumar, R. Vadivel, Meticulous elephant herding optimization based protocol for detecting intrusions in cognitive radio ad hoc networks. Int. J. Emerg. Trends Eng. Res. **8**, 4549–4554 (2020). https://doi.org/10.30534/ijeter/2020/82882020
8. J. Ramkumar, R. Vadivel, Intelligent fish swarm inspired protocol (IFSIP) for dynamic ideal routing in cognitive radio ad-hoc networks. Int. J. Comput. Digit. Syst. **10**, 1063–1074 (2020). https://doi.org/10.12785/ijcds/100196
9. R. Vadivel, J. Ramkumar, QoS-enabled improved cuckoo search-inspired protocol (ICSIP) for IoT-based healthcare applications, pp. 109–121 (2019). https://doi.org/10.4018/978-1-7998-1090-2.ch006
10. J. Ramkumar, R. Vadivel, B. Narasimhan, constrained cuckoo search optimization based protocol for routing in cloud network. Int. J. Comput. Netw. Appl. https://doi.org/10.22247/ijcna/2021/210727
11. J. Ramkumar, R. Vadivel, FLIP: frog leap inspired protocol for routing in cognitive radio ad hoc networks, in *International Conference on Recent Trends in Engineering and Material Sciences (ICEMS-2016)*, Jaipur, p. 248 (2016)
12. J. Ramkumar, R. Vadivel, CSIP—cuckoo search inspired protocol for routing in cognitive radio ad hoc networks, in *Advances in Intelligent Systems and Computing* (Springer, 2017), pp. 145–153. https://doi.org/10.1007/978-981-10-3874-7_14
13. P. Menakadevi, J. Ramkumar, Robust optimization based extreme learning machine for sentiment analysis in big data, in *2022 International Conference on Advanced Computing Technologies and Applications*, pp. 1–5 (2022). https://doi.org/10.1109/ICACTA54488.2022.9753203
14. J. Ramkumar, C. Kumuthini, B. Narasimhan, S. Boopalan, Energy consumption minimization in cognitive radio mobile ad-hoc networks using enriched ad-hoc on-demand distance

vector protocol, in *2022 International Conference on Advanced Computing Technologies and Applications*, pp. 1–6 (2022). https://doi.org/10.1109/ICACTA54488.2022.9752899
15. J. Ramkumar, R. Vadivel, Whale optimization routing protocol for minimizing energy consumption in cognitive radio wireless sensor network. Int. J. Comput. Netw. Appl. **8**. https://doi.org/10.22247/ijcna/2021/209711
16. J. Ramkumar, R. Vadivel, Improved frog leap inspired protocol (IFLIP)—for routing in cognitive radio ad hoc networks (CRAHN). World J. Eng. **15**, 306–311 (2018). https://doi.org/10.1108/WJE-08-2017-0260
17. J. Ramkumar, R. Vadivel, Improved wolf prey inspired protocol for routing in cognitive radio ad hoc networks. Int. J. Comput. Netw. Appl. **7**, 126–136 (2020). https://doi.org/10.22247/ijcna/2020/202977
18. J. Ramkumar, R. Vadivel, Multi-adaptive routing protocol for internet of things based ad-hoc networks. Wirel. Pers. Commun. 1–23 (2021). https://doi.org/10.1007/s11277-021-08495-z
19. M. Lingaraj, T.N. Sugumar, C. Stanly Felix, J. Ramkumar, Query aware routing protocol for mobility enabled wireless sensor network. Int. J. Comput. Netw. Appl. **8**, 258 (2021). https://doi.org/10.22247/IJCNA/2021/209192
20. S. Kim, S. Kim, User preference for an IoT healthcare application for lifestyle disease management. Telecomm. Policy **42**, 304–314 (2018). https://doi.org/10.1016/j.telpol.2017.03.006
21. P. Verma, S.K. Sood, Cloud-centric IoT based disease diagnosis healthcare framework. J. Parallel Distrib. Comput. **116**, 27–38 (2018). https://doi.org/10.1016/j.jpdc.2017.11.018
22. R. Bharathi, T. Abirami, S. Dhanasekaran, D. Gupta, A. Khanna, M. Elhoseny, K. Shankar, Energy efficient clustering with disease diagnosis model for IoT based sustainable healthcare systems. Sustain. Comput. Inf. Syst. **28**, 100453 (2020). https://doi.org/10.1016/j.suscom.2020.100453
23. H. Zhu, P. Podesva, X. Liu, H. Zhang, T. Teply, Y. Xu, H. Chang, A. Qian, Y. Lei, Y. Li, A. Niculescu, C. Iliescu, P. Neuzil, IoT PCR for pandemic disease detection and its spread monitoring. Sens. Actuators B Chem. **303**, 127098 (2020). https://doi.org/10.1016/j.snb.2019.127098
24. P.M. Kumar, S. Lokesh, R. Varatharajan, G. Chandra Babu, P. Parthasarathy, Cloud and IoT based disease prediction and diagnosis system for healthcare using fuzzy neural classifier. Futur. Gener. Comput. Syst. **86**, 527–534 (2018). https://doi.org/10.1016/j.future.2018.04.036
25. Z. Al-Makhadmeh, A. Tolba, Utilizing IoT wearable medical device for heart disease prediction using higher order Boltzmann model: a classification approach. Measurement **147**, 106815 (2019). https://doi.org/10.1016/j.measurement.2019.07.043
26. V. Pathak, K. Singh, A. Aziz, A. Dhoot, Efficient and compressive IoT based health care system for parkinson's disease patient. Procedia Comput. Sci. **167**, 1046–1055 (2020). https://doi.org/10.1016/j.procs.2020.03.441
27. A. Das, P. Rad, K.K.R. Choo, B. Nouhi, J. Lish, J. Martel, Distributed machine learning cloud teleophthalmology IoT for predicting AMD disease progression. Futur. Gener. Comput. Syst. **93**, 486–498 (2019). https://doi.org/10.1016/j.future.2018.10.050
28. T. Nguyen Gia, I.B. Dhaou, M. Ali, A.M. Rahmani, T. Westerlund, P. Liljeberg, H. Tenhunen, Energy efficient fog-assisted IoT system for monitoring diabetic patients with cardiovascular disease. Futur. Gener. Comput. Syst. **93**, 198–211 (2019). https://doi.org/10.1016/j.future.2018.10.029

Detection of Fault Disturbances in a DG Integrated Hybrid Power System Using HS-Transform and Wavelet Transform

Basanta K. Panigrahi, Jyoti Shukla, and Shruti Sahu

Abstract Solar energy penetration into traditional power grid causes numerous problems in power system management and control. Detecting fault disturbances in an electrical power system is a difficult undertaking. This paper discusses a novel method for tracking the fault disturbances in solar operated DG connected in power system. Numerous types of faults like LG, LLG, LL, LLLG, and LLL are considered in this work. It is noticed that both the transforms are effectively identifies the instants of disruption in the voltage. It is observed that the time–frequency resolution in case of HST is comparatively better than WT. The objective of this work is to detect the fault disturbances using HS-transform and wavelet transform in a DG connected hybrid power system. A novel approach based on HS-transform and wavelet transform is presented to detect the LG fault and LLL fault. When signal is passing through WT and HST, it is evaluated that WT is unable to identify the signal due to noise, whereas in HST the disturbances present in the signal in the corresponding instants is nicely captured and detected. This shows the robustness in HST under noisy conditions. It simplifies the complexity in identifying the disturbances which increases the detection accuracy of the system.

Keywords Distributed generation (DG) · Wavelet transform (WT) · Hyperbolic S-transform · Point of common coupling (PCC)

1 Introduction

Recently, extraction of renewable energies in the form of distributed generation (DG) is establishing itself as a major contributor of generation of electrical power to

B. K. Panigrahi (✉)
Department of Electrical Engineering, SOA University, Bhubaneswar, India
e-mail: basanta1983@gmail.com

J. Shukla
Poornima College of Engineering, Jaipur, India

S. Sahu
University College of Engineering, Kota, India

© The Author(s), under exclusive license to Springer Nature Singapore Pte Ltd. 2023

K. Murari et al. (eds.), *Soft Computing Applications in Modern Power and Energy Systems*,
Lecture Notes in Electrical Engineering 975,
https://doi.org/10.1007/978-981-19-8353-5_3

fulfill the increasing demand with its merit as green energy with almost negligible environmental pollution [1]. Among all the renewable sources, wind and solar energy are the most versatile resources. Though these are highly potential sources of energy, but with increased penetration of DGs in conventional power grid will pose various operational and design challenges. Stability is a vital issue so when the system is subjected to different types of symmetrical and unsymmetrical fault conditions [2]. Again, when photovoltaic system is connected to the grid via interfacing converters. The main aspect of power system design is to maintain uninterruptible power supply to the customers. But this condition is disrupted by the different fault disturbances occurred in power system because of natural calamities, mal-operations, physical accidents, lightning, and other operating failures. These will lead to fault conditions such as LG, LL, LLG, LLL, and LLLG which directly or indirectly threaten the stability and reliability in power supply [3, 4]. As solar energy is intermittent which makes it highly uncertain in characteristics and therefore need some storage system like battery or flywheels to improve the system performance. Further, the solar PV system is dependent on different parameters such as solar insolation, temperature of cells, and shadow effects that may cause some abnormal situations indirectly [5]. In addition, different artificial intelligence techniques like fuzzy logic (FL), artificial neural network (ANN), artificial neuro-fuzzy inference system (ANFIS), and support vector machine (SVM) are used to classify the fault disturbances. Artificial neural network (ANN) is popularly used for fault localization and detection classification [6, 7]. ANN alongside wavelet transform was proposed to identify the fault disturbances [8].

Various studies were reported in the literature for the identification and monitoring of fault disturbances. Some used indices like RMS value, peak value, frequency, or voltage change for detecting fault/abnormal conditions. The methods such as Fourier transform (FT) and fast Fourier transform (FFT) are one of the most popular ones for the disturbance study. Many researchers have used other transforms like chirp *Z*-transform, Welch algorithm for observing the electrical-parameters [3, 9]. But sometimes it is very hard to detect non-stationary disturbances due to only frequency data and no time data. Therefore, wavelet transform (WT), S-transform, short-time Fourier transform (STFT), etc., were studied and designed to be applied to fulfil the objective of fault analysis [10, 11].

The article is assembled as follows. Section 2 illustrates the system configuration and description of solar energy-based system. The detection methodologies are describing in Sect. 3, and the simulation results and discussion is mark out in Sect. 4. In the end, the conclusions residue from the research is briefed in Sect. 5.

2 System Configuration and Modeling

The system under study is a solar-based power system as shown in Fig. 1, which is a combination of PV, based DG in grid-connected mode. Solar energy is a valuable renewable energy resource with numerous applications in society, and it is being

employed in the present analysis in conjunction with the traditional power system. The sub-sections that follow gives the modeling and descriptions of such a system.

Figure 1 depicts a PV system that is interconnected to the standard power grid and includes a battery energy storage system. The excess energy is stored in the battery via a bi-directional converter during periods of high solar insolation. The system depicted in Fig. 1a is utilized to investigate disturbances. The basic layout diagram of a solar energy-based system with several elements is shown in Fig. 1a. Figure 1b depicts the detailed interface structure of the power system under consideration.

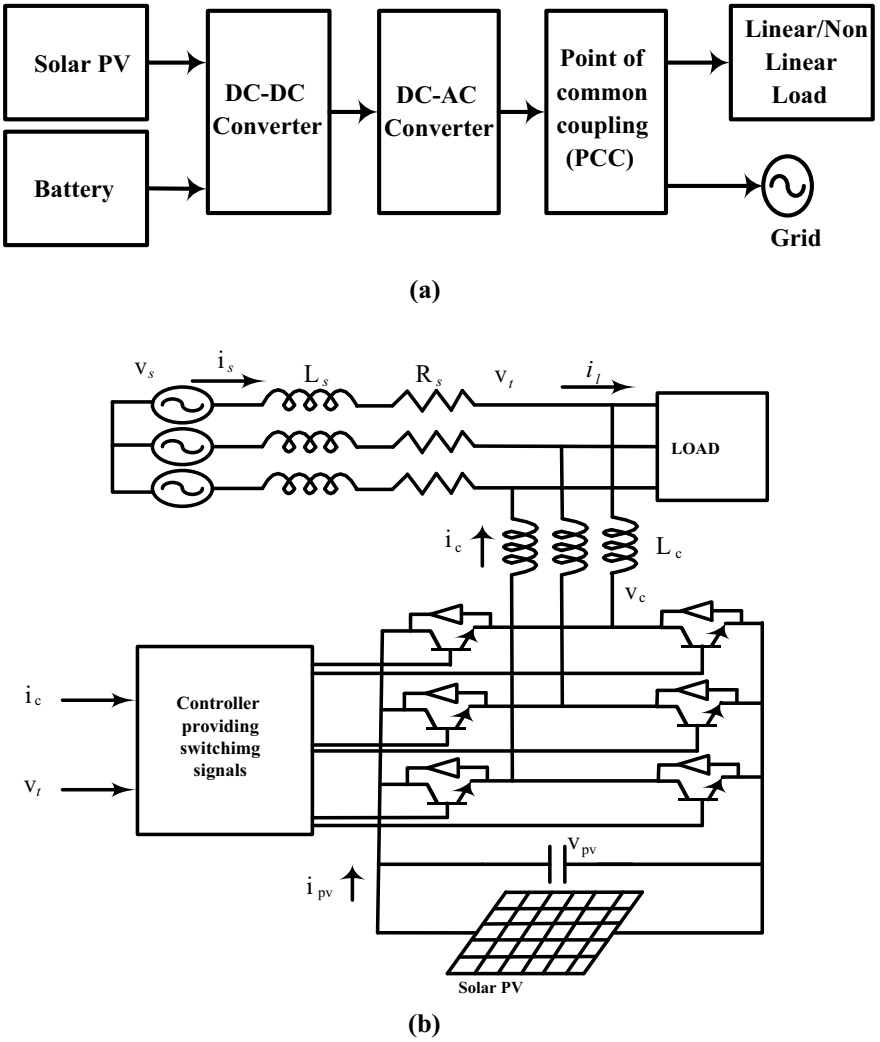

Fig. 1 Basic layout diagram of solar energy-based system, **a** block diagram, **b** detailed interfacing circuit

3 Detection Techniques

The following are descriptions of several detection methods, such as the HS-transform and the wavelet transform:

3.1 HS-Transform

The S-transform (ST), a time–frequency multi-resolution analysis was conducted based on the WT and STFT, is a revised form of the wavelet transform with phasor rectification. It employs a Gaussian variable window with indirectly related width and frequency. But, even in the existence of noise, sometimes S-transform fails to locate disturbances. Thus, in low–high frequencies, HS-transform with pseudo-hyperbolic Gaussian window provides improved time/frequency resolutions. A higher distortion of the window at low frequencies improves the frequency domain width [12].

The hyperbolic window is expressed as

$$W_{\mathrm{hb}} = \frac{2f_s}{\sqrt{2\pi(\alpha_{\mathrm{hb}} + \beta_{\mathrm{hb}})}} \exp\left\{-\frac{-f_s^2 X^2}{2}\right\} \tag{1}$$

where

$$X = \frac{(\alpha_{\mathrm{hb}} + \beta_{\mathrm{hb}})}{2\alpha_{\mathrm{hb}}\beta_{\mathrm{hb}}}(\tau - t - \xi) + \frac{(\alpha_{\mathrm{hb}} - \beta_{\mathrm{hb}})}{2\alpha_{\mathrm{hb}}\beta_{\mathrm{hb}}}\sqrt{(\tau - t - \xi)^2 + \lambda_{\mathrm{hb}}^2} \tag{2}$$

$$0 < \alpha_{\mathrm{hb}} < \beta_{\mathrm{hb}} \text{ and } \xi = \frac{\sqrt{(\beta_{\mathrm{hb}} - \alpha_{\mathrm{hb}})^2 \lambda_{\mathrm{hb}}^2}}{4\alpha_{\mathrm{hb}}\beta_{\mathrm{hb}}}$$

The HS-transform's discrete version is calculated and $G(m_F, n_F)$ represents the Fourier transform of hyperbolic window

$$G(m_F, n_F) = \frac{2f_s}{\sqrt{2\pi(\alpha_{\mathrm{hb}} + \beta_{\mathrm{hb}})}} \exp\left\{-\frac{-f_s^2 X_D^2}{2}\right\} \tag{3}$$

where

$$X_D = \frac{(\alpha_{\mathrm{hb}} + \beta_{\mathrm{hb}})}{2\alpha_{\mathrm{hb}}\beta_{\mathrm{hb}}} t + \frac{(\alpha_{\mathrm{hb}} - \beta_{\mathrm{hb}})}{2\alpha_{\mathrm{hb}}\beta_{\mathrm{hb}}}\sqrt{t^2 + \lambda_{\mathrm{hb}}^2} \tag{4}$$

$H[m_F, n_F]$ is the frequency shifted Fourier transform $H[m_F]$ and is given by

$$H[m_F] = \frac{1}{N}\sum_{m_F=0}^{N-1} h(k)\exp(-i2\pi n_F k) \tag{5}$$

$$S[n_F, j] = \sum_{m_F=0}^{N-1} H(m_F + n_F)G(m_F, n_F)\exp(-i2\pi m_F j) \tag{6}$$

S indicated the S-transform of $h(t)$. τ is a parameter that affects the location of Gaussian window. Here, N is the total sample size. $H[m_F]$ is the fault voltage and current waveform sample.

3.2 Wavelet Transform (WT)

Signal processing techniques also known as transient-based approaches are preferably employed for fault diagnosis mainly for protection, and the wavelet transform has been discovered to be capable of studying transient signals occur during a power system fault condition arises. Owing to its economical speed, frequency resolutions, and dependability of extracting relevant features, the wavelet transform (WT) is viewed as a potential tool for fault detection. The wavelet is made up of translations and dilatations that are formed from a mother wavelet [13, 14]. The discrete wavelet transform (DWT) of a function $f(t)$ can be investigated using the equation.

$$\frac{1}{\sqrt{x_0^m}} \sum_k f(k)\phi * \left(\frac{n - kx_0^m}{x_0^m}\right) \tag{7}$$

In place of x and y, the parameters m and k represent the integer variables. The wavelet is connected with a scaling function, which when combined with the wavelet function. That one level's scaling function can be represented as the sum of the next finer level's scaling function.

$$\phi(t) = \sum_{n=-\infty}^{\infty} h(n)\sqrt{2}\phi(2t - n) \tag{8}$$

The link between both the scaling function and the wavelet function is shown in Eq. (9).

$$\phi(t) = \sum_{n=-\infty}^{\infty} h_1(n)\sqrt{2}\phi(2t - n) \tag{9}$$

$$c_j(k) = \sum_{m=-\infty}^{\infty} c_{j+1}(m)h(m - 2k) \tag{10}$$

$$d_j(k) = \sum_{m=-\infty}^{\infty} c_{j+1}(m)h_1(m - 2k) \tag{11}$$

Equations (10) and (11) illustrate the coefficients at a rough stage that may be obtained by analyzing coordinates at a finer level until they reach their individual filters that would be followed by the implementation of the two, resulting in different numbers of samples at the coarser stage.

4 Simulation Results and Analysis

The simulated outcomes achieved with MATLAB/Simulink are described in this section. The solar PV system in question is connected to the electrical grid, and the complete system is modeled in MATLAB. Different faults are being created in grid side and the corresponding voltage signal at PCC is taken offline. It is then processed through wavelet and S-transforms. The transformed signal is used to determine various statistical characteristics such as standard deviation and entropy. An information set of 500 × 6 is then developed taking into consideration six distinct characteristics and faults in distinct working situations. Half of this collection of information is used for practice, and half is used for testing. The sampling frequency is set to 5 kHz. The detail coefficients out from original images provide more spatial and spectral data. The detail coefficients show where in data set key facts can be found. As a result, the Db4 detail coefficient is used in this proposed study. A grid-connected solar energy generating plant is depicted in the proposed concept. A PV panel, three-phase source, transformers, circuit breakers, and a fault block connected to the load are all included in the model. Figure 2 depicts a single line diagram of the proposed hybrid model.

At PCC, the signal of voltage for LG fault is shown in Fig. 3a. This signal is obtained at PCC and carried through WT and HST, and the findings are displayed in Fig. 3b and c. It is noticed that both the transform very beautifully identifies the instants of disruption in the voltage. Of course, the time–frequency resolution in case of HST is comparatively better than WT. The voltage signal is further given

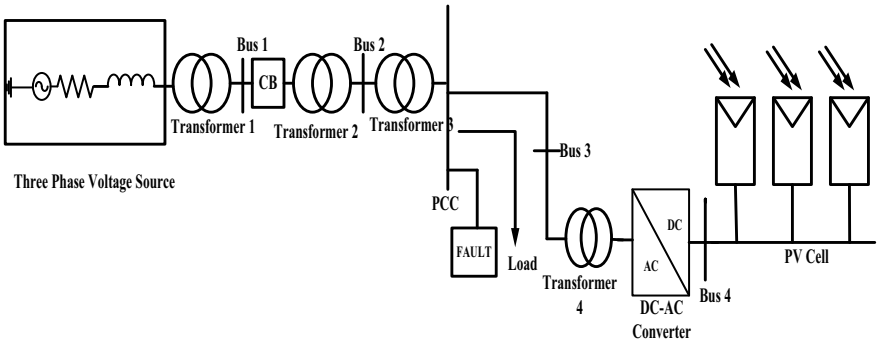

Fig. 2 Single line diagram of proposed Simulink DG integrated hybrid system

a 20 dB noise boost, as illustrated in Fig. 4a. When passing through WT and HST illustrate in Fig. 4b and c, it is evaluated that WT unable to identify the signal due to noise, whereas in HST the disturbances present in the signal in the corresponding instants is nicely captured and detected. This shows the robustness in HST under noisy conditions. Again, the voltage signal for LLL fault is extracted and shown in Fig. 5a. After it is passed through WT and HST, the results are presented in Fig. 5b and c, respectively. It is observed that HST shows better detection capability as compared WT. The detection is determined on the basis of performance measures such as entropy and standard deviation. In a grid-connected PV system, LG and LLL faults are formed, and the relevant voltage signal is retrieved at the PCC (Table 1).

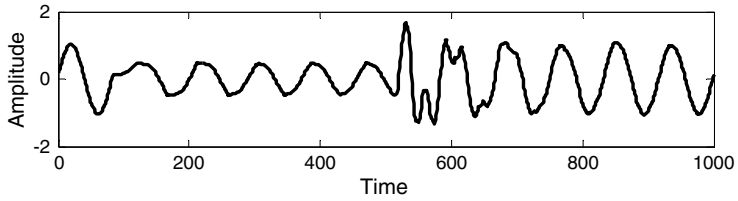

(a)Voltage signal for LG fault at PCC

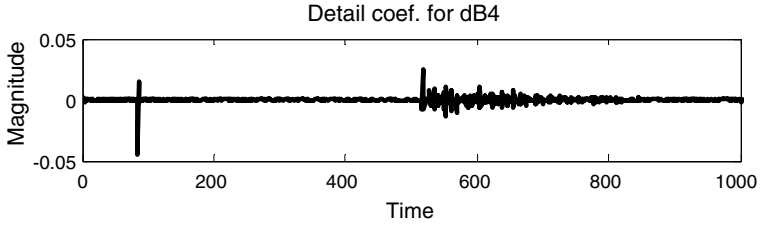

(b) Detection by WT

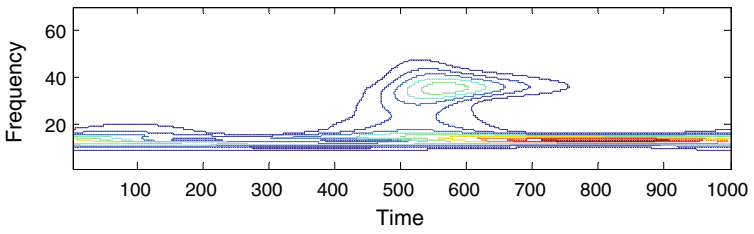

(c) Detection by HST

Fig. 3 LG fault detection, **a** voltage signal for LG fault at PCC, **b** detection by WT, **c** detection by HST

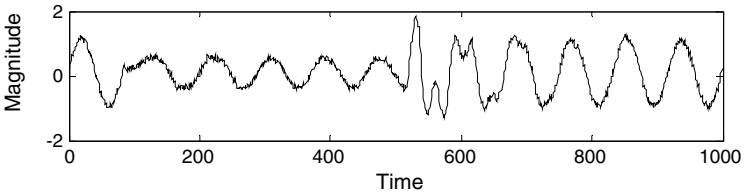

(a) Voltage signal for LG fault at PCC

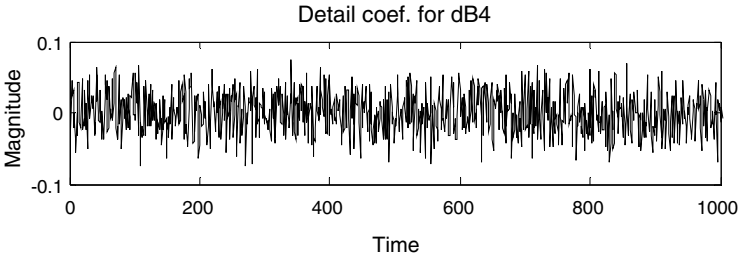

(b) Detection by WT

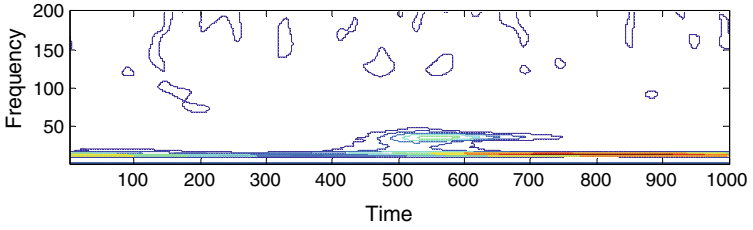

(c) Detection by HST

Fig. 4 LG fault detection with 20 dB noise, **a** voltage signal for LG fault at PCC, **b** detection by WT, **c** detection by HST

5 Conclusion

This paper presents the study of different fault disruption of the grid-integrated solar PV-based power system. The fault disturbances are detected by utilizing WT and HS-transforms. It is noted that HS-transform is more accurate in the detection of disturbances. The effectiveness of the present work has been verified at different noise levels to validate its validity. A comparison of the STD and entropy has been performed. The comparison results show that the proposed strategy provides more consistent and trustworthy outcomes. It has been observed that when noise is injected into the voltage signal, the accuracy of WT will be degrading. Although HST was able to identify the disturbances present in the signal. The simulation results obtained reveal that the proposed method performs well for all types of faults.

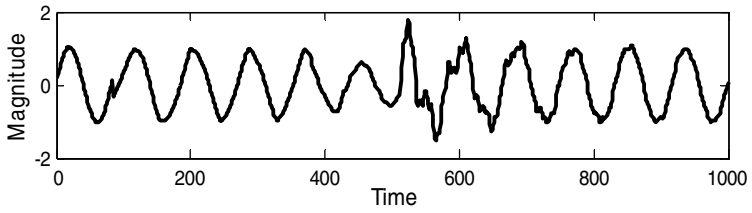

(a) Voltage signal for LLL fault at PCC

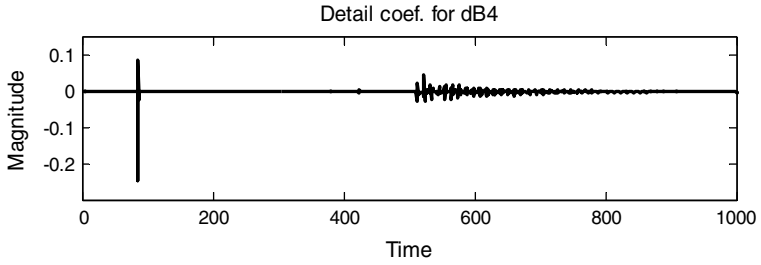

(b) Detection by WT

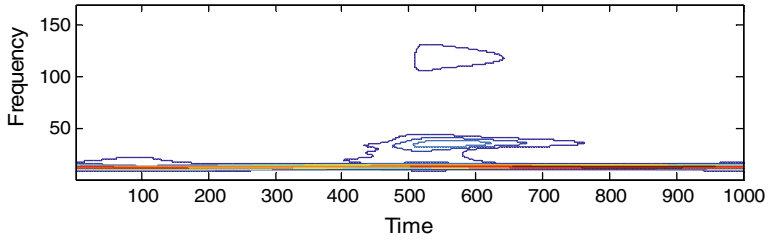

(c) Detection by HST

Fig. 5 LLL fault detection, **a** voltage signal for LG fault at PCC, **b** detection by WT, **c** detection by HST

Table 1 STD and entropy for different faults

Fault	Standard deviation (STD)	Entropy
LG	0.345	0.583
LG with 20 dB noise	0.456	0.838
LLL	0.532	0.638

References

1. K. Moloi, Y. Hamam, J.A. Jordaan, Fault detection in power system integrated network with distribution generators using machine learning algorithms, in *2019 6th International Conference on Soft Computing & Machine Intelligence (ISCMI)* (IEEE, 2019), pp. 18–22
2. M.S. Thomas, P.P. Terang, Interconnection issues for distributed resources in a smart distribution system, in *2012 IEEE 5th India International Conference on Power Electronics (IICPE)* (IEEE, 2012), pp. 1–6

3. P.K. Ray, S.R. Mohanty, N. Kishor, Disturbance detection in grid-connected distributed generation system using wavelet and S-transform. Electr. Power Syst. Res. **81**(3), 805–819 (2011)
4. Y.A. Elshrief, D.H. Helmi, A.D. Asham, B.A. Abozalam, Merits and demerits of the distributed generations connected to the utility grid. Menoufia J. Electron. Eng. Res. **28**(ICEEM2019-Special Issue), 259–262 (2019)
5. P.R. Satpathy, S.B. Thanikanti, A.H. Mahmoud, R. Sharma, B. Nastasi, A TCT-SC hybridized voltage equalizer for partial shading mitigation in PV arrays. IEEE Trans. Sustain. Energy (2021)
6. S. Adhikari, N. Sinha, T. Dorendrajit, Fuzzy logic based on-line fault detection and classification in transmission line. Springer Plus **5**(1), 1–14 (2016)
7. M. Singh, B.K. Panigrahi, R.P. Maheshwari, Transmission line fault detection and classification, in *2011 International Conference on Emerging Trends in Electrical and Computer Technology* (IEEE, 2011), pp. 15–22
8. A. Bhuyan, B.K. Panigrahi, S. Pati, Fault classification for DG integrated hybrid power system using wavelet neural network approach, in *2021 1st Odisha International Conference on Electrical Power Engineering, Communication and Computing Technology (ODICON)* (IEEE, 2021), pp. 1–5
9. P.K. Ray, N. Kishor, S.R. Mohanty, Islanding and power quality disturbance detection in grid-connected hybrid power system using wavelet and $ S $-transform. IEEE Trans. Smart Grid **3**(3), 1082–1094 (2012)
10. B.K. Panigrahi, P.K. Ray, P.K. Rout, S.K. Sahu, Detection and location of fault in a micro grid using wavelet transform, in *2017 International Conference on Circuit, Power and Computing Technologies (ICCPCT)* (IEEE, 2017), pp. 1–5
11. S.R. Samantaray, P.K. Dash, G. Panda, Fault classification and location using HS-transform and radial basis function neural network. Electr. Power Syst. Res. **76**(9–10), 897–905 (2006)
12. S. Agrawal, M.H. Dhend, Wavelet transform based voltage quality improvement in smart grid, in *2016 International Conference on Automatic Control and Dynamic Optimization Techniques (ICACDOT)* (IEEE, 2016), pp. 289–294
13. J. Shukla, B.K. Panigrahi, An analytical approach for optimal size of distributed generation unit, in *International Conference on Recent Advances and Innovations in Engineering (ICRAIE-2014)* (IEEE, 2014), pp. 1–6
14. B.K. Panigrahi, A. Bhuyan, A.K. Satapathy, R. Pattanayak, B. Parija, Fault analysis of grid connected wind/PV distributed generation system, in *International Conference on Intelligent Computing and Communication Technologies* (Springer, Singapore, 2019), pp. 47–54
15. P.K. Ray, B.K. Panigrahi, P.K. Rout, A. Mohanty, F.Y. Eddy, H.B. Gooi, Detection of islanding and fault disturbances in microgrid using wavelet packet transform. IETE J Res. **65**(6), 796–809 (2019)

Clonal Assortment Optimization Procedure to Unravel Cost-Effective Power Dispatch Problem

Vijay Raviprabhakaran

Abstract This article offers an artificial immune logic (AIL) centred optimization methodology to unravel the cost-effective power dispatch problem. Economic power dispatch (EPD) defines the electric generated power produced by the dedicated power-producing units so that the production rate is curtailed as fulfilling the power requirement concurrently. The developed AIL procedure utilized the total production expense as the goal function and is characterized as the affinity rate. The antibodies with high-affinity instruments are generated through genetic progression and grow into the solution. The replication findings expose that the established technique is simple to execute congregated within a satisfactory implementation period and an extremely optimized solution for EPD with the least production expense is attained, while the same is audited on 3, 13 in addition to 40 power-producing schemes. The result also validates that the AIL-based optimization technique is an effective tool for resolving optimal results in EPD problems, which entails a large quantity of generating units while simultaneously fulfilling many limitations when contrasted with other procedures. Still, the purported technique might be valid to obscure real power-producing system hindrances.

Keywords Artificial immune logic · Economic power dispatch · Cost effective solution · Clonal assortment optimization algorithm · Power production expense

V. Raviprabhakaran (✉)
Electrical and Electronics Engineering, CVR College of Engineering, Hyderabad 501510, India
e-mail: vijai.mtp@gmail.com

© The Author(s), under exclusive license to Springer Nature Singapore Pte Ltd. 2023

K. Murari et al. (eds.), *Soft Computing Applications in Modern Power and Energy Systems*,
Lecture Notes in Electrical Engineering 975,
https://doi.org/10.1007/978-981-19-8353-5_4

1 Introduction

Electric power systems are constructed and controlled to meet up the constant deviation of power demand. In power system lessening, the operation rate is very significant. EPD is a way to organize the power generator yields about the load demands and to manage the power system most cost effectively. Throughout the days, numerous struggles have been created to unravel the EPD problem, encompassing several limitations or numerous goals through numerous arithmetic programming and optimization methods. The standard typical approaches include the lambda reiteration procedure, base point approach and participation factor methodology, gradient method, etc. Conversely, the above-mentioned conventional dispatch procedures necessitate the incremental fuel rate curves to be monotonically enhancing or piecewise linear. The response/yield traits of current entities are intrinsically extremely nonlinear (valve-point loading, ramp rate restrictions, etc.,) and have numerous local minimum locations in the fuel rate function. Its attributes remain reckoned to go through the obligations of standard power dispatch processes in the lead to suboptimal answers, then stemming in enormous profits deficit all over the period. The concern of extremely nonlinear traits of the power generating units makes a highly robust set of rules to avert becoming trapped in local optima. The orthodox calculus-centred procedures failed to unravel these sorts of complications.

Recently, stochastic hunt algorithms for instance simulated annealing (SA) [1], genetic algorithm (GA) [2], evolutionary programming (EP) [3], particle swarm optimization (PSO) [4], Grey wolf optimization (GWO) [5], Whale Optimization (WO) algorithm [6], and Communal Spider Optimization (CSO) [7] algorithm have been frightfully cast-off to unravel power organization optimization complications attributable to its facility towards discovering the close-global resolution of a nonconvex optimization delinquent. The simulated annealing is a robust optimization procedure, but in routine, the toughening plan ought to be painstakingly modified else the accomplished answer will even remain locally optimal. Still, a suitable annealing plan frequently entails immense reckoning time. Mutually, GA and EP developed along the simile of real natural training can necessitate a near-global result. EP contrasts with GA in the view that EP differs predominantly in transformation and assortment even though not limited in the same way as in GA. Accordingly, a substantial reckoning period might be hoarded in EP. In malevolence of their beneficial performance, both GA and EP retain approximately weaknesses prominent towards a further computation period and smaller conjunction in the instance of extremely epistatic goal functions. The limitations augmented remain extremely associated. Even though PSO is utilized in the direction of unravelling the nonlinear and non-continuous optimization delinquent, it agonizes from hasty convergence, particularly though supervising complications through further local goals.

Apart from the stochastic algorithm, there is numerous nature-stimulated optimization algorithm, for solving the EPD problem. Every procedure has its advantages and disadvantages [8–12]. The same algorithm is being solved for optimal power and control schemes in generating systems [13, 14].

This article offers the usage of the artificial immune logic (AIL) [15] centred optimization technique utilizing the clonal assortment principle to decipher EPD problems [16]. The acquired AIL software development is employed to ascertain the real power elect spawned by the power generating components in a power production scheme. Which remain imperilled by quite a few disparities and equality limitations to accomplish the smallest production rate though substantial the power mandates instantaneously.

The remaining of this article is outlined as ensues Sect. 2 depicts the EPD problem interpretation. Section 3 is concerning the artificial immune logic algorithm and its study. Section 4 accords the execution of the clonal assortment algorithm to EPD problem. The results and analyses are accompanied in Sect. 5. Conclusions are presented in Sect. 6.

2 EPD Problem Formulation

The goal of EPD remains towards discovering the best result as a result that the bare lowest fuel rate is attained bound by specific equality and inequality restrictions. The delinquent might be conveyed as a role that involves the cost function and the restrictions. The equality limitation considers active power equilibrium, then the inequality limitation indicates the bounds of active power production. Arithmetically, the interpretation is given as follows

2.1 Goal Function

The hybrid system consists of the following characteristics.

The goal function comprises the amount of the rate role of entirely dedicated elements finished in all periods. F is the entire coal rate for the ith power generator (in \$/h), then is typified through the subsequent equivalence.

$$F = \sum_{i=1}^{n} F_i(P_i) \tag{1}$$

The fuel expense attributes of every power-producing unit i is symbolized with a quadratic polynomial equivalence

$$F_i(P_i) = a_i + b_i + c_i P_i^2 \tag{2}$$

where a_i, b_i and c_i are the cost coefficients of the ith generator, and P_i is the output for unit i

2.2 Goal Function with Valve Point Influence

The faucet opening manner of multivalve coal-powered steam turbines creates a wave-similar impact in the temperature rate curvature of the power producers, and it is engaged into consequence in the EPD delinquent by overlaying the fundamental quadratic fuel cost attributes through the modified sinusoidal section as surveys.

$$F_i(P_i) = a_i + b_i + c_i P_i^2 + \left| d_i \sin\left\{ e_i \left(P_i^{\min} - P_i \right) \right\} \right| \tag{3}$$

where e_i and d_i are the coal fuel expense factors of unit i with valve point effect.

The above Eq. (2) can be solved by considering the following constraints.

2.3 Real Power Equilibrium Limitation

For power equilibrium, equality restriction must be convinced. The aggregate produced power must remain identical to the complete load demand combined with the aggregate losses ($P_L = 0$).

$$\sum_{i=1}^{N} P_i - P_D - P_L = 0 \tag{4}$$

where P_i is the power production for taken generating unit i,

N is the number of power generators in the structure,

P_D is the absolute power demand,

P_L is the power transmission network loss.

2.4 Real Power Operating Restrictions

There is a threshold on the extent of power that a division of generators can produce. The generator power production of any unit should not surpass its assessment, nor should it be lower than required for a balanced process. The production yield of every unit would remain sandwiched between upper and lower restrictions. The resultant inequality constraints for every single generator are

$$P_i^{\min} \leq P_i \leq P_i^{\max} \; i \in N \tag{5}$$

where $P_i^{\min}$ and $P_i^{\max}$ are minima and maximum operating output of the relevant unit.

2.5 Generating Unit Ramp Limits

If the power generator ramp rate restrictions are considered then the actual real power operational limits are revised as arise.

$$P_i - P_i^0 \leq \mathrm{UR}_i \qquad \text{If generation enhances}$$

$$P_i^0 - P_i \leq \mathrm{DR}_i \qquad \text{If generation diminishes}$$

$$\max\left(P_i^{\min}, P_i^0 - \mathrm{DR}_i\right) \leq P_i \leq \min\left(P_i^{\max}, P_i^0 + \mathrm{UR}_i\right) i \in N \tag{6}$$

where UR_i DR_i ramp-up and ramp-down rate boundaries of the ith generator, and P_i^0 is the prior operating point of the generator.

3 Artificial Immune Logic Algorithm

The primary intention of the protected scheme is to distinguish all cells (or fragments) inside the body and compartmentalize individual cells as identity or non-identity. The non-identity cells are more catalogued to provoke an apt type of suspicious apparatus. The immune system realizes all overgrowth to characterize treacherous extraneous antigens (e.g. microbes, viruses, etc.) and the body's cells or molecules.

The AIL imitates these biological moralities of clone production, propagation, and evolution. The foremost phases of AIL built on the clonal assortment attitude are stimulation of antibodies, propagation, and discrepancy on the happenstance of cells through antigens, mellowing by booming out affinity mellowing progression, eradicating deep-rooted antibodies to sustain the miscellany of antibodies, and evading untimely conjunction, an assortment of individual antibodies whose sympathies by the antigen are superior. To rival AIL in optimization, the antibodies and affinity are carried as the viable solutions and the objective function correspondingly. The real number is applied to embody the traits of the antibodies.

To recognize the speculative hypothesis of AIL, the biological development of the immune approach needs to be welcomed. The body's defence apparatus varies with the activity of antibodies to acknowledge and eradicate overseas cells termed antigens. The antibodies remain created through lymphocytes over clonal propagation. *B*-lymphocytes and *T*-lymphocytes are the dual key elements in the lymphocyte

assembly. The *B*-lymphocytes are the cells produced by the bone marrow, and the *T*-lymphocytes are the cells formed by the thymus. *A B*-lymphocyte drives and delivers a solo antibody that is located on its outside shell besides performing as a receptor. Regulator procedures of antibody creations are then tweaked by the activities of *T*-lymphocytes.

Figure 1 illustrates the device of the invulnerable system. It reveals that following the discriminatory stimulation over the requisite of antigens, the lymphocytes would redo themselves all through clonal abundance. This is observed by genetic processes on the clones of the plasma cells. Lastly, antibodies are stashed and willing to oblige antigens. Certain lymphocytes would change into prolonged *B* reminiscence cells.

These reminiscence cells distribute all over the blood, lymph, and tissue with the intention of while visible towards a subsequent antigenic impetus. They would discern hooked on substantial lymphocytes that are proficient towards harvesting extraordinary-affinity antibodies to contest alongside the same antigens that encouraged the foremost reply.

The rare computational patterns established that have been centred on immune arrangement ethics are

(i) Immune network representations,
(ii) Negative assortment procedures, and
(iii) Clonal assortment algorithm (CAA).

3.1 Clonal Assortment Algorithm

In the clonal assortment algorithm, a nominee solution for the individual problem is called an antigen or a pathogen, which is identified by the antibody. Each antibody signifies a spot in the hunt area, i.e. a viable solution to the problem. An inhabitant entails a predetermined quantity of antibodies. Every antibody is estimated by the appraisal method to acquire its affinity. Based on this affinity and enduring immune operators, a new population is spawned iteratively with every sequential population, depicted as a production. The CAA utilizes three immune machinists, i.e. cloning, hypermutation, and receptor editing, to invigorate the creation of populations.

While implementing an AIL of the clonal selection rule, the key measure in the algorithm incorporates

(a) Instigation of antibodies.
(b) Propagation and variation on the confrontation of cells with antigens.
(c) Maturation and modification of antibody categories through resounding out sympathy maturing method over accidental hereditary variations.
(d) Confiscating individuals discriminated immune cells, which possess low-kinship antigenic receptors.

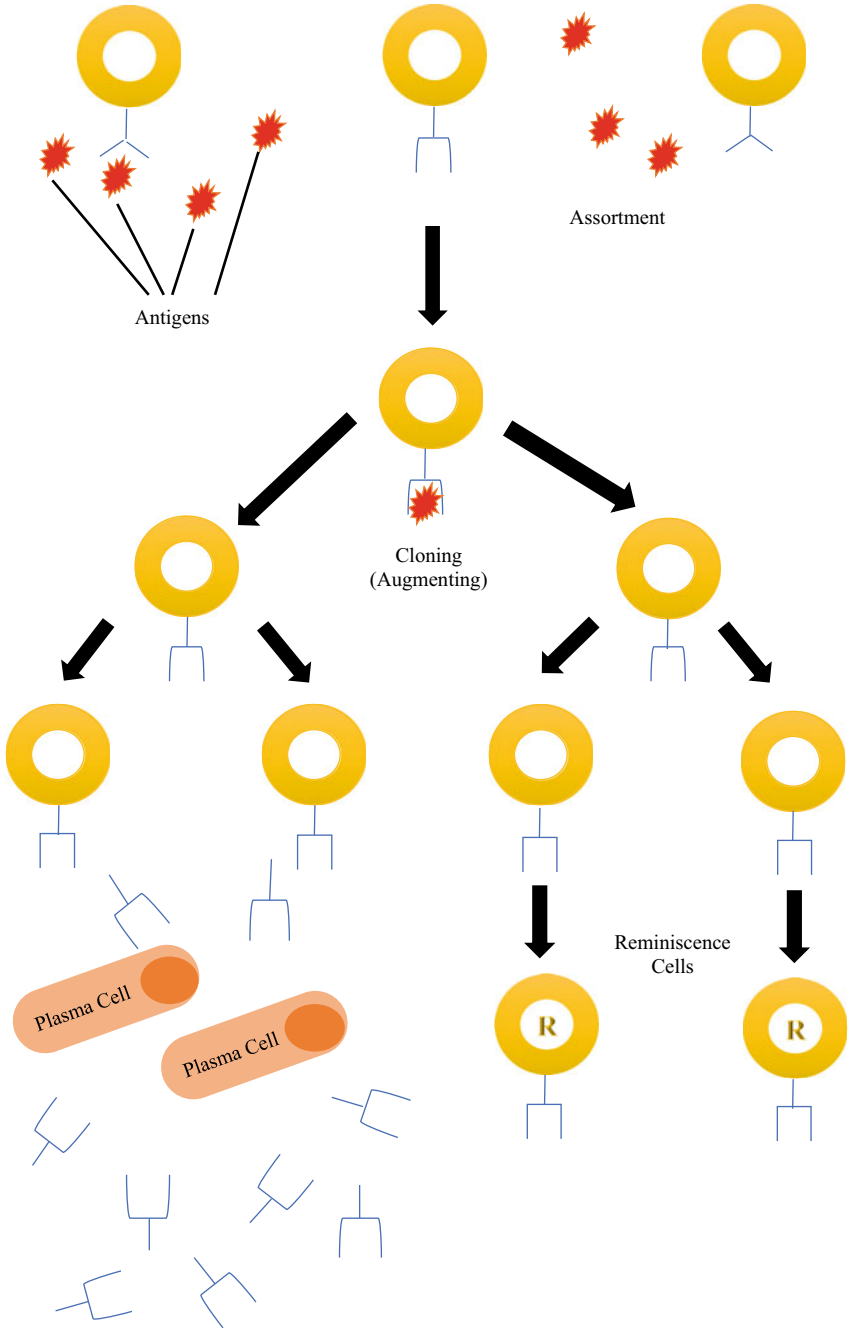

Fig. 1 Progression of the immune system

Once the clonal assortment procedure is executed and intended for cracking the optimization delinquent, a rare revision must be completed as trials.

(i) Now no clear antigen towards being documented, but a goal purpose is to be augmented. Consequently, the empathy of an antibody denotes the appraisal of the goal function.
(ii) All antibodies remain designated and nominated for replicating.
(iii) The quantity of clones engendered through the antibodies is identical
(iv) The consequence of a fluctuating the number of clones produced bestowing to the appropriateness (affinity) of the distinct is inspected here in the article.

The subsequent are the chief steps intricate in the clonal assortment algorithm.

Step 1. Initialization—The chief step comprises expressing an antibody pool of static extent N.
Step 2. Loop—The CAA then incomes by implementing numerous reiterations of divulging the scheme to all acknowledged antigens. A solo round of acquaintance or recapitulation is stated as power production. The quantity of cohorts G the system accomplishes is manipulator configurable; however, the scheme can practise a delinquent explicit hindering state.
Step 3. Choice antigen—A sole antigen is designated arbitrarily deprived of standby (for the current generation) since the pool of antigens.

Step 3.1. Acquaintance—The scheme is bare to the nominated antigen. Affinity ideals are intended for entire antibodies besides the antigen. Kinship is a quantity of resemblance and is delinquent-reliant.
Step 3.2. Selection—A set of n antibodies is designated from the whole antibody pool that has the uppermost attraction with the antigen.
Step 3.3. Cloning—The customary of nominated antibodies is formerly replicated in share to its affinity (rampant-created). The number of clones can be initiated by

$$N_c = \text{round}(\beta * N) \tag{7}$$

where β—Multiplying factor choices from (0–1)
N—Total expanse of antibodies.

The following pseudocode reveals the CAA algorithm with the clonal assortment basis.

Input: *N, n, L, d, β, ρ*

Output: *P*

P ← *Build random cells (N, L);*

While stop condition () do

for

each $p_i \in P$ *do*

affinity (p_i);

end

P_{choose} ← *choose (P, n);*

P_{clones} ← *0;*

for

each $p_i \in P_{choose}$ *do*

$P_{clones} \leftarrow Clone(p_i, \beta)$;

end

for

each $p_i \in P_{clones}$ *do*

hyper mutate (p_i, ρ);

affinity (p_i);

end

$P \leftarrow choose\ (P, P_{clones}, N)$;

$P_{rand} \leftarrow$ *create Random Cells (d, L);*

replace (P, P_{rand})

end

return

Step 3.4. Kinship growth (transmutation)—The clone (customary of replicate antigens) is formerly imperilled to an empathy mellowing practice towards a well-fit antigen.

Step 3.5. Clone disclosure—The clone is then unveiled to the antigen, and responsiveness actions are assessed.

Step 3.6. Contention—The antibodies through the ultimate kinship in the clone are afterwards designated as entrant remembrance antibodies intended for positioning into *N*.

Step 3.7. Substitute—The *d* individuals in the residual antigen tarn through the last possible affinity are substituted with novel arbitrary antibodies.

Step 4. Final texture—Afterwards the accomplishment of the coaching scheme and the remembrance module of the antigen pool are next carried as the set of rules result. Subject to the delinquent purview, the resolution might be a distinct finest distinct antigen or the cooperative of whole antigens in the pool.

4 Execution of Clonal Assortment Algorithm to EPD Problem

The realization of CAA for unravelling the EPD is corresponding to the subsequent process.

(a) The primary inhabitants are constructed from a collection of indiscriminately spawned numbers. Each generated unit is assessed for any limitation infringement using the following Eqs. (4) and (5). Only the values that comply with the restriction are integrated into the inhabitant's set.
(b) The fitness estimate of every number in the inhabitant's usual is weighed employing Eq. (1).
(c) Cloning the individuals in the inhabitants offers growth near a momentary inhabitant of clones.
(d) The inhabitants of clones endure a mellowing development by employing genetic manoeuvres, i.e. metamorphosis on the inhabitants of replicas. The metamorphosed duplicates are interpreted, and their appropriateness values are assessed.
(e) A different population of the identical extent as the initial inhabitants is designated after the metamorphosed clones created for their appropriateness value.
(f) The novel inhabitants will endure identical development as identified in stages 1–5.
(g) This procedure is continued till the elucidation met an optimal value.

5 Results and Analyses

The pertinency and authenticity of the AIL optimization procedure for everyday claims must remain assessed continuously in three examination instances. Instance 1 is a 3-unit system [17], Instance 2 is a 13-unit system [17] besides Instance 3 is a 40-unit arrangement [18]. To substantiate the competence in seeking out the complete or nearby global optimal power equilibrium, power production restrictions and ramp rate limit limitations only are incorporated for evaluation with supplementary practices stated in the prose.

Table 1 Finest power output for a 3-generator arrangement

Unit	GA [19]	PSO [20]	EP [21]	GWO [5]	WOA [6]	AIL (props.)
P_1	300.00	300.27	300.26	300.09	300.02	300.00
P_2	400.00	400.00	400.00	400.00	400.00	400.00
P_3	150.00	149.73	149.74	149.91	149.89	149.99
Total power (MW)	850.00	850.00	850.00	850.00	850.00	850.00
Total charge ($/hr)	8237.60	8235.09	8234.07	8235.93	8234.98	8234.07

Table 2 Convergence characteristics for the 3-unit system

Method	Min. charge ($/hr)	Mean charge ($/hr)	Max. charge ($/hr)
GA [19]	8237.60	8298.58	8359.56
PSO [20]	8235.09	8239.10	NA
EP [21]	8234.07	8248.99	8263.91
GWO [5]	8235.93	8247.40	8258.87
WOA [6]	8234.98	8245.12	8255.26
AIL (props.)	8234.05	8243.59	8253.14

5.1 Instance I

A generating system of three thermal units with the consequences of valve-point loading is scrutinized in this test. In this instance, the load demand is anticipated to be revealed as 850 MW. Based on the data acquired over 100 epochs, the assessments of the three thermal units, assessed by several approaches are exemplified in Tables 1 and 2, which appear that the AIL achieved in obtaining the agreeable result.

5.2 Instance II

A structure of thirteen thermal units with the effects of valve-point loading is explored in this test. In this instance, the power demand is anticipated to be revealed as 2520 MW. Based on statistics obtained over 100 epochs, the analogies of the thirteen thermal units analysed by different approaches are exemplified in Tables 3 and 4, which reveal that the AIL achieved in obtaining a suitable resolution.

Table 3 Finest power yield for 13-generating unit system

Unit	PSO [18]	DE [19]	GWO [5]	WOA [6]	AIL (props.)
P_1	628.32	680.00	629.32	628.40	680.00
P_2	299.20	360.00	298.70	298.38	360.00
P_3	291.90	360.00	290.02	291.51	359.65
P_4	159.73	154.99	159.86	159.79	154.74
P_5	159.73	154.99	159.86	159.79	154.45
P_6	159.73	155.00	159.86	159.79	155.00
P_7	159.73	155.00	159.86	159.79	154.74
P_8	159.73	155.00	159.86	159.79	155.01
P_9	159.73	154.99	159.86	159.79	154.94
P_{10}	114.80	40.00	114.75	114.93	41.65
P_{11}	75.00	40.00	74.98	75.02	40.01
P_{12}	60.00	55.00	60.69	60.52	54.05
P_{13}	92.40	55.00	92.38	92.50	55.76
Total power (MW)	2520.00	2520.00	2520.00	2520.00	2520.00
Total charge ($/hr)	24,252.6	24,083.52	24,079.89	24,077.52	24,075.58

Table 4 Convergence characteristics for 13-generating unit system

Method	Min. charge ($/hr)	Mean charge ($/hr)	Max. charge ($/hr)
PSO [20]	24,252.65	24,246.60	24,265.79
DE [21]	24,083.52	24,169.92	24,264.85
GWO [5]	24,079.89	24,172.83	24,265.78
WOA [6]	24,077.52	24,170.88	24,264.24
AIL (props.)	24,051.58	24,142.98	24,263.56

5.3 Instance III

This instance comprises 40 coal-fired generating units with the power demand of the system of 10,500 MW. Its finest results found all through the AIL are revealed in Tables 5 and 6. All the limitations formerly declared are satisfied.

Comparably, the suppositions show that the intended AIL methodology recommends good quality resolution than those encountered with actual value implied by EP, DE, GWO, and WOA methods. The convergence curve of the 40-unit system with solving with AIL is shown in Fig. 2.

Principally, the insinuated AIL outpaces each more deemed modern optimization system for the over-executed power assessment structures. Because the insinuated logic procedure is picking the elite antibodies for disentangling the intent, cloning

Table 5 Finest results for 40-generating units including 100 epochs

Unit	Generation (MW)	Unit	Generation (MW)	Unit	Generation (MW)
P_1	81.2186	P_{14}	300.1023	P_{27}	147.1183
P_2	61.9359	P_{15}	490.0801	P_{28}	102.1334
P_3	104.6810	P_{16}	409.3752	P_{29}	88.4145
P_4	128.2894	P_{17}	398.1404	P_{30}	84.7519
P_5	91.5206	P_{18}	453.5361	P_{31}	145.2739
P_6	128.3100	P_{19}	482.4879	P_{32}	117.8334
P_7	268.6816	P_{20}	549.1000	P_{33}	150.1571
P_8	267.4955	P_{21}	435.7806	P_{34}	174.6702
P_9	274.6465	P_{22}	436.4504	P_{35}	200.0000
P_{10}	139.4918	P_{23}	459.9832	P_{36}	112.7668
P_{11}	336.0714	P_{24}	380.7259	P_{37}	103.7170
P_{12}	100.9512	P_{25}	517.3195	P_{38}	82.8316
P_{13}	450.7750	P_{26}	533.3150	P_{39}	107.9537
				P_{40}	499.1998
				$\sum_{i=1}^{40} P_i = 10.4999e + 003$	

Table 6 Outcomes of 40-generating units including 100 epochs

Method	Min charge ($/hr)	Mean charge ($/hr)	Max charge ($/hr)
CEP [21]	124,139.67	123,382.13	122,624.35
FEP [21]	124,119.37	123,499.59	122,879.71
DE [21]	122,056.69	121,882.35	121,708.07
GWO [5]	121,102.58	121,379.94	121,657.26
WOA [6]	121,084.34	121,306.87	121,529.26
AIL (Props.)	121,023.58	121,218.54	121,412.64

facilitates the greatest imitation of antibodies and transmutation ameliorates in retentive the suitable antigen. Conclusively, reminiscence comforts to cuddle solvent, antigen for the ensuing rehearsal so that the carried problem extends the finest crux swiftly.

6 Conclusion

A novel method employing a clonal assortment algorithm created AIL to unravel pecuniary power dispatch problems in the power scheme is offered. The expanded

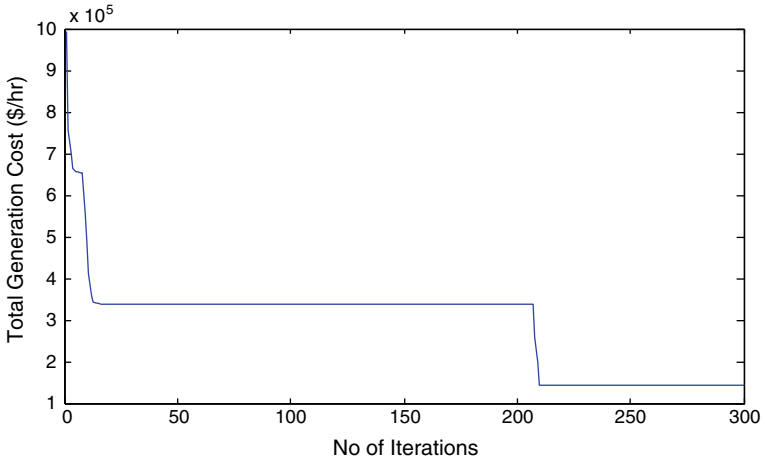

Fig. 2 Convergence nature of AIL in Instance III (40-unit case)

AIL procedure is adept at regulating the power spawned by every power-producing component in the organization so that the expense of power production could be curtailed although sustaining nearly functional limitations. The results attained by the purported technique for 3, 13, and 40 power-producing entities are concomitant with typical and contemporary optimization practices. The analogy reveals that AIL performs healthier than the other considered algorithms. Though, it is realized by prior examination that the meta-evolutionary scheduling procedure requires a retentive accomplishment period to achieve the optimum outcome. Consequently, the analysis indicates that AIL might be a favourable procedure for unravelling intricate optimization complications in the power system.

Acknowledgements The authors would like to thank the management of CVR College of Engineering, Hyderabad, for providing a plentiful space for steering this investigation work.

References

1. C. Yu, A.A. Heidari, H. Chen, A quantum-behaved simulated annealing algorithm-based moth-flame optimization method. Appl. Math. Model. **87**, 1–19 (2020)
2. S. Mirjalili, Genetic algorithm, in *Evolutionary Algorithms and Neural Networks* (Springer, Cham, 2019), pp. 43–55
3. Y.J. Cao, Q.H. Wu, Evolutionary programming, in *Proceedings of 1997 IEEE International Conference on Evolutionary Computation (ICEC'97)* (IEEE, 1997), pp. 443–446
4. J. Kennedy, R. Eberhar, Particle swarm optimization, in *Proceedings of ICNN'95-International Conference on Neural Networks* , vol. 4 (IEEE, 1995), pp. 1942–1948
5. M. Pradhan, P.K. Roy, T. Pal, Grey wolf optimization applied to economic load dispatch problems. Int. J. Electr. Power Energy Syst. **83**, 325–334 (2016)

6. C.K. Faseela, H. Vennila, Economic and emission dispatch using whale optimization algorithm (WOA). Int. J. Electr. Comput. Eng. **8**(3), 1297 (2018)
7. R. Vijay, Performance enrichment in optimal location and sizing of wind and solar pv centered distributed generation by communal spider optimization algorithm. COMPEL - Int. J. Comput. Math. Electr. Electron. Eng. **41**(5), 1971–1990 (2022)
8. V. Raviprabakaran, R.C. Subramanian, Enhanced ant colony optimization to solve the optimal power flow with ecological emission. Int. J. Syst. Assur. Eng. Manag. **9**(1), 58–65 (2018)
9. R. Vijay, Optimal and stable operation of microgrid using enriched biogeography-based optimization algorithm. J. Electr. Eng. **17**(4), 11–11 (2017)
10. V. Raviprabhakaran, C.S. Ravichandran, Enriched biogeography-based optimization algorithm to solve economic power dispatch problem, in *Proceedings of fifth international conference on soft computing for problem solving*, vol. 437 (Springer, Singapore, 2016), pp. 875–888
11. R. Vijay, C.S. Ravichandran, Scheduling practical generating system using an improved bacterial swarm optimization. Tehnicki vjesnik/Technical Gazette **23**(5) (2016)
12. R. Vijay, Quorum sensing driven bacterial swarm optimization to solve practical dynamic power ecological emission economic dispatch. Int. J. Comput. Methods **15**(03), 1850089 (2018)
13. R. Vijay, B. Deepika, Computational modeling and governing of standalone hybrid electric power generation system, in *Intelligent Systems* (Springer, Singapore, 2021), pp. 311–325
14. V. Raviprabhakaran, T.S. Mummadi, Optimal scheme and power controlling aspects in shipboard system. Innov. Electr. Electron. Eng. **626**, 367–379 (2020)
15. D. Dasgupta (ed.), Artificial immune systems and their applications (Springer Science & Business Media, 2012)
16. L.N. de Castro, F.J. van Zuben, Learning and optimization using the clonal selection principle. IEEE Trans. Evol. Comput. **6**(3), 239–251 (June2002)
17. R. Vijay, Intelligent bacterial foraging optimization technique to economic load dispatch problem. Int. J. Soft Comput. Eng. **2**(2), 55–59 (2012)
18. R. Vijay, C.S. Ravichandran, Certain investigation on bio inspired optimization algorithm for application of reliable and optimal operation of power system, Anna University (2017)
19. J.K. Pattanaik, M. Basu, D.P. Dash, Improved real coded genetic algorithm for dynamic economic dispatch. J. Electr. Syst. Inf. Technol. **5**(3), 349–362 (2018)
20. N. Chopra, Y.S. Brar, J.S. Dhillon, An improved particle swarm optimization using simplex-based deterministic approach for economic-emission power dispatch problem. Electr. Eng. **103**(3), 1347–1365 (2021)
21. M. Basu, Fast convergence evolutionary programming for economic dispatch problems. IET Gener. Transm. Distrib. **11**(16), 4009–4017 (2017)

Classification of Fault Disturbances in a DG Integrated Hybrid Power System Using Support Vector Machine and Decision Tree

Kumaresh Pal, Ashok Kumar Akella, Kumari Namrata, and Basanta K. Panigrahi

Abstract To fulfill the increasing load demand, distributed generations are becoming increasingly crucial in the electrical power system. The connection of a distributed generator (DG) to the grid raises a number of challenges related to power system structural protection and control. The consequence of dispersed generations on a grid is that the fault current level fluctuates, which complicates fault investigations. Even after years of in-depth research, categorization of fault remains one of the most important difficulties that arise in a distributed generation integrated power system. The fault disturbances are classified by the pattern recognition techniques like decision tree (DT) and support vector machines (SVM). The study is carried out both graphically as well as in terms of performance indices like standard deviation (STD) and entropy. The objective of this article is to use DT and SVM to categorize fault-related disturbances in a DG-infiltrated hybrid power system. To categorize the Line-Line fault and Line-Line-Ground fault, an unique technique based on SVM and DT is proposed. Based on these analyzes, it is observed that DT Gives the highest viable accuracy as compared to other methods, which proves its robustness in various working situations such as load variability, in the scheme's parameters, there are solar insolation, noise, and harmonics.

Keywords Distributed generator DG) · Support vector machine (SVM) · Decision tree (DT) · Point of common coupling (PCC)

K. Pal · A. K. Akella · K. Namrata
Department of Electrical Engineering, NIT, Jamshedpur, India
e-mail: namrata.ee@nitjsr.ac.in

B. K. Panigrahi (✉)
Department of Electrical Engineering, SOA University, Bhubaneswar, India
e-mail: basanta1983@gmail.com

© The Author(s), under exclusive license to Springer Nature Singapore Pte Ltd. 2023

K. Murari et al. (eds.), *Soft Computing Applications in Modern Power and Energy Systems*,
Lecture Notes in Electrical Engineering 975,
https://doi.org/10.1007/978-981-19-8353-5_5

1 Introduction

At the distribution level, a large number of dispersed generation units are being incorporated into the electrical power system. Distributed generators (DG) are one of the most significant changes in the electrical sector and power grid in the last ten years. Energy being generated close to the point of consumption is referred to as "Distributed Generation" (DG) [1]. Sources of renewable energy such as wind, PV cells, tidal, geothermal heat, and biomass are examples of distributed generation resources. One of the advantages of adopting DG is its proximity to the load of the users. Increasing grid reliability, cutting transmission line losses, improving voltage stability, and improving power quality all require distributed generations [2]. In addition, different artificial intelligence techniques like fuzzy logic (FL), artificial neural network (ANN), and support vector machine (SVM) are used to classify the fault disturbances. Artificial neural network (ANN) is popularly used for fault localization and detection classification [3–6]. ANN alongside wavelet transform was proposed to identify the fault disturbances [7].

Various studies were reported in literature for the identification and monitoring of fault disturbances. Some used indices like rms value, peak value, frequency, or voltage change for detecting fault/abnormal conditions. The methods such as fourier transform (FT) and fast fourier transform (FFT) are one of the most popular ones for the disturbance study. Many researchers have used other transforms like chirp *Z*-transform and Welch algorithm for observing the electrical parameters [8, 9]. But sometimes it is very hard to detect non-stationary disturbances due to only frequency data and no time data. Therefore, wavelet transform (WT), *S*-transform, short-time fourier transform (STFT), etc., were studied and designed to be applied to fulfill the objective of fault analysis [10].

A composite technique on particle swarm optimization (PSO) and artificial neural networks (ANNs) was employed for faulty phase/section detection in power systems as another method for forecasting fault disturbances. Fuzzy logic along with neural network in the form of ANFIS is effectively and correctly used for the same objectives to protect power system and its equipment's [5]. A support vector machine (SVM) is also being considered as a potential candidate for fault classification [11]. But, because of degraded performances of some of the above-mentioned techniques under higher penetration levels of renewable sources, uncertain system inputs like solar insolation in solar PV systems, and abnormal operating conditions in power system in presence of noise are the reasons that why the authors in these papers have proposed a combined approach based on SVM and decision tree (DT). Again, different features from transformed signal are used to formulate data set with reduced size in order to improvise the classification objectives [12, 13].

The article is assembled as follows: Sect. 2 represents the system configuration and description of solar energy-based system. The classification methodologies are describing in Sect. 3, and the result of the simulation and their discussion are marked out in Sect. 4. At the end, the conclusions residue from the research are briefed in Sect. 5.

2 System Configuration and Modeling

The structure of a solar PV cell is identical to that of a *p–n* junction, which transforms light energy into electrical energy. Figure 1 illustrate the circuit equivalent, representation of a solar cell given by a photo-current source I_{ph}, a non-linear diode, internal series and shunt resistances R_s and R_{sh} [14].

The mathematical equation representing a PV cell is given by:

$$I = I_{\text{ph}} - I_s\left(e^{\frac{q}{\text{AkT}}(V+\text{IR}_s)} - 1\right) - \frac{1}{R_{\text{sh}}}(V + \text{IR}_s) \tag{1}$$

where photo-current is represented by I_{ph}, diode saturation current is represented by I_s; q is the charge of an electron; diode ideality factor is A; k is Boltzmann's constant; S is the solar intensity (W/m^2). The photocurrent in terms of temperature and solar intensity is given by:

$$I_{\text{ph}} = \left(\frac{S}{S_{\text{ref}}}\right)\left[I_{\text{ph,ref}} + C_T(T - T_{\text{ref}})\right] \tag{2}$$

S_{ref}, $I_{\text{ph.ref}}$ and T_{ref} are the standard values of solar intensity, photocurrent and cell temperature, respectively. C_T is the temperature coefficient (A/K). Diode saturation current and the semiconductor material's band energy gap is represented as $I_{\text{s.ref}}$ and E_g, respectively, under standard test conditions. PV modules consists of cells that are coupled in series and parallel. The voltage-current characteristic equation for the equivalent model is given by:

$$I = N_p I_{\text{ph}} - N_p I_s\left(e^{\frac{q}{\text{AkT}}\left(\frac{V}{N_s} + \frac{\text{IR}_s}{N_p}\right)} - 1\right) - \frac{N_p}{R_{\text{sh}}}\left(\frac{V}{N_s} + \frac{\text{IR}_s}{N_p}\right) \tag{3}$$

The number of series connected cells and parallel connected cells is denoted by N_s and N_p, respectively. The PV module parameters used in this study were derived from references [15–17].

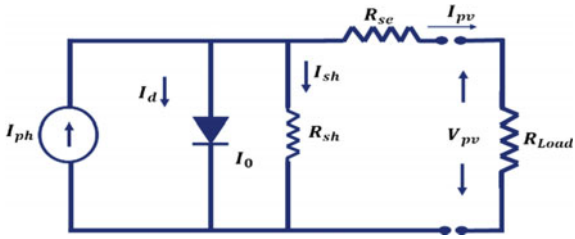

Fig. 1 Equivalent circuit of PV cell

3 Classification Techniques

The description of classification techniques used such as decision tree (DT) and support vector machine (SVM) are described below:

3.1 Decision Tree (DT)

Data can be classified based on checking the similarities between the datasets. Decision trees are effectively employed for data classification, choosing features which maximize and divide the data. These features are divided into various cases repeatedly till the proper ending and categorization [3]. The mathematical model of decision tree is given below:

$$\overline{X} = \{X_1, X_2, \ldots, X_m\}^T \tag{4}$$

$$X_i = \left\{x_1, x_2, \ldots, x_{ij}, \ldots, x_{in}\right\} \tag{5}$$

$$S = \{S_1, S_2, \ldots, S_i, \ldots, S_m\} \tag{6}$$

where m is the amount of observations available, the amount of independent variable s is indicate by n, S is the vector m-dimension of the variable predicted from $\overline{X}$, X_i is the i-th component vector of n-dimension autonomous variables, $x_1, x_2, \ldots, x_{ij}, \ldots, x_{in}$ are autonomous variables of pattern vector X_i, and T is the transpose notation vector. The optimal or correctly sized DT T_{k0} is constructed according to the following issue of optimization:

$$\hat{R}(T_{k0}) = \min_k \left\{\widehat{R}(T_k)\right\}, k = 1, 2, 3, \ldots, K \tag{7}$$

$$\hat{R}(T) = \sum_{t \in \hat{T}} \{r(t)\, p(t)\} \tag{8}$$

where $\hat{R}(t)$ is the error level in misclassification of tree T_k, T_{k0} is the optimal DT for minimizing the error of misclassification, T is a binary tree $\in \{T_1, T_2, T_3, \ldots . T_k, t_1\}$, k denotes the tree's index number, tree node is denoted by t. T is made up of plane partitioning characteristics [18–20].

3.2 Support Vector Machines

SVM is a statistical learning methodology for classification of pattern based on a structural risk mitigation strategy, and it's a good choice for high-dimensional datasets because of its generalization capacity. SVM has improved the accuracy of disturbance classification over ANN and Bays classifiers and is relevant for classification of fault [11]. For inputs of n-dimension $s_i (i = 1, 2, \ldots, M)$, M is the samples number fitting to class1 or class2 with outputs $o_i = 1$ for class1 and $o_i = -1$ for class2, correspondingly. And the distance from the geometry is provided as $\|w\|^2$. The following optimization issue can drive the optimal hyperplane [21, 22]:

Minimize

$$\frac{1}{2}||w||^{-2} + C\sum_{i=1}^{M}\xi_i \tag{9}$$

subject to:

$$o_i\left(w^T s + b\right) \geq 1 - \xi_i \text{ for } i = 1, 2, \ldots, M \tag{10}$$

The unknown data sample s is classified as:

$$s \in \left\{ \begin{array}{c} \text{Class} - 1, f(s) \geq 0 \\ \text{Class} - 2, \text{Otherwise} \end{array} \right\}$$

4 Simulation Results and Analysis

This part describes the simulated outcomes achieved with MATLAB/Simulink. The solar PV system under consideration is interconnected to the power grid, and the entire system is simulated in MATLAB. An information set of 500 × 6 is then developed taking into consideration six distinct characteristics and faults in distinct working situations. Half of this collection of information is used for practice and half is used for testing. At the point of common coupling, the accumulated signal is sampled at 5 kHz of frequency. A grid-connected solar energy electrical power plant is depicted in the presented approach. The proposed model includes a PV panel, three-phase source, circuit breakers, transformers, and a fault block connected to the load. Figure 2 depicts a one-line diagram of the proposed hybrid model. Under varied noise levels, a correlative study of the SVM and DT with the classification accuracy values aids in the discrimination of fault disturbances. Figure 3 illustrates this analysis.

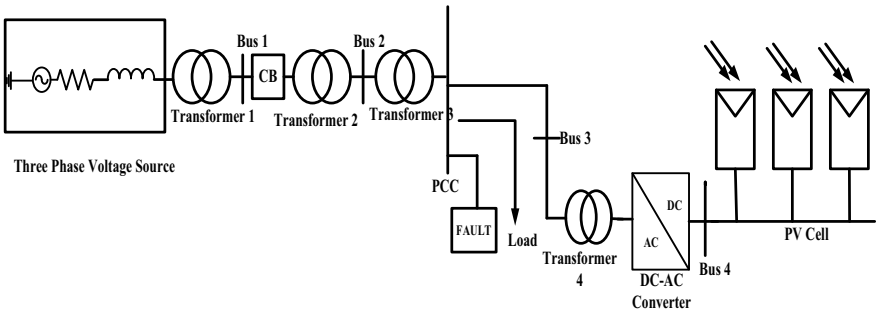

Fig. 2 Single line diagram of proposed Simulink DG integrated hybrid system

The accuracy of DT and SVM classification is illustrated in Fig. 3a and b at distinct of noise level. It is noted that in all working circumstances, DT provides better efficiency relative to SVM. This study is carried out both graphically as well as in terms of performance indices like standard deviation (STD) and entropy. The same can be done by taking other performance indices like energy and skewness. A border plot is also displayed in Fig. 3c three distinct fault disturbances (class1-class3) and comparable curve/contour may be shown in all other instances to differentiate between.

The computation of performance indicators like entropy and standard deviation is used to classify the data. Line-Line fault and Line-Line-Ground faults are formed in a grid-connected PV system, and the standard deviation and entropy are derived as performance indices from the data (PIs). Table 1 lists the PIs for various fault scenarios.

5 Conclusion

SVM and DT are used in this study to classify faults in a PV-connected power system. This paper presents a novel approach based on SVM and DT for the classification of Line-Line fault and Line-Line-Ground fault signals. From the point of common connection, the three-phase voltages and phase currents are derived. This paper presents about the study of different fault disruptions of the grid-integrated solar PV-based power system. SD and entropy are two performance indices that are studied. The fault disturbances were correctly classified utilizing SVM and DT. The accuracy of classification is considerably improved. The effectiveness of the proposed method has been verified at various noise levels. A comparative of the STD and entropy is conducted in this paper. The given method offers a more consistent and trustworthy performance, according to statistical information. The classification precision of DT is better than SVM is observed in different working situations and also the comparative assessment is performed.

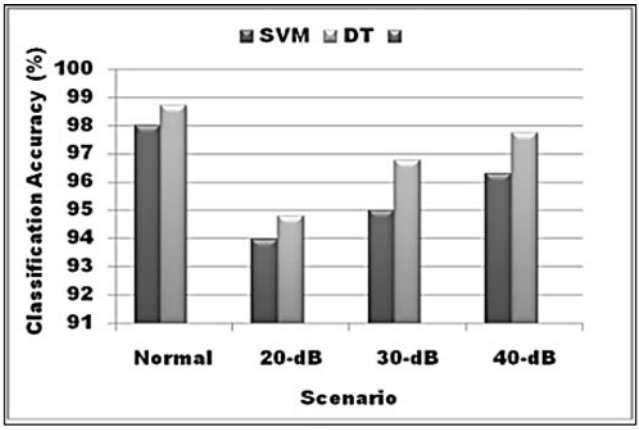

(a)

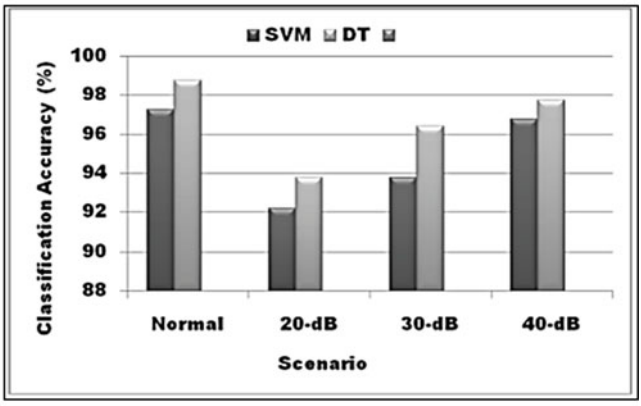

(b)

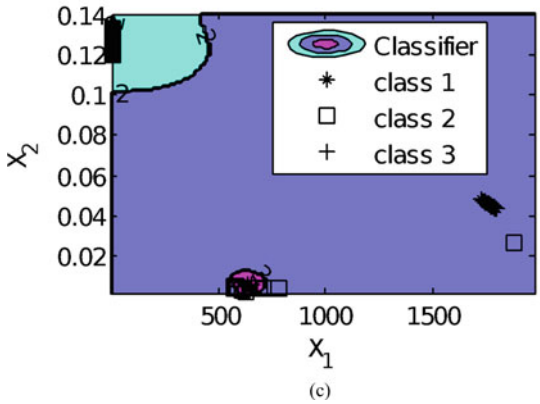

(c)

Fig. 3 **a** For LL fault classification, **b** LLG fault classification, and **c** boundary plot to classify faults using SVM

Table 1 STD and entropy for different faults

Fault	Standard deviation (STD)	Entropy	Standard deviation (STD)	Entropy
	Normal		With 20-dB noise	
L-L	0.432	0.590	0.578	0.796
L-L-G	0.547	0.619	0.656	0.905

References

1. K. Moloi, Y. Hamam, J.A. Jordaan, Fault detection in power system integrated network with distribution generators using machine learning algorithms, in *2019 6th International Conference on Soft Computing and Machine Intelligence (ISCMI)* (IEEE, 2019), pp. 18–22
2. M.S. Thomas, P.P. Terang, Interconnection issues for distributed resources in a smart distribution system, in *2012 IEEE 5th India International Conference on Power Electronics (IICPE)* (IEEE, 2012), pp. 1–6
3. S. Adhikari, N. Sinha, T. Dorendrajit, Fuzzy logic based on-line fault detection and classification in transmission line. Springerplus **5**(1), 1–14 (2016)
4. M. Singh, B.K. Panigrahi, R.P. Maheshwari, Transmission line fault detection and classification, in *2011 International Conference on Emerging Trends in Electrical and Computer Technology* (IEEE, 2011), pp. 15–22
5. L. Tightiz, M.A. Nasab, H. Yang, A. Addeh, An intelligent system based on optimized ANFIS and association rules for power transformer fault diagnosis. ISA Trans. **103**, 63–74 (2020)
6. B.K. Sahoo, S. Pradhan, B.K. Panigrahi, B. Biswal, N.C. Patel, S. Das, Fault detection in electrical power transmission system using artificial neural network, in *2020 International Conference on Computational Intelligence for Smart Power System and Sustainable Energy (CISPSSE)* (IEEE, 2020), pp. 1–4
7. A. Bhuyan, B.K. Panigrahi, S. Pati, Fault classification for DG integrated hybrid power system using wavelet neural network approach, in *2021 1st Odisha International Conference on Electrical Power Engineering, Communication and Computing Technology (ODICON)* (IEEE, 2021), pp. 1–5
8. P.K. Ray, N. Kishor, S.R. Mohanty, Islanding and power quality disturbance detection in grid-connected hybrid power system using wavelet and $ S $-transform. IEEE Trans. Smart Grid **3**(3), 1082–1094 (2012)
9. P.K. Ray, S.R. Mohanty, N. Kishor, Disturbance detection in grid-connected distributed generation system using wavelet and S-transform. Electr. Power Syst. Res. **81**(3), 805–819 (2011)
10. É.M. Lima, C.M. dos Santos Junqueira, N.S.D. Brito, B.A. de Souza, R. de Almeida Coelho, H.G.M.S. de Medeiros, High impedance fault detection method based on the short-time Fourier transform. IET Gener. Transm. Distrib. **12**(11), 2577–2584 (2018)
11. N. Shahid, S.A. Aleem, I.H. Naqvi, N. Zaffar, Support vector machine based fault detection and classification in smart grids, in *2012 IEEE Globecom Workshops* (IEEE, 2012), pp. 1526–1531
12. X.G. Magagula, Y. Hamam, J.A. Jordaan, A.A. Yusuff, Fault detection and classification method using DWT and SVM in a power distribution network, in *2017 IEEE PES PowerAfrica* (IEEE, 2017), pp. 1–6
13. A. Nakho, K. Moloi, Y. Hamam, High impedance fault detection based on HS-transform and decision tree techniques, in *2021 Southern African Universities Power Engineering Conference/Robotics and Mechatronics/Pattern Recognition Association of South Africa (SAUPEC/RobMech/PRASA)* (IEEE, 2021), pp. 1–5
14. P.K. Ray, A. Mohanty, B.K. Panigrahi, P.K. Rout, Modified wavelet transform based fault analysis in a solar photovoltaic system. Optik **168**, 754–763 (2018)

15. B. Dhanalakshmi, N. Rajasekar, A novel competence square based PV array reconfiguration technique for solar PV maximum power extraction. Energy Convers. Manag. **174**, 897–912 (2018)
16. J.C. Teo, R.H.G. Tan, V.H. Mok, V.K. Ramachandaramurthy, C. Tan, Impact of bypass diode forward voltage on maximum power of a photovoltaic system under partial shading conditions. Energy **191**, 116491 (2020)
17. P. Kut, K. Pietrucha-Urbanik, B. Tchórzewska-Cieślak, Reliability-oriented design of a solar-PV deployments. Energies **14**(20), 6535 (2021)
18. Y. Zhao, L. Yang, B. Lehman, J.F. de Palma, J. Mosesian, R. Lyons, Decision tree-based fault detection and classification in solar photovoltaic arrays, in *2012 Twenty-Seventh Annual IEEE Applied Power Electronics Conference and Exposition (APEC)* (IEEE, 2012), pp. 93–99
19. F. Esposito, D. Malerba, G. Semeraro, J. Kay, A comparative analysis of methods for pruning decision trees. IEEE Trans. Pattern Anal. Mach. Intell. **19**(5), 476–491 (1997)
20. A. Jamehbozorg, S.M. Shahrtash, A decision-tree-based method for fault classification in single-circuit transmission lines. IEEE Trans. Power Delivery **25**(4), 2190–2196 (2010)
21. U.B. Parikh, B. Das, R. Maheshwari, Fault classification technique for series compensated transmission line using support vector machine. Int. J. Electr. Power Energy Syst. **32**(6), 629–636 (2010)
22. H.R. Baghaee, D. Mlakić, S. Nikolovski, T. Dragicević, Support vector machine-based islanding and grid fault detection in active distribution networks. IEEE J. Emerg. Sel. Top. Power Electron. **8**(3), 2385–2403 (2019)

Intelligent Excitation System for Efficient Control of Dual Stator Winding Permanent Magnet Synchronous Generator in Hybrid Power System Applications

Appalabathula Venkatesh and Shankar Nalinakshan

Abstract In this paper, the proposed method shows better performance evaluation over conventional DC-DC converter under low power capabilities of system during lower excitation potential levels, by using dual stator winding-controlled permanent magnet synchronous generator and maximum power point position controller techniques in hybrid power system applications. Both PV panel and wind plant were integrated to compensate for the deficit voltage levels during low parameter ranges. An intelligent excitation power electronic control system is proposed to sense and control the operation of synchronous generator. The intelligent excitation system applies the sliding-mode control strategies to balance the stability to control and compensate the control voltage applied to the winding of the developed dual stator winding synchronous generator. The intelligent excitation system operates based upon the power angle curves of the hybrid power system, and it tracks the maximum power point with the help of sliding-mode controller even at low-speed ranges of the proposed synchronous machine. The proposed technique is analysed at the various environmental conditions based on mode shifting conditions using AVR Mega-32 microcontroller.

Keywords HPSA · Intelligent control systems · DSPWM · Excitation control · Mode shifting · Load schedule

A. Venkatesh · S. Nalinakshan (✉)
Electrical and Electronics Engineering, The National Institute of Engineering, Mysuru, Karnataka, India
e-mail: shankar.nalinakshan@nie.ac.in

A. Venkatesh
e-mail: venkatesh@nie.ac.in

© The Author(s), under exclusive license to Springer Nature Singapore Pte Ltd. 2023

K. Murari et al. (eds.), *Soft Computing Applications in Modern Power and Energy Systems*, Lecture Notes in Electrical Engineering 975,
https://doi.org/10.1007/978-981-19-8353-5_6

1 Introduction

Wind energy is one of the world's oldest and best renewable energy sources. Over the past few decade(s), many research and policy changes are upgrading in wind energy and wind plants which makes a significant increase of its contribution in the energy sector and which transforms the world's energy sector, transition from conventional fossil fuels to renewable sources and makes the energy sector as a clean and sustainable development sector. The Global Wind Energy Council reported that wind power capacity is increased by 60 GW in 2019 which is 20% annual increment over previous years. The rapid growth in renewable sources leads to the shift in global warming heat by below 1.5 °C; to achieve this, we need to install at least 100 GW of renewable energy generation for the next decade. The conventional fuel scarcity pushes many of the researchers to work in the concepts of renewable energy sources (like solar and wind sources, etc.)-based power system applications [1]. An efficient way of energy transmission plays a key role in any grid-connected systems [2].

The main challenging tasks in wind plant are the development of new technologies for controlling the drive mechanism of wind turbine generator set which results in development of energy-efficient wind farms. This paper mainly deals with the contribution towards the energy-efficient integrated renewable sources. To develop energy-efficient renewable energy integrated system, one needs to involve better access to evacuation, efficient transmission and supported energy banking infrastructure, which are needed to overcome the intermittency of wind energy [3].

Energy banking infrastructure is also one of the key supporting factors for the development of energy-efficient wind farm which allows the continuity in power supply to the end consumers when there is unavailability or deficiency of wind energy, which in turn provides the reliability to the wind farms. The above concept is achieved by integrating the multi-sources which results in the development of multi-source power system applications called as hybrid power system applications (HPSA) [4]. This paper is mainly dealing with the integration of the wind plant's energy and solar panel energy (WE-SE), which increases the reliability and continuity of the supply [5].

Energy-efficient wind farms are developed when new technologies are adopted in construction-wise of wind turbine generator set, and their corresponding control strategies are found feasible and efficient. Winding construction of stator and rotor plays key role in generators; based upon this factor, many different types of machines are developed. In this paper, dual stator winding-controlled permanent magnet synchronous generator (DSWCPMSG) is proposed and designed, and it is coupled with the wind turbine, based upon the proposed concept for DSWIG [6, 7].

Power electronic converters (PECs) play a major role in an efficient way of operation of the plant with a significant loss of energy. To obtain the desired stable load requirement, controllers are needed. Even though, conventional controllers like PI, PID are simple to tune and easy to integrate with existing system, but they will suffer from the poor transient and sub-transient performance [8, 9], and they require all system parameters' information. But in practical hybrid power system applications,

system dynamics are robust in nature. In such cases, sliding-mode controllers are well suited and give stable results over conventional controllers [10]. The control problem in DC-DC converter has unknown output voltage and unknown dynamics; in such cases, adaptive controllers with state feedback controllers give better performance [11–13].

Integration of intelligence in power transfer capabilities and efficient way of producing pulses to the devices in PEC legs: The integration of intelligence in decision making, controlling and to establish an effective way of communication between the hybrid source and load results into the development of proposed intelligent excitation power electronic control system (IEPECS). In order to address the issues with conventional controller, both linear and nonlinear control techniques are applied for obtaining the fast and stable response. An IEPECS includes boost converter and adapts the sliding-mode control strategies to balance the stability of the DSWCPMSG operation to control and compensate the control voltage applied to the winding of the DSWCPMSG.

The IEPECS operates based upon the power angle curves of the hybrid power system. The IEPECS tracks the MPPPC with the help of SMC even at low-speed and low-frequency ranges of the DSWCPMSG [14, 15]. The proposed technique is analysed at the various environmental conditions based upon on mode shifting conditions (MSC) performed by microcontroller with load scheduling at different intervals. The major concern for control system engineers after designing any system is its stability analysis, while any disturbances are introduced into the system in the form of faults or sudden changes in the supply system which disturbs the steady-state and dynamic-state behaviours of the systems.

The main complication involved in hybrid power system application is shifting or load sharing among the hybrid sources like PV, wind and battery while implementing the hardware circuit. In this paper, the hardware model mainly consists of microcontroller, boost converter and hybrid sources. Here, the microcontroller is mainly used for the purpose of mode selection. It will take signals from the PV panel and wind by time schedule.

This paper is organized in such a way that for achieving the desired objectives which are mentioned in the abstract section. In this section, the necessity of HPSA is discussed. In Sect. 2, analytical-based approach for modelling of DSWCPMSG is discussed, and in Sect. 3, modelling and analysis of IEPECS along with sliding-mode operation are discussed in achieving the MPPC.

In Sect. 4, MPPPC operation along with isolated solar panel and wind plant is discussed. In Sect. 5, integration of DSWCPMSG-HPSA with IEPECS is analysed. In Sects. 1–5, isolated solar and wind plants are operated, and the developed powers, the corresponding voltage and currents and the source parameters are analysed with the help of MATLAB and Simulink results. An integrated solar and wind plant that is operated along with the modified P&O technique is applied for MPPPC and IEPECS operations. A hardware prototype is designed with the help of AVR Mega-32 microcontroller and tested at various load scheduling. Next section deals with the analytical-based approach for the proposed model of DSWCPMSG.

2 Analytical-Based Approach for the Modelling of DSWCPMSG

The proposed generator is a DSWCPMSG, whose stator winding is split into two windings and is supplied with the alternating supply; hence, it produces a rotating magnetic field, and the rotor winding is separately excited by a constant DC supply through brushless excitation. The constant current in rotor winding produces a flux in the air gap which interlinks with the stator-induced emf, and the rotor flux helps its rotor body to rotate along with the stator magnetic fields. This double excitation helps in rotating the rotor at synchronous speed.

Figure 1 represents the proposed DSWCPMSG constructional view [16]. DSWCPMSG is fed by the wind turbine, its rotor is being driven by the wind turbine, and it will be operated as a synchronous generator (SG). As the rotor is always rotating at constant speed, i.e. synchronously rotating speed, hence the synchronously rotating frame is fixed which causes fixed ($d^{se} - q^{se}$) axes. The fixed axes with synchronously rotating frame electrical equivalent circuit model of DSWCPMSG are explained in [17, 18] which are as shown in Fig. 2.

By applying KVL to q^{se} axis, we can obtain Eq. (1)

$$V_{qs1} = i_{qs1}R_{s1} + L_{ls1}\frac{di_{qs1}}{dt} + \omega_e\psi_{ds1} + L_{qm}\frac{d\left(i_{qs1} + i_{qs2} + i_{qr}\right)}{dt}$$

$$V_{qs2} = i_{qs2}R_{s2} + L_{ls2}\frac{di_{qs2}}{dt} + \omega_e\psi_{ds2} + L_{qm}\frac{d\left(i_{qs1} + i_{qs2} + i_{qr}\right)}{dt}$$

$$0 = i_{qr}R_{qr} + L_{lqr}\frac{di_{qr}}{dt} + L_{qm}\frac{d\left(i_{qs1} + i_{qs2} + i_{qr}\right)}{dt} \quad (1)$$

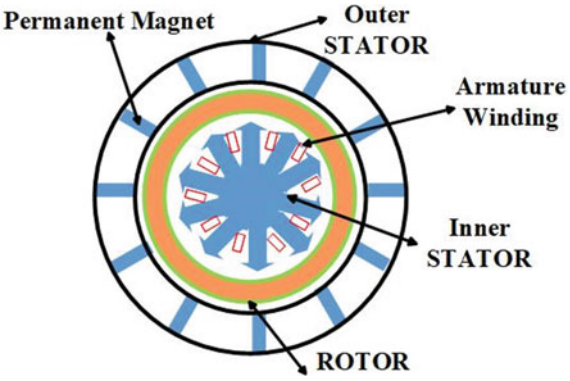

Fig. 1 Constructional view of proposed 5PP-DSWCPMSG

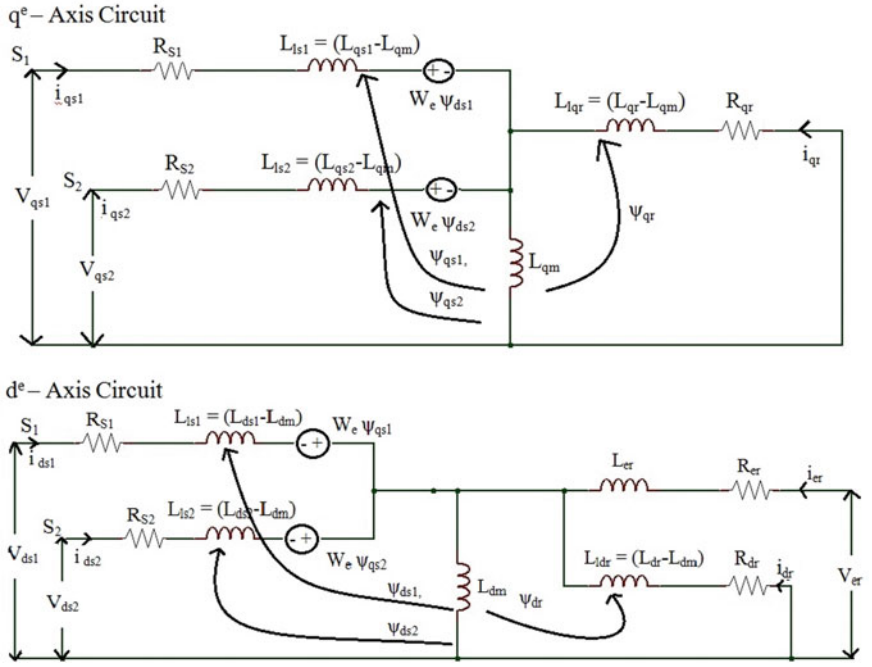

Fig. 2 $(d^{se} - q^{se})$ axes electrical equivalent circuit of DSWDESG

Similarly, KVL to the field circuit is referred to stator-side results in (2)

$$V_{er} = i_{er}R_{er} + L_{er}\frac{di_{er}}{dt} + L_{dm}\frac{d(i_{er} + i_{dr} + i_{ds1} + i_{ds2})}{dt} \tag{2}$$

Similarly, by applying KVL to d^e axis circuit, we can obtain as (3)

$$V_{ds1} = i_{ds1}R_{s1} + L_{ls1}\frac{di_{ds1}}{dt} - \omega_e\psi_{qs1} + L_{dm}\frac{d(i_{ds1} + i_{ds2} + i_{dr})}{dt}$$

$$V_{ds2} = i_{ds2}R_{s2} + L_{ls2}\frac{di_{ds2}}{dt} - \omega_e\psi_{qs2} + L_{dm}\frac{d(i_{ds1} + i_{ds2} + i_{dr})}{dt}$$

$$0 = i_{dr}R_{dr} + L_{ldr}\frac{di_{dr}}{dt} + L_{dm}\frac{d(i_{ds1} + i_{ds2} + i_{dr})}{dt} \tag{3}$$

Different types of used notations which are involved while modelling the DSWCPMSG are listed in Table 1.

Table 1 Notations used for modelling DSWCPMSG

Symbol	Name
s_1, s_2	Double winding stator terminals
a_{s1}, b_{s1}, c_{s1}; a_{s2}, b_{s2}, c_{s2}	Double winding stator phases
$\left(d^e_{s1} - q^e_{s1}\right)$; $\left(d^e_{s2} - q^e_{s2}\right)$	Synchronous rotating frame of stator terminals s_1, s_2
θ_{e1}, θ_{e2}	Phase shift of double winding stator d-axis from stator reference frame (°)
L_{ls1}, L_{ls2}	Double winding stator leakage inductance (H)
R_{s1}, R_{s2}	Double winding stator resistance (Ω)
L_{dm}, L_{qm}	d^{se} and q^{se} axis mutual inductance (H)
V_{ds1}, V_{ds2}; V_{qs1}, V_{qs2}	d^{se} and q^{se} axis stator terminal voltages (V)
i_{ds1}, i_{ds2}; i_{qs1}, i_{qs2}	d^{se} and q^{se} axis stator currents (A)
ψ_{ds1}, ψ_{ds2}; ψ_{qs1}, ψ_{qs2}	d^{se} and q^{se} axis flux linkages (Wb/turn)
V_{er}	Field circuit terminal voltage (V)
i_{er}	Field circuit current (A)
R_{er}	Field circuit resistance (Ω)
L_{er}	Field circuit self-inductance (H)
L_{em}	Field circuit mutual inductance (H)

3 Modelling and Analysis of IEPECS

Input to the wind turbine may not be same in the span of a particular duration, and wind may change its direction and speed based upon the environmental change. In certain durations, the amount of energy may not be sufficient to meet the load (or) grid requirements; in such cases, we need to boost the energy levels, and there is an essence of need in controlling the voltage of control winding. Conventional DC-DC converter (CDC-DC) circuit along with the intelligence control is integrated by applying the sliding-mode operation to satisfy the above statements. In this section, mathematical modelling of conventional DC-DC converter and IEPECS is discussed and compared. Mathematical model equations of dual-input conventional DC-DC converter [19, 20] in different modes are as follows in (4)–(7). To operate proposed conventional DC-DC converter shown in Fig. 3, two modes are required.

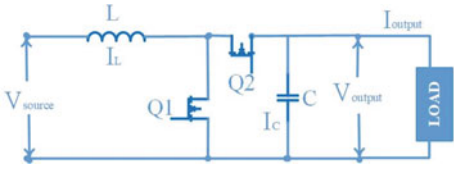

Fig. 3 Block diagram of CDC-DC

Mode-I: When MOSFET-1 is ON, MOSFET-2 is OFF

$$V_{\text{source}} * \delta T_{\text{on}} - L\frac{\mathrm{d}i_L}{\mathrm{d}t} * \delta T_{\text{on}} = 0 \tag{4}$$

$$V_{\text{output}} * \delta T_{\text{on}} - V_c * \delta = 0 \tag{5}$$

$$I_{\text{output}} = I_c \tag{6}$$

Mode-II: When MOSFET-1 is OFF, MOSFET-2 is ON

$$V_{\text{source}} * (1-\delta)T_{\text{off}} = L\frac{\mathrm{d}i_L}{\mathrm{d}t} * (1-\delta)T_{\text{off}} + V_{\text{out}}(1-\delta)T_{\text{off}} \tag{7}$$

Above modelling equations are reframed in state-space form as follows.

$$\begin{aligned} x(k+1) &= Ax(k) + bu(k) \\ y(k) &= cx(k) + du(k) \end{aligned} \tag{8}$$

where $u(t) = V_{\text{source}}$; $y(t) = V_{\text{out}} = x_2$; $I_L = x_1$

$$A = \begin{bmatrix} 0 & -\frac{(1-\delta)}{L} \\ \frac{(1-\delta)}{C} & -\frac{1}{RC} \end{bmatrix}; \quad b = \begin{bmatrix} \frac{1}{L} \\ 0 \end{bmatrix}; \quad c = [0\ 1]; \quad d = [0]$$

The converter output voltage with CDC-DC is as shown in Fig. 4.

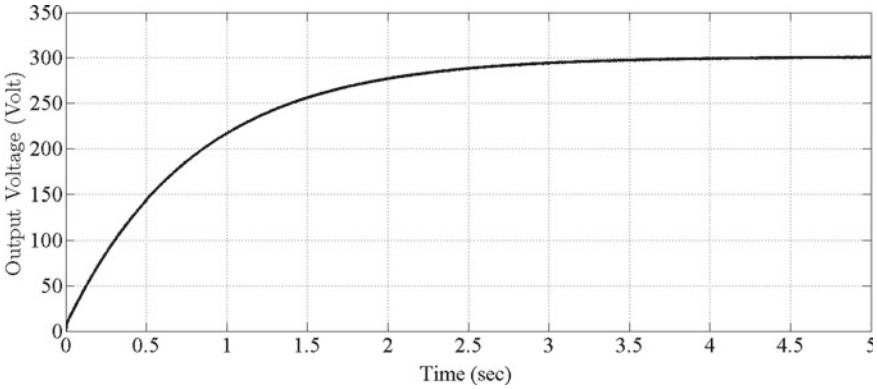

Fig. 4 Converter output voltage with CDC-DC

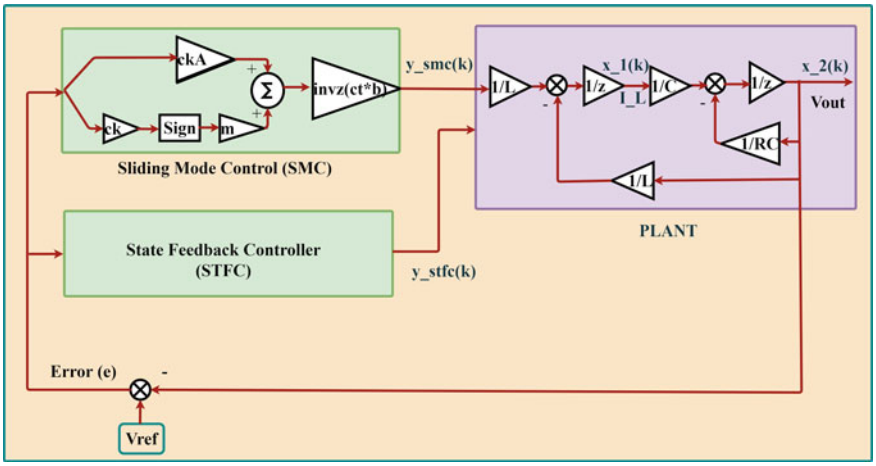

Fig. 5 DC-DC converter block diagram representation with SMC

Sliding-mode control expression to perform the controlling operation [21, 22] is as expressed in Eq. (9)

$$y_{\text{smc}}(k) = -\left[ckAe + m * \text{sign}|cke|\right](ckb)^{-1} \tag{9}$$

The simulation diagram of conventional DC-DC converter along with the control strategy of single input-discrete sinusoidal PWM (DSPWM) technique integrated with proposed IEPECS-SMC is as represented in Fig. 5. Input voltage is set at 50 V, and the reference voltage is maintained at 300 V; for the corresponding desired levels, converter elements are calculated. Similarly, the converter operation is performed with the state feedback control technique. The state feedback controller (STFC) is operated based upon the inclusion of state vector for the desired control action for the control system dynamics.

The modified closed-loop state vector is represented as $A_{\text{closed}} = A - bK$, then state vector in Eq. (8) is rewritten as follows [12]

$$x(k+1) = [A - bK]x(k) + bu(k) \tag{10}$$

Poles are placed at the locations -1500 and -1228 in order to obtain the desired converter response, and the corresponding converter circuit output voltage with both sliding-mode controller and state feedback controller is as shown in Fig. 6. Based on the simulation results in Fig. 6, SMC has shown better performance over STFC. Hence, SMC is proposed for this research study.

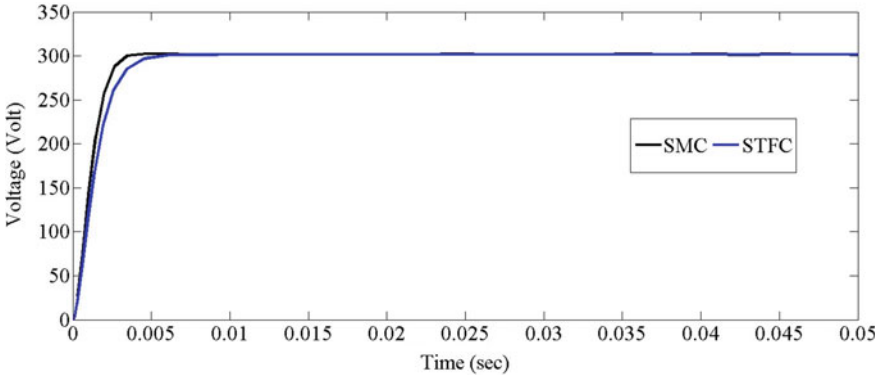

Fig. 6 DC-DC converter output voltage with proposed IECPECS (SMC and STFC)

4 MPPPC Operation with Isolated Solar Panel and Wind Plant

4.1 Isolated SOLAR Plant with MPPPC

4.1.1 Mathematical Modelling of MPPPC-P&O Technique

The block diagram of solar panel along with MPPPC is as shown in Fig. 7. Mathematical modelling of MPPPC-P&O technique is done with the following terms listed in Table 2 which are taken into consideration.

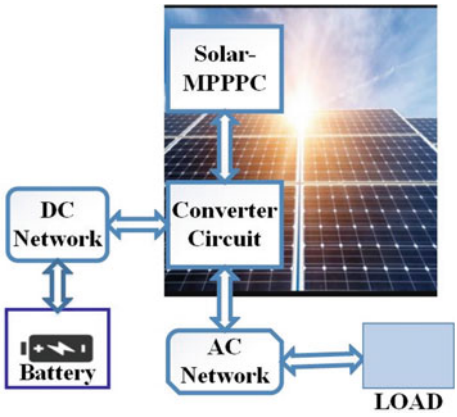

Fig. 7 Block diagram of isolated solar plant with proposed DSWCPMSG

Table 2 Notations used for developing modified MPPPC technique

Symbol	Name
$V_{pv}(k)$	Present-state PV panel voltage
$V_n = V_{pv}(k-1)$	One-step delayed PV panel voltage
$V_b = \int V_n(k-1)\mathrm{d}t$	On integrated step delay V_n
$P_{pv}(k)$	Present-state PV panel power
$P_n = P_{pv}(k-1)$	One-step delayed PV power
$P_b = \int P_n(k-1)\mathrm{d}t$	On integrated step delay P_n

Algorithm for Modified MPPPC

Algorithm for the operation of MPPPC-using modified P&O Technique [23, 24].

Step 1: Read the current state values of voltage and current $V(k)$, $I(k)$ respectively.
Step 2: Estimate the present state value of power using the formula

$$P(k) = V(k) * I(k) \tag{11}$$

Step 3: Estimate the following states using the previous available states

$$V_n = V(k-1)$$

$$V_b = \int V_n(k-1)\mathrm{d}t \tag{12}$$

$$P_n = P(k-1)$$

$$P_b = \int P_n(k-1)\mathrm{d}t \tag{13}$$

Step 4: Find the incremental or decremental changes in voltage and power values which is the difference between V_n and V_b

$$\Delta V = (V_n - V_b) \quad \text{and} \quad \Delta P = (P_n - P_b) \tag{14}$$

Step 5: Determine the product of previously obtained incremental or decremental changes in voltage and power values

i.e., $\Delta V * \Delta P$.

If $\Delta V * \Delta P > 0$ Then go to Step 6
$\Delta V * \Delta P < 0$ Then go to Step 7
Step 6: Then the operating point of P–V characteristics shift towards left side by MPPPC with the sign function + 1. Then the update position is

$$p = \Delta D + D_b \tag{15}$$

where $\Delta D \rightarrow$ Position tolerance shift by MPPPC

$$D_b = \int D(k-1)\mathrm{d}t \tag{16}$$

Go to Step 8

Step 7: Then the operating point of P–V characteristics shift towards right side by MPPPC with the sign function of -1.

Then the update position is

$$p = -\Delta D + D_b \tag{17}$$

where $\Delta D \rightarrow$ Position Tolerance shift by MPPPC

$$D_\mathrm{b} = \int D(k-1)\mathrm{d}t \tag{18}$$

Step 8: Then the obtained position from above steps 'p' is passing through the carrier signals to generate the duty cycle for boost-converter operation.

With the integration of above algorithm of MPPPC in the proposed system, maximum power is to be tracked across the 1-phase grid/load under different loading conditions of 10, 50 and 100 Ω using the modified P&O technique.

The simulation result in Fig. 8 represents the MPPPC operation with the load power.

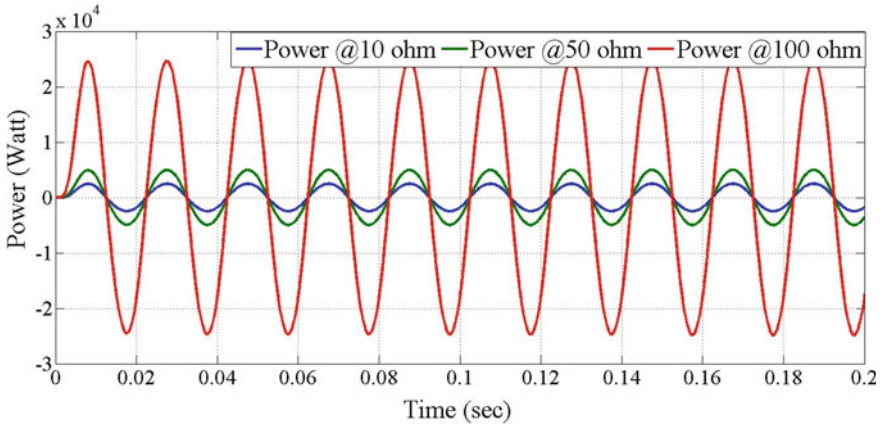

Fig. 8 Maximum tracking power across one-phase load for isolated solar panel with MPPPC

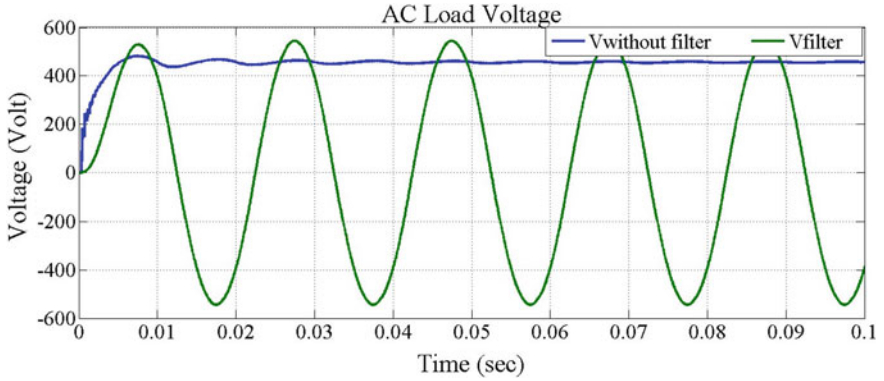

Fig. 9 One-phase load voltage of isolated solar—without and with filter circuit

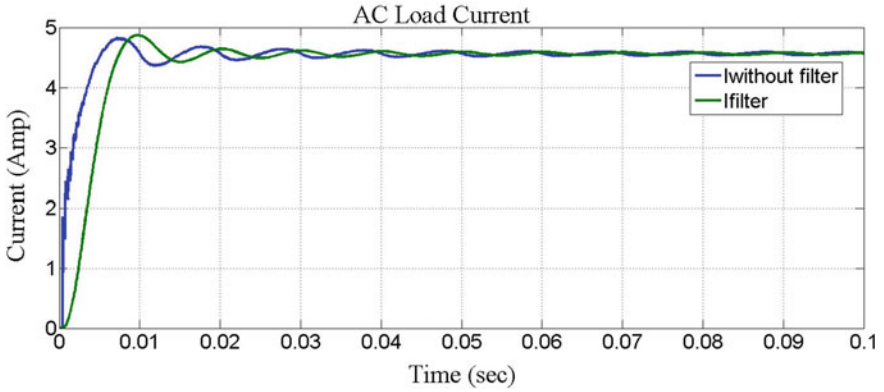

Fig. 10 One-phase load current of isolated solar—without and with filter circuit

The simulation results in Figs. 9 and 10 represent the one-phase load V and I curves without and with filter circuit for the isolated solar panel with MPPPC operation.

4.2 Isolated Wind Plant with MPPPC

The block diagram of isolated wind plant (includes wind turbine + PMSG (PM-synchronous generator)) along with MPPPC operation is as shown in Fig. 11. The distribution of air pressure across the airfoil will be expressed by using the coefficient of pressure (C_p) which will be expressed mathematically [25] as given in Eq. (19)

$$C_p = \frac{P_{\text{Mech,Out}}}{Wp * f(v, \omega, \phi)} \tag{19}$$

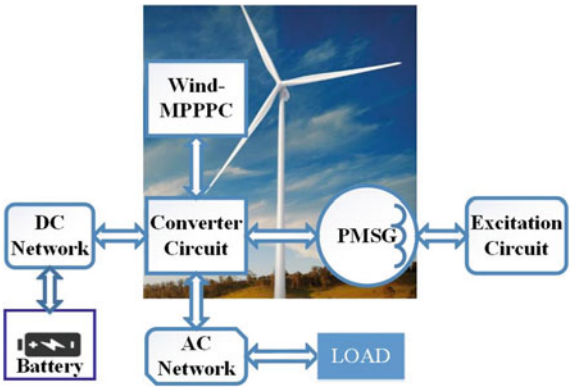

Fig. 11 Block diagram of isolated wind plant with proposed DSWCPMSG

where $C_p \rightarrow$ Coefficient of performance index of wind turbine,
$f(v, \omega, \phi) \rightarrow$ Functional objective of wind turbine,
$P_{\text{Mech,Out}} \rightarrow$ Mechanical output of wind turbine,
$v \rightarrow$ Wind velocity in m/s,
$\omega \rightarrow$ Angular velocity of wind turbine in rad/s,
$\phi \rightarrow$ Pitch angle in degree.

The MPPPC operation is implemented along with the inverter circuit to operate the loads connected to AC/DC grid along with the boost converter. The following simulation results in Figs. 12 and 13 represent the load voltage and currents of a load with and without filter circuit.

With the integration of MPPPC, maximum power is tracked across the 1-phase grid or load under different loading conditions of 10, 50 and 100 Ω. The following simulation results in Fig. 14 represent maximum power tracked across the load for the isolated wind plant with MPPPC operation.

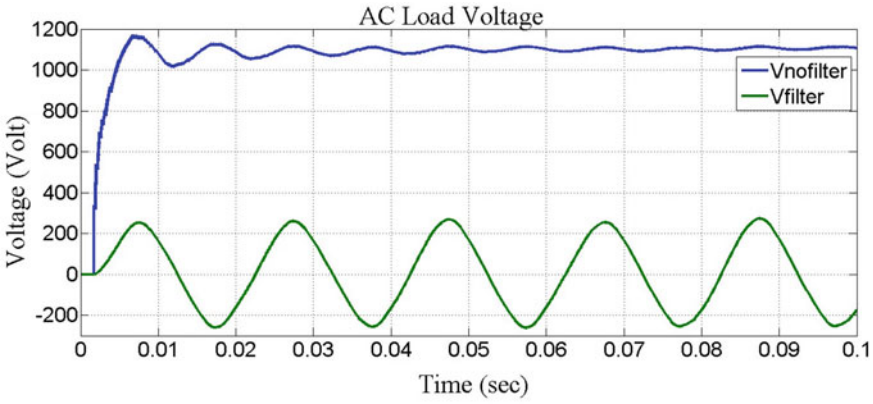

Fig. 12 One-phase load voltage of isolated wind plant—without and with filter circuit

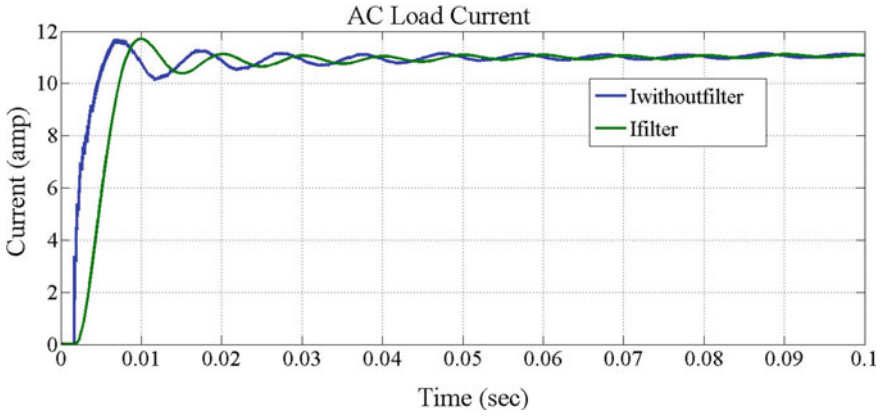

Fig. 13 One-phase load current of isolated wind plant—without and with filter circuit

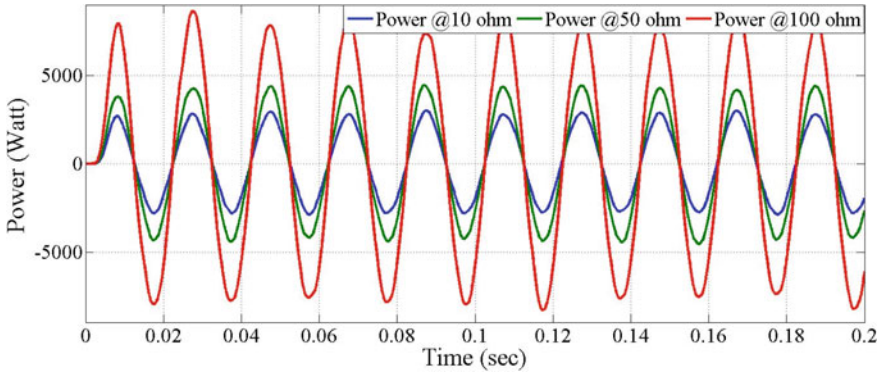

Fig. 14 Maximum tracking power across one-phase load for isolated power plant with MPPPC

Excitation circuit plays the main key role for doubly excited machines like synchronous machines. The excitation circuit acts as a constant current source which is controlled by a power electronic converter circuit with an excitation capacitor at the output terminals of the converter circuit. Simulation results are attached in Fig. 15 which provides the excitation circuits output with different values of excitation capacitors 10, 30, 50, 80 μF. The excitation circuit with the integration of intelligence provides the necessary field current to the stator circuit of the modelled DSWCPMSG. The results suggest that the filter circuit provides stable outputs than without filter circuit.

The excitation characteristics prove that the double-excited synchronous generator can be controlled to different extents based on load requirement.

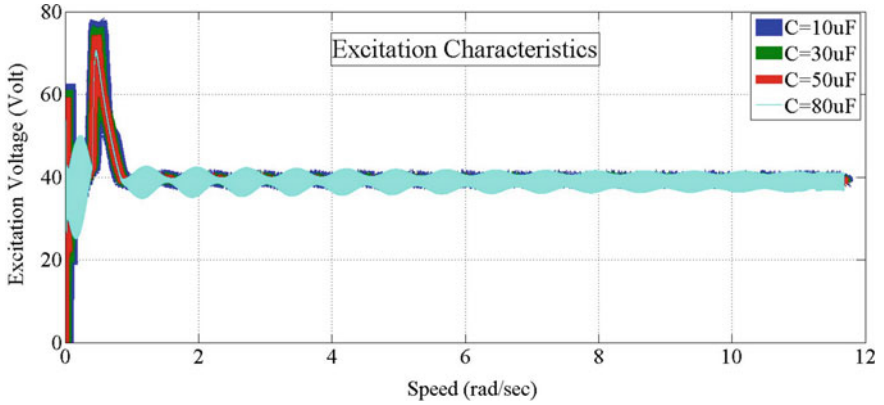

Fig. 15 Excitation characteristics for different excitation capacitor values

5 Integration of DSWCPMSG-HPSA with IEPECS

The reliability of the wind power system application is increased by integrating the solar PV system. The overall integrated system is called as hybrid power system application (HPSA). The overall DSWCPMSG-HPSA system along with IEPECS with a three-phase and a simple DC network is shown in Fig. 16. The simulation results of the proposed system with power characteristics of PV panel in integrated HPSA are shown in Fig. 17, where input to the PV panel is being irradiance which is expressed in W/m^2 and the output of the solar panel is power extracted which is expressed in Watt.

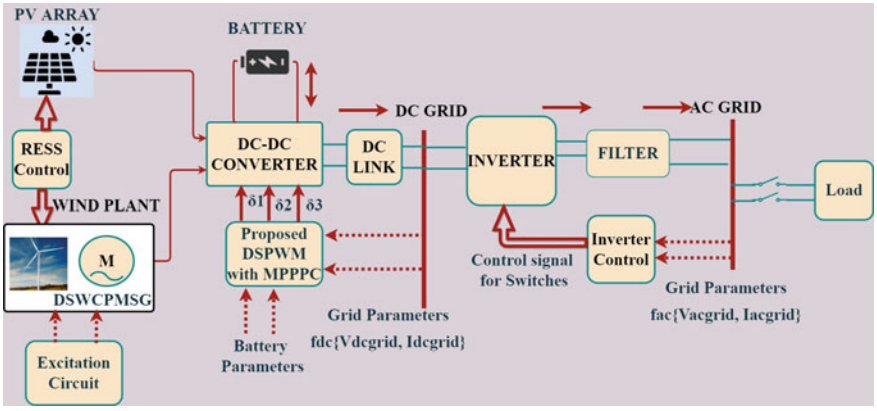

Fig. 16 Block diagram representation of overall system for study

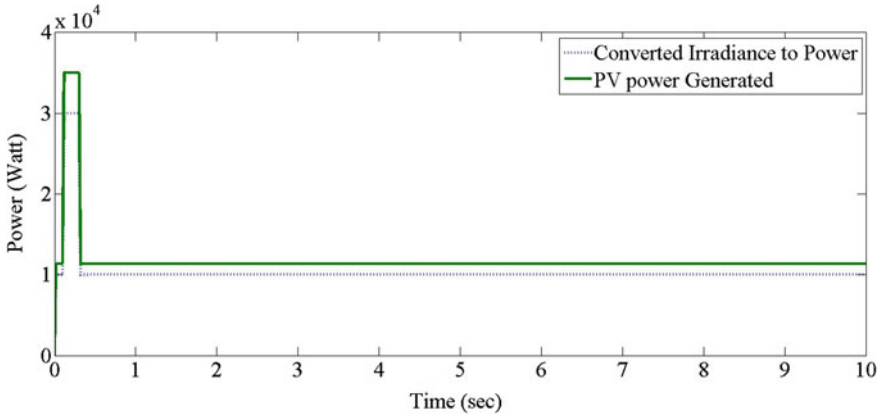

Fig. 17 PV power characteristics in DSWCPMSG-HPSA

5.1 When a Sudden Change in Load Demand

Under loading conditions, the load demand is shared by the hybrid power sources (i.e. the solar panel under variable irradiances and wind plant with variable wind speeds).The additional amount of reactive power required by the load is minimized with the help of an LC filter which is as concluded by comparing simulation results. For testing the system behaviour, a sudden change of 4 kW of load is applied at 2nd sec and maintained up to 3rd sec and a sudden decrement in load of 5 kW is applied at 5th sec and maintained up to 6th sec. The corresponding powers at each primary and auxiliary power sources for the required power demand are in Fig. 18.

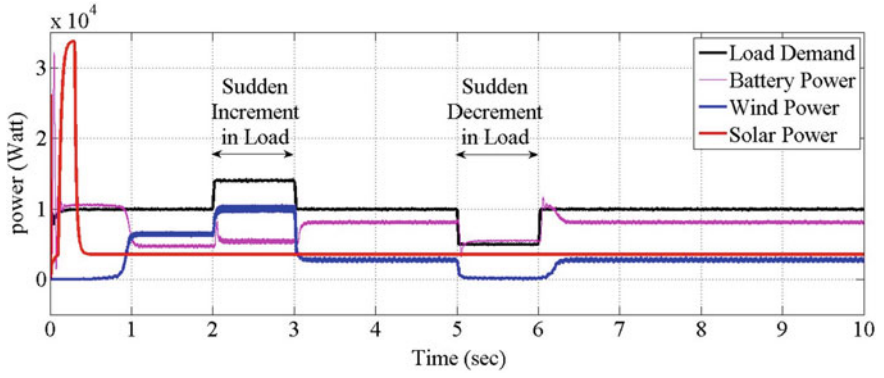

Fig. 18 Power sharing among the sources for the sudden increment and decrement load

Table 3 Load sharing among hybrid sources

Sl. No.	Powers	Load scheduling in kW					
		(0–1)	(1–2)	(2–3)	(3–5)	(5–6)	(6–10)
1	Load demand	10	10	14	10	5	10
2	Battery power	11	5	6	8	5.5	8
3	Wind power	6	6	10	3	3	3
4	Solar power	4	4	4	4	4	4
5	Spinning reserve	11	5	6	5	7.5	5

For the different loading conditions, the power that is shared among the considered hybrid sources, i.e. PV panel and wind plant along with the hybrid energy storage device (battery), is as listed under different loading schedules, and the simulation results are given in Table 3. For the sudden change in load, the IEPECS is adjusted to its pulse angle so as to control the power electronic devices operation; hence, the power flow at DC link is varied, and bidirectional energy flow is controlled by keeping the solar power as constant but varying the wind power by adjusting the excitation characteristics of generator, and based on SoC limits, battery delivery power is adjusted. The corresponding load sharing between the primary and secondary sources is shown in Table 3.

Figure 19 shows voltage variations at the DC link for the respective load changes; with the proposed control techniques, though the voltage fluctuations are occurred due to the sudden changes in load, DC link voltage is restored to constant value of 640 V. The auxiliary source (battery) voltage and currents changes are shown in Fig. 20.

The corresponding AC grid/load currents are for the sudden increment in load at 2nd sec and maintained till 3rd sec, and there is a sudden decrement in load at 5th sec which is shown in Figs. 21 and 22, respectively.

The battery parameters are controlled based on the reference voltage and SoC limits.

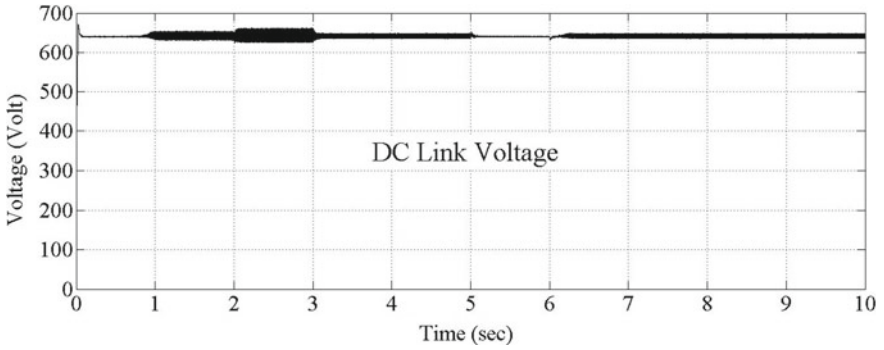

Fig. 19 DC link voltage for sudden changes in load demand

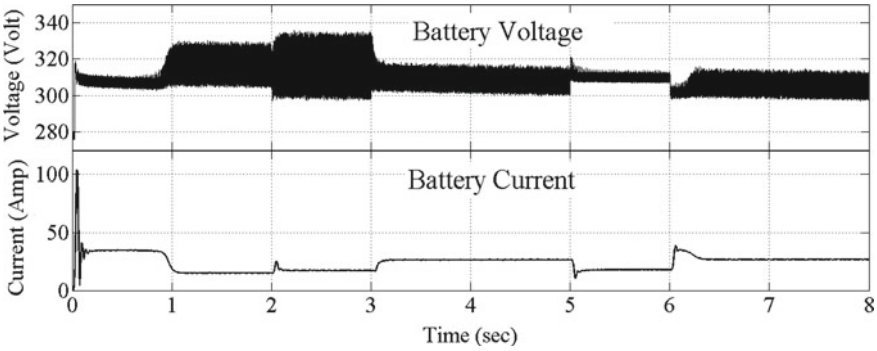

Fig. 20 Battery parameters

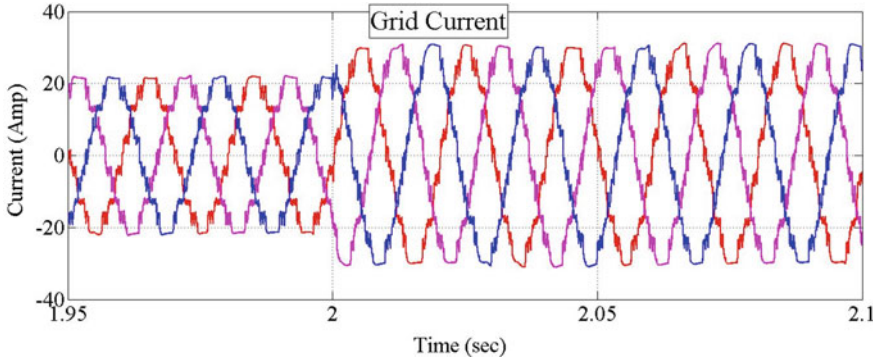

Fig. 21 Grid current variation for the sudden increment in load demand

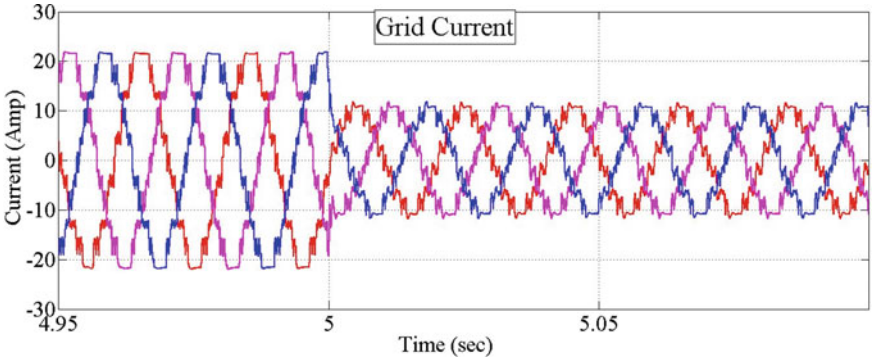

Fig. 22 Grid current variation for the sudden decrement in load demand

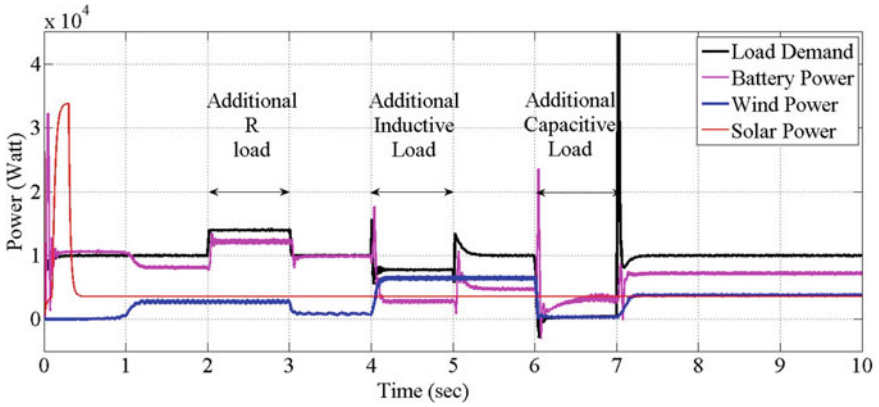

Fig. 23 Powers developed by hybrid sources for the load demand

The stable outputs suggest that there is a smooth control in energy transfer between the primary and secondary sources.

5.2 When Variable Loading Conditions Are Applied in the System

In practical scenario, all the loads are nonlinear in nature. The dynamic behaviour of the developed system is tested with nonlinear loads. A sudden change of 4 kW additional load is applied at 2nd sec and maintained up to 3rd sec. A sudden additional inductive load of 50 kVA is added to the existing 10 kW load at 4th sec and maintained up to 5th sec, and another capacitive load is applied at 6th sec which is added to the existing load of 5 MVA and maintained up to 7th sec. The corresponding simulation results under above-mentioned variable loading conditions are shown in Fig. 23.

The mode shifting operation between the primary and auxiliary sources is done with the help of AVR Mega-32 microcontroller as shown in Fig. 24.

6 Conclusions

In this research paper, dual stator winding-controlled permanent magnet synchronous generator (DSWCPMSG) is implemented with the maximum power point position controller (MPPPC) technique for extracting maximum powers from the hybrid sources. Both PV panel and wind plant were integrated with a secondary source battery, to compensate the deficit voltage levels during low parameter ranges.

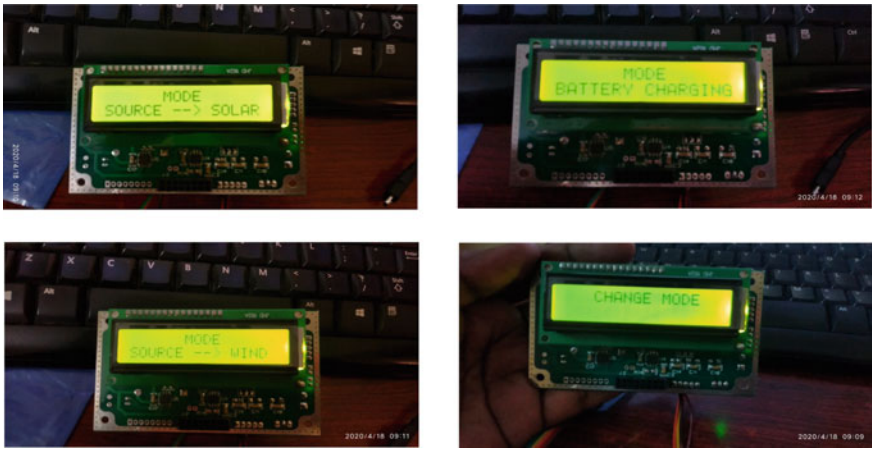

Fig. 24 Mode shifting control with AVR Mega-32 microcontroller

Power electronic converters play key role in smooth operation of power sharing among the sources. Initially, they tested the proposed system with conventional controllers. But they fail to obtain the smooth control operation in the hybrid power system applications where system dynamics will change from instant to instant. Hence, an intelligent excitation power electronic control system (IEPECS) is proposed to sense and control the operation of DSWDESG.

An IEPECS applies the sliding-mode control strategy which is applied to balance the stability of the DSWPMSG operation, to control and compensate the control voltage which is applied to the control winding of the DSWCPMSG. The IEPECS tracks the MPPPC with the help of proposed SMC even at low-speed ranges of the DSWCPMSG.

The proposed system is studied at various loading conditions, and the effects due to sudden changes in load are observed. The proposed system with the IEPECS provides stable output and smooth control of energy flow between the primary and secondary sources. Based on the data from the simulation results, mode shifting among the sources is implemented with the help of AVR Mega-32 microcontroller which is helpful for the future works to implement in the small-scale hardware prototype.

Appendix 1

The proposed DSWCPMSG design specifications:
Two winding stator phase resistances: R_{s1}, $R_{s2} = 0.8\,\Omega$.
Two winding stator phase inductances: $L_{ls1} = L_{ls2} = 3.2\,\text{mH}$.
Mutual inductances: $L_{dm} = 45\,\text{mH}$.
Rotor phase resistances: R_{qr}, $R_{dr} = 0.9\,\Omega$.

Rotor phase inductances: $L_{lqr} = L_{ldr} = 3.6$ mH.
Excitation circuit phase resistance and inductance: $R_{er} = 0.22\,\Omega$; $L_{er} = 4.5$ H.
Excitation capacitance $C_{exct} = 1\ \mu$F.
Phase split resistance $R_{exct} = 1\,\Omega$.
Rotor inertia: $J = 0.01197\,\text{kg m}^2$.
Viscous damping: $D = 0.001189\,\text{Nm s}^{-1}$.
Pole pairs: PP = 5.
Static friction: Neglected.

Appendix 2

PV panel and wind plant data.
Wind plant data:
Nominal power output of turbine 8.5 kW.
Nominal wind speed 13.2 m/s.
Nominal torque: 55.6 Nm.
PV panel data:
Nominal open-circuit voltage $V_{oc} = 406$ V.
Assumed irradiation range: 1–4 kW/m^2 (usual irradiation range: 1–1.37 kW/m^2).
Type of connection: Parallel.
No of strings used: 2.

References

1. S. Saji, N. Kuldeep, A. Tyagi, *A Brief Report on A Second Wind Sector for India's Wind Energy Sector Pathway to Achieve 60 GW* (Published by Council of Energy, Environment and Water (CEEW), 2019)
2. A. Venkatesh, S. Nalinakshan, S.S. Kiran, H. Pradeepa, Energy transmission control for a grid-connected modern power system non-linear loads with a series multi-stage transformer voltage reinjection with controlled converters. Int. J. Eng. Trends Technol. **68**(8), 97–101(2020)
3. A. Urja, Report from renewable energy-new horizons covered by MNRE re round-up for 2018–2019. Sol. Mag. **12**(5) (2019)
4. Report from Alliance for Rural Electrification. Hybrid Power Systems Based on Renewable Energies. https://www.ruralelec.org/sites/default/files/are-wg_technological_solutions_-_brochure_hybrid_systems.pdf
5. X. Yang, Y. Xu, N. Yang, B. Wen, K. Zhao, Y. Zhang, Research on the reliability and capacity allocation of wind power-solar power-pumped storage hybrid power system, in *China International Conference on Electricity Distribution* (IEEE, Tianjin, China, 2018), pp. 2071–2076
6. A. Kavousi, S. Hamid Fathi, J. Milimonfared, M.N. Soltani, Application of boost converter to increase the speed range of dual-stator winding induction generator in wind power systems. IEEE Trans. Power Electron. **33**(11), 9599–9610 (2018). https://doi.org/10.1109/TPEL.2018.2797095

7. M.H. Zamani, G.H. Riahy, M. Abedi, Rotor-speed stability improvement of dual stator-winding induction generator-based wind farms by control-windings voltage oriented control. IEEE Trans. Power Electron. **31**(8), 5538–5546 (2016). https://doi.org/10.1109/TPEL.2015.2495256
8. R. Das, H. Rashid, I.U. Ahmed, A comparative analysis of PI and PID controlled bidirectional DC-DC converter with conventional bidirectional DC-DC converter, in *3rd International Conference on Electrical Information and Communication Technology (EICT)*, pp. 1–6 (2017)
9. H.M. Solaiman, M.M. Hasan, A. Mohammad, S.R. Kawsar, M.A. Hassan, Performance analysis of DC to DC boost converter using different control methods, in *IEEE International Conference on Electrical, Computer and Communication Technologies (ICECCT)* (2015), pp. 1–5
10. H. Li, X. Ye, Sliding-mode PID control of DC-DC converter, in *5th IEEE Conference on Industrial Electronics and Applications* (2010), pp. 730–734
11. M.R. Mahmud, H. Pota, Robust feedback linearizing controller design for DC microgrid connected DC-DC converter, in *2021 IEEE Texas Power and Energy Conference (TPEC)* (2021), pp. 1–6
12. M. Mazlan, N. Haqkimi, C. Charin, N. Fairuz, N. Izni, M. Annuar, State feedback controller using pole placement method for linear buck converter to improve overshoot and settling time. Appl. Mech. Mater. **793**, 211–215 (2015)
13. S. Chincholkar, W. Jiang, C.-Y. Chan, S.S. Rangarajan, A simplified output feedback controller for the DC-DC boost power converter. Electronics **10**(4), 493 (2021)
14. A. Venkatesh, An improved adaptive SMO for speed estimation of sensorless DSFOC induction motor drives and stability analysis using Lyapunov theorem at low frequencies. Int. J. Eng. Res. Technol. (IJERT) **8**(9), 246–253 (2019)
15. S. Kumari, V. Kushwaha, T.N. Gupta, A maximum power point tracking for a PMSG based variable speed wind energy conversion system, in *International Conference on Power Energy, Environment and Intelligent Control (PEEIC)* (IEEE, 2018), pp. 789–794
16. E.E.M. Mohamed, M.S.R. Saeed, A.I.M. Ali, Dual three-phase partitioned stator flux-switching PM machine for wind generating systems, in *12th International Middle East Power Systems Conference (MEPCON)* (IEEE, 2018), pp. 992–997
17. K. Bimal, *Bose: Modern Power Electronics & AC drives* (Prentice Hall PTR, USA, 2002)
18. R. Krishnan, *Electric Motor Drives Modelling, Analysis & Control*, 1st edn. (Prentice Hall, New Jersey, 2001)
19. A. Siva Prasad, S. Kumaravel, S. Ashok, Integration of solar PV/battery hybrid system using dual input DC-DC converter, in *Biennial International Conference on Power and Energy Systems: Towards Sustainable Energy (PESTSE)* (IEEE, 2016), pp. 1–5
20. M.N.B. Akbar, A.S.M. Toha, A.A. Priyo, S. Ghosh, M.Z. Jamil, H.K. Dhar, Performance analysis of multi-input DC-DC boost converter for hybrid power system, in *Innovations in Power and Advanced Computing Technologies (i-PACT)* (IEEE, 2019), pp. 1–6
21. W. Perruquetti, J.P. Barbot, *Sliding Mode Control in Engineering*, 1st edn. (Marcel Dekker, Inc, USA, 2002)
22. B. Draženović, Č. Milosavljević, B. Veselić, Comprehensive approach to sliding mode design and analysis in linear systems, in *Advances in Sliding Mode Control 2013*, LNCIS, vol. 440, ed. by B. Bandyopadhyay, S. Janardhanan, S. Spurgeon (Springer, Heidelberg, 2013), pp. 1–19
23. M. Hlaili, H. Mechrgui, Comparison of different MPPT algorithms with a proposed one using a power estimator for grid connected PV system. Int. J. Photo Energy 1–10 (2016)
24. H.H.Mousa Hossam, A.-R. Youssef, E.M. Mohamed Essam, Improved perturb and observe MPPT algorithm of multi-phase PMSG based wind energy conversion system, in *21st International Middle East Power Systems Conference (MEPCON)* (IEEE, 2019), pp. 97–102
25. A.R. Sudhamshu, M.C. Pandey, N. Sunil, N.S. Satish, V. Mugundhan, Numerical study on effect of pitch angle on performance characteristics of a HAWT. Eng. Sci. Technol. Int. J. **19**(1), 632–641 (2016)

Investigation of New Fuzzy Cascade Controller for Frequency Deviation in Hybrid Power Systems

Prince Sinh, Ujjaval Patel, and Nilesh Chothani

Abstract A new fuzzy cascade controller is proposed to perform the load frequency task and to give reliable operation of a power system. In this study, fuzzy PI-(1 + DD) controller is optimally designed as LFCs scheme for an interconnected multi-area power system via parallel AC/DC transmission links. The presented interconnected microgrids test system comprises thermal power generating unit with reheat, hydro generating unit, photovoltaic (PV) model with MPPT, DG, and SMES. The parameters of proposed controller considered as control variables and integral time absolute error obtain from as fitness function. Big bang–big crunch (BB–BC) algorithm is used for optimal tuning of FPI-(1 + DD) controller structure variables. To evaluate the effectiveness of the proposed design scheme, obtained simulation results have been compared with the results of fuzzy PID controller in terms of settling times and oscillation of the frequency deviation, tie-line power fluctuation. MATLAB/Simulink was used to check dynamic behavior of a test system for this study.

Keywords Automatic generation control · Fuzzy logic · Cascade controller · Load frequency control · Interconnected microgrids · Big bang–big crunch algorithm · HVDC link · Optimization

1 Introduction

A large scale interconnected power system comprises combination of non-renewable and renewable energy resources with the various types of energy storage system

P. Sinh (✉)
EV Division, Epowerx learning technologies pvt ltd, Ahmedabad, India
e-mail: prince.dinanath@skill-lync.com

U. Patel
School of Cyber Security & Digital Forensics, National Forensic Sciences University, Gandhinagar, India
e-mail: ujjaval.patel@nfsu.ac.in

N. Chothani
Department of Electrical Engineering, Pandit Deendayal Energy University, Gandhinagar, India
e-mail: nilesh.chothani@sot.pdpu.ac.in

© The Author(s), under exclusive license to Springer Nature Singapore Pte Ltd. 2023

K. Murari et al. (eds.), *Soft Computing Applications in Modern Power and Energy Systems*, Lecture Notes in Electrical Engineering 975,
https://doi.org/10.1007/978-981-19-8353-5_7

(ESS) such as battery ESS, flywheel energy storage (FES), pumped hydroelectric storage (PHS), and superconducting magnetic energy storage (SMES), which can be placed near to the consumer to supply energy [1–3]. This all storage gets charged when the output power from power plants are at its peak. Also the ESS acts as a spinning reserve and fed power into system as un-interruptible power supply (UPS). Hence, ESS is employed in the electrical grid for absorbing or delivering active power when the power generated by the renewable energy increase or decrease, respectively [4]. The dispatchable power sources such as diesel generator (DG), fuel cell (FC), and micro-turbine (MT) adjust their power output supplied to the electrical grid on demand. Also the increasing penetration of stochasticity and uncertainty at distribution end in the existing power system well as the influence of incorporated structures with the intermittent nature makes the frequency deviation control a complicated task [5, 6]. The foremost responsibility of the any electrical grid is to control and keep the frequency deviations within the limits by using better control strategies. Generally, the LFC is used to maintain the network stability of the power system grid within the particular area in w.r.t system loads changes and profile of power flow in tie-line [1–6]. Research on load frequency control (LFC) has gained a lot of attention in recent years.

Several research papers have discussed LFC with various types of control strategies such as optimal control approaches, classical control approaches, adaptive and self-tuning control approaches, variable structure control approaches, robust control approaches, centralized and decentralized control approaches, soft computing techniques, fuzzy logic-based methods, and bio-inspired optimization algorithm. But very few have addressed solution approaches or methodologies, optimization techniques, and its modeling used in LFC. In the literature survey, one can find various comprehensive review on LFCs. Alhelou et al. [1] presented a critical review of the various approaches for the LFC parameters related to smart power systems. Different control strategies were elaborated especially considering power system with HVDC, deregulation, distributed generation (DG), and renewable energy resources to understand the pros, cons, and limitations of explored approaches and to identify future research gaps. Pappachen et al. [7] explored a critical review on LFC. The review includes key elements of a deregulated power system, difference between conventional and non-conventional energy architecture, and its control strategies. Ramesha et al. [8] reviewed the load frequency control for microgrid (μ-grid) considering solar-wind-based hybrid energy sources. The applications of flower pollination algorithm (FPA) to optimized fractional order proportional-integral-derivative (FOPID) for LFC in μ-grid are also discussed. Figure 1 gives a classification of the variety of existing control approaches of LFC for power networks [9–25].

More numbers of literatures are available on classical control approaches to controlling the frequency deviation in a power system. Mohamed et al. [10] designed Krill Herd algorithm (KHA)-based optimum synthesis for fractional order PID controller (FOPID) controller of conventional power system frequency control. Lamba et al. [11] leveraged interval FO-based PID (INFOPID) controller under system under dynamics uncertainties for two-area frequency response model. Although the authors of [12–15] also presented some classical control approaches,

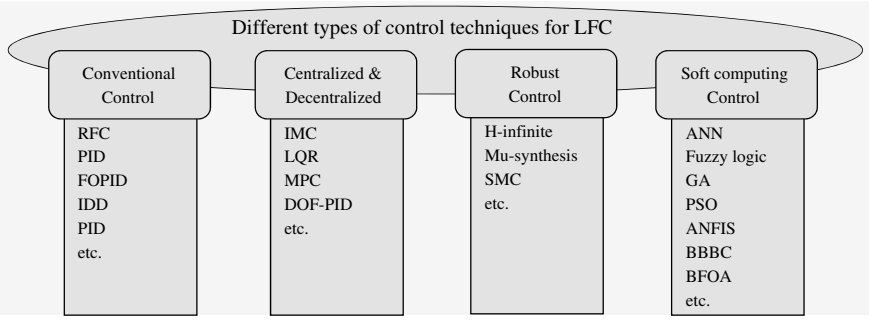

Fig. 1 Control techniques for LFC

however these methods did not give better result when the multi-area interconnected power system consider with nonlinear characteristics. Even under deregulated power system, nominal system parameters also very arbitrarily during a daily cycle. Due to this, these designs are not suitable for the load frequency control (LFC) issues and it resulted in less effective performance.

Centralized and decentralized-based control strategies are reported in [5, 17–19] for the load frequency control issues in interconnected power network. Asghar et al. [5] implemented the decentralized-Model Predictive Control (De-MPC) and Centralized-Model Predictive Control (Ce-MPC) controller to maintain the minimum frequency deviation will be appraising the EVs integrated smart grid (SG) system. Ismail et al. [17] used the modified design of different types of proportional integral (PI) controllers, which is tuned based on fuzzy logic and MPC for a multi-area to control the interconnected power system containing photovoltaics and wind turbine, here with attachment of electrical vehicle (EV) used to analyze adaptive ability of the controller to adapt to the influence of load frequency control (LFC) in different areas. Results generated by MPC and FOPID approached were compared with traditional strategies. Pahasa et al. [18] proposed a novel secondary frequency control approach for microgrid with wind turbine by incorporating the EV using MPC.

Authors of [20–23] illustrated various robust control approaches for LFC issues, adaptive sliding mode control (SMC) algorithm for LFC presented in Dev et al. [20], proposed a nonlinear adaptive super twisting SMC approach, and applied it to a multi-area load frequency control prototype, and designed based on nonlinear disturbance observer. Trip et al. [21] designed some distributed SMCs as the LFC and it analyzed on first-order turbine governor dynamics (TGD) and second-order turbine governor dynamics (TGD) in a unifying way. Davidson et al. [22] proposed an extended version framework of general H-infinity via loop shaping in which the synthesis of the controller can be adjustment of frequency response of whole power system within certain bounds of interest toward the improvement of the closed-loop dynamics performance and stability. In Bevrani et al. [23], this paper addresses mixed H-infinity and Structured Singular Value (mu-synthesis) Control Theory to enhance the frequency control performance and robustness in the presence of islanded

microgrid system, including MT, FC, and ES is investigated. However, in SMC control, chattering is a harmful phenomenon because it leads to low control accuracy.

Nowadays, distributed energy sources with the conventional source of energy have been added to the power system, which increases the complexity of the power system structure. So, the only traditional LFCs may not be capable to give exact result. To overcome this problem, the soft computing techniques along with traditional controllers addressed in such references [16, 24–28]. Li et al. [16] designed centralized data-driven grid-area coordinated LFC (GAC-LFC) approach and considered the inter-sample information using the technique of effective exploration-based multi-agent deep deterministic policy gradient (EE-MADDPG). Such technique has been capable as LFC controller in each area, where each area of power system tends to different agents. Modern LFC system is a typical sampled data system, but the input delay method has not been used so far. Kumar et al. [24] proposed a big bang–big crunch (BB-BC) optimization algorithm control to achieve optimal gains of PID controllers for frequency control in two areas reheat thermal system and four areas thermal reheat system using a generation rate constraint (GRC), and also designed a model predictive control (MPC), PID, and fuzzy cascaded PID controllers. However, this type of optimize LFC controllers are individually use for generating units and area units; therefore, its system frequency regulation ability is restricted. Shayeghi et al. [25] reported an optimal design of fuzzy PD-(1 + I) cascade controller tuned by the mayfly optimization (MO) technique to the LFC task in μ-grid. The six different situations investigated to check the capability of system in comparison with the fuzzy PD-(1 + I) cascade and PID controller under the environment of system parameters variation, load disturbance rejection, and renewable energy sources (RESs) generation changes. Annamraju et al. [26] designed two-stage hybrid FLC for LFC problem of system perturbations in an autonomous microgrid (MG). Also authors have utilized a nature as well as biological inspired techniques such as grey wolf optimization (GWO) and proposed particle swarm optimization (PSO) to optimize the membership functions (MFs) of fuzzy strategy to control the power flow from grid. Table 1 explored literature review articles on LFC and their contribution concerning its control strategies with architecture, nature of energy source, solution approach, and uncertainty handling methodology.

The main contribution of this work is encapsulated as follows:

1. Illustration of the LFC in the power system with its different generating unit.
2. A new controller with fuzzy system is incorporated and investigated for LFC of the 2-area power network with conventional and renewable energy plants.
3. Critical and comparative investigation is achieved via optimizing parameters of the implemented system.
4. 1 + DD parameters is added to the controller to increase stability and robustness.

This research paper is organized as: Second section comprises the mathematical model of the multi-area power system. Third section illuminates main principle of the proposed controller fuzzy PI-(1 + DD), while test system model and the MATLAB/Simulink-based analysis is exhibited in fourth section. Finally, the last section provides the concluding remarks and future scope.

Table 1 Existing literature review on the load frequency control

Sr. No.	References	Number of areas	Nature of generation	Interaction of other devices	Type of controller	Year of publication
1	Li Jiawen et al.	4	TGD	–	EE-MADDPG	2022
2	N. Kumar et al.	2, 4	TPP	–	BBBC + MPC, fuzzy, cascaded PID	2022
3	H. Shayeghi	2	STP, BEG, BTG, MHTG, WT	HEV	MO fuzzy + cascaded PI	2021
4	M. Ramesha et al.		WT, PV, DEG	BESS, SMES, EV	FPA, FOPID	2021
5	A. Latif et al.	2, 4	PV, WT, TPP, HPP	–	FO	2021
6	A. Osman et al.	2	PV, HPP	–	SA, GA, PSO	2021
7	A. Dev et al.	2	TGD	–	Sliding mode	2020
8	R. Mohamed et al.	1	WTG, PV, DEG	FC, FESS, BESS	FOPID	2020
9	R. Asghar et al.	4	WT, TGD	EV	PID, Ce-MPC, De-MPC	2020
10	S. Anbarasi et al.	2, 3, 4	TTP, HPP, WT	HVDC	BFOA	2020
11	R. Lamba et al.	2	TGD	–	INFOPID	2019
12	A. Annamraju et al.	1	PV, WT, DEG	BESS, FC	PSO, GWO + fuzzy PI	2018
13	M. Ismail et al.	4	PV, WT	EV	PI, MPC, FOPID	2018
14	S. Trip et al.	6	TGD	–	Droop based	2017
15	J. Pahasa et al.	1	WT	EV	MPC	2016
16	A. Davidson et al.	2	TGD	–	H-infinity	2016
17	M. Ponnusamy et al.	2	TPP, HPP	SSSC, CES	ICA	2015
18	Y. Zhang et al.	4	TPP, HPP, WT	–	DMPC	2015
19	H. Bevrani et al.	–	DEG, MT, WTG, PV	BESS, FC, FES	Mu-synthesis and H-infinity	2015

(continued)

Table 1 (continued)

Sr. No.	References	Number of areas	Nature of generation	Interaction of other devices	Type of controller	Year of publication
20	P. Bhatt et al.	2	TPP, HPP, WT	TCPS, SMES	GA, CRPSO	2012

TPP Thermal power plant, *HPP* Hydro power plant, *DEG* Diesel engine generator, *STP* Solar thermal power plant, *WT* Wind turbine, *MT* Microturbine, *TGD* Turbine governor dynamics, *PV* Photovoltaic panel, *BESS* Battery energy storage system, *FES* Flywheel energy storage, *EV* Electric vehicle, *FC* Fuel cell, *TCPS* Thyristor controlled phase shifter, *SSSC* Static synchronous series compensator, *CES* Capacitive energy storage, *RFB* Redox flow batteries, *EES* energy storage system

2 Dynamic Mathematics Model of an Interconnected System

In this study, we tested two-area system consisting of four generating stations. This interconnected system comprises hydro power plant (HPP), thermal power plant (TPP), and diesel engine generator (DEG) integrated with a non-conventional energy sources such as PV module in addition to energy storage unit like SMES as shown in Fig. 2. Area-1 is interconnected with Area-2 with the help of parallel ac and dc link to exchange the scheduled megawatt (MW). Hence, load changes or any generation loss in any one area, its effect reflected on another area in terms of the tie-line power flows as well as frequency deviations. As a result, the power flow fluctuations in tie-line and frequency deviations will be minimized by using effective load frequency controllers [1].

As explored above, both area is simply composed by a group of governors, equivalent turbine generator units, and demand loads. The equivalent respective transfer functions (TF) of respective turbine generator unit and a governor in each areas are expressed below.

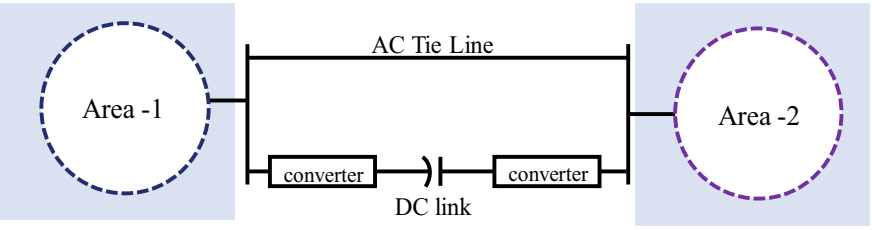

Fig. 2 Interconnected power system

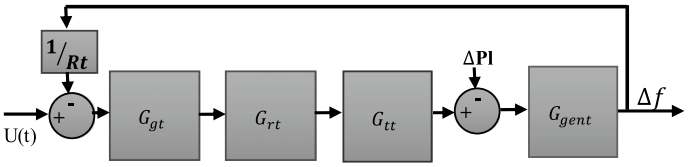

Fig. 3 Thermal generating unit

2.1 Mathematical Modeling of Generating Units

2.1.1 Thermal Generating Unit Dynamics Model

Figure 3 illustrates block diagram of the thermal generating unit, each parameter of block described as follows [25, 27].

$$\text{Governor model} \quad G_{\text{gt}} = \frac{K_{\text{gt}}}{T_{\text{g}}s + 1} \tag{1}$$

$$\text{Reheater model} \quad G_{\text{rt}} = \frac{K_{\text{r}}T_{\text{r}}s + 1}{T_{\text{r}}s + 1} \tag{2}$$

$$\text{Turbine model} \quad G_{\text{tt}} = \frac{K_{\text{t}}}{T_{\text{t}}s + 1} \tag{3}$$

$$\text{Generator model} \quad G_{\text{gent}} = \frac{K_p}{T_p s + 1} \tag{4}$$

2.1.2 Hydro Generating Unit Dynamics Model

Figure 4 explored block diagram of the hydro generating unit 4, each parameter of block described as follows [25, 27].

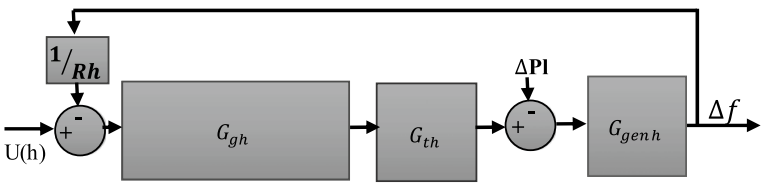

Fig. 4 Hydro generating unit

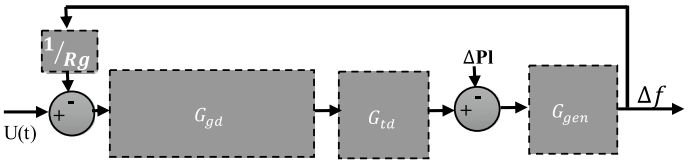

Fig. 5 Block diagram of diesel engine generating unit

$$\text{Governor model} \quad G_{\text{gh}} = \frac{K_{\text{gh}}}{T_{\text{gh}}s + 1} \times \frac{T_{\text{rh}}s + 1}{T_{\text{rh}}s + 1} \tag{5}$$

$$\text{Turbine model} \quad G_{\text{th}} = \frac{-T_{\text{w}}s + 1}{0.5T_{\text{w}}s + 1} \tag{6}$$

$$\text{Generator model} \quad G_{\text{genh}} = \frac{K_{\text{p}}}{T_{\text{p}}s + 1} \tag{7}$$

2.1.3 Diesel Engine Generating Unit Dynamics Model

The block arrangement of the diesel engine generating plant is depicted in Fig. 5, each parameter of block described as follows [29, 30]:

$$\text{Speed governor model} \quad G_{\text{gd}} = \frac{K_{\text{gd}}}{T_{\text{dd}}s + 1} \times \frac{T_{\text{dr}}s + 1}{T_{\text{df}}s + 1} \tag{8}$$

$$\text{Turbine model} \quad G_{\text{td}} = \frac{K_{\text{td}}}{T_{\text{cd}}s + 1} \tag{9}$$

2.1.4 Solar Power Generating Model

Solar cells are generally attached in power network to balance the demand. Usually in PV, the relationship between voltage and current is not exact follow linearity characteristics due to the change of solar radiation throughout the day. Hence, it is essential to maximize energy extraction by using MPPT and also to enhance the output power of the PV. The transfer function (TF) of the solar power generating unit with MPPT can be expressed as follows [30]:

$$\text{T.F of the PV Plant} \quad G_{\text{PV}} = \frac{K_{\text{PV1}}s + K_{\text{PV2}}}{T_{\text{PV1}}s + T_{\text{PV2}} + S^2} \tag{10}$$

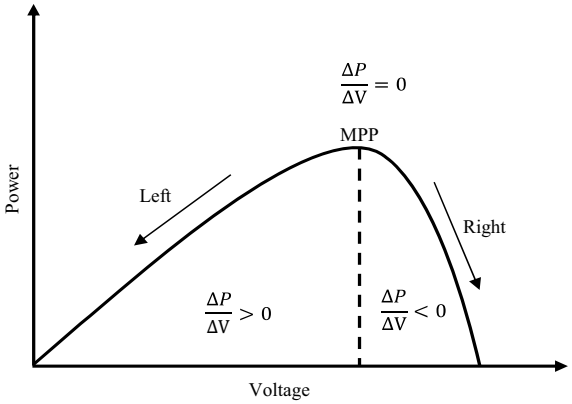

Fig. 6 MPP conditions with IC approaches

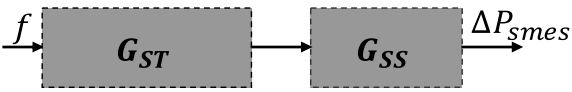

Fig. 7 Transfer function of SMES model

Here, the incremental conductance (IC) scheme is used to detect the slope of the *P–V* curve, which is maximum power point (MPP). The conditions used in IC scheme can be shown in Fig. 6.

2.1.5 SMES Model

Energy storage units are inserted in the grid to store the excess amount or surplus energy [31]. In this study, SMES is used as energy storage unit and its block diagram based on two stage as shown in Fig. 7 [32, 33]. When the consumer side demand is changed suddenly and power requirement increased, the energy discharges from SMES into the grid through the power converter system.

$$G_{\mathrm{st}} = \frac{T_{\mathrm{a}}s + 1}{T_{\mathrm{b}}s + 1} \times \frac{T_{\mathrm{c}}s + 1}{T_{\mathrm{d}}s + 1} \tag{11}$$

$$G_{\mathrm{ss}} = \frac{K_{\mathrm{smes}}}{T_{\mathrm{smes}}s + 1} \tag{12}$$

2.1.6 HVDC Link Model

In HVDC model, the converter dynamics is neglected to reduce the complexity. The transfer function of a HVDC link can be given as [34, 35] (Fig. 8):

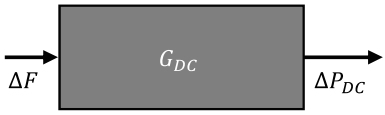

Fig. 8 Transfer function of a HVDC model

$$\Delta P_{\mathrm{DC}} = \frac{K_{\mathrm{DC}}}{T_{\mathrm{DC}}s + 1}\Delta F \tag{13}$$

3 Description of Proposed LFC Scheme

Conventional controllers such as proportional (P), the derivative (D), integral (I), PI, PD, and PID are mostly used in plant control process due to their general structure, availability, and acceptable performance. General dynamic characteristics are difficult for this type of controllers include high-order dynamics and large time delays. Hence, in somehow cases to obtain its optimal setting will be not easy due to their components interaction, to overcome this problem in some applications, using a traditional controller with state space model or cascaded controllers can give satisfactory results. This study presents a new control scheme called PI-(1 + DD) cascade controller arrangement is applied to solve expressed LFC issues. Initially given the detail structure of proposed cascade and then its design from the perspective of optimization is described.

3.1 PI-(1 + DD) Cascade Controller Structure

The proposed multistage or cascade controller is divided in two different stages. The first stage comprises proportional-integral (PI) and second stage is structured one plus double derivative (1 + DD). The block diagram of proposed PI-(1 + DD) cascade controller is shown in Fig. 9.

The s-domain transfer functions (TF) of PI and (1 + DD) controllers can be expressed by

$$G_{\mathrm{PI}}S = K_P + \frac{K_I}{S} \tag{14}$$

$$G_{(1+\mathrm{DD})}S = 1 + SK_{D1} + SK_{D2} \tag{15}$$

$$G_{\mathrm{PI}-(1+\mathrm{DD})}S = \left(K_P + \frac{K_I}{S}\right) \cdot (1 + SK_{D1} + SK_{D2}) \tag{16}$$

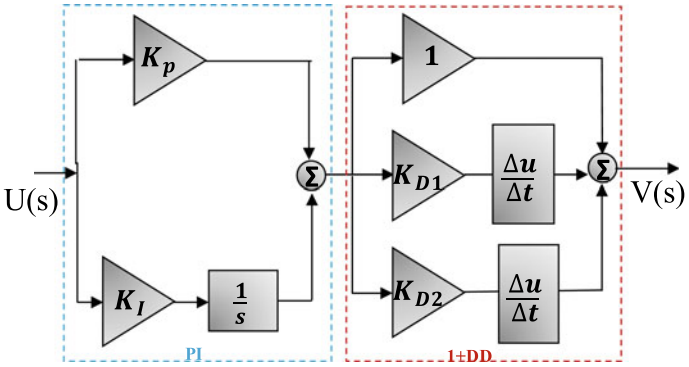

Fig. 9 Structure of PI-(1 + DD) cascade controller

where K_P, K_{D1}, K_{D2}, and K_I are proportional, derivative, derivative, and integral parameters, respectively. Here the input signal of cascade controller is only the respective area control error (ACE), moreover the output signal with its transfer function modeling can be written as

$$V(s) = \Delta P_{\text{ref}} = \left[\text{ACE} \cdot \left(K_P + \frac{K_I}{S}\right)\right] \cdot (1 + SK_{D1} + SK_{D2}) \tag{17}$$

In this paper, the proposed controllers are attached with fuzzy interfacing system (FIS), which has two inputs and one output membership functions will be shown in Fig. 13. One of them input is the area control error (ACE) signal and other is the deviation in area control error (ΔACE) signal, where K_e and K_{de} are the scaling factors for them, respectively, and the output of fuzzy controller is the control function applied for control the system. Thus, ACE for control Area-1 and for control Area-2 are given as

$$\text{ACE}_1(S) = \Delta P_{\text{tie}}(S) + \beta_1 \Delta F_1(S) \tag{18}$$

$$\text{ACE}_2(S) = \Delta P_{\text{tie}}(S) + \beta_2 \Delta F_2(S) \tag{19}$$

To design such FIS, the three basic steps shown in Fig. 10a are followed [36, 37],

Step-1: Fuzzification block converts given inputs to degrees of MFs and match the data with respective rule conditions.
Step-2: Mamdani-type inference engine: This block determined the capability of degree based on inserted IF–THEN rules commands to determine an output response.
Step-3: Defuzzification block convert outputs of the fuzzy engine to crisp values through centroid method. Also, there are twenty-five IF–THEN rules depicted in the fuzzy rules engine. The fuzzy rules base for Mamdani-type inference engine

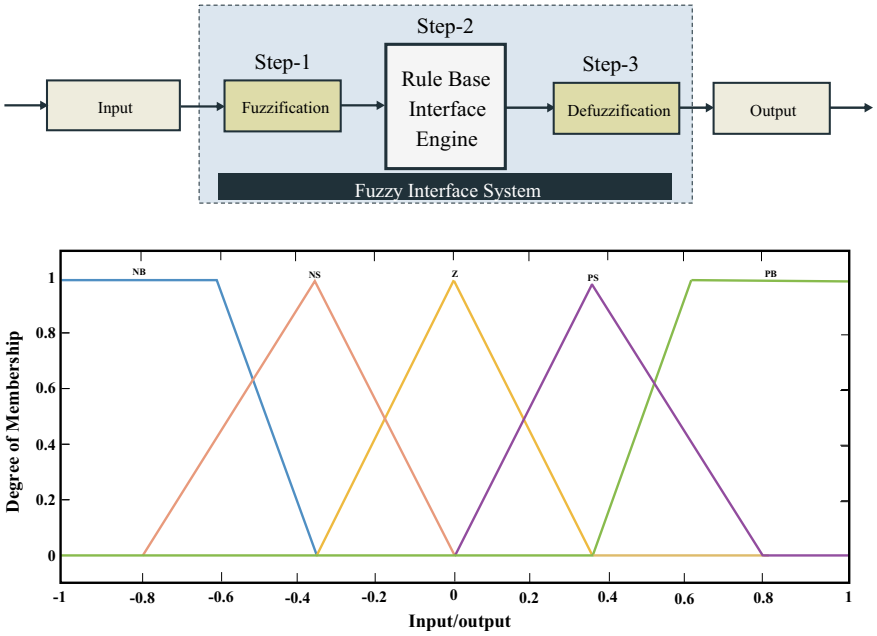

Fig. 10 Fuzzy logic **a** block diagram of FIS and **b** input–output MFs

(FIS) for both controllers is fixed and as given in Table 2, where MFs of the linguistic variables are labeled as Negative Big (NB), Negative Small (NS), zero (Z), Positive Small (PS), and Positive Big (PB). The two inputs represent scaled values between (1:1), and thus each of them are divided into five equal areas of Gaussian.

Table 2 Rule bases for FIS

e	$\dot{e}$				
	NB	NS	Z	PS	PB
NB	NB	NB	NS	NS	Z
NS	NB	NS	NS	Z	PS
Z	NS	NS	Z	PS	PS
PS	NS	Z	PS	PS	PB
PB	Z	PS	PS	PB	PB

3.2 *Objective Function*

The controller structure of PI-(1 + DD) has four independent tuning modes and one constant gain to provide better flexibility in controller design. It also results in the enhancement of system stability by reducing the peak deviation and improving transient response. To obtain improved parameters of proposed optimal controller, we employ optimization methods; there are various error integrating objective functions specified such as ISE, ITAE, ITSE, and IAE, where variables are labeled as integral (I), squared (S), error (E), absolute (A), and time (T) etc. Detailed explanation of these objective functions and several comparisons in the plant system performance are available in literature [21–27]. Expression of ISE and ITAE objective function for proposed two area system is given in Eqs. 20 and 21, respectively.

$$J_s = \text{ISE} = \int_0^{t_{\text{sim}}} [|\Delta f_1| + |\Delta f_2| + |\Delta p_{\text{tie}}|]^2 \mathrm{d}t \tag{20}$$

$$J_s = \text{ITAE} = \int_0^{t_{\text{sim}}} [|\Delta f_1| + |\Delta f_2| + |\Delta p_{\text{tie}}|] \cdot t \cdot \mathrm{d}t \tag{21}$$

As mentioned, ISE and ITAE objective functions can be used to tune the parameters of both controllers. However, it is very difficult to decrease the rise time without increasing overshoot. By reducing the rise time, the system settling period is reduced, while it will generate a greater momentum inertia; thus, there is chance of an overshoot increased. As convergence and step response of both systems clearly explored in Fig. 11, although the response signal for ITAE normalized faster, the convergence velocity of ITAE controller is obviously the best one compared with the other ISE. Since Eq. 21-based objective function offers improved response of system in terms of less settling time and damped oscillation compared to other alternatives [38, 39], hence ITAE objective function is mostly applicable in the load frequency controller tasks.

Where J is objective function, Δf is frequency deviation, and t_{sim} is simulation time. In the current paper, the main focus is to minimize J_s with the help of big bang–big crunch (BB–BC) algorithm. The optimization algorithm can be stated as minimizing objective function J_s under the following constraints:

$$K_{P,i}^{\min} \leq K_{P,i} \leq K_{P,i}^{\max} \tag{22}$$

$$K_{I,i}^{\min} \leq K_{I,i} \leq K_{I,i}^{\max} \tag{23}$$

$$K_{D1,i}^{\min} \leq K_{D1,i} \leq K_{D1,i}^{\max} \tag{24}$$

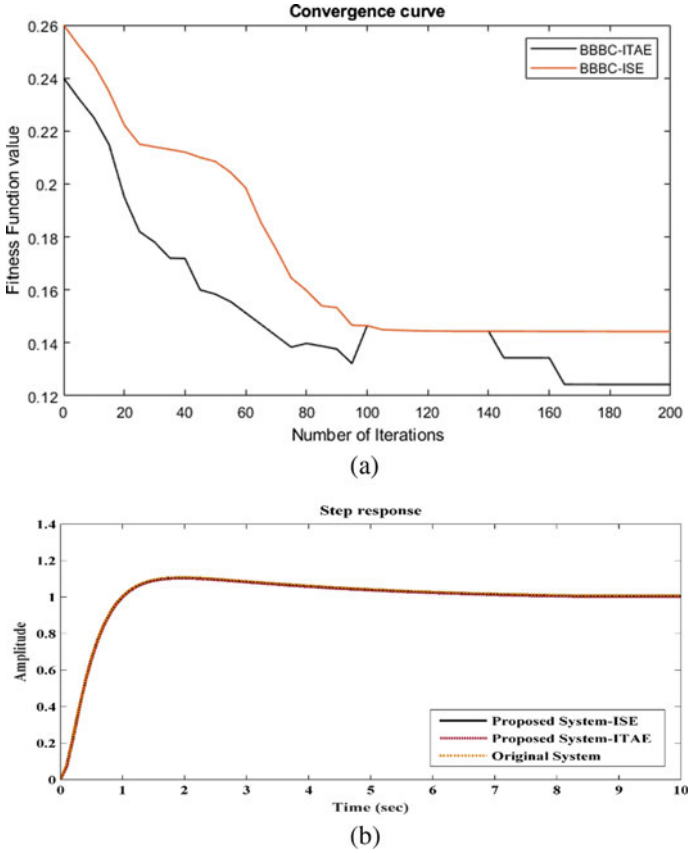

Fig. 11 **a** Convergence and **b** step response of the widely used objective functions

$$K_{D2,i}^{\min} \leq K_{D2,i} \leq K_{D2,i}^{\max} \tag{25}$$

$$K_{e,i}^{\min} \leq K_{e,i} \leq K_{e,i}^{\max} \tag{26}$$

$$K_{De,i}^{\min} \leq K_{De,i} \leq K_{De,i}^{\max} \tag{27}$$

where $K_{P,i}^{\min}$, $K_{I,i}^{\min}$, $K_{D1,i}^{\min}$, $K_{D2,i}^{\min}$ and $K_{P,i}^{\max}$, $K_{I,i}^{\max}$, $K_{D1,i}^{\max}$, $K_{D2,i}^{\max}$ are the minimum and maximum bounds of the PI-(1 + DD) controller. The optimal values of PI-(1 + DD) controller gains have been generated by using the BB–BC algorithm. The BB–BC algorithm is elaborated in the following section.

3.3 Big Bang–Big Crunch (BB–BC) Theory

Among all elaborated optimization algorithms [24–28], BB–BC algorithm proves to be advantageous to start for optimization process because it minimizes objective function very accurately with fast convergence speed and very less computational time [24, 40] etc. Besides this another advantage is, it does not require gradient information, hence optimal tuning possible for average generations [40]. Enrol et al. introduced newly algorithm inspired by big bang theory it is big bang–big crunch (BB–BC) algorithm [37]. It is mainly comprised of two stages: (1) Big bang phase: generation of population, fitness function evaluated and (2) Big crunch phase: implement center of mass (COM) as convergence operator. Proof about its fast convergence for optimization problem reported in [37, 41, 42]. The proposed algorithm is explained as per below steps.

Step 1: Big bang phase: The individual area has its own PI-(1 + DD) controller is considered. The population for each parameter of both area controller can be calculated by using Eq. 28.

$$x_{ij}^{(K)} = x_{i(\min)}^{(K)} + r_i \times \left(x_{i(\max)}^{(K)} - x_{i(\min)}^{(K)} \right) \tag{28}$$

where x represents the PI-(1 + DD) controller parameters, r_i is represent random number, $i = 1, 2, 3,\ldots$ indicates the number of each controller parameter, $K = 1, 2, 3, \ldots$ represents the total number of areas, and $j = 1, 2, 3, \ldots$ determines the population size. $x_{i(\min)}$ is lower limit and $x_{i(\max)}$ is upper limit of ith parameters.
Step 2: Evaluation of selected J_s as per Eq. 21 for each generated population (Eq. 28).
Step 3: Big crunch phase: Calculated the center of mass (COM) by using the knowledge of present position of each parameter in Eq. 28 and the associated objective function value (J_s) as expressed by Eq. 29.

$$X_{\text{COM}}(\text{position vector}) = \frac{\sum_{j=1}^{P} \frac{x_{ij}^{(K)}}{F_j}}{\sum_{j=1}^{P} \frac{1}{F_j}} \tag{29}$$

where P is the population size in BBP, $x_{ij}^{(K)}$ is the ith candidate in Kth iteration of n-dimensional search space.
Step 4: After BCP, new population for each controller parameter is generated in search space, based on the knowledge of COM, expressed as follows.

$$x_{ij(\text{new})}^{K} = \beta X_{\text{COM}} + (1 - \beta) x_{\text{best}} + \delta_i \tag{30}$$

$$\delta_i = r_i \times \frac{\alpha\left(x_{i(\max)}^{(K)} - x_{i(\min)}^{(K)}\right)}{K} \tag{31}$$

where β is the controlling coefficient under the influence of global best solution (x_{best}) on the location of the new candidate solution. If the r_i increases, more scattered the candidate solutions are around COM. δ_i is standard deviation of newly generated candidates w.r.t COM, and α is used to limiting size of the solution space.

Step 5: In this step, updated fitness function calculated w.r.t these newly generated parameters, and this newly generated fitness function compares with the previous one. Finally, the smallest one will be retained and the next parameters are chosen corresponding to the minimum fitness function after comparison.

$$x_{ij}^{K}(\text{next}) = \min\left\{F\left(x_{ij}^{K}(\text{previous})\right), F\left(x_{ij}^{K}(\text{new})\right)\right\} \tag{32}$$

Step 6: Compute the difference between the present and old fitness function value for all generations $e_{ij}^{K} = x_{ij}^{K}(\text{new}) - x_{ij}^{K}(\text{previous})$ and if stopping criterion has been met, iteration run end with optimum fitness function value which further help to obtain the optimum parameters of the proposed controllers, otherwise return to step number 2.

During this study, it has been found that big bang–big crunch (BB–BC) algorithm is good choice for optimization process. However, the main setback of proposed BB–BC theory that it does not imbibe velocity factor for center of mass under influence of gravity, which does not completely imitate scientific theory of universe created.

3.4 Implementation of BB–BC Algorithm with FPID and FPI-(1 + DD) for LFC Problem

In this paper, BB–BC optimization algorithm is implemented to find optimal coefficients and MFs in separate repetitive stages for FPID and FPI-(1 + DD) to solve LFC issues in multi-area power system network. The algorithmic steps divided in three stages of the proposed approaches are enumerated in Fig. 12.

Stage 1: To optimize the controller parameters by applying fixed MFs (Fig. 10) for fuzzy to determine suitable range of the parameters w.r.t objective function Eq. 21.

Stage 2: In this stage, by using generated coefficients (from stage-1) triangular MFs for fuzzy will be optimized with the different ranges for various inputs and output signals.

Stage 3: Simultaneous optimize controller parameters and MFs for fuzzy based on Eq. 21. These three stages counties repeated until condition ($J_s^k - J_s^{k-1} < \varepsilon$) is

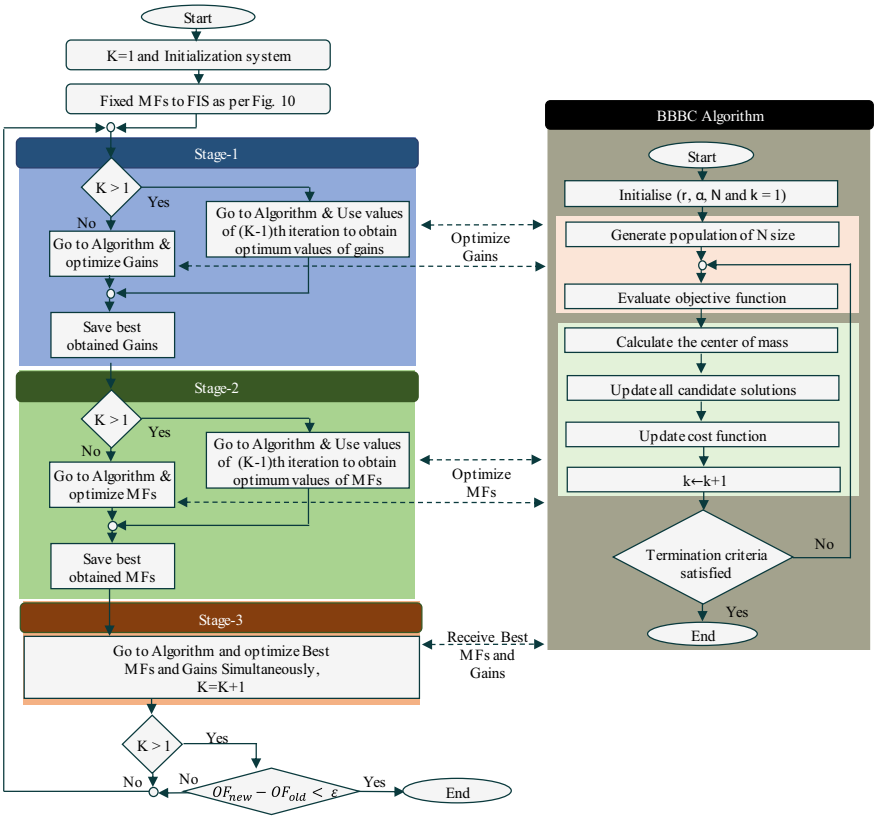

Fig. 12 Flow diagram of optimization process for the fuzzy cascade controllers

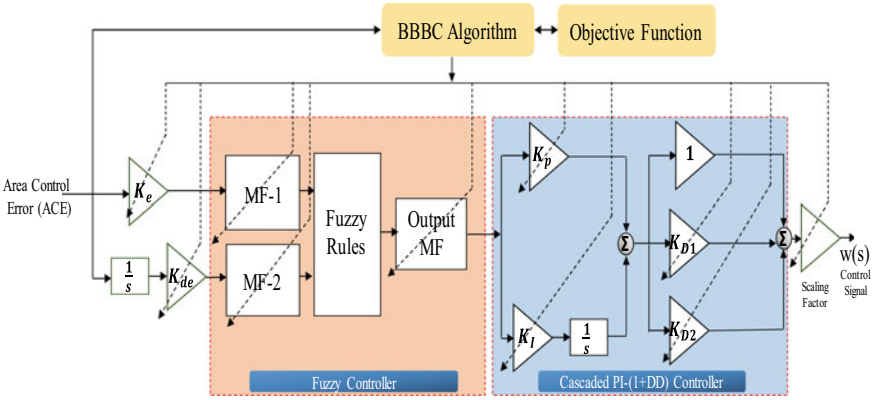

Fig. 13 FPI-(1 + DD) controller and parameters optimization with BB–BC algorithm

satisfied. Figure 13 illustrates flow diagram of optimization process of coefficients and decision variables for proposed controller with the BB–BC algorithm.

4 Test System Simulation and Results Discussion

In this section, the simulation and results of the proposed test system simulated under MATLAB/Simulink environment for the frequency deviation of the prescribed two area power system network are presented using different types of controllers. The proposed interconnected test system model consists of two areas as shown in Fig. 14. The first area includes thermal generating unit, hydro power generating unit with solar power (PV) generating unit, the second one is comprising thermal generating unit and diesel engine generating unit (DG) coupled with wind turbine. The detailed block diagrams of various generating units are built as per the model given in Sect. 2. The parameters values of the constructed system are given in Table 6 in Appendix.

In order to check the robustness of the proposed test system with FPI-(1 + DD) controller and another FPID controller, we simulated our test system model running with BB–BC algorithm under MATLAB/Simulink environment. The simulation is performed for 200 iterations, and the results are illustrated in Fig. 15, which compare

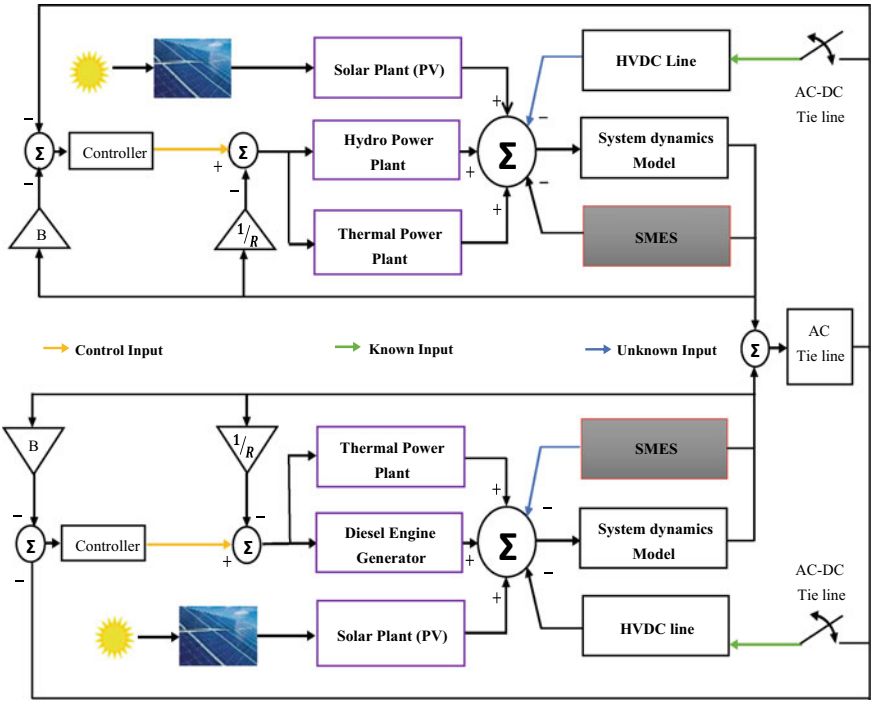

Fig. 14 Test system model of two area system

the frequency deviation for the both the area, respectively, with FPI-(1 + DD) and FPID controllers. Figure 15a shows the frequency deviation of the test system for the first area; it can find that both controllers settle the frequency deviation to zero, while the settling time for the FPI-(1 + DD) controller is very fast compare with FPID controller, respectively. Hence, the FPI-(1 + DD) gives the best performance in terms of very fast its set time with minimum overshoot, while the FPID gives average. The same performance can be found second area as well, which depicts in Fig. 15. Figure 15c shows the power exchange in tie-line between interconnected areas. The time taken to settle and peak overshoot and under shoot of the frequency deviation and power fluctuation in the tie-line are depicted in Tables 3, 4 and 5 for the selected two area power system model by using FPI-(1 + DD) and FPID controllers.

5 Conclusion

The conducted work demonstrated the utilization of FPI-(1 + DD) controller as new LFC approach for multi-source hybrid power system with SMES and HVDC link under deregulated power system environment. Each area has been considered with an individual FPI-(1 + DD) controller for analysis. The parameters of the proposed controller were optimized by applying BB–BC as a novel approach for optimization problems with ITAE as an objective function. From the in-depth simulation of test system elaborated in Sect. 4, followed by the analysis of it. Practically, LFC is system to adjust the mechanical power input to generator and match the electrical power demand and keep the rotational speed, and hence electrical frequency, nominal. The obtained simulation results (Fig. 15) confirmed that FPI-(1 + DD) controller effective to minimize mean square of area control error, frequency deviation, and power fluctuations in tie-line, and it is more efficiently and effective as compared to the conventional FPID controller for system under study. Also, this new technique is succeeded to improve the controller performance by reducing the percentage overshoot. Hence, it can be inferred that the FPI-(1 + DD) controller with BB–BC outperforms applied for LFC of a multi-source hybrid power system. The further modifications in the processes followed in BB–BC theory are suggested for the future work to improve the local optimum solutions of proposed system.

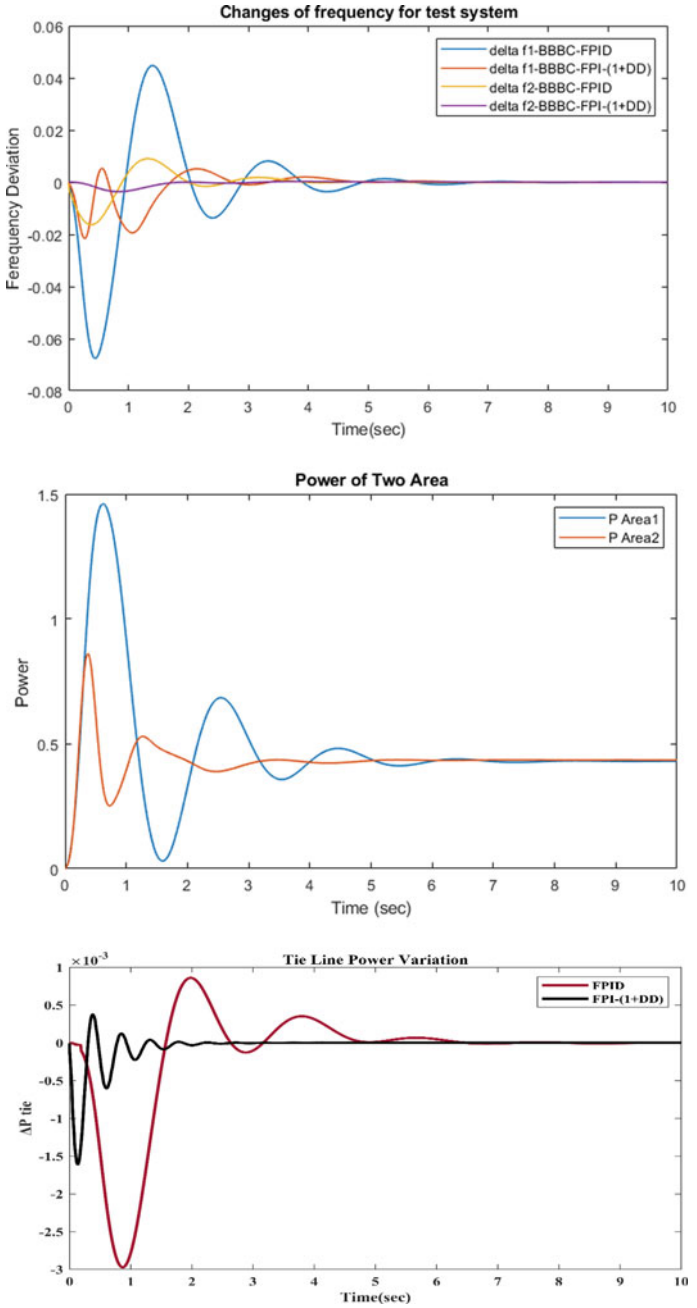

Fig. 15 Test system responses: **a** frequency deviation (rad/s), **b** power flow in the two area (p.u.) and **c** tie-line power fluctuation (p.u.)

Table 3 Comparative study of settling time (s)

Controllers	ΔF		ΔP_{tie}
	Area1	Area2	
FPI-(1 + DD)	6.85	4.5	3.2
FPID	8.48	7.6	8.4

Table 4 Comparative study of peak overshoots (p.u.)

Controllers	ΔF		ΔP_{tie}
	Area1	Area2	
FPI-(1 + DD)	0.0053	0.0025	0.0037
FPID	0.0446	0.009	0.0085

Table 5 Comparative study of undershoot (p.u.)

Controllers	ΔF		ΔP_{tie}
	Area1	Area2	
FPI-(1 + DD)	− 0.0216	− 0.0035	− 0.0016
FPID	− 0.0675	− 0.0163	− 0.0029

Appendix

See Tables 6 and 7.

Table 6 System parameters and nomenclature

Grid component	Parameters		Values	Unit
Thermal power generating unit	K_{gt}	Coefficient of steam turbine governor	1	p.u.
	T_g	Steam turbine governor time constant	0.25	s
	K_r	Coefficient of reheat steam turbine	0.33	p.u.
	T_r	Reheat steam turbine time constant	0.3	sec
	K_t	Coefficient of steam turbine	1	pu
	T_t	Steam turbine time constant	10	sec
Hydro power generating unit	K_{gh}	Coefficient of hydro turbine governor	1	pu

(continued)

Table 6 (continued)

Grid component	Parameters		Values	Unit
	T_{gh}	Hydro turbine governor time constant	0.2	s
	T_r	Rest time for speed governor	5.0	s
	T_w	Water time constant	1	s
	T_{rh}	Time constant of transient droop	28.75	s
Diesel engine generating unit	K_{gd}	Diesel turbine governor gain	1.0	p.u.
	T_{dd}	Speed governor time constant	2.0	s
	T_{dr}	Time constant	1.0	s
	T_{df}	Speed governor time constant	0.025	s
	K_{td}	Diesel turbine gain	0.1	p.u.
	T_{cd}	Diesel turbine time constant	3.0	s
Solar power generating unit	K_{PV1}	Gain of the PV system	−1/18	p.u.
	K_{PV2}	Gain of the PV system	1/900	p.u.
	T_{PV1}	PV system time constants-1	100	s
	T_{PV2}	PV system time constants-2	50	s
Superconducting magnetic energy storage (SMES)	K_{smes}	Gain of the SMES	0.2035	p.u.
	T_{smes}	Time constants	0.03	s
	T_a	Time constants of the SMES	0.2333	s
	T_b	Time constants of the SMES	0.016	s
	T_c	Time constants of the SMES	0.7087	s
	T_d	Time constants of the SMES	0.2481	s
Power system parameters	K_{ps}	Power system coefficient dynamics	0.06	p.u.
	T_{ps}	Time constant of power system dynamics	20	s
	B	System coefficients	2.4	p.u.
	R	System coefficients	0.425	p.u.

(continued)

Table 6 (continued)

Grid component	Parameters		Values	Unit
HVDC link parameters	K_{DC}	HVDC link coefficient	1.0	p.u.
	T_{DC}	HVDC link time constant	0.2	s

Table 7 Controllers' parameters

Controller	Parameters		Values
PID	Proportional coefficient	K_p	0.8901
	Integral coefficient	K_i	1.523
	Derivative coefficient	K_d	0.7851
PI-(1 + DD)	Proportional coefficient	K_p	1.6569
	Integral coefficient	K_i	3.5562
	Derivative coefficient	K_{d1}	1.0136
	Derivative coefficient	K_{d2}	0.8564
Fuzzy	Scaling factors	K_e	5000
	Scaling factors	K_{de}	200

References

1. H. Alhelou, E. Golshan, R. Zamani, E. Forushani, P. Siano, Challenges and opportunities of load frequency control in conventional, modern and future smart power systems: a comprehensive review. J. Energ. **11**(10), 01–35 (2018)
2. Y. Arya, Automatic generation control of two-area electrical power systems via optimal fuzzy classical controller. J. Energ. **355**(05), 2662–2688 (2018)
3. H. Khoobana, T. Niknama, F. Blaabjerg, T. Dragicevi, A new load frequency control strategy for micro-grids with considering electrical vehicles. Electr. Power Syst. Res. **143**, 585–598 (2017)
4. I. Hussain, S. Ranjan, D. Das, N. Sinha, Performance analysis of flower pollination algorithm optimized PID controller for wind-PVSMES-BESS-diesel autonomous hybrid power system. Int. J. Renew. Energy Res. **7**(2), 2019–2021 (2017)
5. R. Asghar, A. Ali, F. Rehman, R. Ullah, K. Ullah, Z. Ullah, M.A. Sarwar, B. Khan, Load frequency control for EVs based smart grid system using PID and MPC, in *International Conference on Computing, Mathematics and Engineering Technologies* (2020)
6. S. Pandey, S. Mohanty, N. Kishor, A literature survey on load–frequency control for conventional and distribution generation power systems. Renew. Sustain. Energy Rev. **25**, 318–334 (2013)
7. A. Pappachen, A. Fathima, Critical research areas on load frequency control issues in a deregulated power system: a state-of-the-art-of-review. Renew. Sustain. Energy Rev. **72**, 163–177 (2017)
8. M. Ramesha, A. Yadav, P. Pathak, An extensive review on load frequency control of solar-wind based hybrid renewable energy systems. J. Energy Sources Part A: Recov. Util. Environ. Effects **23**(5), 2484–2494 (2021)

9. A. Latif, S. Hussain, D. Das, T. Ustun, A. Iqbal, A review on fractional order (FO) controllers' optimization for load frequency stabilization in power networks. Energy Rep. **07**, 4009–4021 (2021)
10. R. Mohamed, M. Helaimi, R. Taleb, A. Gabbar, A. Othman, Frequency control of microgrid system based renewable generation using fractional PID controller. Indones. J. Electr. Eng. Comput. Sci. **19**(2), 745–755 (2020)
11. R. Lamba, S. Singla, S. Sondhi, Design of fractional order PID controller for load frequency control in perturbed two area interconnected system. J. Electr. Power Comp. Syst. **47**(11–12), 998–1011 (2019)
12. Y. Hote, S. Jain, PID controller design for load frequency control: past, present and future challenges. J. Electr. Power Comp. Syst. **51**(4), 604–609 (2018)
13. S. Taher, M. Fini, S. Aliabadi, Fractional order PID controller design for LFC in electric power systems using imperialist competitive algorithm. Ain Shams Eng. J. **5**(1), 121–135 (2014)
14. Z. Zhou, G. Huang, S. Bhattacharyya, Modern PID controller design for load frequency control, in *North American Power Symposium (NAPS)* (2016)
15. B. Nayak, P. Nayak, R. Prusty, Application of FPA based on PID controller for LFC of two-area multi-source hydrothermal power system, in *International Conference on Renewable Energy Integration into Smart Grids: A Multidisciplinary Approach to Technology Modelling and Simulation (ICREISG)* (2020)
16. J. Li, J. Gengb, T. Yua, Grid-area coordinated load frequency control strategy using large-scale multi-agent deep reinforcement learning. Energy Rep. **08**, 255–274 (2022)
17. M. Ismail, A. Bendary, Load frequency control for multi area smart grid based on advanced control techniques. Alex. Eng. J. **57**(4), 4021–4032 (2018)
18. J. Pahasa, I. Ngamroo, Coordinated control of wind turbine blade pitch angle and PHEVS using MPCS for load frequency control of microgrid. IEEE Syst. J. **10**(1), 97–105 (2016)
19. Y. Zhang, X. Liu, Y. Yan, Model predictive control for load frequency control with wind turbines. J. Control Sci. Eng. **8**(1), 233–242 (2015)
20. A. Dev, S. Anand, M.K. Sarkar, Nonlinear disturbance observer based adaptive super twisting sliding mode load frequency control for nonlinear interconnected power network. Asian J. Control **23**(5), 2484–2494 (2020)
21. S. Trip, C. Persis, Distributed optimal load frequency control with non-passive dynamics. IEEE Trans. Control Netw. Syst. **5**(3), 1232–1244 (2018)
22. A. Davidson, S. Ushakumari, H-infinity loop-shaping controller for load frequency control of an uncertain deregulated power system, in *International Conference on Electrical, Electronics, and Optimization Techniques* (2016)
23. H. Bevrani, M.R. Feizi, S. Ataee, Robust frequency control in an islanded microgrid: H-infinite and mu-synthesis. IEEE Trans. Smart Grid **07**(02), 706–717 (2015)
24. N. Kumar, A. Singh, Load frequency control for multiarea power system using secondary controllers. Trends Sci. J. **19**(02), 2044–2055 (2022)
25. H. Shayeghi, A. Rahnama, H. Alhelou, Frequency control of fully-renewable interconnected microgrid using fuzzy cascade controller with demand response program considering. IEEE Trans. Smart Grid **07**(1), 6077–6094 (2021)
26. A. Annamraju, S. Nandiraju, Robust frequency control in an autonomous microgrid: a two-stage adaptive fuzzy approach. Alex. Eng. J. **46**(1), 83–94 (2018)
27. M. Ponnusamy, B. Banakara, S. Dash, M. Veerasamy, Design of integral controller for load frequency control of static synchronous series compensator and capacitive energy source based multi area system consisting of diverse sources of generation employing imperialistic competition algorithm. Int. J. Electr. Power Energy Syst. **73**(1), 863–871 (2015)
28. P. Bhatt, S. Ghoshal, R. Ranjit, Coordinated control of TCPS and SMES for frequency regulation of interconnected restructured power systems with dynamic participation from DFIG based wind farm. Renew. Energy Int. J. Renew. Energy **40**(1), 40–50 (2012)
29. C. Srinivasarathnam, C. Yammani, S. Maheswarapu, Load frequency control of multi-microgrid system considering renewable energy sources using grey wolf optimization. J. Energ. **07**(3), 198–217 (2019)

30. R. Wagle, B. Pariyar, Mathematical modeling of isolated wind-diesel-solar photo voltaic hybrid power system for load frequency control. Int. J. Sci. Res. **07**(3), 960–966 (2018)
31. A. Kumar, S. Suhag, Effect of TCPS, SMES, and DFIG on load frequency control of a multiarea multisource power system using multiverse optimized fuzzy-PID controller with derivative filter. JVC/J. Vib. Control **24**(24), 5922–5937 (2018)
32. J. Shi et al., Integrated design method for superconducting magnetic energy storage considering the high frequency pulse width modulation pulse voltage on magnet. Appl. Energy **248**, 1–17 (2019)
33. M. Nandi, C.K. Shiva, V. Mukherjee, Frequency stabilization of multi-area multi-source interconnected power system using TCSC and SMES mechanism. J. Energy Storage **14**, 348–362 (2017)
34. G. Sharma, I. Nasiruddin, K.R. Niazi, Robust AGC regulators for a two-area power system interconnected via AC/DC tie-lines considering new structures of matrix Q. IET Gener. Transm. Distrib. **10**(14), 3570–3579 (2016)
35. Y. Arya, N. Kumar, AGC of a multi-area multi-source hydrothermal power system interconnected via AC/DC parallel links under deregulated environment. Int. J. Electr. Power Energy Syst. **75**(2), 127–138 (2016)
36. H. Azadi, J. Berg, A, Prasetyo, G. Hosseininia, Sustainability in rangeland systems: introduction of fuzzy multi objective decision making. Curr. World Environ. **4**(1), 19–32 (2009)
37. H.M. Genc, A.K. Hocaoglu, Bearing-only target tracking based on Big Bang–Big Crunch algorithm, in *The Proceedings of the 3rd International Multi-conference on Computing in the Global Information Technology (ICCGI '08)*, vol. 1 (2008), pp. 229–233
38. A. Osman, M. Magzoub, A. Salem, Load frequency control in two area power system using GA, SA and PSO algorithms: a comparative study, in *Australasian Universities Power Engineering Conference* (2021)
39. B. Mohanty, S. Panda, P. Hota, Controller parameters tuning of differential evolution algorithm and its application to load frequency control of multi-source power system. Int. J. Electr. Power Energy Syst. **54**(3), 77–85 (2014)
40. A. Tormási, L. Kóczy, Meta-heuristic optimization of a fuzzy character recognizer. *Fifty Years of Fuzzy Logic and its Applications*, vol. 326 (Springer, 2015), pp. 227–244
41. E. Yesil, L. Urbas, Big Bang-Big Crunch learning method for fuzzy cognitive maps. Eng. Technol. **7** (2010)
42. A. Kaveh, S. Talatahari, Size optimization of space trusses using Big Bang-Big Crunch algorithm. Comput. Struct. **87**(17–18), 1129–1140 (2009)

Frequency Regulation in Microgrid Considering Virtual Inertia with Firefly Algorithm Optimized Controller

Padmasetty Kasi Rao, More Raju, Shivcharan Gupta, and Kishan Dharawat

Abstract In this paper, a virtual inertia (*VI*) control-based virtual synchronous generator mechanism is proposed to improve the frequency dynamics of a microgrid by considering the renewable sources and electric vehicles. The considered microgrid is powered by a diesel generator and solar-thermal unit. In this study, firefly algorithm (FA) optimization technique is proposed to tune parameters of the proportional–integral–derivative (PID) controller. The performance of PID controller is found superior over PI controller. The microgrid system performance is evaluated for both step and randomized natures of the demands. In both cases, the *VI* influence is studied separately with PID controller. It is seen from the results that the dynamics are showing superior performance when *VI* is incorporated into the system. The above statement is also supported by the cost function analysis. The *VI* mechanism also works superiorly in the event of increased step magnitudes and varied solar field conditions.

Keywords Electric vehicles · Firefly algorithm · PID controller · Microgrid · Virtual inertia · Synchronous generator

1 Introduction

The complex power system network is generally interconnected in nature due to which it is able to supply power to different locations and for various types of loads [1]. Owing to geographical constraints and distant locations of conventional power plants, there is a requirement of transmission lines through which power is supplied to the end user (consumer). Due to this, in long-length transmission lines, the transmission losses are more and thereby efficiency of the power system reduces.

It is well known that due to several reasons like modernization, growth in population and industrialization, etc., the requirement of electricity is increasing day by day [2]. With the reduction in cost of power generation and transmission losses, the

P. K. Rao · M. Raju (✉) · S. Gupta · K. Dharawat
Maulana Azad National Institute of Technology Bhopal, Bhopal, India
e-mail: rajunitt1@gmail.com

© The Author(s), under exclusive license to Springer Nature Singapore Pte Ltd. 2023

K. Murari et al. (eds.), *Soft Computing Applications in Modern Power and Energy Systems*,
Lecture Notes in Electrical Engineering 975,
https://doi.org/10.1007/978-981-19-8353-5_8

efficiency of the system can be increased through the microgrid. The term microgrid represents a small-scale power supply network and is designed to produce power using the localized sources [3]. With the help of microgrids, we can supply power to near loads and decrease the peak load demand on main grid. The microgrid generally includes renewable sources that are highly unpredictable and depends upon weather conditions. The three main goals of microgrids are consistency, sustainability, and economic efficiency [3]. The microgrids can be operated in two modes, namely grid-connected mode and islanded mode. In grid-connected mode, microgrid is connected to the utility grid, but in islanded mode, it is not connected to the utility grid. The gap between the generation and load is the major problem to be addressed in both the modes. In grid-connected mode, power transfers between the microgrid and utility grid when there is more load demand. But in case of islanded mode, power is not transferred between utility grid and main grid as it acts as standalone. The power gap problem in islanded mode can be solved by implementing a proper control scheme [4].

The load frequency control is a challenging issue in microgrid. When the microgrid operating in grid-connected mode, the frequency of microgrid is regulated by utility grid. But in case of islanded mode, the frequency of microgrid can be regulated by distributed renewable energy sources like solar photovoltaic (PV) and wind. The researchers in [5] have described the maintenance of microgrid frequency using wind energy. Similarly, in [6], the authors have proposed frequency regulation of microgrid using solar power. In [7], the authors have proposed frequency regulation in autonomous microgrid by using wind, diesel, and distributed energy sources. In [8], the authors have proposed the frequency regulation of islanded microgrid using electric vehicles.

In olden days, for power generation, the larger synchronous machines are used that run on fossil fuels such as coal. But due to the alarming environmental conditions, the power generation from the renewables is increasing year by year. As per the International Renewable Energy Agency (IRENA) [9], the trends in the energy capacity of renewable energy sources (MW) from the year 2015 to 2020 are shown in Fig. 1. From Fig. 1, it can be seen that the there is a considerable increment in capacities year by year.

To interface the renewable energy sources to the microgrid, the power electronic converters are necessary. These inertia less power electronic converters can cause more frequency deviation in microgrid [10]. A control technique called virtual synchronous machine (VSM) is used to provide virtual inertia (*VI*) in microgrid [10, 11]. The concept of VSM is nothing but reproduction of the dynamic characteristics of real synchronous machine to the microgrid [11]. The *VI* property is nothing but controlling active power flow from energy storage devices to the grid. From the synchronous machines, the rotational inertia is available, whereas from the energy storage devices, the virtual inertia. Fini and Golshan [12] have presented the determination of optimal *VI* and frequency control parameters for frequency stabilization in microgrid. The *VI* effect along with storage system for stability improvement of microgrid was studied by Kerdphol et al. [13]. The frequency regulation issue with

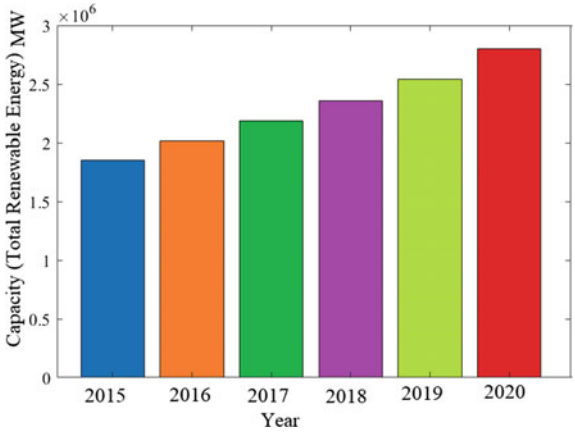

Fig. 1 Total renewable energy capacities, year wise

electric vehicles and *VI* is addressed in [11]. The electric vehicles as controllable loads can contribute to the frequency regulation [14, 15].

By observing the literature, it is seen that some studies have been attempted to include the solar-thermal renewable energy to the automatic generation control problem [16]. The concentrated solar power can store the energy in the form of thermal energy, and this can be used for electricity production in the absence of irradiance [16]. However, the solar-thermal system with EVs and *VI* for frequency regulation is not studied so far.

In literature, various studies have been applied to regulate the frequency in microgrid in the past. Maneesh in [17] has proposed the PI controller-based microgrid frequency regulation. In [18], the author proposed intelligent fuzzy PI controller for isolated microgrid comprising of EVs. The PID controllers, due to the simple structure and ease in maintenance, are still superior choice for most of the industrial/real-time applications.

To tune the controllers effectively, author in [17] utilized manual and Ziegler-Nichols methods. The tuning of PI controller was performed using Big Crunch algorithm (BBBA) [19]. The genetic algorithm (GA)-tuned PID controller is suggested for regulation of frequency in [20] by the researchers. In the present article, the firefly algorithm, a biologically evolved meta-heuristic optimization method, is proposed to tune the PID controller gains. The authors in [21] proved the superiority of firefly algorithm over particle swarm optimization, bacterial foraging algorithm, and artificial bee colony algorithm. Hence, owing to its superiority in this manuscript, firefly is implemented. The FA technique was developed by Yang [21, 22] which is based on flashing nature of the fireflies. The FA technique is not applied so far to retrieve the PID controller gains for microgrid system having solar-thermal, EVs, and diesel generator along with the *VI* mechanism.

The cost function used in this optimization is integral absolute error (IAE) given by Eq. (1).

$$J = \int_0^t |\Delta f| \mathrm{d}t \tag{1}$$

Owing to the above-mentioned discussion, the prime objectives of the present research are:

(a) To model an isolated microgrid (MG) system having diesel generator, solar-thermal, and EVs.
(b) To apply PI and PID controllers for regulation of frequency and to decide best between these.
(c) To extract the suitable gains of the controllers in (b) using firefly algorithm and to compare the system dynamics for step and randomized loads.
(d) To study the effect of increments in load demand on system frequency response.

2 System Investigated

The considered microgrid system is having diesel generator, solar-thermal, and electric vehicles. Five number of electric vehicles are used in the present study. For frequency regulation, the PID controller is employed. For effective regulation of the frequency in microgrid, the virtual inertia (*VI*) is incorporated in the system. The effect of *VI* is tested for step and randomized loads using FA-tuned PID controller subjected to Eq. (1). The implemented system and its Simulink model are given in Fig. 1. A separate controller is employed for virtual inertial system (Fig. 2).

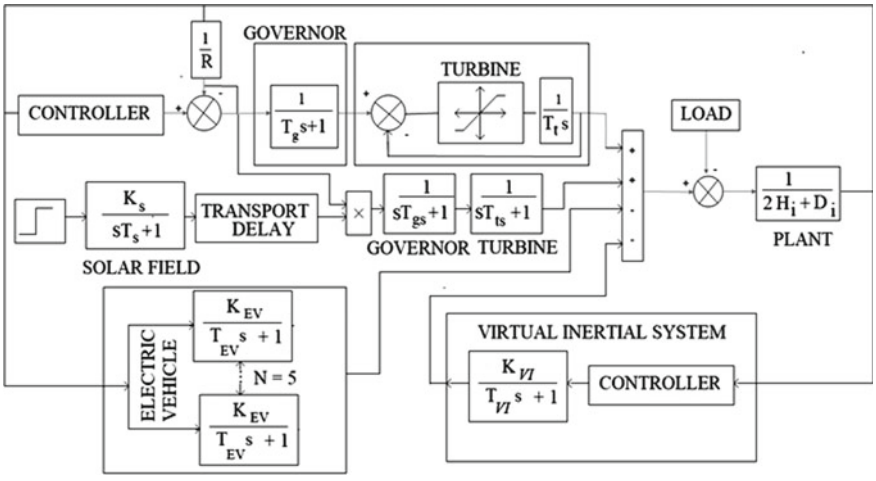

Fig. 2 Studied islanded microgrid system

Table 1 Parameters of islanded microgrid

Parameter	D (PU/Hz)	H (PU)	R (Hz/s)	T_g	T_t	$I_{inertia}$	$K_{inertia}$
Value	0.12	0.10 s	2.4	0.1 s	0.40 s	10	1.0
Parameter	K_P	T_{EV}	K_{EV}	T_{gs}	T_{ts}	K_S	T_S
Value	2.51	0.28 s	1.0	1 s	3 s	1.8	1.8 s

The renewable energy sources like wind, solar-thermal, etc., influence the system inertia if their penetration is high. To find the frequency deviation in microgrid, the frequency change rate function is using. So virtual inertia control also uses frequency rate function to calculate Δf. Based on this Δf, virtual inertia control block adds the necessary real power to set point of the islanded microgrid during high-level diffusion of renewable energy sources and in emergency conditions.

The frequency change rate (FCR) is calculated using the derivative control which is the main concept of the virtual inertia control.

$$\text{FCR} = \frac{\mathrm{d}}{\mathrm{d}t}(\Delta f) \tag{2}$$

The proposed microgrid system is supported by virtual inertia during the high deviation of frequency and high penetration of renewable energy sources.

$$\Delta P_{\text{inertia}} = \frac{K_{\text{inertia}}}{T_{\text{inertia}} s + 1}\left(\frac{\mathrm{d}}{\mathrm{d}t}\Delta f\right) \tag{3}$$

where T_{inertia} is the virtual inertia time constant for islanded microgrid and K_{inertia} is the gain of virtual inertia control in the islanded microgrid. The parameters of the microgrid system are given in Table 1.

3 Firefly Algorithm

In this paper, popularly known optimization technique named firefly optimization technique is used. It was developed by Yang [22, 23]. The firefly algorithm is a bio-inspired meta-heuristic algorithm that is inspired by flashing behaviors of fireflies. The following assumptions are made for FA:

i. Fireflies are attracted by themselves.
ii. Attractiveness is proportional to intensity.
iii. Less-intensity firefly is attracted to the brighter intensity firefly.
iv. As distance between two fireflies increases, the attractiveness toward other firefly decreases.
v. If intensity is similar for both fireflies, they move arbitrarily.

From the Law of Physics, it is identified that the intensity of light varies as inverse with square of distance.

$$\beta(r) = \beta_0 e^{-\gamma r^2} \tag{4}$$

where β_0 is the attractiveness at $r = 0$.

If a firefly is located at X_J and is brighter than other firefly situated at X_i, then firefly at X_i moves toward X_J.

The position updating of firefly is done by using Eq. (5).

$$X_i^{t+1} = X_i^t + \beta_0 e^{-\gamma r^2}(X_j^t - X_i^t) + \alpha(\text{rand} - 0.5) \tag{5}$$

where "t" denotes the iteration number, α denotes the randomization parameter with range [0, 1], β_0 denotes attractiveness at $r = 0$, and γ denotes parameter related to scaling L.

Here, the second term in Eq. (5) reflects the position change due to attractiveness. Similarly, the third term in Eq. (5) includes random movement parameter (α), and *rand* is a random number generator that is uniformly distributed in the range (0, 1). The FA flowchart is given in Fig. 3. The values of α, β_0, and γ are taken as 0.25, 0.2, and 1, respectively. The population count (n) is taken as 20 with iterations (T) as 500.

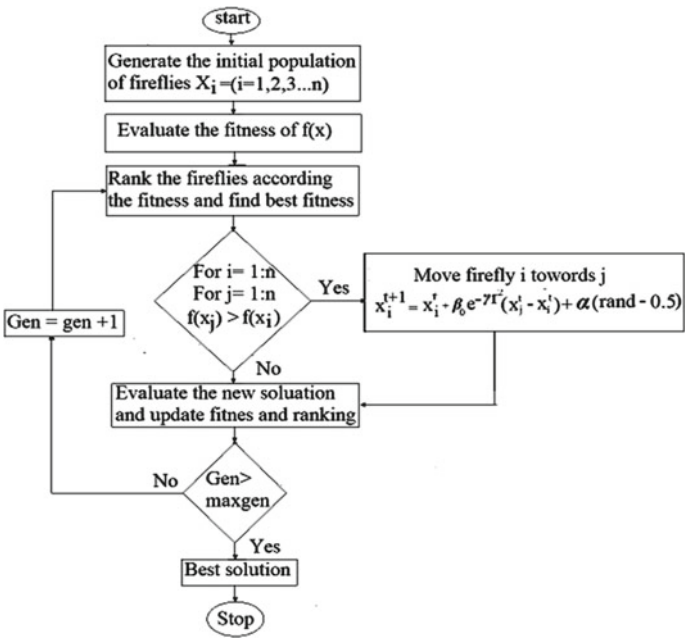

Fig. 3 Flowchart of firefly algorithm

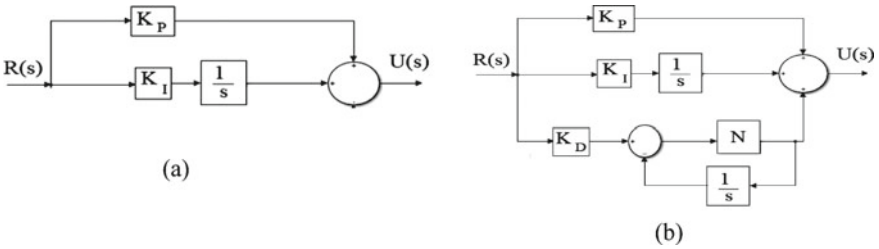

Fig. 4 Block diagram of PID controller

4 PI and PID Controllers

In this research, for frequency regulation in microgrid, PI and PID controllers are employed. Firefly algorithm is selected for tuning of PID parameters. The objective of tuning is that to obtain the optimal gains which will be robust for system uncertainties like load variations. The two- and four-term PI and PID controllers are taken for study (Fig. 4). The controller parameters K_P, K_I, K_D, and N denote the proportional, integral, differential, and filter constants. The first three constants are treated in the range of [0 1], and the last term is tuned within the range of [0 100] using FA constraining to Eq. 1. The PID transfer function in Laplace transform domain is given in Eq. (6).

$$\mathrm{TF_{PID}} = K_P + \frac{K_I}{s} + K_D \frac{N}{1 + \frac{N}{s}} \tag{6}$$

5 Results and Discussion

In this section, the islanded microgrid performance is tested with and without virtual inertia is analyzed and simulation results for the same are implemented/obtained using MATLAB software for step and randomized load demands.

5.1 Performance Evaluation of the Microgrid with PI and PID Controllers

In this scenario, the studied microgrid performance with the proposed control strategy is expounded with help of the PI and PID controllers. The FA-tuned PI and PID (FA-PID) controllers' gains obtained for without *VI* are given in Eqs. (7) and (8).

$$\mathrm{TF_{PI}} = 1.0000 + \frac{1.0000}{s} \tag{7}$$

$$\mathrm{TF_{PID}} = 0.5713 + \frac{0.8563}{s} + 0.2994\frac{65.673}{1 + \frac{65.673}{s}} \tag{8}$$

With the above firefly-tuned PI and PID controllers, the frequency variant is graphed in responses (Figs. 5 and 6). And also, their comparison is given in Fig. 7.

The following observations are made from Fig. 7. The peak overshoot, peak undershoot, and settling time are more in case of PI controller when compared to PID controller. So, by using PID controller, dynamics are superior. So, for remaining all scenarios, the preferable controller is PID (Table 2).

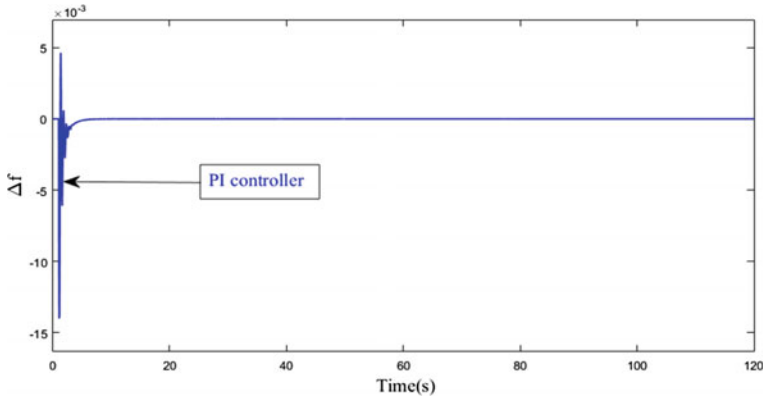

Fig. 5 Frequency regulation with PI controller

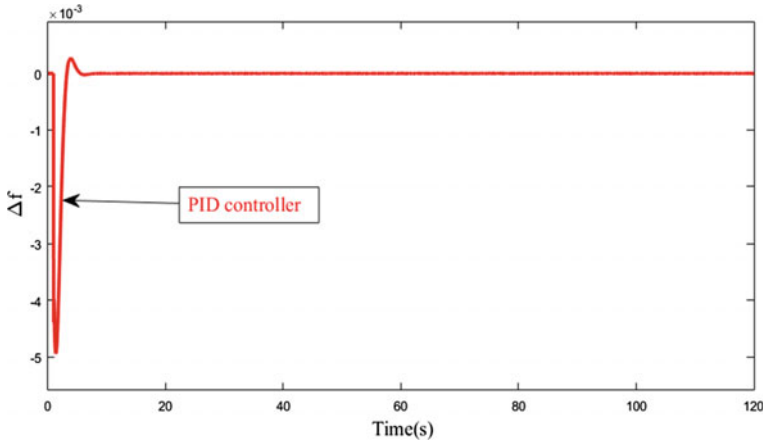

Fig. 6 Frequency regulation with PID controller

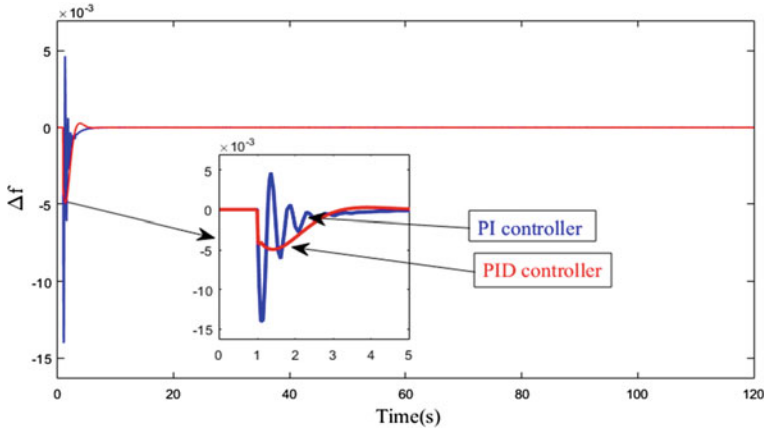

Fig. 7 Frequency regulation comparison with PI and PID controllers

Table 2 Comparison of performance indices for PI and PID controllers

Parameter	PI	PID
Peak overshoot	5×10^{-3}	0
Peak undershoot	14×10^{-3}	5×10^{-3}
Settling time (s)	5	3

5.2 *Performance Evaluation of the Microgrid with Step Load of 0.02 (PU)*

In this scenario, the studied microgrid system performance with the proposed control strategy is expounded with help of the step form of the load (Fig. 8) demand with and without virtual inertia (*VI*). The FA-tuned PID (FA-PID) controller obtained for with and without *VI* is given Eqs. (9)–(11).

$$\mathrm{TF_{PID}} = 0.5713 + \frac{0.8563}{s} + 0.2994\frac{65.673}{1 + \frac{65.673}{s}} \tag{9}$$

$$\mathrm{TF_{PID}} = 0.8722 + \frac{1}{s} + 0.0329\frac{28.8798}{1 + \frac{28.8798}{s}} \tag{10}$$

$$\mathrm{TF_{PID}} = 0.5038 + \frac{0.5308}{s} + 0.5377\frac{55.5308}{1 + \frac{55.5308}{s}} \tag{11}$$

With the above FA-PID controller, the frequency variant is graphed in responses (Figs. 9 and 10). And also, their comparison is given in Fig. 11. The following observations are made from Fig. 11. The settling time is 8 and 6 s for without and

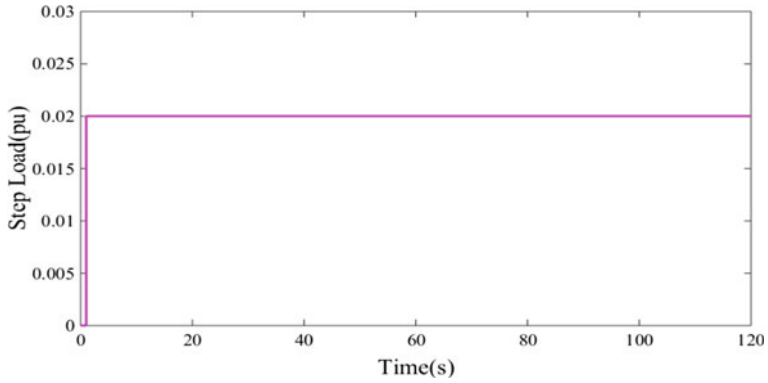

Fig. 8 Step load diagram

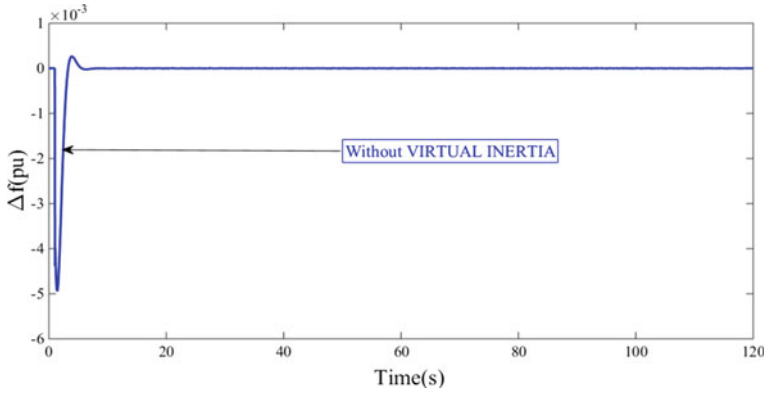

Fig. 9 Frequency regulation without virtual inertia

with *VI*. The value of maximum overshoot is 2.7×10^{-4} for without *VI* and is Nil with *VI*. Similarly, undershoots are found as 4.95×10^{-3} and 4.29×10^{-3} for without and with *VI*.

The performance measures such as peak overshoot, peak undershoot, and settling time for the scenario 2 are given in Table 3.

5.3 Performance Evaluation of Microgrid with Randomized Load

In this scenario, the randomized load as shown in Fig. 12 is treated as load for the system given in Fig. 1. Here also, the PID controller is tuned with FA, and the values and corresponding PIDs are given in Eqs. (12)–(14).

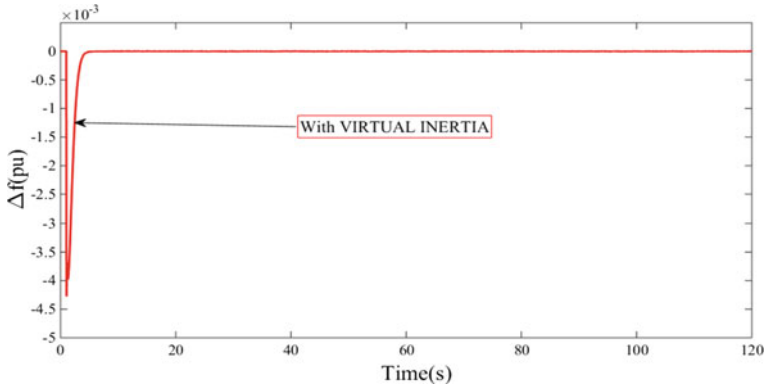

Fig. 10 Frequency regulation with virtual inertia

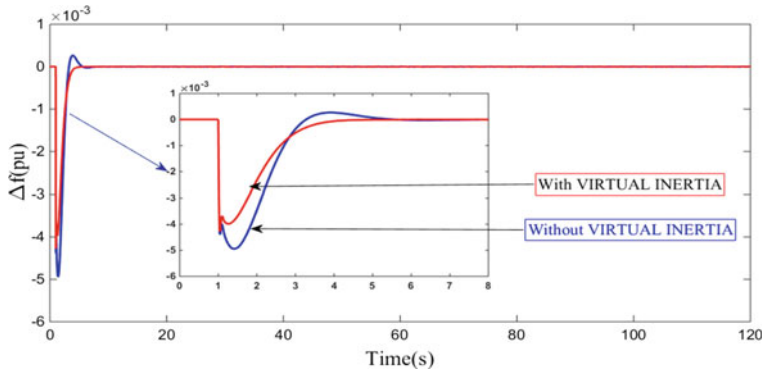

Fig. 11 Comparison of frequency regulation with and without *VI*

Table 3 Performance measures for step input of 0.02 PU

Name of parameter	Peak overshoot	Peak undershoot	Settling time (s)
Without *VI*	0	4.29×10^{-3}	6
With *VI*	2.7×10^{-4}	4.95×10^{-3}	8

$$\mathrm{TF_{PID}} = 0.7415 + \frac{1}{s} + 0.1566\frac{18.2858}{1 + \frac{18.2858}{s}} \tag{12}$$

$$\mathrm{TF_{PID}} = 0.9997 + \frac{1}{s} + 0.2256\frac{62.5040}{1 + \frac{62.5040}{s}} \tag{13}$$

$$\mathrm{TF_{PID}} = 0.8596 + \frac{0.2014}{s} + 0.6178\frac{71.5451}{1 + \frac{71.5451}{s}} \tag{14}$$

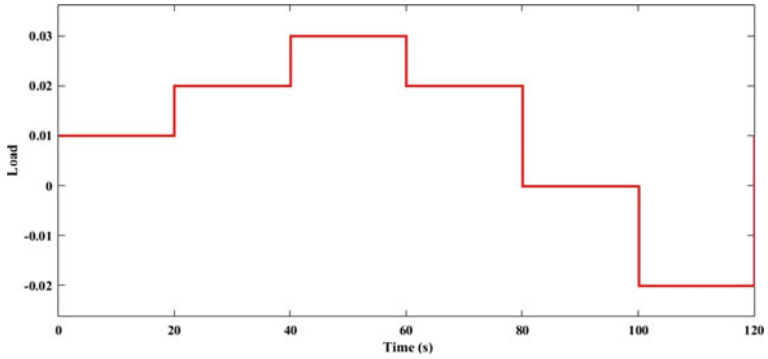

Fig. 12 Randomized load model

With the above FA-PID controllers, the deviated graphs of frequency are represented in Figs. 13 and 14 for without and with *VI*. The comparison of the above figures is made in Fig. 15. Keen observation in Fig. 15 reveals that without *VI*, the fluctuations are more in frequency when compared to without *VI*.

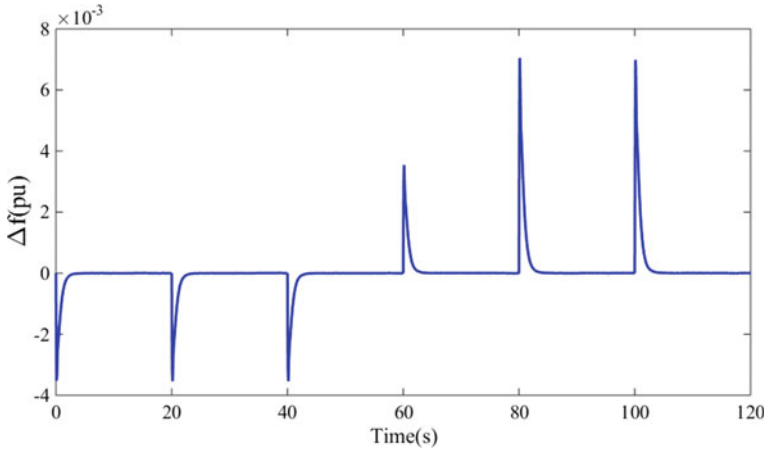

Fig. 13 Frequency regulation without virtual inertia for randomized load model

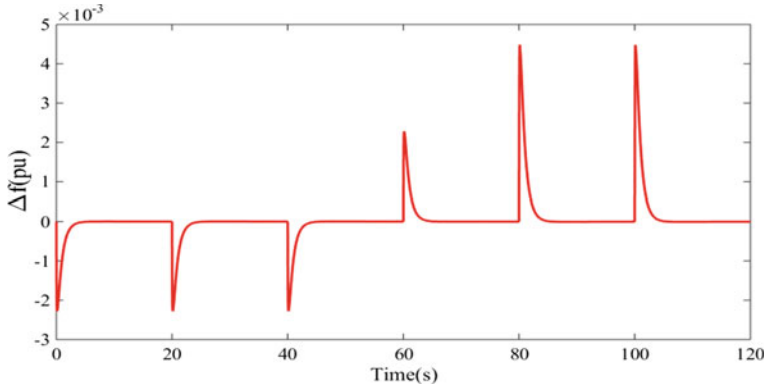

Fig. 14 Frequency regulation with virtual inertia for randomized load model

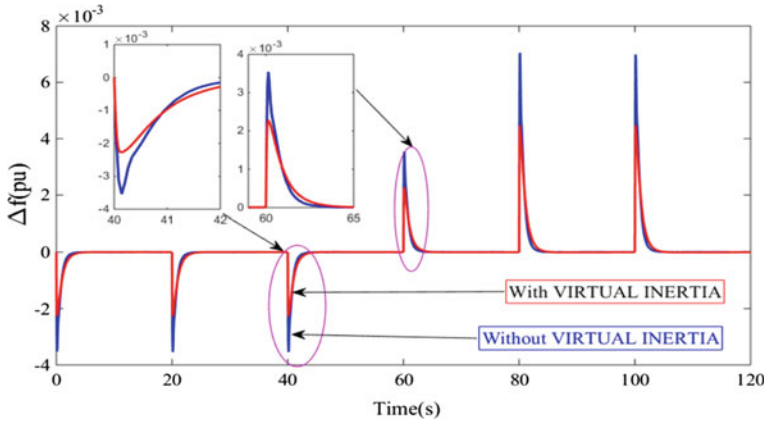

Fig. 15 Frequency regulation with and without virtual inertia for randomized load model

6 Case Studies

6.1 Increased Step Load Conditions

In this case, the studied microgrid system is examined with increased magnitude of load demand of 0.02 PU. In all the varied steps, the microgrid regulation performance is observed with and without *VI*. Equations (15)–(23) represent the PID controller gains for 0.04 PU, 0.06 PU, and 0.08 PU loads. Critical evaluation of the responses (Figs. 16, 17 and 18) confirms the superiority in the presence of *VI*.

$$\mathrm{TF_{PID}} = 0.8496 + \frac{1}{s} + 0.0619\frac{43.9615}{1 + \frac{43.9615}{s}} \tag{15}$$

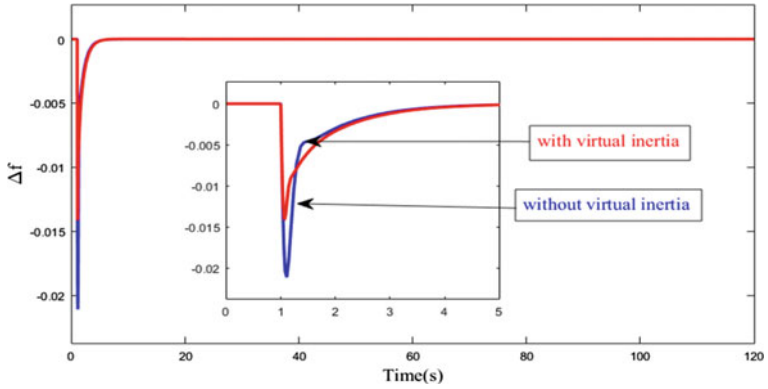

Fig. 16 Comparison of frequency regulation with and without *VI* for 0.04 PU load

$$\mathrm{TF_{PID}} = 0.9865 + \frac{1}{s} + 0.0495\frac{41.6359}{1 + \frac{41.6359}{s}} \tag{16}$$

$$\mathrm{TF_{PID}} = 0.8906 + \frac{0.3747}{s} + 0.3602\frac{53.9376}{1 + \frac{53.9376}{s}} \tag{17}$$

$$\mathrm{TF_{PID}} = 0.7466 + \frac{1}{s} + 0.0816\frac{63.3930}{1 + \frac{63.3930}{s}} \tag{18}$$

$$\mathrm{TF_{PID}} = 0.9132 + \frac{1}{s} + 0.2576\frac{57.2201}{1 + \frac{57.2201}{s}} \tag{19}$$

$$\mathrm{TF_{PID}} = 0.3523 + \frac{0.0686}{s} + 0.4525\frac{39.4415}{1 + \frac{39.4415}{s}} \tag{20}$$

$$\mathrm{TF_{PID}} = 0.8349 + \frac{1}{s} + 0.1007\frac{77.7241}{1 + \frac{77.7241}{s}} \tag{21}$$

$$\mathrm{TF_{PID}} = 0.9677 + \frac{1}{s} + 0.1229\frac{27.0657}{1 + \frac{27.0657}{s}} \tag{22}$$

$$\mathrm{TF_{PID}} = 0.2336 + \frac{0.2009}{s} + 0.3320\frac{29.9302}{1 + \frac{29.9302}{s}} \tag{23}$$

6.2 Variable Solar Field for with and Without Inertia

In this case, constant solar field of 0.01 PU which is considered earlier is replaced by variable solar field pattern as shown below in Fig. 19. With PID controller, the *VI*

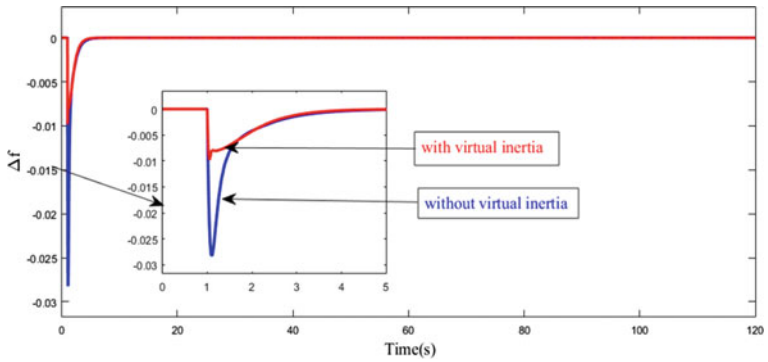

Fig. 17 Comparison of frequency regulation with and without *VI* for 0.06 PU load

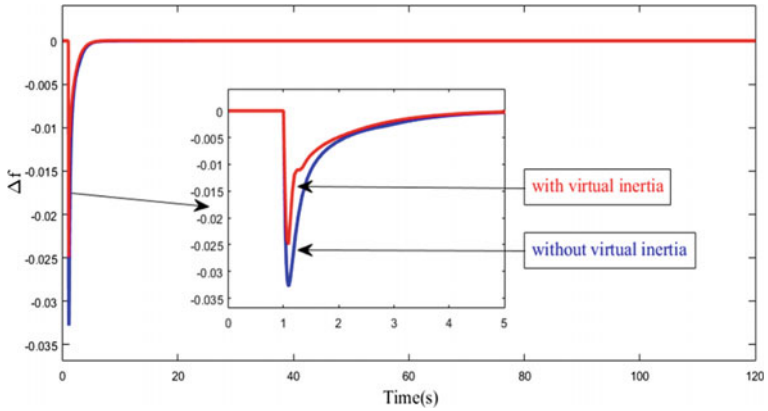

Fig. 18 Comparison of frequency regulation with and without *VI* for 0.08 PU load

importance is again shown. For this, the PID gains are obtained using FA technique with and without *VI*. The dynamics of the frequency responses are plotted in Fig. 20. The red-marked responses correspond to with *VI* and blue is for without *VI*. Critical observation of Fig. 20 reveals that when the load demand increases, the *VI* controls the dynamics effectively as it is restricting the oscillations to minimum than without *VI* case (Tables 4 and 5).

6.3 Sensitivity Study

This analysis is done to show how effective is the proposed PID controller parameters for wide variations in the time constant of solar-thermal turbine constant (T_{ts}). When the T_{ts} is changed by an increment of 50%, the frequency response is drawn and

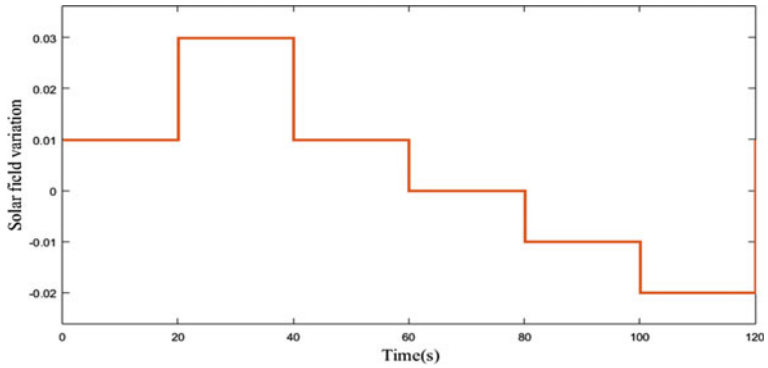

Fig. 19 Solar field variation

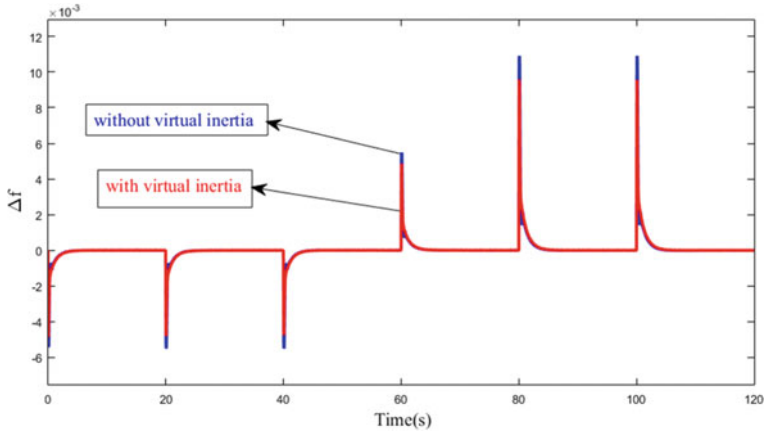

Fig. 20 Comparison of frequency with and without *VI* for variable solar field

Table 4 Undershoots' comparison for various cases

Step load (PU)	Peak undershoot		% improvement in undershoots
	Without *VI*	With *VI*	
0.04	22×10^{-4}	14×10^{-3}	57
0.06	29×10^{-3}	10×10^{-3}	190
0.08	33×10^{-3}	25×10^{-3}	32

compared with that of the unchanged T_{ts}. It is seen from Fig. 21 that these dynamics are more or less same (overlapping) which reveals the robustness against variations of T_{ts}.

Table 5 Cost comparison for various scenarios

S. No.	Case study	Solar field	Cost	
			Without *VI*	With *VI*
1	0.02	Constant (0.01)	0.0065	0.0051
2	0.04	Constant (0.01)	0.0100	0.0050
3	0.06	Constant (0.01)	0.0150	0.0099
4	0.08	Constant (0.01)	0.0201	0.0151
5	Randomized load	Constant (0.01)	0.0150	0.0148
6	Randomized load	Variable	0.0151	0.0148

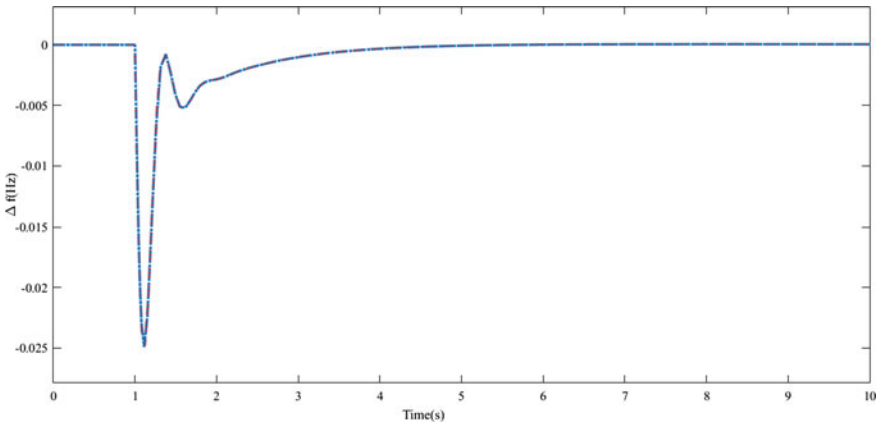

Fig. 21 Comparison of frequency with and without changed T_{ts}

6.4 Comparison of Performance Between PSO and FA Algorithms

The PID controller parameters are also optimized using particle swarm optimization. The optimized PID controller is as follows (Eq. 24).

$$\mathrm{TF}_{\mathrm{PID,PSO}} = 0.3656 + \frac{0.4348}{s} + 0.8708\frac{0.0906}{1 + \frac{0.0906}{s}} \tag{24}$$

The cost obtained with PSO is 0.0388 while with FA is 0.0065. With FA-PID, the cost value is less which is superior to that of PSO-PID controller. Here, the N value is restricted between [0 1].

7 Conclusion

In this research, we performed the frequency regulation of an islanded microgrid with help of PID controller whose parameters are tuned with FA. The step and randomized load cases are taken for assessment with and without considerations of the virtual inertia, *VI*. The regulation of frequency is found more effective when *VI* is considered for both step and randomized loads. The cost is also found less when *VI* is integrated into the microgrid system. Interestingly, it is observed that when the constant pattern of load incremented in magnitudes, the dynamics are well in control with *VI* incorporation. A special case study in regard to the randomized solar field reveals that in the presence of *VI*, the system dynamics are superior without *VI*. Future research may use more sophisticated controllers which can be tuned using newly proposed optimization methods. And also, more additional number of generations can be added to the system to draw more realistic microgrid performance. It is also worthwhile to incorporate the energy storage technology into the proposed microgrid in the future.

References

1. P.K. Ray, A. Mohanty, A robust firefly swarm hybrid optimization for frequency control in wind/PV/FC based microgrid. Appl. Soft Comput. **85**, 105823 (2019)
2. M.H. Saeed, A review on microgrid challenges & perspectives. IEEE Access **9**, 166502–166517 (2021)
3. E. Hossain, Microgrid testbeds around the world: state of art. Energy Convers. Manag. **86**, 132–153 (2014)
4. D. Kanakadhurga, N. Prabaharan, Demand side management in microgrid: a critical review of key issues and recent trends. Renew. Sustain. Energy Rev. **156**, 111915 (2022)
5. K.J. Bunker, W.W. Weaver, Microgrid frequency regulation using wind turbine controls, in *Power and Energy Conference at Illinois* (2014), pp. 1–6
6. L.D. Watson, J.W. Kimball, Frequency regulation of a microgrid using solar power, in *Twenty-Sixth Annual IEEE Applied Power Electronics Conference and Exposition* (2011), pp. 321–326
7. L. Bhukya, Robust frequency control in a wind-diesel autonomous microgrid: a novel two-level control approach. Renew. Energy Focus **36**, 21–30 (2021)
8. P. Li, W. Hu, X. Xu, Q. Huang, Z. Liu, Z. Chen, A frequency control strategy of electric vehicles in microgrid using virtual synchronous generator control. Energy **189**, 116389 (2019)
9. *Renewable Electricity Generation Country Ranking 2019* (Int. Renew. Energy Agency, Abu Dhabi, United Arab Emirates, 2019)
10. V. Thomas, S. Kumaravel, S. Ashok, Reduction of frequency oscillations in solar PV microgrid using virtual synchronous machine, in *International Conference on Power Electronics Applications and Technology in Present Energy Scenario* (2019), pp. 1–5
11. H. Abubakr, T.H. Mohamed, M.M. Hussein, J.M. Guerrero, G.A. Tinajero, Adaptive frequency regulation strategy in multi area microgrids including renewable energy and electric vehicles supported by virtual inertia. Int. J. Electr. Power Energy Syst. **129**, 106814 (2021)
12. M. Hajiakbari, M.E.H. Golshan, Determining optimal virtual inertia and frequency control parameters to preserve the frequency stability in islanded microgrids with high penetration of renewables. Electr. Power Syst. Res. **154**, 13–22 (2018)

13. T. Kerdphol, M. Watanabe, Y. Mitani, V. Phunpeng, Applying virtual inertia control topology to SMES system for frequency stability improvement of low-inertia microgrids driven by high renewables. Energies **12**, 3902 (2019)
14. M.H. Khooban, T. Niknam, F. Blaabjerg, T. Dragicevic, A new load frequency control strategy for micro-grids with considering electrical vehicles. Electr. Power Syst. Res. **143**, 585–598 (2017)
15. H.M. Hasanien, A.A.E. Fergany, Salp swarm algorithm-based optimal load frequency control of hybrid renewable power systems with communication delay and excitation cross-coupling effect. Electr. Power Syst. Res. **176**, 105938 (2019)
16. Y. Sharma, L.C. Saikia, Automatic generation control of a multi-area ST—thermal power system using Grey Wolf Optimizer algorithm based classical controllers. Int. J. Electr. Power Energy Syst. **73**, 853–862 (2015)
17. Maneesh, Frequency control of a microgrid by using PI controller, in *International Conference on Energy, Power and Environment Towards Sustainable Growth* (2015), pp. 1–5
18. M.U. Jan, A. Xin, M.A. Abdelbaky, H.U. Rehman, S. Iqbal, Frequency regulation of an isolated micro-grid integrated with electric vehicles using adaptive and fuzzy PI controllers, in *The 16th IET International Conference on AC and DC Power Transmission*, vol. 8 (2020), pp. 87621–87632
19. M. Sedighizadeh, M. Esmaili, A.E. Moarref, Voltage and frequency regulation in autonomous microgrids using Hybrid Big Bang-Big Crunch algorithm. Appl. Soft Comput. **52**, 176–189 (2017)
20. A. Singh, Sathans, GA optimized PID controller for frequency regulation in standalone AC microgrid, in *2016 7th India International Conference on Power Electronics* (2016), pp. 1–5
21. S. Debbarma, L.C. Saikia, N. Sinha, Robust two-degree-of-freedom controller for automatic generation control of multi-area system. Int. J. Electr. Power Energy Syst. **63**, 878–886 (2014)
22. X.S. Yang, *Nature Inspired Met Heuristic Algorithms* (Luniver Press, UK, 2008)
23. X.S. Yang, Firefly algorithm for multimodal optimization, in *Stochastic Algorithms: Foundations and Application*, Lecture Notes on Computer Science, vol. 5792 (Springer, 2009), pp. 169–178

A Report on Multi-agent System Application in Power System

Subhranshu Sekhar Puhan, Renu Sharma, and Saumya Ranjan Lenka

Abstract This paper presents different ways in which Multi-Agent Systems (MAS) can be applied in power systems. This paper provides following details (a) outlines regarding fundamental concept of MAS, (b) How the multiagent system can be approached? and (c) How MAS technologies can be utilized in solving the complexities in the operation of this evolving power system. This paper also describes the specific applications which are already existent and technical challenges that need to be addressed for upgrading the MAS technology.

Keywords Multi-agent system (MAS) · Phasor measurement unit (PMU) · Remote terminal unit (RTU)

1 Introduction

The definition of agent used above is problematic in terms of power engineering; this is because it does not differentiate the agents from existing software or hardware systems. Under such definition, some of the existing elements in the power system can come under agents, like protection relay. It can be called an agent according to the above definition, because it also reacts to changes in the atmosphere of transmission lines, automatically as per the condition of the atmosphere. There is no benefit in renaming such existing technologies as protection relays as agents because there is nothing new gain to technology in naming like that. According to [1], 'An agent is meant to be a tool for analyzing systems.' Therefore, instead of saying 'agent,' the term 'intelligent' agent is proposed, just to distinguish the agent from an existing system (such as protection relays). According to [2], an agent, which

S. S. Puhan · R. Sharma · S. R. Lenka (✉)
Department of Electrical Engineering, ITER, SOA Deemed To Be University, Bhubaneswar, India
e-mail: saumyaranjanlenka@gmail.com

S. S. Puhan
e-mail: subhranshusekharpuhan@soa.ac.in

R. Sharma
e-mail: renusharma@soa.ac.in

© The Author(s), under exclusive license to Springer Nature Singapore Pte Ltd. 2023

K. Murari et al. (eds.), *Soft Computing Applications in Modern Power and Energy Systems*, Lecture Notes in Electrical Engineering 975,
https://doi.org/10.1007/978-981-19-8353-5_9

displays flexibility in its automatic decision-making to changes in atmosphere, is called an intelligent agent. Such an agent has the following characteristics:

1. According to the goals the agent is required to achieve, an intelligent agent must be able to react to the changes in the atmosphere in which it is situated, at the appropriate time.
2. Pro-activeness: Pro-activeness means the ability of an agent to take the initiative [2].

Therefore, an intelligent agent must be able to take the initiative from itself whenever the system is behaving out of way. For example, if agent-1 needs to fulfill some services of agent-2 in order to achieve its goal (of agent-1), and at some time suddenly it loses communication with agent-2, then agent-1 has to automatically initiate itself to establish a connection with other agents in the same atmosphere, thus get information from them so as to fulfill its services associated with agent-2. Thus, overall agent-1 is then known as goal directed.

An intelligent agent is supposed to interact with other agents, not simply bypassing data, but by their ability to interact and negotiate very cooperatively. That ability is possible by Agent Communication Language (ACL) [3–5], which allows agents to converse rather than just passing of data between them. Thus an agent must have reactivity, at least some form of pro-activeness and social ability, if not everything is perfect, in order to term that agent as an intelligent agent. A system consisting of one or more such intelligent agents is known as a 'Multi-Agent System.' Thus in a Multi-Agent System, we can see that there are only the local goals of each intelligent agent but the not overall goal of that system. And, the application of Multi-Agent Systems can only be realized by the system designer by introducing multiple such intelligent agents with their local goals. An example of this system is shown in Fig. 1, Here, we see a number of loads, distributed generators (DG), switches (SW), circuit breaker (CB), and transformers (TR) give their information to the intelligent agents, which in turn take decision with the help of provided database (DB), and thus provide an interface to the user or equipment desired by the user.

The rest of the paper is arranged as follows: in Sect. 2—the basic ways of application of MAS in power systems are described, and Sect. 3 deals with MAS application in a real-life situation. Sections 4 and 5 deal with the matured application of MAS and technical challenges in MAS in the present-day power system.

2 Basic Ways of Application of MAS in Power System

In order to know how MAS can be made use so as to apply it best in power systems, it is required to understand the basic ways in which MAS can be made use. MAS can be made used in two ways of approaches: It can be used as an approach to the construction of flexible, extensible, and robust systems and a modeling approach. Something robust means strong enough to withstand or overcome intellectual challenges. The term 'robust' in this context can be understood as the ability to withstand

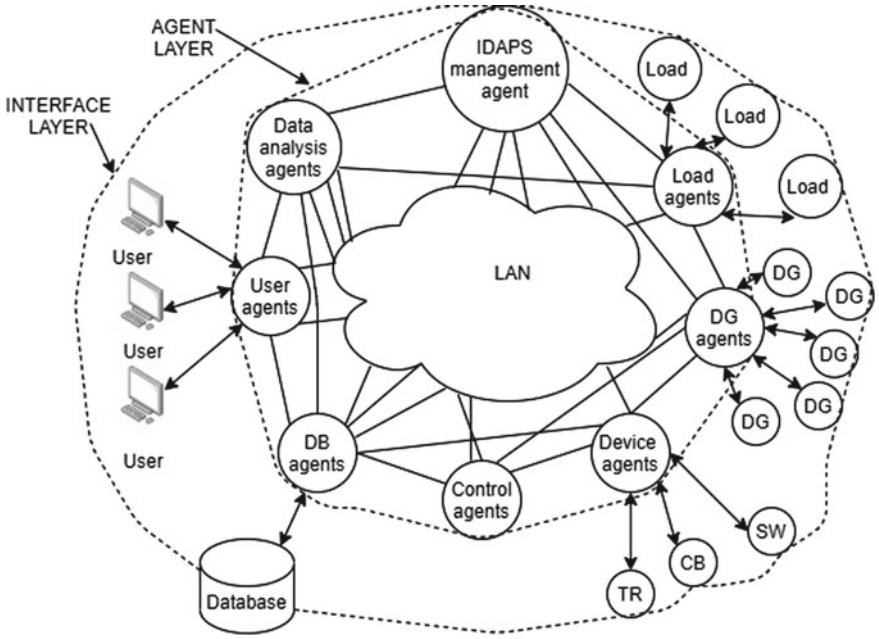

Fig. 1 Basic MAS architecture [6]

the major changes in the system or atmosphere. Secondly, the term 'flexibility' means the ability of the same topology of MAS to support various situations in the same or different atmosphere. That also means the ability to respond to various dynamic changes in the system. It must be noted that the automatic action of an agent is different from the flexibility of an agent: Being automatic means the ability of the agent to schedule its actions, and flexibility means choosing one possible action in a number of such actions (which is best). Thirdly, extensibility means the ability of a system to easily add a new function to the existing system. It can be either appending to the original system or upgrading the original system. An example for appending is that of the condition monitoring system, on which a new sensor can be introduced, and thus, new data analysis is to be added. An example for upgrading is that of the state estimation system, where a faster load flow estimation algorithm can be introduced to upgrade the older one. Along with the construction of such robust, flexible, and extensible systems in power engineering, there is also a need for fault tolerance in the system and also need the ability of the system to meet the design objective if part of the system fails. Thus, Multi-Agent Systems have the capability to provide a way to build such systems, with all the above-discussed characteristics.

The properties of Multi-Agent Systems that produce the above qualities are:

1. **First Property: Agent Encapsulation and Self Decision making**: In fact, an agent capsulizes, i.e., condenses a task or set of functions, in a way similar to object-oriented programming or modular programming. Thus, Multi-Agent

Systems also have standard interfaces and information hiding tools, by use of standard Agent Communication Language (ACL), with the additional capability of automatic and flexible action. In object-oriented programming, external signals call a function that the module is bound to execute and does not have any other choice. But in agent programming, external signals give messages to the agent, but the agent has the choice of which one to execute, which is helpful in case of the agent receiving many requests at the same time. Thus, more flexible and extensible systems are provided by agents. Thus, agent programming provides the functionality for messaging and service location, which means that new agent integration and communications are handled without effort from the system designer.

2. **Open MAS Architectures**: Earlier, the system architectures are closed architectures. Closed architecture means new agents cannot be added to that system, and even if new agents are added, other agents cannot access or locate it or communicate it. Thus, a closed architecture has no possibility of being extensible and flexible. But, open architectures do allow flexible communication with an agent. This is possible by all agents sticking to the same standards of messaging. Thus, there has to be a common messaging language for inter-agent communication. There is such a set of standards for an open architecture defined by the Foundation of Intelligent Physical Agents (FIPA) [3]. The FIPA standards cover the framework within which FIPA agents exist. Thus, these standards define standards for not only communicating with agents but also creating, locating, and removing the agents. This is called an agent platform. The second requirement is to locate agents within the particular platform. Under FIPA standards, this is achieved through a separate agent called the directory facilitator, which manages a searchable list of services offered by other agents within the platform.
3. **Third Property: Single Platform for Distributed Systems**: One agent, situated in one atmosphere, must be able to achieve its goals and abilities in different atmospheres also. Nevertheless, that particular atmosphere impacts the actions which the agent takes. In practical systems, this property of the distribution of agents which generally don't have a fixed atmosphere is supported by the agent platform. This platform is run on every computer that invites agents into the system.
4. **Fourth Property: Fault Tolerance**: Fault tolerance means tolerance to faults in agent or agent communication. To make the Multi-Agent System fault tolerant, one of the basic approaches is redundancy. Thus, redundancy here means proving other duplicate agents for one agent. Thus if agent-1 requires service from agent-2, and agent-2 fails, agent-1 can take the help of the duplicate agent-2 using the directory facilitator mentioned above. This property of fault tolerance is fault specific, and therefore may not be obtained simply by duplication of agents. However, the open MAS architecture discussed before is automatically faulted tolerant if designed with good social ability.

3 MAS as an Approach to Modeling Real-Life Situations

Multi-Agent Systems can be made use, not only as construction of robust, flexible, and extensible systems in power engineering but also can be made use as an approach to modeling any given system by giving a way to view the real-life situations. An agent system can also be represented as a real-world situation with interacting entities; thus, the MAS system can be helpful in viewing how complex the real-world situations can emerge. In the various power system area viz. power system dynamics of generators and control etc. such kind of realizations are possible. Generators have a degree of automatic control by Automatic Voltage Regulators (AVRs), and they can be indirectly affected by external systems. Thus, they can be represented by different agents to model the generator system. Thus, Multi-Agent Systems offer very appreciable approaches for modeling and analyzing the power system. Therefore, many of the applications, like real-time planning, decision-making, control of equipment, simulation, and modeling, can make use of Multi-Agent Systems for increased efficiency. The two main approaches by which the Multi-Agent System can be intelligently applied in power systems are described in the above discussions. The applications of power systems that display the following characteristics are best suited for fields in which MAS can be applied:

1. When there is a need for frequently implementing new functions within the existing systems (like existing plant items or control systems). For example, implementing newer and newer algorithms or functions in a numerical relay for different protections like out-of-step protection or power system blocking.
2. When there is a need for interaction between the control stations or any distinct conceptual entities. For example, controlling the microgrid where the control subsystem must take its inputs from voltage for voltage control at different stations and renewable energy stations as well.
3. When there is the involvement of a large number of entities and interaction among them, where it is not possible to model the overall behavior of the system. For example, simulating the energy marketplace in which every generator, every system operator, and the customer has to be modeled. Without the need for communication with the central point, enough data is available at any substation locally to take any decision (by agents). For example, monitoring of transformer internal as well as incipient faults, at a particular substation for which local data is sufficient for handling.
4. When there is a need for functionality to be added in the existing system, continuously over a period of time. For example, management of different assets in the power system using real-time condition monitoring of the system. In accordance with the above characteristics, there can be many fields in which MAS can be applied, out of which few are described below.

4 Matured Applications of MAS in Power Systems

Adding to the above-mentioned applications of Multi-Agent Systems in power systems, the MAS technology also has the potential for several other diverse range of applications in the area of power systems. Few of such applications which reached the maturity of application are Control of microgrid, Protection Engineering Diagnostic Agents (PEDA), and Intelli TEAM II (commercial product) [7]. National Technical University of Athens (NTUA) developed the application of agents in control of microgrids [1]. The physical demonstration of this system using agents has been employed successfully on a test electrical network. University of Strathclyde developed PEDA for making the analysis of power system data automatic. This system was not only developed in laboratory but also at the utility successfully; pointing that MAS technology has become mature enough to achieve significant industrial applications. All these matured applications are explained briefly as follows.

A. **PEDA**

The PEDA system is created for post-fault analysis. It uses, not only SCADA, but also digital fault recorder (DFR) data, for analysis. What mainly PEDA does is that, it integrates many of the intelligent agents in MAS, and finally draws conclusions of the system, at the same time communicating with other agents for useful information through FIPA communication standards. It uses expert system to identify the key information such as fault occurrence and clearance times and the type of fault or generator tripping. The information from different agents is collected using an agent named collation agent, and finally conclusion is provided to an engineer, through an agent named engineering assistant agent. Using PEDA system led to significant advancements in techniques to achieve maintainability and stability. The main advantages lies in MAS structure, incorporating Protection Engineering diagnostic agents integrates supervisory data acquisition system along with digital fault recorder data. With inclusion of digital fault recorder, the protection engineer will get the fault data and fault behavior in a very short span of time but to design such a sophisticated integration system is quite cumbersome task [8].

B. **COMMAS**

The condition Monitoring Multi-Agent System (COMMAS) [9] is developed for the purpose of fault diagnosis in the plant items such as transformers. It was essentially applied in transformer condition monitoring system, after initial implementation in gas turbine start up sequence. For example, monitoring of Partial Discharge in transformer. Partial Discharge gathered through sensors and fed into feature extract agent [10], and diagnosis agents use feature extract agents for classifying the defect as Partial Discharge. The information of all the agents was collected by corroboration agent, and finally information agent provides the conclusion to the engineer. Because the agents located at different locations through the DF, extra diagnosis agents could be added to the system and their

diagnoses were smoothly collected by the Corroboration Agent, this approach was used for extensible system development. The integration of PEDA system and COMMAS has been discussed in detail manner [11] for increased benefits to the system operator. With inclusion of condition monitoring features in the COMMAS architecture, early diagnosis of faults is quite easy. With inclusion of COMMAS feature, there are several features added in conventional MAS structure like cross sensor corroboration, data fusion, incorporation of more than one computational intelligent system techniques in the system [12].

C. **SPID**

In power system, there are few events which make the system vulnerable to cascaded tripping of huge generators and black out, if they take place. In order to discover and resolve those events and hidden failure components that can leave the system prone to cascading events [13], the Strategic Power Infrastructure Defense (SPID) System was developed using MAS. In SPID, the agents were arranged in different layers depending on the influence of the event on occurrence of cascaded events [14]. Finally, signal for reconfiguring the network or generating a restoration plan after an incident is given to the engineer. For practical industrial solution, robust tools for implementation of SPID are very essential. By incorporating MAS technologies, SPID system is able to assess power system vulnerability, monitor hidden failures for protective devices to work upon, and more over it provides adaptive control action with preparedness for any catastrophic failures. The main disadvantages of SPID system are that the adaptive control action depends on machine learning capabilities.

D. **Intelli TEAM II**

Intelli TEAM II Automatic Restoration System [15] was produced by S&C company in order to determine and execute the restoration plan after isolation of faulted segment of the line. This is made possible by communication with agents responsible for the faulted segment of line. The intelligent agents in this system have power to control switches and reclosers of faulted segment, but controlling is only done after confirmation with the neighboring agent. This system was implemented with the ENMAX Power Corporation in Canada.

E. **Power Matcher**

In constrained networks, an agent-based solution to demand side management is developed as a commercial product named Power Matcher. Its main objective is to dynamically match supply and demand in local area, through an open market. Power Matcher has been deployed in more than three field systems and is in the advanced stages of field testing, confirming that Power Matcher can perform its required tasks in practical system. The Power Matcher phase of MAS structure determine the idea about the demand and supply side of electricity market. By utilizing the power matcher we can easily predict the power market behavior. But the only drawback of this power matcher is that it is only suitable for small

and medium sized market and is not fit for predicting the behavior of large-sized market.

F. **AuRA-NMS**

The objective of Autonomous Regional Active Network Management System (AuRA-NMS) is to include multiple techniques to operate distribution networks efficiently. The decision-making for voltage control, network optimization, and power flow management is made automatic using agent technology as an integral part for these techniques.

G. **Smart Grid**

On the other hand, the MAS technology can be best made use of in the Smart Grids [16, 17], allowing flexibility in the complex system. There is need to allow different objectives like as voltage regulation, power flow management, and automated restoration within the smart grid management system. Also care should be taken that actions taken to meet one objective should not negatively impact another objective unless intentionally done. Multi-Agent Systems aim to fulfill many features, making agent technology substantial for delivery of smart grid capability. Multi-Agent Systems in distributed smart Grid is discussed in [10]. Besides the above mentioned applications, there are still ongoing researches in many other areas of power systems like relay coordination using JADE [14, 18], especially the smart grid. The progress of Multi-Agent Systems in the practical industrial application is briefly described in this section, showing that this technology can help solving the complex industrial problems in power systems. Thus, this technology is progressing toward robust industrial implementations.

H. **Demand Response**

Demand response (DR) is a change in the way energy is consumed by the client of may be an electricity company, as energy demand is better adjusted to the offer. DR is a way to respond to cases of maximum energy demand so that users can be restricted from accessing all or part of their network energy consumption when they are asked to do so. MAS structure as discussed in [19, 20] applied to model the electricity markets and in [21] MASCEM structure is used to model the irregulated power systems. Even some of the researchers also started using MAS with basic learning systems for the modeling of market in power system. With inclusion of basic learning system, the modeling of power system market will be quite easier and comprehensive to access idea about demand response [22].

5 Technical Challenges in Application of MAS

Different applications and potential benefits of MAS technology have been addressed in the before sections. Along with this, it is worthy to identify the important challenges that need to be overcome for most efficient use of MAS. These key challenges are

1. Security: Because the agents are distributed throughout, the security has to be taken care of. There must be sufficient tools to measure the level of trust in case a new agent smoothly joins the agent community without prior permission. For example, only limited services can be offered to agents from competitor utility, giving then the lower trust rating.
2. Design of Intelligent agent: There is a need to train the industrial implementers and new researchers on the knowledge of agents, how the agent should be designed and the available options to design. There are different strategies that give rise to agents with varying degrees of pro-activeness, social ability and reactivity. All these strategies must be well equipped by the new researcher to design a system of intelligent agents, so that they may be suitable for applications in power systems.
3. Toolkits: In power systems, there is need to reuse the existing agent designs and functionality, to stick on to the specific standards for agents. Thus, the role of toolkits, which facilitate the reuse of existing agent capabilities and behavior, is very vital. There is need for such toolkits to be developed.
4. Agent knowledge domain and communication languages: The social ability of agents is only possible if there is common communication language. How an agent exchanges information, communicates, or negotiates is dependent on the Agent Communication Language. The Foundation for Intelligent Physical Agents (FIPA) [3, 16] has set the international standards for communication languages and protocols. Therefore, there should be agreement within the community to adopt appropriate communication languages for agents, so that all the agents are able to cooperate and interoperate.
5. Necessity for common platform: Because there are many platforms in which any agent can exist, it is extremely important for all the agents to exist on one standard platform. This is necessary for agents to interact with each other in a flexible and extensible manner. It is also prime necessary to develop an open architecture.

Keeping aside the applications and technical uses of MAS described above, due to the fact that use of Multi-Agent Systems is new to industry, and because lack of experience of engineers, there is a worry for both manufacturers and utilities to consider the Multi-Agent System solutions. But putting MAS solutions into practice is a significant step in power systems, because it increases reliability and robustness of the system. With the proper communication and by training the operators and researcher from industry regarding the operation of MAS Technology (condition of operation and failure of MAS Technology) power system could be made more reliable and robust.

6 Conclusion and Future Scope

The paper came out with different characteristics of MAS which facilitate its use in power systems. The discussion is made here in about the basic applications of MAS in different areas like power system monitoring, fault diagnostics, modeling and simulation, system protection, and possibility of distribute dc control. The specific applications of MAS in power systems, namely PEDA, COMMAS, SPID, Power Matcher, Intelli TEAM II, and AuRA-NMS were also discussed in brief, thus describing the practical benefits derived from MAS. However, many different areas of research are still in progress in order to increase the flexibility and degrees of freedom of control of complex systems. Moreover, industrial applications and demonstrations should be encouraged in order give a way for further advancements in Multi-Agent System Technology.

References

1. S.D.J. McArthur et al., Multi-agent systems for power engineering applications—Part I: Concepts, approaches, and technical challenges. IEEE Trans. Power Syst. **22**(4), 1743–1752 (2007)
2. K. Hopkinson et al., EPOCHS: a platform for agent-based electric power and communication simulation built from commercial off-the-shelf components. IEEE Trans. Power Syst. **21**(2), 548–558 (2006)
3. S.D.J. McArthur et al., Toward a model integration methodology for advanced applications in power engineering. IEEE Trans. Power Syst. **18**(3), 1205–1206 (2003)
4. S. Sheng et al., Agent-based self-healing protection system. IEEE Trans. Power Deliv. **21**(2), 610–618 (2006)
5. D.V. Coury et al., An agent-based current differential relay for use with a utility intranet. IEEE Trans. Power Deliv. **17**(1), 47–53 (2002)
6. Multi Agent System of a Smart Grid. http://www.itee.uq.edu.au/pssl/drupal7withinnTheme/?q=node/358
7. S&C Electric Company (2007). http://www.sandc.com/products/Energyline/IntelliTEAM
8. E.M. Davidson, S.D.J. McArthur, J.R. McDonald, T. Cumming, I. Watt, Applying multi-agent system technology in practice: automated management and analysis of SCADA and digital fault recorder data, in *2006 IEEE Power Engineering Society General Meeting* (2006), p. 1. https://doi.org/10.1109/PES.2006.1708863
9. R. Giovanini et al., A primary and backup cooperative protection system based on wide area agents. IEEE Trans. Power Deliv. **21**(3), 1222–1230 (2006)
10. V.M. Catterson, E.M. Davidson, S.D.J. McArthur, Practical applications of multiagent systems in electric power systems. Eur. Trans. Electr. Power **22**(2), 235–252 (2012)
11. V.M. Catterson, E.M. Davidson, S.D.J. McArthur, Issues in integrating existing multi-agent systems for power engineering applications, in *Proceedings of the 13th International Conference on Intelligent Systems Application to Power Systems, 2005* (IEEE, 2005)
12. E.E. Mangina, S. Mcarthur, J.R. Mcdonald, COMMAS (COndition Monitoring Multi-Agent System). Auton. Agent. Multi-Agent Syst. **4**, 279–282 (2004)
13. C.-C. Liu et al., The strategic power infrastructure defense (SPID) system. A conceptual design. IEEE Control Syst. **20**(4), 40–52 (2000)
14. H. Wan, K.P. Wong, C.Y. Chung, Multi-agent application in protection coordination of power system with distributed generations, in *2008 IEEE Power and Energy Society General*

Meeting—Conversion and Delivery of Electrical Energy in the 21st Century (2008), pp. 1–6. https://doi.org/10.1109/PES.2008.4596261
15. D.M. Staszesky, D. Craig, C. Befus, Advanced feeder automation is here. IEEE Power Energy Mag. **3**(5), 56–63 (2005)
16. Z. Yahouni, A. Ladj, F. Belkadi, O. Meski, M. Ritou, A smart reporting framework as an application of multi-agent system in machining industry. Int. J. Comput. Integr. Manuf. **34**(5), 470–486 (2021)
17. W. Khamphanchai, S. Pisanupoj, W. Ongsakul, M. Pipattanasomporn, A multi-agent based power system restoration approach in distributed smart grid, in *2011 International Conference & Utility Exhibition on Power and Energy Systems: Issues and Prospects for Asia (ICUE)* (2011), pp. 1–7. https://doi.org/10.1109/ICUEPES.2011.6497754
18. O.P. Mahela et al., Comprehensive overview of multi-agent systems for controlling smart grids. CSEE J. Power Energy Syst. **8**(1), 115–131 (2022). https://doi.org/10.17775/CSEEJPES.2020.03390
19. F. Bellifemine, A. Poggi, G. Rimassa, JADE—a FIPA-compliant agent framework, in *Proceedings of the PAAM*, London, UK, 30 April 1999, vol. 99, p. 33
20. I. Praça, C. Ramos, Z.A. Vale, Competitive electricity markets: simulation to improve decision making, in *Proceedings of the 2001 IEEE Porto Power Tech Proceedings*, Porto, Portugal, 10–13 Sept 2001, vol. 1
21. I. Praça, C. Ramos, Z. Vale, M. Cordeiro, MASCEM: a multiagent system that simulates competitive electricity markets. IEEE Intell. Syst. **18**, 54–60 (2003)
22. Z. Vale, T. Pinto, I. Praca, H. Morais, MASCEM: electricity markets simulation with strategic agents. IEEE Intell. Syst. **26**, 9–17 (2011)

Inspection of Overhead Power Transmission Conductors with Autonomous Quadcopter

MD. Faiyaz Ahmed and J. C. Mohanta

Abstract Inspection of overhead power transmission lines and components is crucial for the reliability and availability of power supply. The main drawback of existing traditional methods of inspection is, it is cumbersome on installations of power lines and lack of adaptability to modern methods of inspection and improper maintenance to electrocution for human operators. Thus, inspection of overhead power transmission lines with Unmanned Aerial Vehicles (UAV)/Quadcopter has been attracting the power utility companies since their inception. This article explains about the quadcopter-based inspection of overhead power transmission conductors and their failures due to the poor connection between connecting clamps/spacers and conductors and fusing failures. The investigation by thermal analysis explains that, if the conductor's temperature is higher than the spacer/clamp then it leads to poor contact of clamps and conductors. The thermal imaging of the conductor also reveals that it generates heat in the form of an equidistant helix. The captured thermal image provides some practical explanation regarding the defects of conductor and power line components enabling the timely maintenance and system reliability.

Keywords Unmanned aerial vehicles · Overhead power transmission lines · Thermal imaging · Equidistant helix · Clamp/spacer · Conductors

1 Introduction

The demand for electricity is increasing day by day across the globe. In 2018, around 4% more production rate of electricity was observed which was twice compared to the global energy demand [1]. Electricity supply is an emerging demand in the present world due to the current development in society. There is a huge pressure on power grids and transmission sectors due to different factors such as increase

MD. Faiyaz Ahmed (✉) · J. C. Mohanta
Department of Mechanical Engineering, MNNIT-Allahabad, Prayagraj, India
e-mail: mahmed@mnnit.ac.in

J. C. Mohanta
e-mail: jcmohanta@mnnit.ac.in

© The Author(s), under exclusive license to Springer Nature Singapore Pte Ltd. 2023

K. Murari et al. (eds.), *Soft Computing Applications in Modern Power and Energy Systems*,
Lecture Notes in Electrical Engineering 975,
https://doi.org/10.1007/978-981-19-8353-5_10

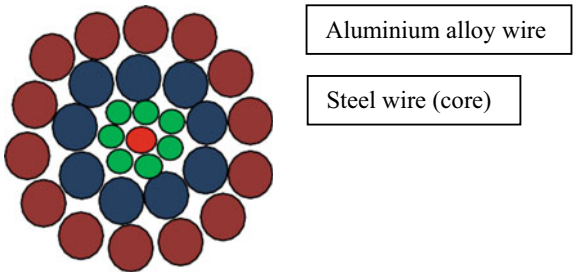

Fig. 1 Cross section of ACSR conductor

of power load, electrical networks, implementation of renewable [2, 3], flexibility and decentralization of power [4, 5], introducing on road electric vehicles [6] and integration of European market [5]. The rate of construction for new transmission lines is very low compared to the demand of power supply. So, there is need to multiple the number of newly constructed transmission lines for increasing the power generation and supply [7–9].

The overhead transmission lines across the globe are in their forties or fifties old, and the power line components such as conductors, insulators, pylons, spacers and clamps are reaching the first stage of deterioration [10]. Therefore, it is difficult to identify and rectify these deteriorations in conductors, insulators and spacers which are physically not accessible. The power transmission line conductor mainly consists of the spacer connector and the aluminium conductor with the steel core material. The general type of conductors mostly used is Aluminium Conductor Steel Reinforced (ACSR) as shown in Fig. 1.

The major challenge in the life span of overhead power line conductors is the wind induced Aeolian vibrations. The conductor or insulators exposed to bad weather conditions such as pollution, rain, sulphur dioxide and vegetation lead to electro-chemical corrosion [11]. When cross-checked with the positive pole, the corrosion degree for the inner layer is least, whereas the degree of corrosion for second layer is at most and the corrosion rate for outer layer lies between them [12]. This results in increase of maximum resistance in the second layer, leading to the formation of higher temperature between the inner and second layer of conductor. The temperature of the conductor affects the total capacity of overhead electrical transmission lines. The formation of corrosion between these two layers leads to the increase of power consumption and even in some worst cases results in breakage or blast of conductors and fire hazards, etc. resulting in the breakage of normal power sully and operational issues in power grids. So, the role of ACSR in power utilities plays a major role in terms of performance, consumption of power and reliability and security.

In order to have a smooth function of power lines under safety conditions, there is a need to figure out the changes occurred with respect to temperature between the layers (first and second) of conductors. The overall capacity of transmission system depends on the temperature of conductors, so the limited space between the spacers and conductor joints is to be maintained regularly as it can cause the overheating and melting of steel wires and aluminium. So, the main failure of transmission conductor

occurs at joints [13, 14]. In order to execute the fast and accurate inspection of these overhead power transmission conductors and insulators, implementation of Unmanned Aerial Vehicles (UAS) is highly preferred due to their structure and ability to hover above the power transmission conductors.

This manuscript studies the defects of power transmission conductors by using visual and thermal cameras. The thermal images show the results of defective conductors and spacers/clamps. The results of this research will enable the guidance and future direction for autonomous inspection of power transmission conductors and improve the performance and reliability of power transmission systems.

2 Related Works

Researchers across the globe have mostly concentrated on electrochemical corrosion problems and only a few studies are carried on conduction of heat on power transmission conductor. Inspection of these power transmission lines and components is executed with the traditional methods such as foot patrolling [15] and helicopter-based inspection. In foot patrolling, two or more skilled technicians will walk on the surface of conductors by wearing the Infrared (IR)/thermal goggles and vision inspection devices for locating the defects. However, this type of inspection is considered to be dangerous as in the most cases, technicians will get electrocuted and it is a time-consuming process, whereas in helicopter-based inspection, a crew with three or four members will hover the helicopter around the power transmission lines and collect the data with the help of recording devices and later this data will be cross checked on ground control station (GCS) for the presence of anomalies. This type of inspection is also considered to be dangerous, expensive and the data collected is not accurate due to the flying conditions of helicopter [16].

The use of robotic platforms such as UAS or climbing robots for inspection of power transmission lines is highly preferred by the power utility companies. Ahmed et al. [17] have developed and fabricated a smart quadcopter for inspection of power transmission lines. Chen et al. [18] explained about the path planning of UAS around power transmission conductors for avoiding obstacles by using the methods of Voronoi Diagram (VD). Basso et al. [19] developed an UAS with on-board hardware components and software-based data inspection. The UAS was used for capturing the images of crop rows and later processed them in GCS for defect detection. The same procedure can be applied foe power line inspection. Mohanta et al. [20] have proposed a low cost flying UAS with a planned trajectory for real-time navigation. The control scheme for path planning is developed in MATLAB Simulink, in which PID controller is designed for stable navigation.

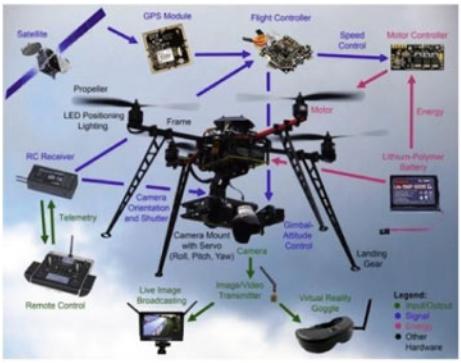

(a) Schematic of quadcopter with multiple onboard components

(b) Fabricated autonomous quadcopter

(c) HereLink for autonomous operations

Fig. 2 Autonomous quadcopter for inspection of power transmission conductors and insulators

3 Autonomous Quadcopter and On-Board Components

An autonomous quadcopter is fabricated with multiple components for performing the online inspection of power transmission conductors as shown in Fig. 2. The on-board components mounted on quadcopter are listed in Table 1.

4 Thermal Rating of Overhead Power Transmission Conductors

The overhead power transmission lines and conductors operate according to the thermal rating and temperature. This rating ensures the proper supply and consumption of electricity among all the line spans of conductors exposing to multiple weather

Table 1 List of components mounted on quadcopter

S. No.	Component	Quantity	Weight (g)
1	S-500 frame and landing gear	1	150
2	BLDC motors	4	265
3	ESC's	4	155
4	Pixhawk orange cube controller	1	124
5	Receiver with antennas	1	50
6	Tarot 3D gimbal	1	78
7	Go Pro Hero 8 camera	1	55
8	Lipo battery	2	312
9	GNSS antenna	1	35

conditions [8]. Temperature and time have a direct impact on loss of tensile strength which showcases the effect on temperature of conductors. The conductor temperature depends on the weather conditions such as wind speed, pressure, temperature, and solar heating and instantaneous current level flowing through the line [21].

4.1 Sag and Tension on Overhead Transmission Conductors

Sag is defined as the vertical distance between the midpoint of the span and the straight line joining the two support structures/points of the conductor in overhead power transmission lines, as shown in Fig. 3. Transmission line structures are computed using phase-to-tower and phase-to-phase clearances in order to survive galloping, sudden voltage surges and conductor swinging during poor weather.

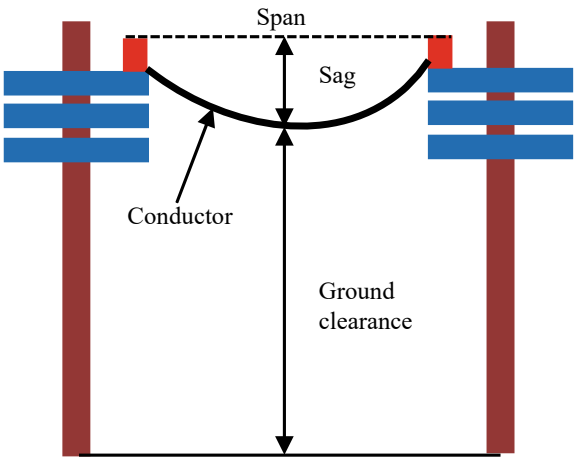

Fig. 3 Sag and tension on overhead power transmission conductors

The temperature of sag should be stable for ACSR conductor's, i.e. 75 °C, if the temperature exceeds beyond this point, then it is considered as defective [21]. If the temperature is above 90 °C, then the mechanical strength of ACSR conductor losses with time resulting in sag and decrease in clearance between the conductor and spacer/clamps. Therefore, the operational limitation of ACSR conductors lays between 75 and 85 °C for continuous and safe operation. If the temperature lies between 100 and 150 °C, then it is considered for anomalies [22]. Equation 1 summarizes the thermal models derived by [23–25] for transient and steady state circumstances. According to Eq. 1, the quantity of heat supplied to the conductor equals the amount of heat dissipated, leading the conductor to thermal equilibrium.

$$\underbrace{P_{\text{Joule}} + P_{\text{Magnetic}} + P_{\text{Solar}} + P_{\text{Corona}}}_{\text{Heating mechanisms}} = \underbrace{P_{\text{Connective}} + P_{\text{Radiative}} + P_{\text{Evaporative}}}_{\text{Cooling mechanisms}} \ \text{W/m} \tag{1}$$

Simultaneously under transient conditions, the equation for heat balance is in (2).

$$mc\frac{\mathrm{d}T}{\mathrm{d}t} = P_{\text{Joule}} + P_{\text{Magnetic}} + P_{\text{Solar}} + P_{\text{Corona}} - P_{\text{Connective}} - P_{\text{Radiative}} - P_{\text{Evaporative}} \ \text{W/m} \tag{2}$$

m = mass of the conductor/unit length and c = specific heat capacity.

4.2 *Theoretical Analysis and Laboratory Work*

When a conductor is tested in laboratory by supplying the required amount of current, it is found that, in the faulty conductor, the contact between the line and clamp will be much larger compared to new conductor and clamp. This indicated that there is an internal heat source due to the presence of anomaly inside the conductor and joint as shown in Fig. 4.

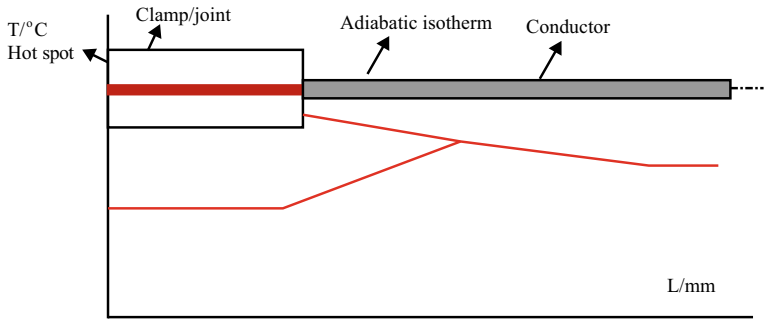

Fig. 4 Model of heat transfer in conductor (theoretical) [26]

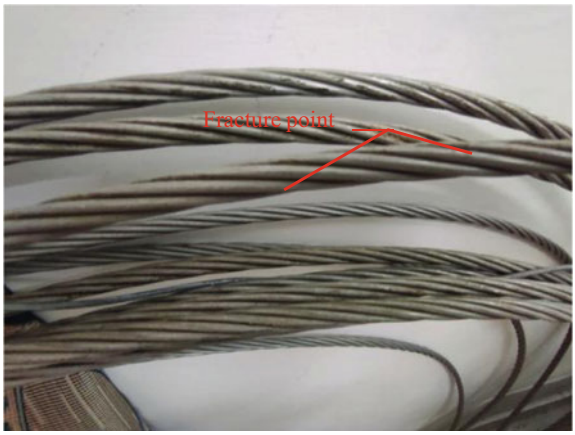

Fig. 5 Erosion and fusion on outer layer of conductor

The existing hotspot transfers the heat linearly on to the surface of transmission conductor and then transfers axially. Nonetheless, the rate of heat transfer in the direction of cross section is stronger compared to axial direction. The main reason identified while experimenting for fusing failure in conductors is the gap between the conductor and clamp occurred due to temperature variation and anomalies [26, 27].

According to [24], the disassembly inspection will include 48 aluminium strands, with 10 in the inner layer, 22 in the outer layer, 16 in the second layer and 7 in the steel core. Figure 5 depicts the erosion and fusion of the conductor's outer layer.

4.3 Quadcopter-Based Inspection of Conductors

An autonomous quadcopter with the support of HereLink is used to fly around the overhead power transmission lines. In order to implement the autonomous navigation task, an on-board computer such as Nvidia Jetson Nano with ARM processor and 32-bit Pixhawk orange cube controller with in-built companion computer is used.

Capturing images and videos is carried by GoPro Hero 8 action camera equipped with wide angled lens. The latitude and longitude of the experimental location are 25.4920° N, 81.8639° E, respectively. A Flir C5 thermal imager camera is used for capturing the thermal images of conductor and power transmission tower. The quadcopter-based inspection around the overhead power transmission conductors is shown in Fig. 6a–d.

According to Figs. 7a and 8, the heat-producing conductor's thermal image resembles an equidistant helix and there were still some hotspots in the conductor layers. However, the distribution of current among the lines was in line with the expectations. The temperature diagram of power transmission conductor with respect to histogram and oscilloscope is shown in Fig. 7b. The infrared thermal images and contour of overhead power transmission lines and components are shown in Fig. 9a.

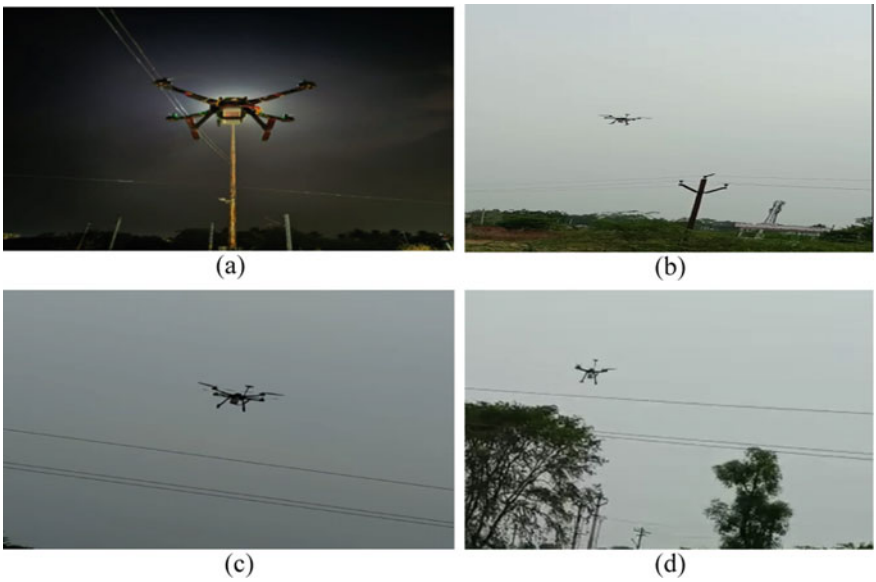

Fig. 6 Hovering of quadcopter around power transmission conductors

As it can be seen in Fig. 9a, left image, the jointer or spacer was reflecting the indication of hotspot leading to the fusing failure and threat to power transmission line. Before the transmission line shut down out of operation, the location of hotspot was informed to the power utility staff for maintenance of the detected fault. The temperature diagram of power transmission line and components with respect to histogram and oscilloscope is shown in Fig. 9b.

5 Conclusion

In this manuscript, an autonomous quadcopter is used for inspection of overhead power transmission conductors and components. The autonomous quadcopter has followed the predetermined waypoints for the inspection of power transmission conductors. Throughout the inspection, it is observed that, the main cause for the fusing failure of conductor is the poor contact between spacer and transmission line. Irregular maintenance for a long time and environmental impacts such as air oxidation, vegetation and salty environment leads to the permanent damage of power transmission line and sometimes blackout. Laboratory experiments are performed on the transmission conductor and it is observed that most of the broken strands are found in outer layer and the cracks were found mostly between the range of 110 and 185 mm from the clamp and spacer. The thermal imaging of conductors and power transmission line site showcased the poor contact of spacer and conductor. It is also noticed

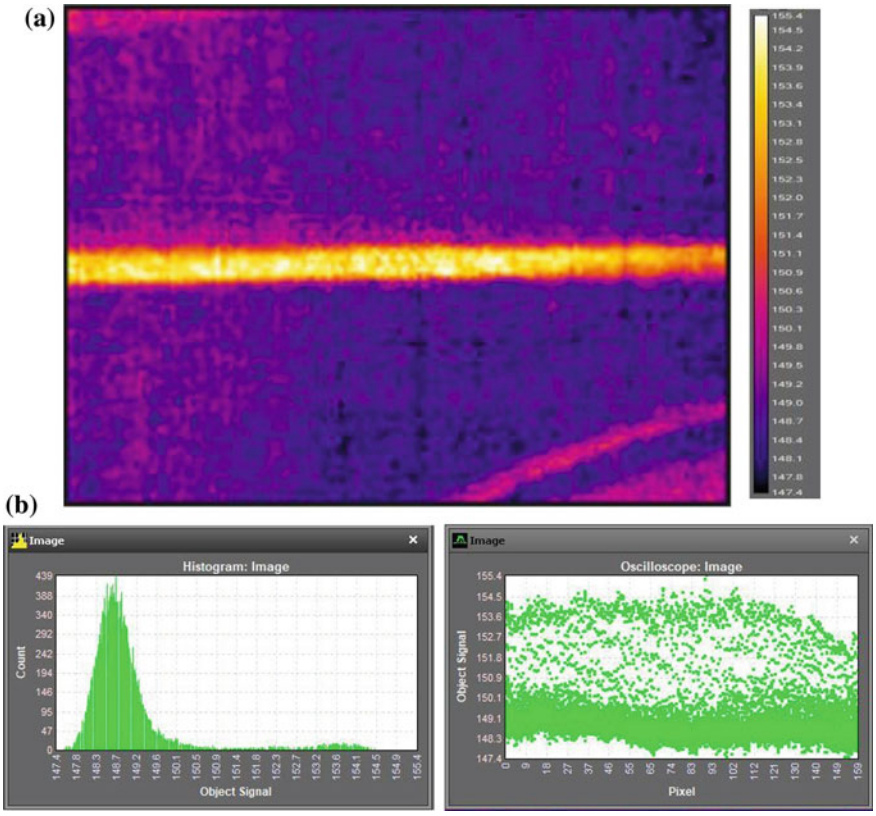

Fig. 7 **a** Thermal image of power transmission conductor. **b** Temperature diagram in histogram and oscilloscope

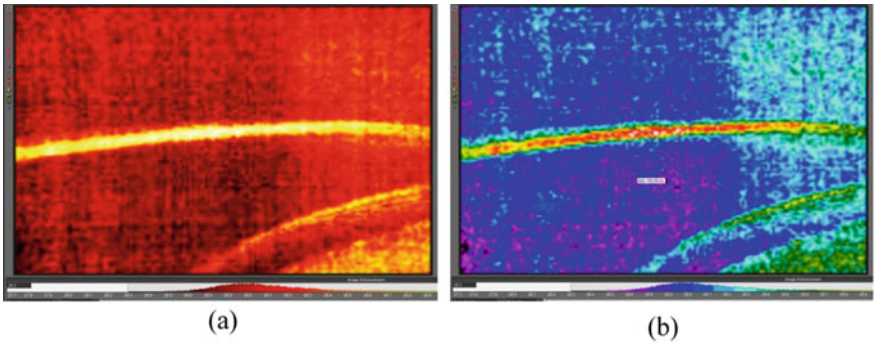

Fig. 8 Infrared thermal and contour image of power transmission contour

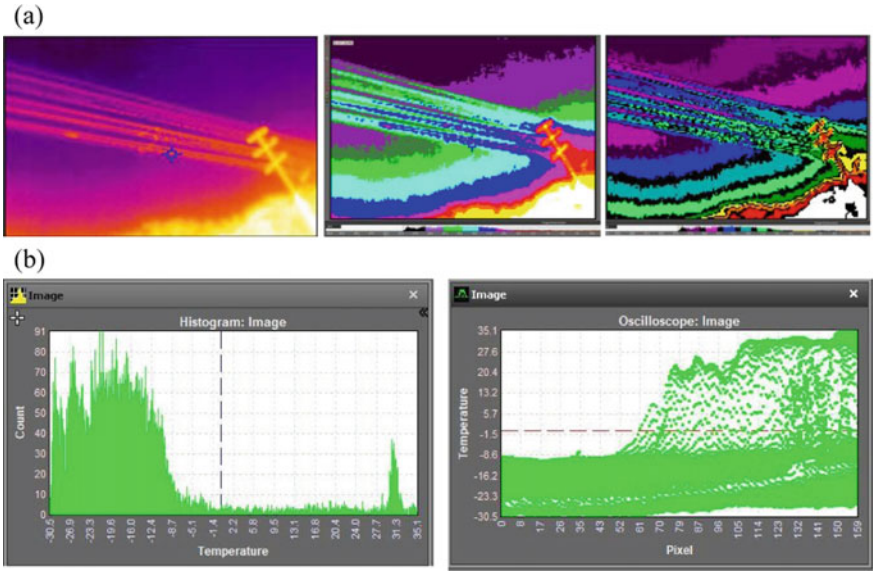

Fig. 9 **a** Infrared and contour thermal image of power transmission line. **b** Temperature diagram in histogram and oscilloscope

that, the temperature of spacer or joint was higher than the conductor like an equidistant helix. Timely inspection of power transmission line with autonomous quadcopter and thermal camera leads to the successful maintenance and repair of identified hotspot which is a vital importance in order to ensure uninterrupted operation of the power transmission line and equipment.

Acknowledgements The authors would like to thank the project 'Quadcopter application for live inspection of power transmission lines' (Ref no: T-32) funded by ICPS-DST, India, for supporting this research.

Conflicts of Interest The authors declare no conflict of interest.

References

1. A.A.P. Silva, J.M.B. Bezerra, Applicability and limitations of ampacity models for HTLS conductors. Electr. Power Syst. Res. **93**, 61–66 (2012)
2. S. Beryozkina, Evaluation study of potential use of advanced conductors in transmission line projects. Energies **12**(5), 822 (2019)
3. A. Alassi, S. Banales, O. Ellabban, G. Adam, C. MacIver, HVDC transmission: technology review, market trends and future outlook. Renew. Sustain. Energy Rev. **112**(1), 530–554 (2019)
4. International Energy Agency, Global Energy & CO_2 Status Report 2019. The Latest Trends in Energy and Emissions in 2018

5. M. Baumann, M. Weil, J.F. Peters, N. Chibeles-Martins, A.B. Moniz, A review of multicriteria decision making approaches for evaluating energy storage systems for grid applications. Renew. Sustain. Energy Rev. **107**, 516–534 (2019)
6. Y. Zheng, S. Niu, Y. Shang, Z. Shao, L. Jian, Integrating plug-in electric vehicles into power grids: a comprehensive review on power interaction mode, scheduling methodology and mathematical foundation. Renew. Sustain. Energy Rev. **112**, 424–439 (2019)
7. F. Capelli, J.-R. Riba, D. Gonzalez, Thermal behavior of energy-efficient substation connectors, in *2016 10th International Conference on Compatibility, Power Electronics and Power Engineering (CPE-POWERENG)* (2016), pp. 104–109
8. Cigre, Technical brochure 244. Conductors for the uprating of existing overhead lines, Paris (France) (2019)
9. F. Capelli, J.-R. Riba, J. Sanllehí, Finite element analysis to predict temperature rise tests in high-capacity substation connectors. IET Gener. Transm. Distrib. **11**(9), 2283–2291 (2017)
10. C.R.F. Azevedo, T. Cescon, Failure analysis of aluminum cable steel reinforced (ACSR) conductor of the transmission line crossing the Paraná River. Eng. Fail. Anal. **9**(6), 645–664 (2002)
11. P. Hadimani, S.C. Kulkarni, Static and dynamic analysis of transmission line tower (2017)
12. E. Pultrum, R. Gruntjes, B. Verhoeven, The value of type testing cables and accessories, in *CIRED 2009—The 20th International Conference and Exhibition on Electricity Distribution—Part 2* (2009), pp. 1–2
13. C. Lihua, *Analysis of Electric and Heating Mixed Field of Transmission Lines and Electrical Equipment* (North China Electric Power University, 2013)
14. C. Barbosa et al., Analysis of critical field procedures for power HV overhead transmission line splices installed after restructuring of Brazilian electrical sector. Eng. Fail. Anal. (2011)
15. J. Katrasnik, F. Pernus, B. Likar, A survey of mobile robots for distribution power line inspection. IEEE Trans. Power Deliv. **25**(1) (2010)
16. L. Zhang, L. Yan, L. Meng, X. Li, S. Huang, The application study of helicopter airborne photoelectric stabilized pod in the high voltage power line inspection, in *International Conference on Optoelectronics and Microelectronics (ICOM)*, Changchun, China (2012)
17. Md. Ahmed, J. Mohanta, M. Zafar, Development of smart quadcopter for autonomous overhead power transmission line inspections. Mater. Today: Proc. (2021). https://doi.org/10.1016/j.matpr.2021.05.271
18. X. Chen, G.-y. Li, X.-m. Chen, Path planning and cooperative control for multiple UAVs based on consistency theory and Voronoi diagram, in *Control and Decision Conference (CCDC), 2017 29th Chinese* (IEEE, 2017), pp. 881–886
19. M. Basso, E. Pignaton de Freitas, A UAV guidance system using crop row detection and line follower algorithms. J. Intell. Robot. Syst. **97**, 605–621 (2020)
20. J.C. Mohanta, D.R. Parhi, S.R. Mohanty et al., A control scheme for navigation and obstacle avoidance of autonomous flying agent. Arab. J. Sci. Eng. **43**, 1395–1407 (2018)
21. IEEE Power and Energy Society, 1283-2013—IEEE guide for determining the effects of high-temperature operation on conductors, connectors, and accessories, New York (2013)
22. CIGRE Green Books, *Overhead Line*s (Malters, Switzerland, 2017)
23. Cigre Working Group 22.12, Thermal Behaviour of Overhead Conductors (2002)
24. M.F. Ahmed, M.N. Zafar, J.C. Mohanta, Modeling and analysis of Quadcopter F450 frame, in *2020 International Conference on Contemporary Computing and Applications (IC3A)* (2020), pp. 196–201. https://doi.org/10.1109/IC3A48958.2020.233296
25. S.N. Yeole, F. Ahmed, Fabrication and testing of quadcopter prototype for surveillance. Int. J. Mech. Prod. Eng. Res. Dev. (IJMPERD) (2018)
26. Y. Jin, M. Quan, S. Yan, Y. Yan, M. Cui, Y. Liu, Analysis of overhead transmission lines fusing failure due to poor contact between conductors and clamps. Eng. Fail. Anal. **118**, 104858 (2020). ISSN: 1350-6307
27. F. Ahmed, J.C. Mohanta, A. Keshari et al., Recent advances in unmanned aerial vehicles: a review. Arab. J. Sci. Eng. (2022). https://doi.org/10.1007/s13369-022-06738-0

Quasi-oppositional Whale Optimization Algorithm for Solving Multi-objective Optimal DG Emplacement Problem in Radial Distribution Network

Himanshu Lahoti, Avinit Kumar Singh, Sneha Sultana, and Sourav Paul

Abstract Optimization of system losses and quality power is still a major concern for many researchers. DG, i.e., Distributed Generation is a newly developed effective technology, when placed optimally in power system helps in raising overall efficiency and quality of power by minimizing distribution losses. This paper presents a methodology based on quasi-oppositional whale optimization algorithm (QOWOA) to locate DG with appropriate size in distribution system for reducing losses along with minimization of voltage deviance and enhancement of voltage stability index. The above-mentioned methodology is tested on three different test systems consisting of 33, 69 and 118 buses. The computer simulation results obtained using projected methodology is compared with the earlier optimization techniques proposed by various author.

Keywords Distributed generation · Whale optimization algorithm · Quasi-oppositional whale optimization algorithm · Power loss minimization · Voltage deviance improvement

1 Introduction

Distribution network connects the power station with the consumer located far away for the transfer of electricity. Consumers called for load demand is obtained through distribution system. With the advancement of human civilization and technology, demand for superior quality electric power has reached the maximum capability

H. Lahoti (✉) · A. K. Singh · S. Sultana · S. Paul
Department of Electrical Engineering, Dr B.C Roy Engineering College, Durgapur 713206, India
e-mail: himanshulahoti20@gmail.com

A. K. Singh
e-mail: avinit14663@gmail.com

S. Sultana
e-mail: sneha.sultana@bcrec.ac.in

S. Paul
e-mail: sourav.paul1@bcrec.ac.in

© The Author(s), under exclusive license to Springer Nature Singapore Pte Ltd. 2023

K. Murari et al. (eds.), *Soft Computing Applications in Modern Power and Energy Systems*,
Lecture Notes in Electrical Engineering 975,
https://doi.org/10.1007/978-981-19-8353-5_11

of the existing radial distribution network (RDN). This causes distribution system operation to become more complex, having tendency to failure and discontinuity. Therefore, the very objective of power system is haltered. Moreover, bulk power exchange that takes place in the distribution system incorporates huge power loss in the form of I^2R resulting in reducing power system efficiency.

Thus, distribution network is drawing much attention of researchers for ascertaining solutions to the existing problem in supplying load demand and making the power system reliable. One solution to above-mentioned difficulty could be modification or enhancing the capacity of the existing distribution system network. But it will not be an easy task and at the same time, it is not economical. Another most effective and efficient solution could be integrating DG with the existing power system. Bhatt et al. [1] gives an overview concerning integration of DG, its impact in steady-state operation, and dynamic behavior. Integration of DG helps in the minimization of distribution system losses, enhancing voltage profile and reliability. Moreover, DG's acts as a support to grid distribution system by fulfilling both active and reactive power requirements and also assist in future network enhancement. Robert et al. [2] suggested a solution to rural electrification problem by extending central power grid with the help of renewable energy generation and storage.

Many researchers have used analytical methods for finding solution to optimum DG allocation (ODGA) problem. Viral and Khatod [3], Hung et al. [4], and Acharya et al. [5] utilized an analytical methodology to locate DG with appropriate size in the RDN with the purpose to minimize loss in the system. A hybrid method by combining sensitivity and power factor method to find optimum DG size and location was introduced by Mirzaei et al. [6]. Dulau et al. [7] suggested extended version Newton–Raphson methodology for emplacement of DG in RDN taking into account power loss at each bus with which it is connected. Babu et al. [8] put forward power loss sensitivity (PLS) and nonlinear programming (NLP) method to obtain optimality in finding correct position of DG with exact size in the distributed network for considerable reduction in system losses. Zaineb et al. [9] proposed load flow analysis method to solve ODGA problem in RDN to deal with losses and voltage stability.

Analytical techniques for finding solutions to ODGA problem are easy to implement and shows good convergence rate while dealing with small-scale optimization problem but it has some limitations. The complexity of the problem increases with multi-DG in a diverse load-generation condition. Analytical methods often deal with by considering some unrealistic assumption which causes an error in the output when implemented on real system. Moreover, the probabilistic techniques used for finding solution to (ODGA) problem requires large amount of computational data and huge processing ability. On the other hand, meta-heuristic methods are capable of producing near-optimal solution to ODGA problem considering single or multi-DG with satisfactory computational speed and processing capability.

In recent decades, meta-heuristic methods have become very popular for finding solution to optimum location of DG and its sizing. In Refs. [10–14] a partial swarm optimization (PSO) based methodology is utilized to obtain the DG site in RDN for the synchronous power loss optimization with voltage enhancement. Ahmed

et al. [15] considered DG in the RDN to convert radial section to loop using PSO algorithm. Legha et al. [16], Ud Din et al. [17] utilized genetic algorithm (GA) for finding solution to ODGA problem in the RDN. In Ref. [18], an optimization technique based on GA and ds evidence theory to find optimal allocation of DG with minimum system losses was discussed by Zhao et al. Kanaan et al. [19] presented a simple method established on the comparison of fast voltage stability index (VSI) and simulated annealing (SA) to find optimum location and appropriate DG size. The suggested methodology was simulated on MATLAB and MATPOWER software and the results obtained resembles that the losses in system and voltage profile depends on appropriate location and DG size. Sultana et al. [20] applied a modified teaching-learning-based optimization methodology to obtain optimum DG siting with side-by-side reduction in power loss, voltage variation- and voltage stability index enhancement in RDN. Cuckoo search algorithm to solve optimization problem related to DG with sizing in a distribution system has been addressed in Nguyen et al. [21]. Muthukumar et al. [22] presented harmony search algorithm (HSA) to search for both allocating DG and compensating device with the significant reduction in power loss. Hashemabadi et al. [23] used bacteria foraging algorithm and binary genetic algorithm to obtain optimum location of DG to cut down system loss and variation in voltage. The search for optimal location and sizing of multi-DG in presence of SVC using adaptive differential search algorithm (DSA) for reducing system losses was developed by Mahdad et al. [24]. An improved differential search algorithm (IDSA) for solving optimization problem related to DG allocation and sizing with the technical, financial benefits of DG was objective was introduced by Injeti et al. [25]. A firefly algorithm (FA) in balanced/unbalanced distribution system for optimal sitting of voltage operated DG was utilized by Othman et al. [26]. Katamble et al. [27] presented a fuzzy logic to find candidate node for DG installation with reduced power loss and voltage deviance. In Ref. [28], a hybrid imperialistic competitive algorithm (ICA) method for getting optimum location of DG for the purpose of loss reduction was introduced by Poornazaryan et al. Home-Ortiz et al. [29] proposed mixed integer conic programming (MICP) that shows better potential and performance in find optimum DG place in RDN. Nguyen and Vo [30] introduced a stochastic fractal search algorithm (SFSA) for minimizing loss, enhancing voltage profile and stability with the satisfaction of various constraints. Reddy et al. [31] proposed whale optimization algorithm (WOA) and power loss index (PLI) to locate DG with appropriate size for loss minimization and improvement in voltage profile in RDN.

Moreover, according to "no-free-lunch" theorem, there is no optimization technique which is well-defined for all types of optimization problems. This motivated the author to come up with a new algorithm to solve the desired objective function, namely, Quasi-Oppositional Whale Optimization Algorithm to solve multi-objective optimal DG emplacement problem in RDN as well as improvement of voltage profile and voltage stability index. QOWAO is relatively new, much simpler, and more robust optimization algorithm on comparison to other optimization problems. This paper used quasi-oppositional whale optimization algorithm (QOWOA)

for obtaining optimum DG location and size for the minimization losses and betterment voltage profile and stability index in distribution system. Simulation outcomes obtained with the help of MATLAB software are described in comparison to other techniques proposed by different authors in the later part of paper.

The arrangement of paper is done in following manner. Mathematical formulation is described under Sect. 2. The Whale Optimization algorithm is described under Sect. 3. Oppositional-based learning is described under Sect. 4. QOWOA applied to ODGA problem is discussed under Sect. 5. Results and discussion are described under Sect. 6. Conclusion is described under Sect. 7.

2 Mathematical Formulation

2.1 Multi-objective Function

Multi-objective optimization is also known as Pareto optimization having more than one decision-making criteria that mainly concern with the optimization of more than one objective functions. This paper aims at minimizing system power loss ($\mathrm{Of_{Ploss}}$) and voltage deviance ($\mathrm{Of_{vpi}}$), and voltage stability index ($\mathrm{Of_{vsi}}$) enhancement by optimally sizing and allocating DG. This multi-objective function expressed as:

$$\mathrm{Of} = \min[\mathrm{Of_{ploss}} + \alpha_1 \mathrm{Of_{vpi}} + \alpha_2 \mathrm{Of_{vsi}}] \tag{1}$$

where,

$$\mathrm{Of_{ploss}} = \min(P_{\mathrm{loss}}) \tag{2}$$

$$\mathrm{Of_{vpi}} = \sum_{i=1}^{N} (v_i - v_{\mathrm{rated}})^2 \tag{3}$$

$$\mathrm{Of_{vsi}} = v_i^4 - 4(p_{i+1} r_i + q_{i+1} x_i) v_i^2 - 4(p_{i+1} x_i - q_{i+1} r_i)^2 \tag{4}$$

$$p_{\mathrm{loss}} = \sum_{i=1}^{N} \sum_{j=1}^{N} c_{ij}(p_i p_j + q_i q_j) + d_{ij}(q_i p_j - p_i q_j) \tag{5}$$

$c_{ij} = \frac{r_{ij}}{|v_i||v_j|} \cos(\phi_i - \phi_j)$, $d_{ij} = \frac{r_{ij}}{|v_i||v_j|} \sin(\phi_i - \phi_j)$, q_i and q_j, p_i and p_j are the respective reactive, active power of ith and jth bus; v_i and v_{rated} are the voltage and the rated voltage of ith bus respectively; p_{i+1} and q_{i+1} are $i + 1$th bus power, i.e., active reactive; v_j is the jth bus voltage, resistance, reactance of the line associated in-between the buses ith and jth are r_{ij} and x_{ij} severally.

2.2 Constraints

Load Equilibrium Constraints

For the purpose of power equilibrium, the sum of the power generated by DG ($p_{\mathrm{DG},i}$ and $q_{\mathrm{DG},i}$) at a particular bus ith and that supplied by the substation ($p_{\text{sub - station}}$ and $q_{\text{sub - station}}$) must meet the total demand ($p_{\mathrm{TD},i}$ and $q_{\mathrm{TD},i}$) at ith bus and system losses. The load equilibrium constraints given below:

$$p_{\text{sub - station}} + \sum_{i=1}^{N} p_{\mathrm{DG},i} = \sum_{i=1}^{N} p_{\mathrm{TD},i} + p_{\mathrm{loss}} \tag{6}$$

$$q_{\text{sub - station}} + \sum_{i=1}^{N} q_{\mathrm{DG},i} = \sum_{i=1}^{N} q_{\mathrm{TD},i} + q_{\mathrm{loss}} \tag{7}$$

Bus Voltage Limit

Bus voltage must be in the range of its maximum and minimum voltage limit for guaranteed system stability and quality of power given by;

$$v_{i,\min} \leq v_i \leq v_{i,\max} \tag{8}$$

Voltage Angle Limit

Voltage angle at the bus must be in-between the maximum ($\partial_{i,\max}$) and minimum ($\partial_{i,\min}$) angle limit.

$$\partial_{i,\min} \leq \partial_i \leq \partial_{i,\max} \tag{9}$$

3 Whale Optimization Algorithm

The WAO [32] is a swarm intelligence-based meta-heuristic method first introduced by Lewis and Mirjalili in the year 2016. The WAO technique is rooted on the hunting or foraging behavior in humpback whales, also referred to as bubble-net foraging. This optimization is designed on the distinctive hunting method of humpback whales to find small fish or prey on the surface by forming bubbles in a 9-shaped path in order to search the prey. WAO has mathematically designed three different behaviors used by humpback whales during hunting, which are prey encircling, bubble-net attacking, and prey searching.

3.1 Encircling Prey

Humpback whales can perceive the prey's location and encircle them. To emulate the procedure presuming that the present optimal solution is the final optimal solution or near it. After which, other search agents will move towards the best searching agent present there and hence updating their position. This can describe as below:

$$\overrightarrow{R} = \left| \overrightarrow{H} \cdot \overrightarrow{L}^{*}(T) - \overrightarrow{L}(T) \right| \tag{10}$$

$$\overrightarrow{L}(T+1) = \overrightarrow{L}^{*}(T) - \overrightarrow{E}\,\overrightarrow{R} \tag{11}$$

where T indicates the present iteration, $\overrightarrow{A}$ and $\overrightarrow{B}$ are co-efficient vectors, L^{*} is the position vector of the best solution in every particular iteration, $\overrightarrow{L}$ is the position vector, $\|$ is the absolute value and. is an element-by-element multiplication.

The $\overrightarrow{E}$ and $\overrightarrow{H}$ vectors are,

$$\overrightarrow{E} = 2\overrightarrow{\alpha} \cdot \overrightarrow{x} - \overrightarrow{\alpha} \tag{12}$$

$$\overrightarrow{H} = 2.\overrightarrow{x} \tag{13}$$

where α is linearly decreased from 2 to 0 amidst the iterations and $\overrightarrow{x}$ is a random vector in [0, 1].

3.2 Bubble Net Attack Method

This method uses two different outlooks where humpback whales swim across the prey in a spiral-shaped path along a shrinking circle where bubble nets are created during the entire process to hunt down their prey. The mathematical formulation is as follows:

$$\overrightarrow{R'} = \left| \overrightarrow{L^{*}}(T) - \overrightarrow{L}(T) \right| \tag{14}$$

$$\overrightarrow{L}(T+1) = \overrightarrow{R'} e^{yz} \cdot \cos(2\pi z) + \overrightarrow{L^{*}}(T) \tag{15}$$

where y is a constant for defining the shape of logarithmic spiral and z is random number in $[-1, 1]$.

While swimming around its prey, the whale swims in a shrinking circle and spiral-shaped path concurrently which can be mathematically given together for optimization as:

$$\overrightarrow{L}(T+1) = \begin{cases} \overrightarrow{L}^*(T) - \overrightarrow{E} \cdot \overrightarrow{R} & \text{if } n < 0.5 \\ \overrightarrow{R} \cdot e^{yz} \cdot \cos(2\pi z) + \overrightarrow{L}^*(T) & \text{if } n \geq 0.5 \end{cases} \tag{16}$$

3.3 Prey Search

Humpback whales arbitrarily hunt on the perception of the prey. The location in the searching phase is arbitrarily updated and taken as the best solution.

$$\overrightarrow{R} = \left| \overrightarrow{H} \cdot \overrightarrow{L}_{\text{rand}} - \overrightarrow{L} \right| \tag{17}$$

$$\overrightarrow{L}(T+1) = \overrightarrow{L}_{\text{rand}} - \overrightarrow{E} \cdot \overrightarrow{R} \tag{18}$$

where $\overrightarrow{L}_{\text{rand}}$ is the number of random whales at the present situation.

4 Quasi-oppositional Based Learning

In general, Oppositional Based Learning is a Novel soft computing or intelligence-based concept to enhance various optimization techniques, first introduced by Tizhoosh [33], apparently one of the most successful concepts in computational intelligence, which enhances the searching abilities of the conventional population-based optimization techniques in solving nonlinear optimization problems. The main objective in OBL is to consider the opposite or reciprocal of a guess or an assumption thereby comparing it with the original assumption and accordingly improve the chances of finding a solution faster. The OBL algorithm starts with the initialization of initial estimate that is based on some prior information about the solution or randomly. Optimal Solution could be in any direction or at least in opposite direction. For convergence opposite set of estimates is considered, which iteratively replaces the initial estimates for better solution in the direction of optimality.

4.1 Opposite Number

Let, $P \in [y, z]$ be a real number. Its opposite number P° is defined by:

$$P^\circ = y + z - P \tag{19}$$

4.2 Opposite Point

Let $R = (X_1, X_2, ..., X_n)$ be a point in n-dimensional space, where $P_r \in [y_r, z_r]$, $r \in \{1, 2, \ldots, n\}$. The opposite point $R^\circ = (X_1^\circ, X_2^\circ, \ldots, X_n^\circ)$ is defined by its components:

$$P_r^\circ = y_r + z_r - P_r \tag{20}$$

4.3 Quasi-opposite Number

Let P be a real number between $[y, z]$. The quasi-opposite number P^{Qo} is defined as:

$$P^{Qo} = \text{rand}(C, \breve{P}) \tag{21}$$

where C is given by:

$$C = \frac{y + z}{2}$$

4.4 Quasi-opposite Point

Let P be a real number between $[a, b]$. The quasi-opposite point P_r^{Qo} is defined as:

$$P_r^{Qo} = \text{rand}(C_r, \breve{\underset{r}{P}}) \tag{22}$$

where $C_r = \frac{y_r + z_r}{2}$, $P_r \in [y_r, z_r]$; $r = \{1, 2, 3, \ldots, n\}$.

5 QOWOA to Solve ODGA Problem in RDN

This paper developed QOWOA by emerging the conception of QOBL in WOA.

The key points involved in above-mentioned methodology are mentioned below.

Point 1: The read data for the system with constraints, size of population (P_n), the maximal iteration count, the maximal DG count that is to be set up in the network, and the parametric quantity of WOA.

Point 2: The randomly generated DG size is normalized between the running limits. The *i*th DG value is normalized to P^i for satisfying the capacity constraint as given below:

$$P^i = P^i_{\min} + r^*(P^i_{\max} - P^i_{\min}) \tag{23}$$

The KW rating and location of all setup DGs, make a sender S_k representing starting status of each factor for ODGA problem.

$$S_k = [\text{loc}_{k,1}, \text{loc}_{k,2}, \ldots, \text{loc}_{k,N}, P_{k,1}, P_{k,2}, \ldots, P_{k,N}] \tag{24}$$

Depending on size of the population, starting solvent S is created as given below:

$$S = [S_1, S_2, \ldots, S_k, \ldots, S_{N,P}) \tag{25}$$

Point 3: Start the load flow for finding power losses utilizing BIBC matrix and BCBV matrix [34].

Point 4: The motion status for each of the whale is updated using different steps encircling Prey, bubble net attack method, and prey search Eqs. (11), (16), and (18).

Point 5: The starting status for each one of the whales is modified using (19). The *i*th solution to ODGA problem represents *i*th whale starting status.

Point 6: The jumping rate is used for the generation of opposite population given by:

$$\underset{1}{\breve{x}}, = a + b - x$$

$$\underset{i}{\breve{x}} = p_i + q_i - y_i$$

Point 7: Choose the fittest individual N_p from the current and the oppositional population. Check if the experimental value is larger than the above limit then set the obtained value as maximum. If the experimental value is smaller than the lower limit then set the obtained value as minimum.

Point 8: The point from 3 to 8 is repeated until and unless the maximum count for the iteration is attained.

6 Results and Discussions

To examine the utility and superiority in finding solution to ODGA problem, the above-proposed methodology QOWOA is tested with three different test systems consisting 33, 69 and 118 buses, with operating voltage 12.66 kV. The simulations are done on MATLAB software using a computer having Intel i3-7020U @ 2.30 GHz and

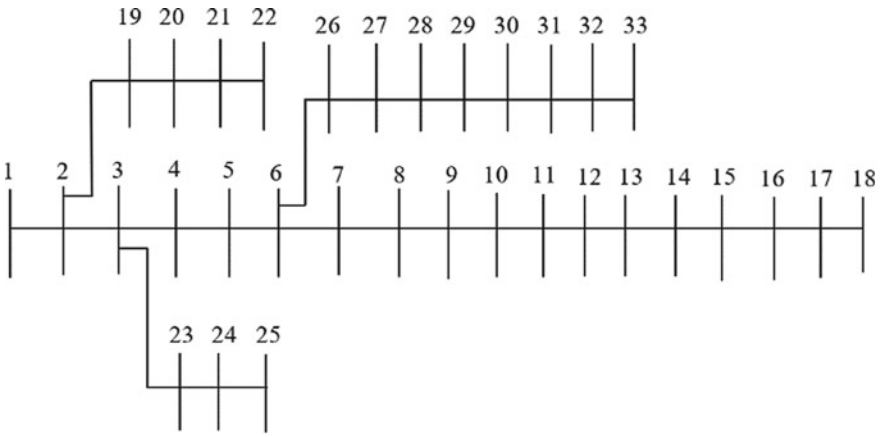

Fig. 1 33-Bus test RDN

8 GB of RAM. For the algorithm population size and iteration count are considered as 50 and 100, respectively.

6.1 33-Bus Test Radial Distribution Network

The QOWOA methodology is tested on 33-bus test RDN that have 33 buses and 32 branches are shown in Fig. 1. The line values and respectively real (3.7 MW) and reactive (2.3 MVAR) power demand for the systems are obtained from Ref. [35]. The voltage stability index, deviance in voltage, and power loss for 33-bus test system with QOWOA are 0.9543, 0.0009 p.u, 0.10235 MW respectively. Results are obtained using QOWOA optimization techniques are indicated in Table 1. The multi-objective of power loss minimization is greatly achieved with the simultaneous enhancement of voltage stability and profile.

6.2 69-Bus Test Radial Distribution Network

The above-mentioned methodology i.e., QOWOA is tested on 69-bus large distribution network consisting of 69 buses and 68 branches are shown in Fig. 2. The line values and respective real (3.8 MW) and reactive (2.69 MVAR) power demand for the systems are obtained from Ref. [36]. The simulation outcomes for the methodology are indicated in Table 2. The obtained results then are compared with the results of various author derived using different optimization. The result shows the effectiveness QOWOA algorithm with side by side by optimization of voltage deviance

Table 1 Computational results of different approaches for 33-bus RDN

Algorithm	DG optimum location	DG optimum size in MW	Losses in MW	Voltage deviance (p.u)	Voltage stability index	CPU time in seconds
GA [38]	11, 29, 30	1.500, 4.288, 1.071	0.1063	0.0407	0.9490	12.55
PSO [38]	8, 13, 32	1.176, 0.981, 0.829	0.1053	0.0335	0.9256	NA
GA/PSO [38]	11, 16, 32	0.925, 0.863, 1.200	0.10340	0.0124	0.9508	NA
TLBO [20]	12, 28, 30	1.1826, 1.1913, 1.1863	0.1246	0.0011	0.9503	12.63
QOTLBO [20]	13, 26, 30	1.0834, 1.1876, 1.1992	0.103409	0.0011	0.9530	12.55
WOA	13, 28, 30	1.1698, 1.19987, 0.89472	0.11148	0.001166	0.9295	NA
QOWOA	13, 26, 30	1.0834, 1.1876, 1.1992	0.10235	0.0009	0.9543	NA

(0.00069), power loss (0.079085), and voltage stability index (0.9872) better than other techniques in comparison.

6.3 118-Bus Test Radial Distribution Network

With the intention of showing the superiority of QOWOA methodology, it is applied to 118 bus test system consisting of 118 buses and 116 branches shown in Fig. 3. System base values are 100 $(\text{MVA})_b$ and 11 $(\text{KV})_b$. The respective reactive, real power demands are 17.04 Mega-VAR and 22.70 MW severally. The line and load data are taken form [37]. The simulation result considering 7 DGs at different locations is shown in Table 3. System loss, voltage deviance, and index of voltage stability for the system under consideration come out to be 0.67646 MW, 0.0121 p.u, and 0.8890, respectively. The result shows its potency in comparison to the methodologies proposed by other authors.

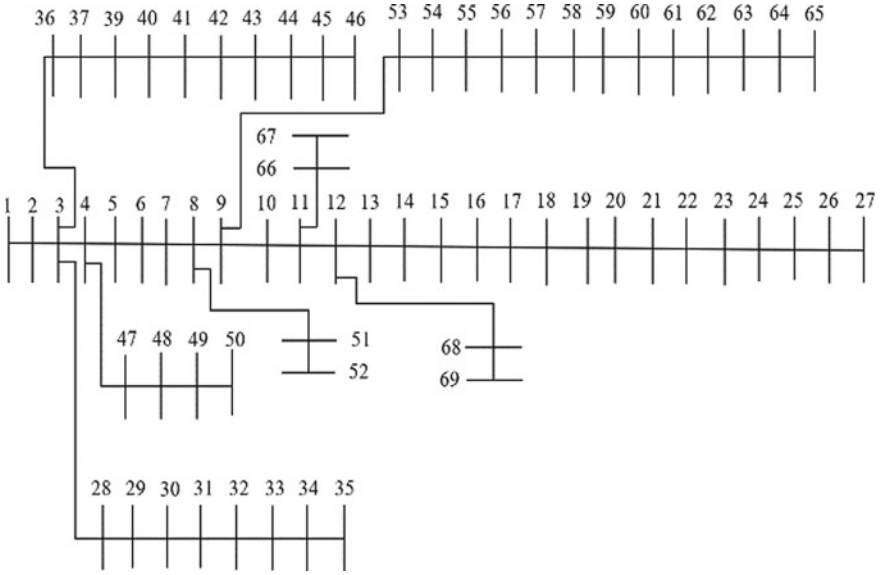

Fig. 2 69-Bus test RDN

Table 2 Computational results of different approaches for 69-bus RDN

Algorithm	DG optimum location	DG optimum size in MW	Losses in MW	Voltage deviance (p.u)	Voltage stability index	CPU time in seconds
GA [38]	21, 62, 64	0.9297, 1.072, 0.9848	0.0890	0.0012	0.9705	NA
PSO [38]	17, 61, 63	0.9925, 1.198, 0.7956	0.0832	0.0049	0.9676	NA
GA/PSO [38]	21, 61, 63	0.9105, 1.126, 0.8849	0.0811	0.0031	0.9768	NA
TLBO [20]	13, 61, 62	1.0134, 0.9901, 1.1601	0.082172	0.0008	0.9745	15.77
QOTLBO [20]	15, 61, 63	0.8114, 1.1470, 1.0022	0.080585	0.0007	0.9769	15.71
WOA	14, 61, 62	0.9201, 1.1232, 1.03445	0.081912	0.00053	0.9770	NA
QOWOA	15, 61, 63	0.8114, 1.147, 1.0022	0.0790	0.00069	0.9872	NA

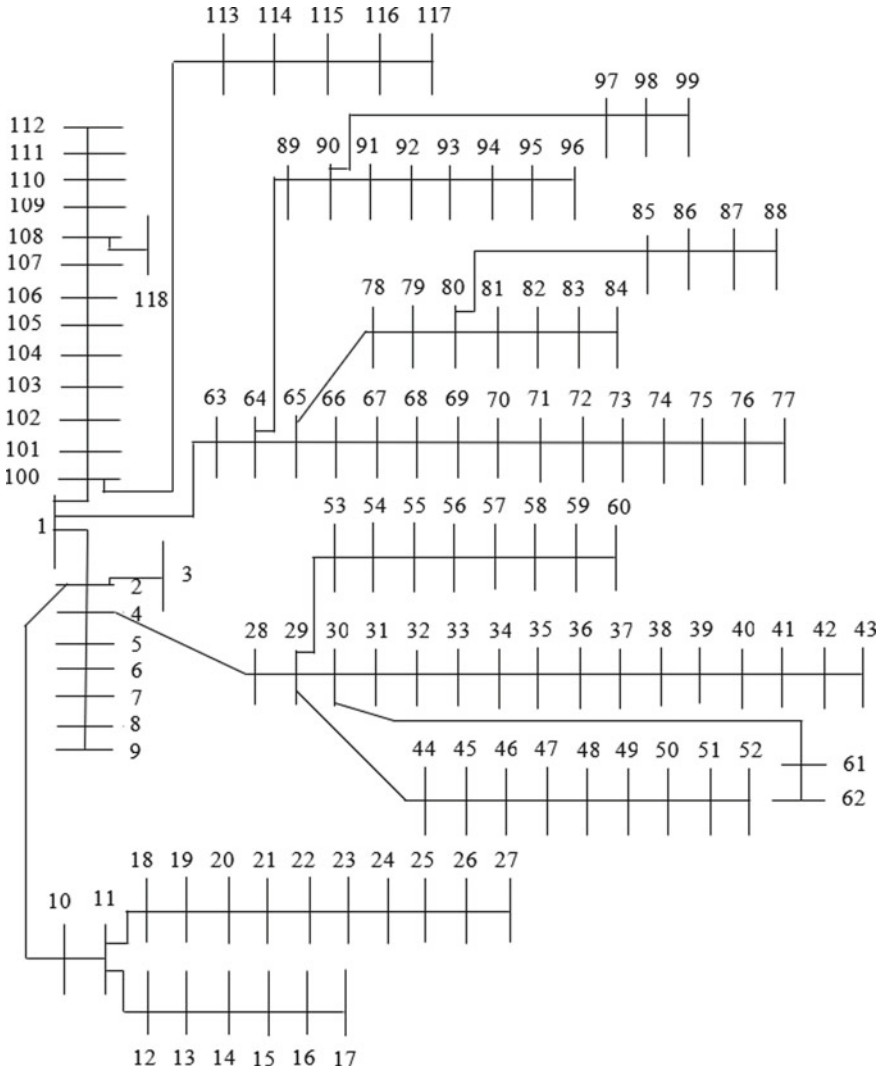

Fig. 3 118-Bus test RDN

7 Conclusion

The paper presents WOA and QOWOA for finding ideal site for DG installation with appropriate size in RDN for multi-objective optimization along with the satisfaction of system constraints. The methodology analysis is done with 33, 69 and 118 bus test system with more than one DG at different locations. The results exhibit the potency of the proposed QOWOA to solve multi-objective optimal DG emplacement problem in RDN. The results clearly demonstrate that QOWOA converges to better

Table 3 Computational results of different approaches for 118-bus RDN

Algorithm	DG optimum location	DG optimum size in MW	Losses in MW	Voltage deviance (p.u)	Voltage stability index	CPU time in seconds
LFSA [39]	36, 48, 56, 75, 88, 103, 116	7.4673, 0.7109, 3.6739, 2.824, 2.2979, 5.0503, 0.4606	0.9001885	NA	0.7561	25.29
TLBO [20]	35, 48, 65, 72, 88, 99, 111	3.2462, 2.8864, 2.4307, 3.305, 1.9917, 1.6040, 3.5984	0.7058980	0.0327	0.8548	20.91
QOTLBO [20]	43, 49, 54, 74, 80, 94, 111	1.5880, 3.8459, 0.9852, 3.1904, 3.1632, 1.9527	0.6775881	0.0233	0.8794	20.85
WOA	35, 48, 65, 72, 86, 99, 111	3.3331, 2.8864, 2.6843, 3.3054, 1.9908, 1.6421, 3.5984	0.71513	0.0318	0.8556	NA
QOWOA	43, 49, 54, 74, 80, 94, 111	1.5879, 3.845, 0.9852, 3.1903, 3.1631, 1.19526, 3.6013	0.67646	0.0121	0.8890	NA

quality solutions co whereas WOA provides quite inferior solutions on comparison to QOWOA. The results obtained are compared with the results of other methodologies to show the effectiveness of the proposed techniques. The results establishes that the proposed QOWOA gives better results in finding solution to ODGA problem with simultaneous optimization of losses along with the voltage profile enhancement in the RDN.

References

1. V.C. Bhatt, S.K. Modi, R.K. Chauhan, Integration of distributed generation systems: a review. Int. J. Sci. Eng. Res. **7**(12), 119 (2016). ISSN: 2229-5518
2. F.C. Robert, S. Gopalan, Low cost, highly reliable rural electrification through a combination of grid extension and local renewable energy generation. Sustain. Cities Soc. **42**, 344–354 (2018)
3. R. Viral, D. K. Khatod, An analytical approach for sizing and siting of DGs in balanced radial distribution networks for loss minimization. Int. J. Electr. Power Energy Syst. **67**, 191–201 (2015)
4. D.Q. Hung, N. Mithulananthan, K.Y. Lee, Optimal placement of dispatchable and nondispatchable renewable DG units in distribution networks for minimizing energy loss. Int. J. Electr. Power Energy Syst. **55**, 179–186 (2014)
5. N. Acharya, P. Mahat, N. Mithulananthan, An analytical approach for DG allocation in primary distribution network. Int J. Electr. Power Energy Syst. **28**, 669–678 (2006)
6. M. Mirzaei, J. Jasni, H. Hizam, N.I.A. Wahab, S.E.G. Mohamed, An analytical method for optimal sizing of different types of DG in a power distribution system, in *2014 IEEE Int. Conference on Power and Energy (PECon)*, NSPEC accession no. 14999900
7. L.I. Dulau, M. Abrudean, D. Bica, Optimal location of a distributed generator for power losses improvement, in *9th INTER-ENG 2015*, Romania, Oct 2015. Procedia Technol. **22**, 734–739 (2016)
8. P.V. Babu, S.P. Singh, Optimal placement of DG in distribution network for power loss minimization using NLP & PLS technique, in *ICAER 2015*, 15–17 Dec 2015, Mumbai, India. Energy Procedia **90**, 441–454 (2016)
9. A. Zaineb, J. Sridevi, Novel method for loss reduction and voltage profile improvement with multiple DGs. Int. J. Sci. Eng. Res. **8**(11) (2017). ISSN: 2229-5518
10. P. Kayal, C.K. Chanda, Placement of wind and solar based DGs in distribution system for power loss minimization and voltage stability improvement. Int. J. Electr. Power Energy Syst. **53**, 795–809 (2013)
11. O.A. Zongoa, A. Oonsivilai, Optimal placement of distributed generator for power loss minimization and voltage stability improvement, in *2017 International Conference on AEDCEE 2017*, 25–26 May 2017, Thailand. Energy Procedia **138**, 134–139 (2017)
12. T.S. Tawfeeka, A.H. Ahmed, S. Hasanc, Analytical and particle swarm optimization algorithms for optimal allocation of four different distributed generation types in radial distribution networks, ICEER 2018. Energy Procedia **153**, 86–94 (2018)
13. H. HassanzadehFard, A. Jalilian, Optimal sizing and location of renewable energy-based DG units in distribution systems considering load growth. Elect. Power Energy Syst. **101**, 356–370 (2018)
14. D.B. Prakash, C. Lakshminarayana, Multiple DG placements in distribution system for power loss reduction using PSO algorithm, global colloquium in RAEREST 2016. Procedia Technol. **25**, 785–792 (2016)
15. A.H. Ahmed, S. Hasan, Optimal allocation of distributed generation units for converting conventional radial distribution system to loop using particle swarm optimization, ICEER 2018. Energy Procedia **153**, 118–124 (2018)
16. M.M. Legha, M. Mohammadian, M. Darini, Loss reduction and reliability improvement with optimization of DGs placement using genetic algorithm—a case study on the electrical distribution network of North Kerman Area. IJSER **5** (2014). ISSN: 2229-5518
17. F. Ud Din, A. Ahmad, H. Ullah, A. Khan, T. Umer, S. Wan, Efficient sizing and placement of distributed generators in cyber-physical power system. J. Syst. Archit. **97**, 197–207 (2019)

18. Q. Zhao, S. Wang, K. Wang, B. Huang, Multi-objective optimal allocation of distributed generations under uncertainty based on D-S evidence theory and affine arithmetic. Electr. Power Energy Syst. **112**, 70–82 (2019)
19. H.A.M. Kanaan, S.K. EL-Sayed, M.A.A. Mehanna, Impact of distributed generator on power system network. Int. J. Sci. Eng. Res. **7**(4), 142 (2016). ISSN: 2229-5518
20. S. Sultana, P.K. Roy, Multi-objective quasi-oppositional teaching learning based optimization for optimal location of distributed generator in radial distribution systems. Int. J. Electr. Power Energy Syst. **63**, 534–545 (2014)
21. T.T. Nguyen, A.V. Truong, T.A. Phung, A novel method based on adaptive cuckoo search for optimal network reconfiguration and distributed generation allocation in distribution network. Electr. Power Energy Syst. **78**, 801–815 (2016)
22. K. Muthukumar, S. Jayalalitha, Optimal placement and sizing of distributed generators and shunt capacitors for power loss minimization in radial distribution networks using hybrid heuristic search optimization technique. Electr. Power Energy Syst. **78**, 299–319 (2016)
23. M.A. Hashemabadi, M.M. Legha, A.K. Ravari, Optimal DG placement for power loss reduction and improvement voltage profile using smart methods. Int. J. Sci. Eng. Res. **5** (2014). ISSN: 2229-5518
24. B. Mahdad, K. Srairi, Adaptive differential search algorithm for optimal location of distributed generation in the presence of SVC for power loss reduction in distribution system. Eng. Sci. Technol. Int. J. **19**, 1266–1282 (2016)
25. S.K. Injeti, A Pareto optimal approach for allocation of distributed generators inradial distribution systems using improved differential search algorithm. J. Electr. Syst. Inf. Technol. **5**, 908–927 (2018)
26. M.M. Othman, W. El-Khattam, Y.G. Hegazy, A.Y. Abdelaziz, Optimal placement and sizing of voltage controlled distributed generators in unbalanced distribution networks using supervised firefly algorithm. Electr. Power Energy Syst. **82**, 105–113 (2016)
27. S. Katamble, S. Palled, V. Gaikwad, V. Shetty, Reconfiguration of distribution system by optimal placement of distributed generator. Int. J. Sci. Eng. Res. **10**(5) (2019). ISSN: 2229-5518
28. B. Poornazaryan, P. Karimyan, G.B. Gharehpetian, M. Abedi, Optimal allocation and sizing of DG units considering voltage stability, losses and load variations. Electr. Power Energy Syst. **79**, 42–52 (2016)
29. M. Home-Ortiz, M.P. Kasmaei, M. Lehtonen, J.R.S. Mantovani, Optimal location-allocation of storage devices and renewable-based DG in distribution systems. Electr. Power Syst. Res. **172**, 11–21 (2019)
30. T.P. Nguyen, D.N. Vo, A novel stochastic fractal search algorithm for optimal allocation of distributed generators in radial distribution systems. Appl. Soft Comput. **70**, 773–796 (2018)
31. P.D.P. Reddy, V.C.V. Reddy, T.G. Manohar, Optimal renewable resources placement in distribution networks by combined power loss index and whale optimization algorithms. J. Electr. Syst. Inf. Technol. **5**, 175–191 (2018)
32. S. Mirjalili, A. Lewis, The whale optimization algorithm. Adv. Eng. Softw. **95**, 51–67 (2016)
33. H.R. Tizhoosh, Opposition-based learning: a new scheme for machine intelligence, in *International Conference on Agents, Web Technologies and Internet Commerce*, Vienna, Austria (2005), pp. 695–701
34. J.H. Teng, A direct approach for distribution system load flow solutions. IEEE Trans. Power Deliv. **18**(3), 882–887 (2003)
35. M.A. Kashem, V. Ganapathy, G.B. Jasmon, M.I. Buhari, A novel method for loss minimization in distribution networks, in *International Conference on Electric Utility Deregulation and Restructuring and Power Technologies 2000*, City University, London, 4–7 April 2000, pp. 251–256
36. M. Chakravorty, D. Das, Voltage stability analysis of radial distribution networks. Int. J. Electr. Power Energy Syst. **23**(2), 129–135 (2001)

37. D. Zhang, Z. Fu, L. Zhang, An improved TS algorithm for loss-minimum reconfiguration in large-scale distribution systems. Electr. Power Syst. Res. **77**(5–6), 685–694 (2007)
38. M.H. Moradi, M. Abedini, A combination of genetic algorithm and particle swarm optimization for optimal DG location and sizing in distribution systems. Int. J. Electr. Power Energy Syst. **34**(1), 66–74 (2012)
39. I.S. Kumar, N.P. Kumar, A novel approach to identify optimal access point and capacity of multiple DGs in a small, medium and large-scale radial distribution system. Int. J. Electr. Power Energy Syst. **45**(1), 142–151 (2013)

Sooty Tern Optimization Algorithm for Economic Emission Dispatch Problem Integration with Wind Energy

Jatin Soni and Kuntal Bhattacharjee

Abstract In order to reduce total fuel costs and greenhouse gas emissions, thermal generating units now use renewable energy sources. Incorporating renewable energy sources like wind energy makes the multi-objective economic emission dispatch (EED) issue very difficult and non-linear. The wind-thermal model's emissions and costs have been optimised using the sooty tern optimization algorithm (STOA), which takes wind output unpredictability into account. Migration and assault, the two key components of the method, aid search agents in avoiding local optimum and obtaining global optimum with a shorter convergence time. In order to verify the suggested algorithm's efficacy, it has been tested in ten thermal producing units with fifty wind units while taking into account different operational restrictions. The proposed method's findings show that, when compared to other recently developed algorithms, the STOA algorithm performs better in terms of computing efficiency and solution quality.

Keywords Economic emission load dispatch · Sooty tern optimization algorithm · Valve point loading effect · Wind energy second

1 Introduction

The small scale of the centralized power system is called a microgrid [1]. The amount of loads, energy sources, and distributed generating (DG) units that have been incorporated into the microgrid [2]. The DG units can be thermal generating units or renewable energy sources [3]. In order to meet load demand, the thermal producing units should be run as cheaply as possible while taking into account numerous operational restrictions, such as the valve point loading effect (VPLE), ramp-rate limit (RRL), power balancing, and transmission loss [4]. Economic dispatch (ED) is the name given to this issue. In recent years, the government has imposed strict rules

J. Soni (✉) · K. Bhattacharjee
Institute of Technology, Nirma University, Ahmedabad 382481, Gujarat, India
e-mail: 20ptphde231@nirmauni.ac.in

© The Author(s), under exclusive license to Springer Nature Singapore Pte Ltd. 2023

K. Murari et al. (eds.), *Soft Computing Applications in Modern Power and Energy Systems*,
Lecture Notes in Electrical Engineering 975,
https://doi.org/10.1007/978-981-19-8353-5_12

on thermal power plants to reduce the emission of harmful fuel gases like sulfur oxides (SO_X), nitrogen oxides (NO_X), and carbon oxides (CO_X). In order to reduce overall fuel costs and pollution emissions, researchers have suggested the integrated multi-objective economic emission dispatch (EED) [5]. Using the price penalty factor (PPF), the EED model's multi-objective function has been reduced to a single objective function [6]. The classical approaches like Newton-Raphson method, linear programming, quadratic programming, and gradient method. However, these methods fail to solve complex and non-linear objective function. The EED problem has therefore been addressed by scholars using a variety of meta-heuristic optimization strategies [7].

Renewable energy sources (RES) have been combined with the thermal producing units to further minimise pollution emissions, overall fuel costs, and the impact of global warming [8]. Due to their lower running costs, wind and solar power facilities have typically been combined with thermal units [9]. Therefore, the EED model becomes highly complex and non-linear after integrating RES with the thermal units. By treating the emission as a limitation, The particle swarm optimization (PSO) [10], artificial bee colony algorithm (ABC) [11], and summation-based multi-objective differential evolution (SMODE) [12] have been utilised to lower the overall cost of gasoline. The EED model with the wind model based on the Weibull distribution has been solved using the craziness-based differential evolution approach [13]. Several other meta-heuristic techniques like a chaotic quantum genetic algorithm (CQGA) [14], Jaya algorithm (JA) [15], Exchange Market Algorithm (EMA) [16], gravitational acceleration enhanced PSO (GAEPSO) [17], and summation-based multi-objective differential evolution (SMODE) [18] have been applied to solve the EED problem integrated with wind energy. The probabilistic EED model has been proposed by considering uncertainties of output wind and solar power [19]. The dragonfly algorithm (DA) has solved the beta distribution-based solar model with the EED model [20]. The wind energy chance-constrained EED issues have been solved using the chaotic sine-cosine algorithm (CSCA) [21]. However, the global optimal solution may not be reached even with the use of the aforementioned techniques [22]. Therefore, to resolve the extremely difficult EED problem integration with RES, a powerful optimization approach is needed [23].

Recently, Dhiman et al. unveiled the swarm intelligence-based Sooty Tern Optimization Algorithm (STOA) [24]. The sooty tern's natural behaviour has served as an inspiration for the STOA method. The STOA technique offers a very excellent balance between the exploration and exploitation strategy, which aids in avoiding local optima and accelerating convergence to global optima [25]. Previously, the STOA technique has been widely used in other fields like feature selections, signal processing, and financial stress prediction. Therefore, the present authors have proposed a first-time STOA algorithm for the EED problem with RES. The following are this paper's key contributions:

- A bio-inspired swarm intelligence soft computing technique called the Sooty Tern Optimization Algorithm (STOA) has been proposed by Dhiman et al. [24]. Dhiman et al. improved the 44 benchmark functions to show the reliability of the

aforementioned method [24]. It has been observed that STOA produces significantly better outcomes than the majority of newly created algorithms. To resolve exceedingly challenging and non-linear EED issues utilising RES, the STOA has been applied for the first time in this work.

- Numerous operational constraints, including valve point loading influence, ramp-rate, transmission loss, generation limit, and generation balance, have been considered to make the system more realistic.
- Wind speed has been randomly generated using the Weibull distribution.
- Several test systems have been used to validate the proposed work.
- A comparison of the proposed algorithm with certain existing methods demonstrates the utility and superiority of the STOA algorithm.

In Sect. 2, the EED problem with RES problem formulation is provided. Information on the original STOA approach is provided in Sect. 3. In Sect. 4, the steps for utilising STOA to solve the EED problem are covered. The simulation results of a test scenario are displayed in Sect. 5. Section 6 highlights the manuscript's conclusion.

2 Problem Formulation

The main objective of the EED problem is to lower total fuel costs and pollution output by adhering to all system limits [26]. After integrating with wind farms, the goal function develops into a very complicated, non-linear function [27]. The EED issue with RES is expressed mathematically in the diagram below.

2.1 Objective Function

The boiler has been linked to the various steam valves. To achieve the maximum feasible efficiency for the specified output, valves are opened successively [28]. Therefore, the goal function now includes the sinusoidal term [29]. The following table lists the goal function of the ED problem and emission dispatch model.

$$C_T = \sum_{i=1}^{N} a_{\mathrm{iT}} + b_{\mathrm{iT}} T_{\mathrm{iT}} + c_{\mathrm{iT}} T_{\mathrm{iT}}^2 + |e_{\mathrm{iT}} \sin\{f_{\mathrm{iT}}(T_{\mathrm{iT}}^{\min} - T_{\mathrm{iT}})\}| \tag{1}$$

$$E_T = \sum_{i=1}^{N} \alpha_{\mathrm{iT}} + \beta_{\mathrm{iT}} T_{\mathrm{iT}} + \gamma_{\mathrm{iT}} T_{\mathrm{iT}}^2 + \zeta_{\mathrm{iT}} \exp(\lambda_{\mathrm{iT}} T_{\mathrm{iT}}) \tag{2}$$

where $a_{\mathrm{iT}}, b_{\mathrm{iT}}, c_{\mathrm{iT}}$ are constant of thermal cost for iTth unit; e_{iT} and f_{iT} are constant of thermal iTth unit representing VPLE; N is the number of linked thermal units; T_{iT} is each thermal generator's output power; $T_{i\,\min}$, $T_{i\,\max}$ are each generator's limit values

for lowest and maximum power; α_{iT}, β_{iT} and γ_{iT} are emission constant of iTth unit; ξ_{iT} and λ_{iT} are constant of emission for iTth unit with VPLE. The multi-objective EED problem may be reduced to one objective using the linear weighting technique. To equalise the weight of each element, the PPF incorporates the cost of pollutants and gasoline [30]. The following is the total cost's mathematical expression.

$$\text{Total cost} = \min[(w \times C_T) + (1 - w) \times \text{PPF} \times E_T] + \sum_{k=1}^{N_w} W_{p,k} \times C_{w,k} \quad (3)$$

where $W_{P,j}$ is power output for jth wind unit; C_{wj} is cost constant of jth wind unit in \$/h; N_s is a number of wind farms overall; w is a uniformly distributed weighting factor that ranges from 0 to 1.

2.2 Constraints

The system should take into account the different operational restrictions to make it more realistic [31]. In conducting this research, the following restrictions have been taken into account.

Thermal Generator Operating Constraints For reliable and continuous operation, the output power from thermal and wind farms should be between the boundary limits [32].

$$T_i^{\min} \leq T_i \leq T_i^{\max}; \quad i = 1, 2, 3, \ldots, N \quad (4)$$

$$0 \leq w_j \leq w_{r,j}; \quad j = 1, 2, 3, \ldots, N_w \quad (5)$$

where $w_{r,j}$ is the power output for jth wind plants.

Power Balance Constraints The combined output of the thermal and wind power plants should be equal to the sum of the load requirements plus the sum of the transmission losses in the lines [33].

$$\sum_{i=1}^{N} T_i + \sum_{k=1}^{N_w} W_{p,k} - (T_D + T_L) = 0 \quad (6)$$

where P_L is total transmission loss; P_D is total load demand. The Kron's loss formula, which is shown below, may be used to compute the overall transmission losses [34].

$$T_L = \sum_{m=1}^{N} \sum_{n=1}^{N} T_m B_{mn} T_n + \sum_{m=1}^{N} B_{m0} T_m + B_{00} \quad (7)$$

where B_{mn}, B_{m0}, and B_{00} are components of the matrix B. The formulation of the aforementioned equation is:

$$T_L = \sum_{m=1}^{N-1}\sum_{n=1}^{N-1} T_m B_{mn} T_n + 2T_N \left(\sum_{m=1}^{N-1} B_{Nm} T_m\right) + B_{NN} T_N^2 + \sum_{m=1}^{N-1} B_{0m} T_m + B_{0N} T_N + B_{00} \tag{8}$$

2.3 Modelling of Wind Plant

Wind speed has been a determining factor in wind farm production power. The wind speed has therefore been generated at random using the Weibull distribution [35]. The following gives the wind velocity's mathematical expression.

$$f_v(v) = \frac{k}{c}\left(\frac{v}{c}\right)^{k-1} \exp\left[1 - \left(\frac{v}{c}\right)^k\right]; \quad \text{for } 0 < v < \infty \tag{9}$$

where k and c are the wind turbine's form and scale factors; the immediate wind speed is v. Here are some examples of how wind power is expressed:

$$W_{\mathrm{p}} = \begin{cases} 0; & : \ v < v_{\mathrm{in}}, v > v_{\mathrm{out}} \\ W_{\mathrm{pt}}\left(\frac{v - v_{\mathrm{i}}}{v_{\mathrm{r}} - v_{\mathrm{i}}}\right) & : \ v_{\mathrm{r}} < v < v_{\mathrm{out}} \\ W_{\mathrm{pr}}; & : \ v_{\mathrm{r}} < v < v_{\mathrm{out}} \end{cases} \tag{10}$$

where v_{i} and v_{r} are instantaneous speed and rated velocity of wind unit; v is output speed from the PDF; v_{in} and v_{out} are cut in and cut out the velocity of wind unit; W_{p} and W_{pt} are output power and rated power of wind turbine.

3 Sooty Tern Optimization Algorithm (STOA)

Dhiman et al. originally suggested the STOA approach in 2019 [24]. There have been different sizes and weights of sooty terns. Insects, reptiles, fish, earthworms, amphibians, and other creatures are all eaten by these sooty terns, which are seabirds. To draw worms that are buried by feet, they create the sound of rain [36]. Additionally, the sooty utilise baking crumbs to encourage the fish [37]. Most of the time, these sooty dwell in groups and employ their intelligence to find and attack prey [25]. The seasonal sooty then searches the environment for sources of appropriate energy. Therefore, migration and attack are the two primary traits of sooty terns. The other sooty terns migrate toward the stronger one during migrating steps and change their positions to avoid colliding [38]. Mathematically, the sooty terns' behaviour may be described as follows:

$$C_{\mathrm{st}} = S_A \times P_{\mathrm{st}}(z) \tag{11}$$

$$S_A = C_f - z \times \frac{C_f}{\text{Iter}_{\max}} \tag{12}$$

where C_{st} is where sooty terns are located, P_{st} is where sooty terns are at the moment, The most recent iteration is z, S_{DA} the sooty terns' movement in the search area, S_f is flexible for regulating S_A. Then, each sooty tern advances toward the largest one [39]. This motion can be described numerically as:

$$M_{\text{st}} = C_B \times (P_{\text{bst}}(z) - P_{\text{st}}(z)) \tag{13}$$

$$C_B = 0.5 \times R_{\text{and}} \tag{14}$$

where M_{st} is the sooty terns' altered posture, P_{bst} is the top sooty tern, C_B is an uncontrolled variable, Rand is a chance number from 0 to 1. The top sooty terns are ranked differently by each tern.

$$D_{\text{st}} = C_{\text{st}} + M_{\text{st}} \tag{15}$$

where between each sooty tern and the strongest sooty tern, there is a difference called S_{st}. The sooty terns attack in a spiral motion while varying their speeds. These properties can be stated numerically as:

$$x' = R_{\text{adi}} \times \sin(i) \tag{16}$$

$$y' = R_{\text{adi}} \times \cos(i) \tag{17}$$

$$z' = R_{\text{adi}} \times i \tag{18}$$

$$r = u \times e^{\text{kv}} \tag{19}$$

where R_{adi} is the diameter of each spiral turn, i is not consistent, v and u are constants, e is the logarithm. The location of sooty terns may be described numerically as

$$P_{\text{st}}(z) = D_{\text{st}} \times (x' + y' + z') \times P_{\text{bst}}(z) \tag{20}$$

where P_{st}(z) then provides the best answer after updating the location of another sooty tern.

3.1 Sequential Steps of STOA

Step 1: Setting up each search agent's lower and higher bound limits. Establish the population size and total number of iterations. Initialize S_A and C_B.
Step 2: When calculating the goal, input variables are taken into account.

Step 3: Use an objective function to assess each population's fitness function value. Look for the most robust sooty tern P_{bst}.
Step 4: If the value of the fitness function is less than the value before, local minima are taken into consideration.
Step 5: The population's altered values are examined to see if they were violated or not. If so, set their boundaries.
Step 6: To locate global optima, the search agents will roam across the whole search space. Revise the parameter S_A and C_B. Calculate the search agent's fitness value and update P_{bst}.
Step 7: In the exploitation stage, the people will travel there after the destination point has been identified.
Step 8: Follow steps 3 through 7 again until the termination requirements are met.

4 STOA Used in EED Problem with RES

Figure 1 shows the STOA flowchart that was utilised to resolve the EED problem using wind energy. The steps to solving the issue are as follows:

Step 1: Set the lower bound, higher bound, number of heat generators, population size, and all other parameters to their starting settings.
Step 2: For thermal power plants, each search agent randomly initialises the population matrix and assesses the fitness function.
Step 3: At this stage, the STOA algorithm starts doing its heavy lifting. Randomly generate S_A and C_B parameters.
Step 4: Based on fitness value, choose the best swarm (strongest sooty tern)
Step 5: Each search agent's position should be updated using Eq. (20).
Step 6: Each search agent's position should be updated using Eq. (20).
Step 7: Calculate the fitness function and update each search agent's local best position. Best mean cost and SD updates.
Step 8 Up until the termination requirement is met, repeat step 5 as necessary.

5 Results and Discussion

The STOA approaches have been used on an EED model with ten thermal producing units and fifty wind units. The STOA method's outcomes are contrasted with those of other newly created methodologies. The simulations were carried out on a machine with a 1.7 GHz Intel CPU and 4 GB of RAM running the MATLAB 2021a programme.

Each of the 50 wind turbines in the wind farms is rated to produce 2 MW of power. The wind turbine's parameter has been specified in [40]. The thermal unit input values were acquired from in [41]. The system needs 2000 MW of electricity.

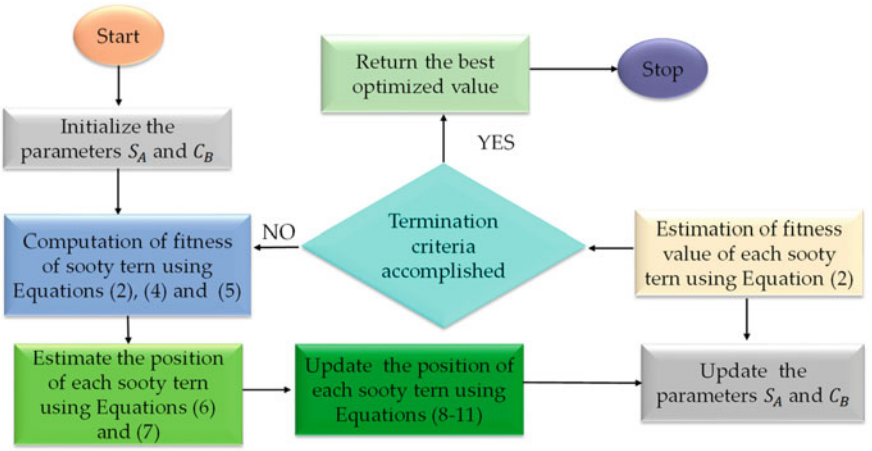

Fig. 1 Flowchart of STOA algorithm applied in EED problem with RES

Table 1 Results for best fuel cost, best emission, and the best compromise solution

	Fuel cost minimization		Emission minimization		Best compromise solution	
	CSCA	TSA	CSCA	TSA	CSCA	TSA
T_1	54.42	55.00	54.10	46.72	54.72	51.29
T_2	79.49	80.00	77.01	75.62	79.78	73.72
T_3	99.44	107.61	78.34	81.06	88.03	111.94
T_4	101.18	111.26	77.82	91.34	80.53	47.52
T_5	79.80	66.43	160.00	160.00	130.19	151.30
T_6	81.69	97.19	237.92	234.00	150.84	184.91
T_7	296.88	267.38	296.09	283.92	296.60	236.29
T_8	335.47	340.00	280.66	242.98	315.61	320.93
T_9	470.00	470.00	417.26	426.01	434.44	443.37
T_{10}	470.00	437.59	384.16	388.09	434.66	386.88
W_P	17.33	49.54	17.06	48.25	17.53	68.84
C_T, \$/h	110,355.35	109,138.85	115,292.06	11,311.22	111,798.83	110,223.36
E_T, tonnes/h	4496.61	4382.33	3878.40	3863.14	4101.73	3919.89
P_L, MW	85.7046	81.99	80.41	77.88	82.93	77.60

This test system has been made more realistic by taking into account the transmission loss, VPLE, and generation capacity limits. The matrix of the B constants was extracted from [42]. Table 1 contains the best result from 50 consecutive runs of the STOA technique in both a single-objective compromise solution and a multi-objective compromise solution. The fuel cost and emission attained by the STOA method are 110,223.36 \$/h and 3919.89 tones/h respectively. As shown in Table 2,

Table 2 Comparison of the best, worst, and average compromise solutions obtained by STOA with other algorithms

Algorithm	Fuel cost minimization				Emission minimization			
	Best	Worst	Average	Std.	Best	Worst	Average	Std.
STOA	110,223.36	111,012.11	110,875.62	24.58	3919.89	4112.69	3998.21	15.74
CSCA	111,798.83	112,457.69	111,875.96	36.96	4101.73	4201.96	4151.26	24.95
GAEPSO	112,968.21	113,145.11	112,999.14	42.11	4251.01	4369.18	4311.21	38.65
GSA	113,845.11	114,541.56	113,987.54	52.96	4336.22	4498.57	4369.25	66.96
PSO	115,962.04	116,412.51	116,112.85	82.21	4415.21	4512.69	4489.15	98.65

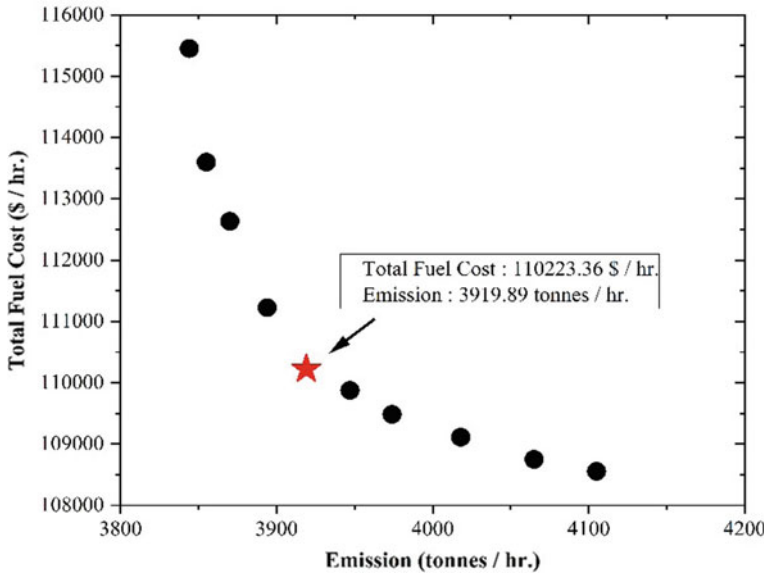

Fig. 2 Trade-off curve obtained by STOA algorithm

the best, worst, and average fuel prices and emission results achieved by the STOA algorithm have been compared with those of other methods. Figure 2 depicts the trade-off curve derived by the STOA approach for the multi-objective EED issue.

5.1 Tuning the Parameter of the STOA

To get the best result in the shortest amount of time for computing, the STOA algorithm's parameters should be adjusted. The different values of the parameters 'S_A and C_B' provide various minimum gasoline prices. For solitary values S_A parameter, the values of another parameter 'C_B' must be changed in all conceivable combinations.

Table 3 The minimum fuel cost for different values of STOA parameters

S_A	C_B	Minimum fuel cost ($/h)	Minimum emission (tones/h)
0.1	0.40	111,236.22	4152.69
0.2	0.45	109,635.32	4256.96
0.3	0.50	111,454.69	4222.32
0.4	0.55	109,965.11	4111.69
0.5	0.60	110,223.36	3919.89
0.6	0.65	111,362.44	3888.62
0.7	0.70	111,962.32	4015.22
0.8	0.75	111,745.62	4145.32

To exhibit here, a very huge space is required. Table 3 displays the results of the minimal fuel costs for all feasible combinations after 100 trail runs. The parameters' ideal values are provided as follows: $S_A = 0.5$ and $C_B = 0.6$.

5.2 Discussion

The best compromise solution for the multi-objective EED issue in the test system is 110,223.36 $/h (fuel cost) and 3919.89 tons/h (emission). When compared to the more current CSCA approach, the STOA method results in lower fuel costs and emissions. 2,008,162 MW, 68.83 MW, 77.6 MW, and 2000 MW correspondingly represent the power generated by the test system's thermal, wind farm, transmission loss, and load demand. Results from recently developed PSO, GSA, and GAEPSO approaches outperform those from STOA methods by a wide margin. Since the thermal generator was integrated with wind farms, the cost of fuel and amount of emissions have both fallen.

6 Conclusion

To reduce overall fuel costs and hazardous gas emissions, the multi-objective EED model has been introduced to coordinate electricity generation from wind farms and thermal generating units. To deal with stochastic variables under the limitations, the Weibull probability density function has been introduced. Wind energy multi-objective EED issues have been tackled using the STOA algorithm, which is based on swarm intelligence. The different system restrictions, including power balance, transmission losses, VPLE, and generator operating limits, have been taken into account. The STOA approach has been proven to be effective in resolving the eco-

nomic emission dispatch issue in the test systems for the ten units. In comparison to other newly created approaches like CSCA, PSO, GSA, and GAEPSO, the STOA method produces better outcomes. The outcomes demonstrate that the suggested approach offers an effective and encouraging optimal solution in a relatively short amount of computing time.

References

1. J.M. Soni, D.V. Patel, R.V. Patel, H.P. Modha, A strategic community control-based power flow between grid-integrated PV houses, in *Electronic Systems and Intelligent Computing* (Springer, 2020), pp. 1061–1071
2. K. Bhattacharjee, K. Shah, J. Soni, Solving economic dispatch using artificial eco system-based optimization. Electr. Power Compon. Syst. **49**, 1–18 (2021)
3. K. Bhattacharjee, Economic dispatch problems using backtracking search optimization. Int. J. Energy Optim. Eng. (IJEOE) **7**(2), 39–60 (2018)
4. K. Bhattacharjee, N. Patel, A comparative study of economic load dispatch with complex non-linear constraints using salp swarm algorithm. Sci. Iran. (2020)
5. K. Bhattacharjee, N. Patel, An experimental study regarding economic load dispatch using search group optimization. Sci. Iran. **27**(6), 3175–3189 (2020)
6. H. Nourianfar, H. Abdi, Solving power systems optimization problems in the presence of renewable energy sources using modified exchange market algorithm. Sustain. Energy Grids Netw. **26**, 100449 (2021)
7. Y. Zhang, F. Yao, H.H.-C. Iu, T. Fernando, K.P. Wong, Sequential quadratic programming particle swarm optimization for wind power system operations considering emissions. J. Mod. Power Syst. Clean Energy **1**(3), 227–236 (2013)
8. A. Gholami, J. Ansari, M. Jamei, A. Kazemi, Environmental/economic dispatch incorporating renewable energy sources and plug-in vehicles. IET Gener. Transm. Distrib. **8**(12), 2183–2198 (2014)
9. G. Piperagkas, A. Anastasiadis, N. Hatziargyriou, Stochastic PSO-based heat and power dispatch under environmental constraints incorporating CHP and wind power units. Electr. Power Syst. Res. **81**(1), 209–218 (2011)
10. G. Liu, Y. Zhu, Z. Huang, Dynamic economic dispatch with wind power penetration based on non-parametric kernel density estimation. Electr. Power Compon. Syst. **48**(4–5), 333–352 (2020)
11. H. Jadhav, R. Roy, Gbest guided artificial bee colony algorithm for environmental/economic dispatch considering wind power. Expert Syst. Appl. **40**(16), 6385–6399 (2013)
12. B.-Y. Qu, J.J. Liang, Y. Zhu, Z. Wang, P.N. Suganthan, Economic emission dispatch problems with stochastic wind power using summation based multi-objective evolutionary algorithm. Inf. Sci. **351**, 48–66 (2016)
13. H. Jadhav, A. Deb, R. Roy, A craziness based differential evolution algorithm for thermal-wind generation dispatch considering emission and economy with valve-point effect, in *2011 10th International Conference on Environment and Electrical Engineering* (IEEE, 2011), pp. 1–5
14. G.-C. Liao, A novel evolutionary algorithm for dynamic economic dispatch with energy saving and emission reduction in power system integrated wind power. Energy **36**(2), 1018–1029 (2011)
15. S. Basak, B. Bhattacharyya, B. Dey, Combined economic emission dispatch on dynamic systems using hybrid CSA-JAYA algorithm. Int. J. Syst. Assur. Eng. Manag. 1–22 (2022)
16. A. Rajan, T. Malakar, Optimum economic and emission dispatch using exchange market algorithm. Int. J. Electr. Power Energy Syst. **82**, 545–560 (2016)

17. S. Jiang, Z. Ji, Y. Wang, A novel gravitational acceleration enhanced particle swarm optimization algorithm for wind-thermal economic emission dispatch problem considering wind power availability. Int. J. Electr. Power Energy Syst. **73**, 1035–1050 (2015)
18. B.-Y. Qu, J.J. Liang, Y. Zhu, Z. Wang, P.N. Suganthan, Economic emission dispatch problems with stochastic wind power using summation based multi-objective evolutionary algorithm. Inf. Sci. **351**, 48–66 (2016)
19. Y. Yang, W. Wu, B. Wang, M. Li, T. Zhu, Optimal decomposition of stochastic dispatch schedule for renewable energy cluster. J. Mod. Power Syst. Clean Energy **9**(4), 711–719 (2021)
20. D. Das, A. Bhattacharya, R.N. Ray, Dragonfly algorithm for solving probabilistic economic load dispatch problems. Neural Comput. Appl. **32**(8), 3029–3045 (2020)
21. T. Guesmi, A. Farah, I. Marouani, B. Alshammari, H.H. Abdallah, Chaotic sine-cosine algorithm for chance-constrained economic emission dispatch problem including wind energy. IET Renew. Power Gener. **14**(10), 1808–1821 (2020)
22. X. Zhao, H. Chen, S. Liu, X. Ye, Economic & environmental effects of priority dispatch of renewable energy considering fluctuating power output of coal-fired units. Renew. Energy **157**, 695–707 (2020)
23. L.-L. Li, Z.-F. Liu, M.-L. Tseng, S.-J. Zheng, M.K. Lim, Improved tunicate swarm algorithm: solving the dynamic economic emission dispatch problems. Appl. Soft Comput. **108**, 107504 (2021)
24. G. Dhiman, A. Kaur, STOA: a bio-inspired based optimization algorithm for industrial engineering problems. Eng. Appl. Artif. Intell. **82**, 148–174 (2019)
25. H.H. Ali, A. Fathy, A.M. Kassem, Optimal model predictive control for LFC of multi-interconnected plants comprising renewable energy sources based on recent sooty terns approach. Sustain. Energy Technol. Assess. **42**, 100844 (2020)
26. F. Nazari-Heris, B. Mohammadi-Ivatloo, D. Nazarpour, Economic dispatch of renewable energy and CHP-based multi-zone microgrids under limitations of electrical network. Iran. J. Sci. Technol. Trans. Electr. Eng. **44**(1), 155–168 (2020)
27. A. Nandi, V.K. Kamboj, A meliorated Harris hawks optimizer for combinatorial unit commitment problem with photovoltaic applications. J. Electr. Syst. Inf. Technol. **8**(1), 1–73 (2021)
28. K. Bhattacharjee, A. Bhattacharya, S.H. nee Dey, Solution of economic emission load dispatch problems of power systems by real coded chemical reaction algorithm. Int. J. Electr. Power Energy Syst. **59**, 176–187 (2014)
29. S. Roy, K. Bhattacharjee, A. Bhattacharya, A modern approach to solve of economic load dispatch using group leader optimization technique. Int. J. Energy Optim. Eng. (IJEOE) **6**(1), 66–85 (2017)
30. N. Patel, K. Bhattacharjee, A comparative study of economic load dispatch using sine cosine algorithm. Sci. Iran. **27**(3), 1467–1480 (2020)
31. K. Bhattacharjee, A. Bhattacharya, K. Shah, N. Patel, Backtracking search optimization applied to solve short-term electrical real power generation of hydrothermal plant. Eng. Optim. 1–19 (2021)
32. X. Li, J. Xu, Z. Lu, Differential evolution algorithm based on state transition of specific individuals for economic dispatch problems with valve point effects. J. Electr. Eng. Technol. 1–14 (2021)
33. N. Shouman, Y.G. Hegazy, W.A. Omran, Hybrid mean variance mapping optimization algorithm for solving stochastic based dynamic economic dispatch incorporating wind power uncertainty. Electr. Power Compon. Syst. **48**(16–17), 1786–1797 (2021)
34. M. Ghasemi, E. Akbari, M. Zand, M. Hadipour, S. Ghavidel, L. Li, An efficient modified HPSO-TVAC-based dynamic economic dispatch of generating units. Electr. Power Compon. Syst. **47**(19–20), 1826–1840 (2019)
35. K. Dasgupta, P.K. Roy, V. Mukherjee, A novel oppositional learning-based chaotic sine cosine algorithm for the dynamic thermal–wind economic dispatch problem. Eng. Optim. 1–19 (2021)
36. K.Z. Zamli, M. Kader, S. Azad, B.S. Ahmed et al., Hybrid henry gas solubility optimization algorithm with dynamic cluster-to-algorithm mapping. Neural Comput. Appl. **33**(14), 8389–8416 (2021)

37. A. Singh, A. Sharma, S. Rajput, A.K. Mondal, A. Bose, M. Ram, Parameter extraction of solar module using the sooty tern optimization algorithm. Electronics **11**(4), 564 (2022)
38. A. Singh, A. Sharma, S. Rajput, A.K. Mondal, A. Bose, M. Ram, Parameter extraction of solar module using the sooty tern optimization algorithm. Electronics **11**(4), 564 (2022)
39. L.-L. Li, Z.-F. Liu, M.-L. Tseng, S.-J. Zheng, M.K. Lim, Improved tunicate swarm algorithm: solving the dynamic economic emission dispatch problems. Appl. Soft Comput. **108**, 107504 (2021)
40. M. Basu, Economic environmental dispatch using multi-objective differential evolution. Appl. Soft Comput. **11**(2), 2845–2853 (2011)
41. M. Basu, Dynamic economic emission dispatch using non-dominated sorting genetic algorithm-II. Int. J. Electr. Power Energy Syst. **30**(2), 140–149 (2008)
42. C. Panigrahi, P. Chattopadhyay, R. Chakrabarti, M. Basu, Simulated annealing technique for dynamic economic dispatch. Electr. Power Compon. Syst. **34**(5), 577–586 (2006)

Bid-Based Economic Load Dispatch in Coordination with Virtual Power Plant

Gautam Kumar, Lalit Kumar, Manoj Kumar Kar, and Sanjay Kumar

Abstract The bid-based dynamic economic load dispatch plays an essential role in power system planning. It aims to proper scheduling the power dispatch in a deregulated electricity market while maximizing the social profit. This paper uses a newly developed meta-heuristic algorithm, Gravitational Search Algorithm, to solve the bid-based dynamic economic load dispatch problem on the five conventional generators and a Virtual Power Plant. In the paper, to test the effectiveness of Virtual Power Plant in maximizing social profit, optimization is performed on the test system with two different cases, including Virtual Power Plant and another case, without considering Virtual Power Plant. The independent system operator collects each generator's generating limits and cost coefficient data and calculates the market-clearing price from the Nash SFE equation. To verify the efficacy of the proposed algorithm, the optimized result obtained from GSA is compared with the other contemporary meta-heuristic algorithm.

Keywords Bid-based dynamic load dispatch · Virtual Power Plant · Distributed Generations · Gravitational Search Algorithm

G. Kumar (✉) · L. Kumar · M. K. Kar · S. Kumar
EE Department, NIT, Jamshedpur, Jharkhand, India
e-mail: 2021rsee002@nitjsr.ac.in

L. Kumar
e-mail: lalitnitjsr@gmail.com

M. K. Kar
e-mail: manojkar132@gmail.com

S. Kumar
e-mail: sanjay.ee@nitjsr.ac.in

© The Author(s), under exclusive license to Springer Nature Singapore Pte Ltd. 2023

K. Murari et al. (eds.), *Soft Computing Applications in Modern Power and Energy Systems*,
Lecture Notes in Electrical Engineering 975,
https://doi.org/10.1007/978-981-19-8353-5_13

1 Introduction

As all the power generating units are shifting towards clean and green energy generation, this leads to clean and green energy through various Distributed Generations (DGs). The problem associated with the DGs is they cannot be used on a large scale and in multiple areas [1]. As a result, the twenty-first century economy demands an advanced electric grid smarter than the conventional plants established at the end of the nineteenth century, whereas "Virtual Power Plant (VPP)" combines distributed generating with digital information and communication technologies to meet the needs of the modern economy [2]. These VPPs are enabled with bidirectional energy flows and knowledge within the VPP, enhancing reliability and energy efficiency [3]. The introduction of non-conventional energy sources (such as PV, wind, and biomass), demand responses, and active participation of customers will enhance the performance of VPP [4]. VPP stores the data of power generation, local load, reserve power, etc. of each DG integrated into it. In this era where the electricity demand is changing so drastically, VPP can be proven a great market model to increase the efficacy and profit of the whole market model [5].

For a distribution company (DISCO), Economy Load Dispatch (ELD) is always a big concern for optimal power dispatch at the minimum cost. The conventional static economic load dispatch has been converted into dynamic economic load dispatch to tackle the considerable load variation in real time [6]. In a deregulated environment, the generating companies run the DED problem to find the optimum operating point of its power and reserve to be sold in the wholesale electricity market to increase profit. It is popularly known as price-based DED (PBDED) [7]. Sometimes, large consumer and load-serving entity also participates in the market. In this study, the independent system operator (ISO) will perform the DED problem to gain increased social profit, i.e. customer profit and producer profit. And it is popularly known as bid-based DED (BBDED). In BBDED, considering only the supply side in the bidding deal, i.e. single side bidding (where only sellers are participated to satisfy the predicted load demands), makes the market inefficient. But double side bidding (Where both buyers and sellers are experienced) is proven efficient and profitable for the electricity market [8].

An intensive literature survey found that VPP can be very helpful in energy dispatch and can minimize the generation cost of CPP and VPP subjected to dynamic load demand [9]. For the implementation of load shifting to reduce the peak time loading, VPP seems more beneficial [10]. As the renewable generation is limited to small areas and is not reliable, VPP can increase the reliability and continuity of power supply [11]. Many papers have used a game-theoretical approach for deciding the energy price in the deregulated market for bid-based economic load dispatch [12]. And to collect the bids from the different market participants of a pool market, independent system operator (ISO) has been used [13]. Strategic bidding can also be used in the deregulated electricity market to increase the profit of each power supplier, where the benefit of each supplier depends on the difference in the degree of imperfection of the rival suppliers' information [14].

Mathematical optimization problems have become increasingly complicated in recent years, necessitating highly productive approaches. Speed and accuracy are critical outcomes [15]. A meta-heuristic calculation methodology is used to get the optimum position of a single- or multi-variable fitness functions. Traditional deterministic methods do an exhaustive search within constrained processing resources based on simple calculus laws and cannot produce efficient solutions as heuristic (trial-and-error) methods [16]. The non-deterministic techniques, like meta-heuristic algorithms, have produced excellent outcomes in many practical, real-world optimization problems. Modern heuristic algorithms can reduce the time consumption for solving a concentrated engineering problem. It can minimize calculation and give a perfect computational result [17, 18]. Aside from animals and inspections, fundamental physics, chemistry, and mathematics occurrences have developed unique optimization strategies. The Gravitational Search Algorithm (GSA) is based on the Archimedes principle of physics [19].

In this paper, bid-based dynamic economic load dispatch (BBDED) has been performed on five conventional generator units and a VPP (shown in Fig. 1) using the proposed GSA. Here, it is assumed that ISO will collect the bids from producers and consumers, and the load is being satisfied by the coordinated dispatch operation (i.e. CPP and VPP).

2 Problem Formulation

The main objective of the energy dispatch problem is to get maximum social profit through the active participation of CPP and VPP. ISO will collect the load demand of consumers and generation capacities of all generating units (CPP and VPP) and market-clearing price (MCP). ISO maximizes social profit by properly scheduling generator units based on this information (load demand and generation capacities).

A. *Objective function*

The objective function of this work is given by Eq. (1), and mathematically expressed as follows:

$$\text{Maximize social profit} = F_2 - F_1 \tag{1}$$

$$F_1 = \left\{ \sum_{i=1}^{N^{\text{CPP}}} F_i^{\text{CPP}}\left(P_{di}^{\text{CPP}}\right) \right\} + F^{\text{VPP}}\left(P^{\text{VPP}}\right) \tag{2}$$

$$F_2 = \left\{ \sum_{i=1}^{N^{\text{CPP}}} \text{MCP}\left(P_{di}^{\text{CPP}}\right) \right\} + (\text{MCP} + \lambda)\left(P^{\text{VPP}}\right) \tag{3}$$

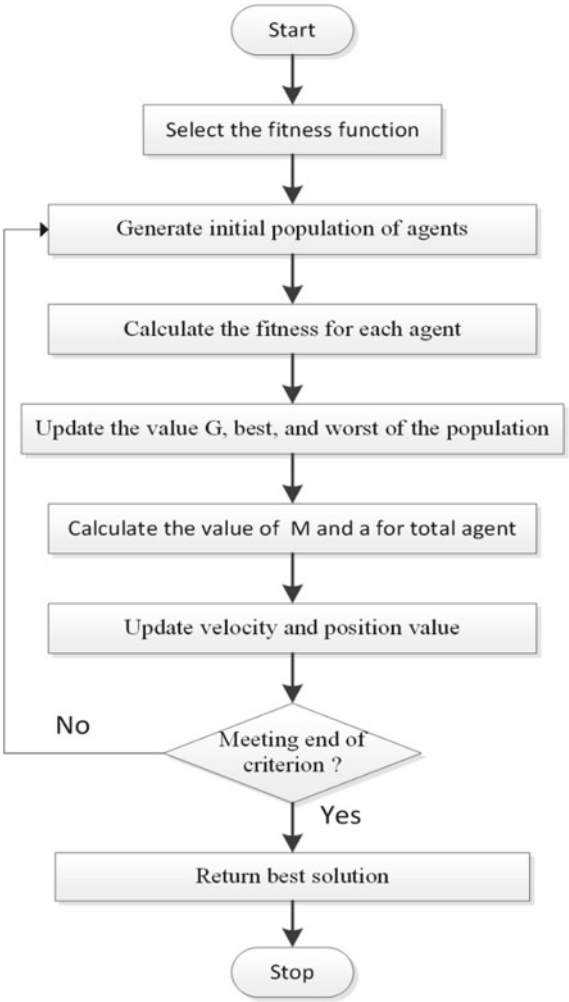

Fig. 1 Flow chart for GSA algorithm

where F_1 and F_2 are the generation cost and revenue given in Eqs. (2) and (3), respectively, $F_i^{\mathrm{CPP}}\left(P_{gi}^{\mathrm{CPP}}\right)$ is the cost function for conventional power plant (CPP) in Eq. (4) and $F^{\mathrm{VPP}}\left(P^{\mathrm{VPP}}\right)$ is the cost function of a virtual power plant (VPP) in Eq. (5), N and M are the no. of generating units in CPP and VPP, respectively, λ is the operation and maintenance cost of VPP, and MCP is the market-clearing price calculated from Eq. (6) [20].

$$F_i^{\mathrm{CPP}}\left(P_{gi}^{\mathrm{CPP}}\right) = \alpha_i^{\mathrm{CPP}} + \beta_i^{\mathrm{CPP}} P_{gi}^{\mathrm{CPP}} + \gamma_i^{\mathrm{CPP}} P_{gi}^{\mathrm{CPP}^2} \tag{4}$$

$$F^{\mathrm{VPP}}\left(P^{\mathrm{VPP}}\right) = \beta^{\mathrm{VPP}} P^{\mathrm{VPP}} + \gamma^{\mathrm{VPP}} P^{\mathrm{VPP}^2} \tag{5}$$

$$\text{MCP} = \frac{P_d + \sum_{i=1}^{N+M} \frac{\beta_i}{\gamma_i}}{\sum_{i=1}^{N+M} \frac{1}{\gamma_i}} \tag{6}$$

where α, β and γ are the coefficients of the cost function.

B. *Equality Constraints*

Active power balance constraints

Active power balance constraints result in the stable operation of the whole power system. Here, the total load demand is being fulfilled by CPP and VPP as shown in Eq. (7).

$$\sum_{i=1}^{N^{\text{CPP}}} \left(P_{gi}^{\text{CPP}}\right) + P^{\text{VPP}} = P_D \tag{7}$$

where P_{gi}^{CPP} is the generation quantity of each generator in CPP, P_{gj}^{VPP} is the generation quantity of each generator in VPP, and P_D is the load demand of consumers.

C. *Inequality Constraints*

Generating limit constraints

Each generating unit of a conventional power plant is designed with a specific maximum and minimum generating capacity; for the power system's stable operation, a generator must generate power within its limits. The limits for CPP and VPP are shown in Eqs. (8) and (9), respectively.

$$P_{ai}^{L,\text{CPP}} \leq P_{ai}^{\text{CPP}} \leq P_{ai}^{U,\text{CPP}} \tag{8}$$

$$0 \leq P_{aj}^{\text{VPP}} \leq P_{aj}^{U,\text{VPP}} \tag{9}$$

3 The Proposed Methodology

GSA is a heuristic search method based on Newton's equations of gravity and mass in relation to each other. Due to its heavy mass, the item experiences gravitational attraction. Due to the overall movement of the object towards the heavier mass, the heavier mass object was attracted to the lower mass object. GSA is used to solve a variety of electrical optimization problems. Due to fewer parameters, it has a very robust and broader search capabilities.

Initialization of position of the αth agent as in Eq. (10):

$$X_\alpha = \left(x_\alpha^1, x_\alpha^2, \ldots x_\alpha^d, \ldots x_\alpha^n\right), \quad \alpha \in N \tag{10}$$

where x_α^d = position of αth agent in the dth dimension

n = search space dimension

The attractive force over mass 'α' by mass 'β' at a given time t is expressed in Eq. (11):

$$F_{\alpha\beta}(t) = G(t)\frac{M_{p\alpha}(t) * M_{a\beta}(t)}{R_{\alpha\beta}(t) + \varepsilon}\left(x_\beta(t) - x_\alpha(t)\right) \tag{11}$$

where $M_{a\beta}$ = active gravitational mass connected to βth agent

$M_{p\alpha}$ = passive gravitational mass connected to αth agent

ε is the arbitrary constant of small magnitude

$G(t)$ = At time t, the gravitational Newtonian constant

$R_{\alpha\beta}(t)$ = The Euclidian distance between "α" and "β" agents that can describe themselves in Eq. (12):

$$R_{\alpha\beta} = \left\| X_\alpha(t) \cdot X_\beta(t) \right\|_2 \tag{12}$$

In GSA, G stands for the starting value G_0 at time t, which may be written as shown in Eq. (13):

$$G(t) = G_0 * \mathrm{e}^{\left(-\gamma \frac{t}{t_{\max}}\right)} \tag{13}$$

where γ is decreasing constant, $t_{\max}$ = maximum iteration.

$F_\alpha(t)$ is the total force operating on the αth agent, which can be expressed as shown in Eq. (14):

$$F_\alpha(t) = \sum_{\beta=1, \beta \neq \alpha}^{N} \mathrm{rand}_\beta * F_{\alpha\beta}(t) \tag{14}$$

where rand_β are arbitrary values in a range [0, 1].

The fitness values are used to calculate distinct masses. As a result, each groups are updated as Eq. (15):

$$M_{a\alpha} = M_{p\alpha} = M_{\alpha\alpha} = M_\alpha, \quad \alpha = 1, 2, \ldots, N$$

$$M_\alpha(t) = \frac{m_\alpha(t)}{\sum_{\beta=1}^{N} m_\beta(t)} \tag{15}$$

where $m_\alpha(t) = \frac{\mathrm{fit}_\alpha(t) - \mathrm{worst}(t)}{\mathrm{best}(t) - \mathrm{worst}(t)}$

$\mathrm{fit}_\alpha(t)$ is the αth agent fitness value at time t

$\mathrm{best}(t) = \min(\mathrm{fit}_1(t), \mathrm{fit}_2(t), \ldots, \mathrm{fit}_N(t))$

$\text{worst}(t) = \max(\text{fit}_1(t), \text{fit}_2(t), \ldots, \text{fit}_N(t))$

Now, at time t, the αth agent acceleration is given in Eq. (16):

$$a_\alpha(t) = {}^{F_\alpha(t)}\!/_{M_\alpha(t)} \tag{16}$$

Finally, the agent's velocity and position values are updated using Eqs. (17) and (18), respectively.

$$v_\alpha(t+1) = \text{rand}_\alpha * V_\alpha(t) + a_\alpha(t) \tag{17}$$

$$x_\alpha(t+1) = x_\alpha(t) + v_\alpha(t+1) \tag{18}$$

The position is adjusted iteratively using the above equation until the GSA algorithm hits the global minima. The GSA flow chart is shown below:

The following steps propose the GSA-based optimization:

- Initialization of the αth agent's position
- Determine the proposed function's value X_α
- Enhance the latest position of $G(t)$, best(t), and worst(t).
- Calculate the valuation of $a_\alpha(t)$, $M_\alpha(t)$ and $V_\alpha(t)$.
- Examine the existing position of $x_\alpha(t+1)$ where, $a = 1, 2, \ldots N$
- Until the global minima are reached in the final iteration.

The reactive sources (such as generator reactive power, tap changer, SVC, TCSCs, and a shunt capacitor) are used as a string form in the proposed problem. Each agent is represented by a single string with a mass and a fitness value computed using the specified functions. The algorithm flow chart for GSA approaches is as follows:

4 Results and Analysis

GSA is used to solve the bid-based dynamic economic load dispatch (BBDED) using the test system with five conventional generators and a VPP. To test the search capability of GSA, results are compared with three different optimization methods. Furthermore to verify the effectiveness of VPP, another case, i.e. without VPP is considered with the same test system and compared with the VPP results. Their cost coefficient data and generation limit are specified in Tables 1 and 2. The load to the test system is assumed to be varying from 180 to 220 MW. Here, social profit is calculated as per Eq. (1). MCP calculation is done from the Nash SFE equilibrium Eq. (6) to ensure that none of the generator units will face losses while supplying the scheduled power. For showing the efficacy of the proposed GSA, two different case studies are considered, and the results are compared with other three meta-heuristic algorithms, i.e. Particle Swarm Optimization (PSO), Ant Bee Colony optimization (ABC), and Competitive Swarm Optimization (CSO).

Table 1 Cost coefficients of generating units

No. of units	Power plant units		Virtual power plant units		
	β($/MWh)	γ($/MWh^2)	β($/MWh)	γ($/MWh^2)	λ($/MW)
1	15	0.02	16.89	0.03134	1.9
2	14.75	0.0175			
3	16	0.025			
4	14	0.0625			
5	16.1	0.025			

Table 2 Generation limit of generating units

No. of units	Power plant units		Virtual power plant units	
	P_{Min} (MW)	P_{Max} (MW)	P_{Min} (MW)	P_{Max} (MW)
1	15	80	0	39
2	15	80		
3	5	40		
4	5	50		
5	5	30		

4.1 Case 1 (With VPP)

It is assumed that five generators and a consumer have submitted their bid to ISO. The generator data have been given in Tables 1 and 2. As we can see from Table 3, the total power is scheduled at 216.8 MW, and scheduling for the respective generator and VPP is mentioned in this table. From this table, we can observe that the most ssoptimum social profit is obtained by using GSA, i.e. 1449.616$ and the least optimum value is given by PSO, i.e. 1258.294$. The proper utilization of VPP is obtained from CSO and GSA, but the best result of social profit is obtained from GSA. The optimization is carried out using MATLAB R2015a, and for the optimization purpose, the maximum iteration is taken as 200, and the population is 30.

The convergence plot for case 1 (with VPP) is shown in Fig. 1, and profit share of each generator in Fig. 2. This graph shows four curves, i.e. GSA, CSO, ABC, and PSO. The bottom-most curve represents PSO convergence, the most uneven curve among all these four algorithms. The curve almost converges at roughly 150 iterations and has the most optimum result. ABC convergence curve is also quite uneven and converges roughly at 160 iterations. Still, the result is more optimum than PSO but least optimum compared to the other two. And the curve of CSO algorithms is the smoothest and converges almost at just 40 iterations. GSA convergence curve is not as smooth as CSO, but the GSA result is the most optimum and converges at 80 iterations.

Table 3 Simulation results of case 1 (with VPP)

No. of units	With VPP (case 1)			
	PSO	ABC	CSO	GSA
P_{G1}(MW)	71.23548	64.2354	57.43861	53.24046
P_{G2}(MW)	62.15487	44.15485	65.58699	55.93093
P_{G3}(MW)	18.25485	32.9655	19.91088	28.5441
P_{G4}(MW)	21.5489	29.0044	25.36435	31.03694
P_{G5}(MW)	21.32145	26.41402	21.91089	22.59617
P_{CPP}(MW)	194.515	196.774	190.21172	191.3486
P_{VPP}(MW)	22.232	19.511	25.888277	25.451393
P_D(MW)	216.8		216.8	
Social profit ($)	1258.294	1286.256	1377.446	1449.616
Avg comp. time (sec)	120.46	131.85	102.45	87.51

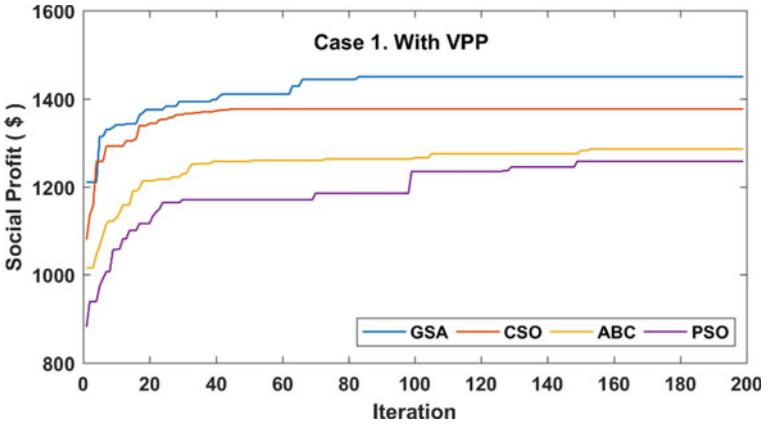

Fig. 2 Convergence plot for case 1 (with VPP)

4.2 Case 2 (Without VPP)

To check the effectiveness of GSA and VPP, we have taken another case study, i.e. without VPP. The scheduling of the total load (216.8 MW) is done by conventional generators only; and the study is given in Table 4, and the convergence curve is shown in the figure. From Table 4, we can see the total load is 216.8 MW, and the power scheduling of each conventional generator is mentioned in the table. From the table, we can absorb that the most optimum result from GSA is 1286.256$ and the least optimum among them from PSO, which is 1035.235$. The optimization is done on MATLAB R2015a, and for the optimization purpose, the maximum iteration is taken as 200, and the population is 30.

Table 4 Simulation results of case 2 (without VPP)

No of units	Without VPP (case 1)			
	PSO	ABC	CSO	GSA
P_{G1}(MW)	68.5875	72.2657	63.5249	73.5628
P_{G2}(MW)	65.2578	78.2542	72.9659	62.4862
P_{G3}(MW)	33.2658	32.5486	21.5441	26.5441
P_{G4}(MW)	24.5658	23.4548	38.2658	35.8576
P_{G5}(MW)	25.1245	10.2587	20.5961	18.2495
P_{CPP}(MW)	216.8	216.8	216.8	216.8
P_{VPP}(MW)	0	0	0	0
P_D(MW)	216.8		216.8	
Social profit ($)	1035.235	1108.854	1258.294	1286.256
Avg comp. time (sec)	116.84	124.57	96.54	80.53

The convergence plot for case 2 (without VPP) is shown in Fig. 3. And the profit share of each generator is in Fig. 4. The graph shows the convergence of social profit of all four optimization techniques (GSA, PSO, CSO, and ABC) without the influence of VPP. In this case, also CSO converses more quickly, about 40 iterations, and GSA takes 80 iterations to converse. And also, in case two, GSA gives the more optimum result compared to other optimization techniques (Fig. 4).

Sensitivity Analysis of GSA Parameters

Since meta-heuristic algorithms are stochastic and generate varying solutions each time, like other optimization algorithms, GSA also has a few tuning parameters such as $C1$, $C2$, $C3$, and $C4$. Change in these parameters gives the changing result. For the most optimum result, the sensitivity analysis of these tuning parameters is much

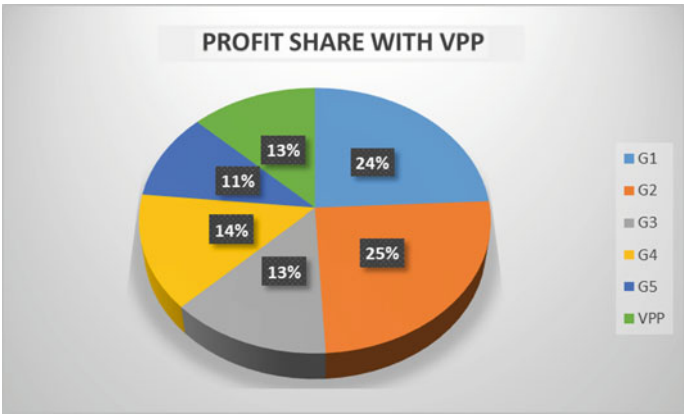

Fig. 3 Profit share of each generator, including VPP

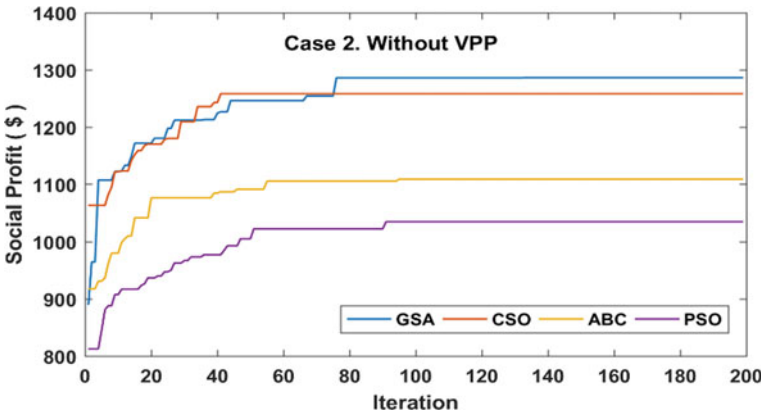

Fig. 4 Convergence plot for case 1 (without VPP)

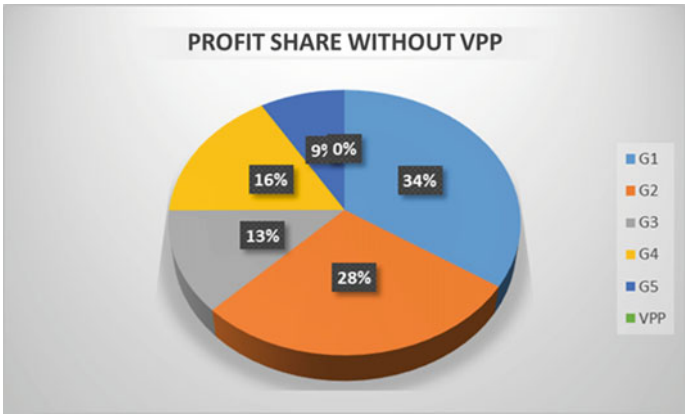

Fig. 5 Profit share of each generator without VPP

needed. The GSA converges much quickly, so the maximum iteration population size for the sensitivity analysis is 200 and 30, respectively.

The selected test system is a six-dimensional system with five conventional generators and a VPP. The objective function for the GSA is a BBDED problem, which is a social profit maximization problem. For optimal social profit, the GSA is tested in several combinations of tuning parameters $C1 \in \{1, 2\}$,$C2 \in \{2, 4, 6\}$,$C3 \in \{1, 2\}$ and $C4 \in \{0.5, 1\}$. After trying all 24 combinations for the given objective function, the optimum social profit for each combination is specified in Table 5, and GSA achieved the best social profit at $C1 = 1$, $C2 = 4$, $C3 = 2$, and $C4 = 0.5$.

A. Statistical Analysis

To test the proposed Gravitational Search Algorithm (GSA), statistical analysis of GSA is required, along with other simulated optimization methods. For this, a test

Table 5 Sensitivity analysis of GSA parameters for different scenarios

Sl. No.	Parameters values				Social profit
	Cl	C2	C3	C4	Objective function
1	1	2	1	0.5	1405.706
2	1	2	1	1	1372.833
3	1	2	2	0.5	1380.546
4	1	2	2	1	1357.248
5	1	4	1	0.5	1408.238
6	1	4	1	1	1402.587
7	**1**	**4**	**2**	**0.5**	**1449.616**
8	1	4	2	1	1347.488
9	1	6	1	0.5	1333.552
10	1	6	1	1	1380.695
11	1	6	2	0.5	1352.478
12	1	6	2	1	1416.967
13	2	2	1	0.5	1374.653
14	2	2	1	1	1430.752
15	2	2	2	0.5	1417.974
16	2	2	2	1	1398.544
17	2	4	1	0.5	1351.615
18	2	4	1	1	1444.542
19	2	4	2	0.5	1362.148
20	2	4	2	1	1440.636
21	2	6	1	0.5	1357.201
22	2	6	1	1	1395.264
23	2	6	2	0.5	1356.254
24	2	6	2	1	1406.769

Bold represents the value of parameters corrosponding to optimum result

is performed to explore the performance of proposed GSA in comparison with other meta-heuristic methods; in this test, the search capability and implementation of the optimization techniques are compared with their best, worst, and mean values (Table 6).

5 Conclusion

This paper uses a newly developed meta-heuristic algorithm, namely Gravitational Search Algorithm (GSA) to solve the BBDED problem on the five conventional

Table 6 Statistical analysis of optimization technique

Optimization technique	Mean	Worst	Best	Max iter	Pop _size	Convergence
With VPP						
GSA	1391.584	1333.552	1449.616	200	30	80
CSO	1341.347	1305.248	1377.446	200	30	40
ABC	1255.354	1224.452	1286.256	200	30	160
PSO	1227.0827	1195.875	1258.294	200	30	160
Without VPP						
GSA	1237.762	1189.268	1286.256	200	30	80
CSO	1225.06	1191.826	1258.294	200	30	40
ABC	1082.785	1056.716	1108.854	200	30	100
PSO	1016.8	998.52	1035.2	200	30	100

generators and a Virtual Power Plant (VPP). In this paper, to test the effectiveness of VPP in maximizing social profit, optimization is performed on the test system with two different cases, i.e. including VPP and without considering VPP. The independent system operator collects each generator's generating limits and cost coefficient data and calculates the market-clearing price from the Nash SFE equation. To verify the efficacy of the proposed algorithm, the optimized results obtained from GSA is compared with the other contemporary meta-heuristic algorithms. From the analysis, following observations have been made:

- Integrating the virtual power plant into the energy scheduling virtual power plant itself generates profit without affecting the profit of conventional power plant as it generates power according to the load demand.
- GSA is more robust and converges more quickly than other meta-heuristic algorithms in the energy dispatch problem of a power system.

References

1. A.K. Singh, S.K. Parida, A review on distributed generation allocation and planning in deregulated electricity market. Renew. Sustain. Energy Rev. **82**, 4132–4141 (2018)
2. L. Yavuz et al., ransformation of microgrid to virtual power plant–a comprehensive review. IET Gener. Transm. Distrib. **13**(11), 1994–2005 (2019)
3. B. Behi et al., Advanced monitoring and control system for virtual power plants for enabling customer engagement and market participation. Energies **14**(4), 1113 (2021)
4. C. Huang, D. Yue, J. Xie, Y. Li, K. Wang, Economic dispatch of power systems with virtual power plant based interval optimization method. CSEE J. Power Energy Syst. **2**(1), 74–80 (2016). https://doi.org/10.17775/CSEEJPES.2016.00011
5. S. Yu et al., Uncertainties of virtual power plant: problems and countermeasures. Appl. Energy **239**, 454–470 (2019)

6. A. Bhadoria et al., A solution to non-convex/convex and dynamic economic load dispatch problem using moth flame optimizer. INAE Letters **3**(2), 65–86 (2018)
7. J.F. Rivera, S.M. Shahidehpour, Application of games with incomplete information for. IEEE Trans. Power Syst. **13**(1), 184–189 (1998)
8. V.K. Jadoun et al., Integration of renewable energy sources in dynamic economic load dispatch problem using an improved fireworks algorithm. IET Renew. Power Gener. **12**(9), 1004–1011 (2018)
9. S.M. Nosratabadi, R.A. Hooshmand, Stochastic electrical energy management of industrial virtual power plant considering time-based and incentive-based demand response programs option in contingency condition. Int. J. Emerg. Electr. Power Syst. 1.ahead-of-print (2020)
10. A. Thavlov, H.W. Bindner, Utilization of flexible demand in a virtual power plant set-up. IEEE Trans. Smart Grid **6**(2), 640–647 (2015). https://doi.org/10.1109/TSG.2014.2363498
11. N. Naval, R. Sánchez, J.M. Yusta, A virtual power plant optimal dispatch model with large and small-scale distributed renewable generation. Renew. Energy **151**, 57–69 (2020)
12. H.H. Alhelou et al., Decentralized fractional order control scheme for LFC of deregulated nonlinear power systems in presence of EVs and RER, in *2018 International Conference on Smart Energy Systems and Technologies (SEST)* (IEEE, 2018)
13. S. Gorgizadeh, F.A. Akbari, A.M. Amir, Strategic bidding in a pool-based electricity market under load forecast uncertainty. 164–176 (2012)
14. S. Sharma, A.R. Abhyankar, Optimal bidding strategies of GENCO under uncertain information of rivals using CVaR. in *2014 Eighteenth National Power Systems Conference (NPSC)*, (IEEE, 2014)
15. S.M. Elsayed, R.A. Sarker, D.L. Essam, On an evolutionary approach for constrained optimization problem solving. Appl. Soft Comput. **12**(10), 3208–3227 (2012)
16. S. Consoli, K. Darby-Dowman, *Combinatorial optimization and metaheuristics* (Brunel University, 2006)
17. E.H. Houssein, M.R. Saad, F.A. Hashim, H. Shaban, M. Hassaballah, L' evy flight distribution: a new metaheuristic algorithm for solving engineering optimization problems. Eng. Appl. Artif. Intell. **94**, 103731 (2020)
18. A.A. Heidari, S. Mirjalili, H. Faris, I. Aljarah, M. Mafarja, H. Chen, Harris hawks optimization: algorithm and applications. Future Gener. Comput. Syst **97**, 849–872 (2019)
19. E. Rashedi, H. Nezamabadi-Pour, S. Saryazdi, GSA: a gravitational search algorithm. Inf. Sci. **179**(13), 2232–2248 (2009)
20. H. Nezamabadi, P. Nezamabadi, M. Setayeshnazar, G.B. Gharehpetian, Participation of virtual power plants in energy market with optimal bidding based on Nash-SFE Equilibrium Strategy and considering interruptible load, in The 3rd Conference on Thermal Power Plants, (2011), pp. 1–6

Development of Fractional Order Controller for Water Level Coupled Tank System Using Different Optimization Techniques

Km Hemlata and Pragya Varshney

Abstract The paper represents the control of the desired water level for the coupled tank system. In order to obtain a stable system, various controller classifications as well as optimization approaches have been applied and the minimization of Integral of Square Error (ISE) is taken as target of the system. MATLAB is used for simulation purpose, and the various step response parameters like settling time, rise time, and overshoot are compared for the system. The variables of the controllers have been optimized by using TLBO and PSO along with implementation of fractional order PID and PID controllers also obtained and overall achieved outcomes of the configurations have been analyzed with comparative study.

Keywords Control of water level · Approaches of PID Tuning · Coupled Tank System (CTS) · PID controllers

1 Modeling of Coupled Tank System

An understanding of the behavioral statistical analysis of the double tank system is very important. This design uses an indirect model to perform the line process along with the recognition of flexible non-line modeling.

Km Hemlata (✉)
Department of Electrical Engineering, NSUT, New Delhi, India
e-mail: khemlata.ee20@nsut.ac.in

P. Varshney
Department of Instrumentation & Control Engineering, NSUT, New Delhi, India
e-mail: pragya.varshney@nsut.ac.in

© The Author(s), under exclusive license to Springer Nature Singapore Pte Ltd. 2023

K. Murari et al. (eds.), *Soft Computing Applications in Modern Power and Energy Systems*,
Lecture Notes in Electrical Engineering 975,
https://doi.org/10.1007/978-981-19-8353-5_14

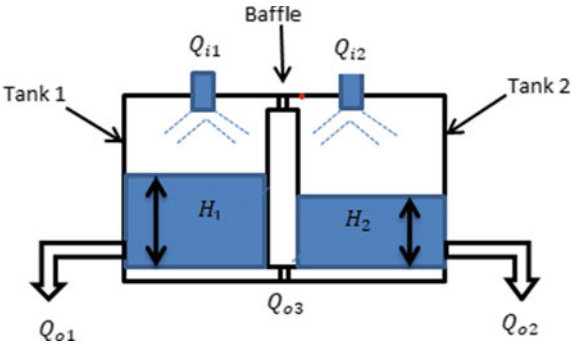

Fig. 1 Layout of couple tank system

For a coupled tank system, the fluid levels of Tank 1 and Tank 2 are considered as $H1$ and $H2$ as shown in Fig. 1. When basic weight balance is used, the fluid flow in the tank is related to the rate of fluctuation of the fluid in each tank, so conceptually, the construction of the mathematical formula for tanks 1 and 2 is represented as [1, 2].

$$A_1 \frac{\mathrm{d}H_1}{\mathrm{d}t} = Q_{i1} - Q_{o1} - Q_3 \tag{1}$$

$$A_2 \frac{\mathrm{d}H_2}{\mathrm{d}t} = Q_{i2} - Q_{o2} + Q_3 \tag{2}$$

where:

H_1, H_2 = Heights of liquid for tanks 1 and 2, respectively.

A_1, A_2 Cross-section Area of Tank 1 and Tank 2, respectively.

Q_3 = Fluid flow rate in both tanks.

Q_{i1}, Q_{i2} = The flow rates of the liquid going into tanks 1 and 2 respectively.

Q_{o1}, Q_{o2} = The flow rates of the liquid coming out from tanks 1 and 2, respectively.

Individual discharge channel may be mathematically represented in the form of a single outlet. According to Bernoulli's equation of stable, viscous, non-compressed fluid, the outflow from all tanks corresponds to the tank's water head square root. The square root of the change in pressure is equal to the flow speed between the tanks 1 and 2. Hence:

$$Q_{o1} = \alpha_1 \sqrt{H_1} \tag{3}$$

$$Q_{o2} = \alpha_2 \sqrt{H_2} \tag{4}$$

$$Q_3 = \alpha_3 \sqrt{H_1 - H_2} \tag{5}$$

where the proportionality constants α_1, α_2 and α_3 are based on discharge coefficients, inter area of every orifice, and gravity constant. The equations that characterize the system dynamics of the CTS apparatus are obtained [3] by substituting (3), (4), and (5) into (2) and (1):

$$A_1 \frac{\mathrm{d}H_1}{\mathrm{d}t} = Q_{i1} - \alpha_1\sqrt{H_1} - \alpha_3\sqrt{H_1 - H_2} \tag{6}$$

$$A_2 \frac{\mathrm{d}H_2}{\mathrm{d}t} = Q_{i2} - \alpha_2\sqrt{H_2} + \alpha_3\sqrt{H_1 - H_2} \tag{7}$$

In the 2nd-order, the process, which includes variables to be controlled h_2, q_1, and q_2, is assumed as zero, and again in the same second-order configuration, q_1 is the variable that is to be manipulated, and h_2 is the operation variable provided, $q_2 = 0$.

$$\frac{h_2(s)}{q_1(s)} = \frac{k_1k_2}{(T_1s+1)(T_2s+1) - k_{12}k_{21}} = \frac{k_1k_2}{T_1T_2s^2 + (T_1+T_2)s + (1-k_{12}k_{21})} \tag{8}$$

Here:

$$\begin{aligned} T_1 &= \frac{A_1}{\left(\frac{\alpha_1}{2\sqrt{H_1}}\right) + \left(\frac{\alpha_3}{2\sqrt{H_1-H_2}}\right)} \\ T_2 &= \frac{A_2}{\left(\frac{\alpha_2}{2\sqrt{H_2}}\right) + \left(\frac{\alpha_3}{2\sqrt{H_1-H_2}}\right)} \end{aligned} \tag{9}$$

$$\begin{aligned} k_1 &= \frac{1}{\left(\frac{\alpha_1}{2\sqrt{H_1}}\right) + \left(\frac{\alpha_3}{2\sqrt{H_1-H_2}}\right)} \\ k_2 &= \frac{\alpha_3}{\left(\frac{\alpha_2}{2\sqrt{H_2}}\right) + \left(\frac{\alpha_3}{2\sqrt{H_1-H_2}}\right)} \\ k_{12} &= \frac{\alpha_3}{\left(\frac{\alpha_1}{2\sqrt{H_1-H_2}}\right) + \left(\frac{\alpha_3}{2\sqrt{H_1-H_2}}\right)} \\ k_{21} &= \frac{\alpha_3}{\left(\frac{\alpha_2}{2\sqrt{H_1}}\right) + \left(\frac{\alpha_3}{2\sqrt{H_1-H_2}}\right)} \end{aligned} \tag{10}$$

The listed parameters in Table 1 are used to obtain plant's transfer function.

After entering all the parameters of Table 1 into Eq. (8), the plant's transfer function will be obtained, which is represented as follows:

$$G_p(s) = \frac{h_2(s)}{q_1(s)} = \frac{0.0361}{36.9406s^2 + 12.1565s + 0.4514} \tag{11}$$

Table 1 Parameters of coupled tank system

Parameters	Value	Unit
H_1	17	cm
H_2	15	cm
α_1	10.78	$cm^{3/2}/s$
α_2	11.03	$cm^{3/2}/s$
α_3	11.03	$cm^{3/2}/s$
A_1	32	cm^2
A_2	32	cm^2

Open Loop Stability Analysis

Figure 2 displays the CTS response open-loop system when there is no controller. It can be seen that the output cannot reach its maximum value. Therefore, it is clear, the open loop control system cannot be sustainable.

In Eq. (4), the distinctive equations of system A are provided by

$$[\lambda I - A] = 0 \tag{12}$$

Open-loop system eigen values are as follows

$$\lambda_1 = -0.2864 \text{and} \lambda_2 = -0.0427.$$

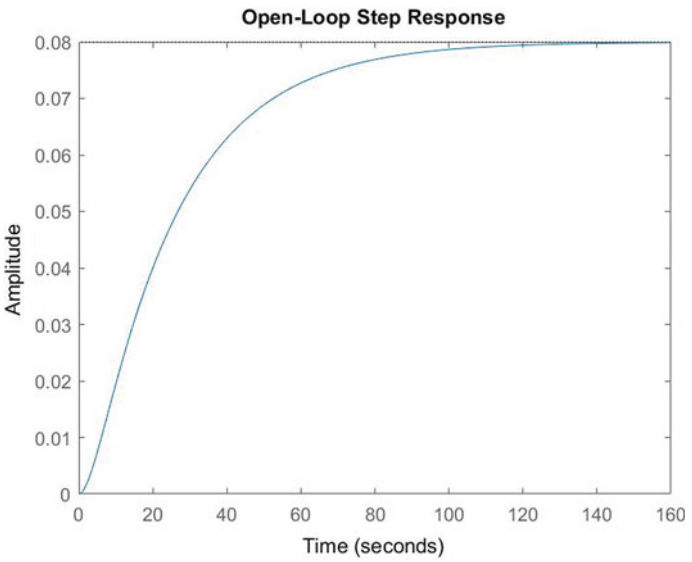

Fig. 2 Open loop response of CTS

It can be shown in the performance response of Fig. 2 that the use of the controller is just mild, so the controller's production strategy must be right.

2 Analysis of Observability and Controllability

The LTI system's state equation is represented.

$$\dot{x}(t) = Ax(t) + Bu(t) \tag{13}$$

The $p \times p$ matrix of the system is represented by 'A', the control matrix is represented by 'B', and the $r \times 1$ input vector is represented by 'u' (Fig. 3).

One way for determining controllability is to verify the matrix rank, $Q = [B\ AB\ A2B \ldots An{-}1B]$. We may state that the system is controlled in equation if the matrix rank Q equals order 'q'. In other words, determinant of Q is non-zero.

$$Q = \begin{bmatrix} 1 & -0.3291 \\ 0 & 1 \end{bmatrix} \tag{14}$$

The ranking of matrix Q is equal to the order of 'q' implying that the system is controllable.

Similarly, one way for determining the system's observability is to examine the matrix rank such that, $L = [C\ CA\ CA2 \ldots C\ An{-}1]$.

If the rank of the calculated matrix L is 'l', we may say that the system is observable in Eqs. (14).

$$L = \left(1.0{*}\mathrm{e}^{-3}\right) * \begin{bmatrix} 0 & 0.9772 \\ 0.9772 & 0 \end{bmatrix} \tag{15}$$

Here, the rank of matrix L is identical to that of A, as well as the order of L, implying that the system is observable.

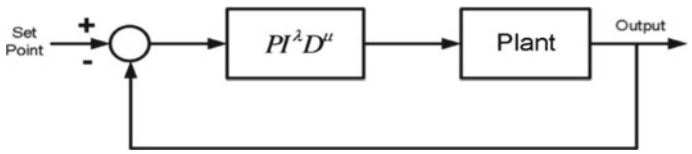

Fig. 3 Block diagram of FOPID controller

3 Controller

3.1 Proportional Integral Derivative Controller (PID)

In this controller, control actions include output, measurement, and integration actions. $e(t)$ represents error signal which is difference of reference signal and output signal.

$$e(t) = V_{\text{ref}}(t) - V(t) \tag{16}$$

$u(t)$ Output provided by controllers in time domain [4], where.

- K_p: proportional gain
- K_d: the gain of the derivative part
- K_I: the gain of the integral part

$$u(t) = K_p{*}e(t) + K_d{*}\frac{\mathrm{d}_e(t)}{\mathrm{d}t} + K_I \int_0^t e(t){*}\mathrm{d}\tau \tag{17}$$

Step Response Using PID CONTROLLER

See Fig. 4.

3.2 Fractional Order PID Controller (FOPID)

A fractional PID controller is a variant of a PID controller that is unique from a standard PID controller and is more flexible than other controllers in adjusting the gain and phase characteristics but it shows very slow switching features to control system and control features [5]. The fractional order PID is considered a powerful tool for designing a robust control system because of its flexibility, and one of the major advantages is that using FOPID with few tuning knobs gives the same robustness as achieved by using a higher-order integral controllers.

This fractional PID controller's generalized transfer function is provided by:

$$C(s) = \frac{U(s)}{E(s)} = K_P + \frac{K_I}{s^{\lambda}} + K_D s^{\mu}, \quad (\lambda,\ \mu \geq 0)$$

where integrator and differentiator order's λ and μ are respectively. All conventional PID controllers are considered unique examples of fractional controllers in which λ and μ are equal to unity [6].

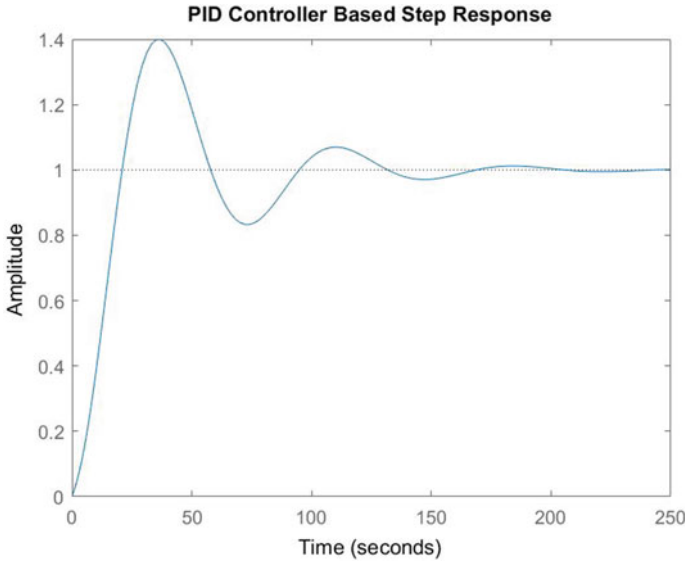

Fig. 4 Step response of the system including PID controller

4 Particle Swarm Optimisation (PSO)

The embedded computing community is paying attention to PSO, a population-based optimization method [7, 8]. It's an effective tool for a variety of multimodal as well as the multi-dimensional problems.

Algorithm of PSO is as follows [9]:

- Every particle has a fitness value assigned to it.
- The best-performing particles are updated.
- Create a set of particles with the greatest performance and update it in the same way.
- Then, by analyzing the finest group performance and single performance particle, the particle velocities are modified.

The PSO algorithm is made up of two formulas [10], one for updating location and the other for updating velocity.

Formula for updating velocity [11]:

$$v_{t\text{in}+1} = v_{t\text{in}} + c_1 * r_1 * (p_{t\text{best}} - v_{t+1} - x_{t\text{in}}) + c_2 * r_2 * (g_{t\text{best}} - x_{t\text{in}}) \tag{18}$$

Position updating formula [11]:

$$x_{t\text{in}+1} = x_{t\text{in}} + v_{t\text{in}+1} \tag{19}$$

The procedure below represents the modified equation for updating the rate of the particle, but the approach for updating the location will remain the same.

$$v_{(t+1)\text{in}} = \omega * v_{t\text{in}} + c_1 * r_1 * (p_{t\text{best}} - v_{t+1} - x_{t\text{in}}) + c_2 * r_2 * (g_{t\text{best}} - x_{t\text{in}}) \quad (20)$$

5 Teacher's Learning Based Algorithm (TLBO)

The TLBO algorithm is inspired by a teaching and learning procedure which is based on the impact of a teacher in a class on a learner's outcome. The algorithm explains two primary learning methods: (i) the teaching period (teaching from a teacher) and (ii) the student period (Learning through mutual interaction of learners). The population examined in this method is a group of learners, with various subjects supplied to the learners serving as additional design factors in the optimization problem. The optimization problem's 'fitness' value is analogous to a learner's outcome [12].

The best option for the population is to hire a teacher. The objective function variable is design variables in the provided optimization issue, and the optimum value for the target function is the optimal result.

TLBO is a human-inspired algorithm that influences the teaching and learning process in the classroom. This method requires standard control parameters, such as generation's number and population size, and does not require any control algorithm-specific control parameters. The two functional phases of the TLBO are the 'teacher phase' and the student phase. In both cases, the operation is described below.

5.1 Teacher's Period

Learners learn through the teacher in the first section of our TLBO algorithm. A teacher, through the phase, tries boosting the class's mean result in the subject explained by them depending on their ability. For any iteration 'i', assuming 'm' design variables (i.e. topics number), 'n' population size (i.e. number of learners, $k = 1, 2, 3, 4, \ldots n$), $M_{j,i}$, is the learner's mean result in a specific subject 'j' ($j = 1, 2, 3, 4, 5, \ldots m$). The complete best effect Xtotal-$k$best, i in consideration of all the issues collected attained in the learners' whole population may be viewed as $k$best, the best learner. Though the teacher is a well-trained person who provides training to learners to have improved output, the top learner recognized is viewed by the algorithm as the teacher [12]. The present mean effect of every subject, as well as the analogous impact for each subject of the teacher, has the difference between them given by [13],

$$\text{Difference\_Mean}_{j,k,l} = r_i \left(M_{j,k\text{best},i} - T_F M_{j,i} \right)$$

Here,

The well learner's output in subject j is $X_{j,\,k\text{best},\,i}$. The teaching factor (TF) chooses the changing mean's value, and the number ri is randomly selected from [0,f 1] range. The value is randomly determined for T_F with equivalent chances as,

$$T_F = \text{round}[1 + \text{rand}(0,\,1)\{2 - 1\}] \tag{21}$$

T_F is not a TLBO algorithm's parameter. The T_F value attained by the algorithm is random from Eq. (21) and is not given as input. In conclusion, the algorithm's performance is better if the value lies between 1 and 2 for T_F, which is obtained after conducting several tests on various benchmark functions. According to the following expression, depend on the Difference. $\text{Mean}_{j,k,i}$, the current result is revised in the teacher phase.

$$X'_{j,k,i} = X_{j,k,i} + \text{Difference\_Mean}_{j,k,l} \tag{22}$$

The regenerated value of $X_{j,k,i}$ is represented as $X''_{j,k,i}$, which upgrades the function parameters. At the completion of the teaching period, function values are accepted and become the learning period input. The learner phase is inextricably linked to the instructor phase.

5.2 Learner's Period

Learners improve their knowledge through communicating with one another in the second phase. The students form informal networks in order to improve their abilities to interact with other students. If another student has greater capacity than the learner, the learner has the opportunity to acquire new things. With a size of population 'n,' the learning factors of this stage are given below [12].

Suppose P and Q are two learners, and X'total-P, iX'total-Q , i (where X'total-P , i and X'total-Q , i are the renewed function values of Xtotal-P , i and Xtotal-Q , i of P and Q at the conclusion of the teacher phase, respectively) [13].

$$\begin{aligned} &X''_{j,k,i} = X'_{j,P,i} + r_i\left(X'_{j,P,i} - X'_{j,Q,i}\right), \\ &\text{If } X'_{\text{total}-P,i} < X'_{\text{total}-Q,i} \end{aligned} \tag{23}$$

$$\begin{aligned} &X''_{j,P,i} = X'_{j,P,i} + r_i\left(X'_{j,Q,i} - X'_{j,P,i}\right), \\ &\text{if } X'_{\text{absolute}-Q,i} < X'_{\text{absolute}-P,i} \end{aligned} \tag{24}$$

$X''_{j,P,I}$ will be acceptable only if it provides suitable function value. Equations (23) and (24) will solve the minimization issue, and Eqs. (25) and (26) will solve the maximization problem.

$$X''_{j,P,i} = X'_{j,P,i} + r_i\left(X'_{j,P,i} - X'_{j,Q,i}\right), \quad \text{if } X'_{\text{total}-Q,i} < X'_{\text{total}-P,i} \tag{25}$$

$$X''_{j,P,i} = X'_{j,P,i} + r_i\left(X'_{j,Q,i} - X'_{j,P,i}\right), \quad \text{If } X'_{\text{total}-P,i} < X'_{\text{total}-Q,i} \tag{26}$$

OBJECTIVE FUNCTION

The integral of the squared error during the optimization simulation period is assumed to be the target function of the system for the performance index optimization.

$$\text{Targetfunction} = \int_0^{Tss} e^2(t) \cdot dt \; W1 * \int_0^{Tss} e^2(t).dt \tag{27}$$

$w1$ represents weight of ISE output.

6 Results and Discussion

The results and graphs obtained from an uncontrolled open-loop system are presented, and a flexible system is obtained, which is depicted in Fig. 2. The stability of the system is maintained by using controllers. Therefore, a closed-loop model has been developed by considering FOR-PID and PID controllers, which efficiently stabilize the system and enhance the control parameters, minimize the design error and distortions and Controls, Maintain reduction in rising time, Maximum overshoot, Stop time, and undershoot applying TLBO and PSO approach (Tables 2 and 3).

i. Step output of PSO-based PID Controller (Fig. 5).
ii. Step output of PSO-based on FOPID Controller (Fig. 6).
iii. Step output of TLBO based on PID Controller (Fig. 7).
iv. Step Response of TLBO based on FOPID Controller (Fig. 8).

Table 2 Gains of various factors of different controllers configurations

Optimization technique	Controller	K_p	K_i	K_d	Λ(Lambda)	μ (Mu)
PSO	PID	86.7484	10.2961	94.6968	–	–
PSO	FOPID	86.8152	5.6300	64.0057	0.9971	0.346
TLBO	PID	126.9171	4.1818	129.6055	–	–
TLBO	FOPID	99.9922	6.3539	98.0928	0.918	0.498

Table 3 Comparison of several parameters of distinct controllers configurations

Parameter / Controller	Rise time	Overshoot	Undershoot	Settling time	ISE
PID PSO	5.4182	27.48	2.497	34.4514	0.4685
FOPID-PSO	4.6414	9.013	1.089	16.2679	0.4843
PID-TLBO	4.917	8.649	1.281	21.880	0.299
FOPID-TLBO	4.392	8.11	1.208	12.797	0.24

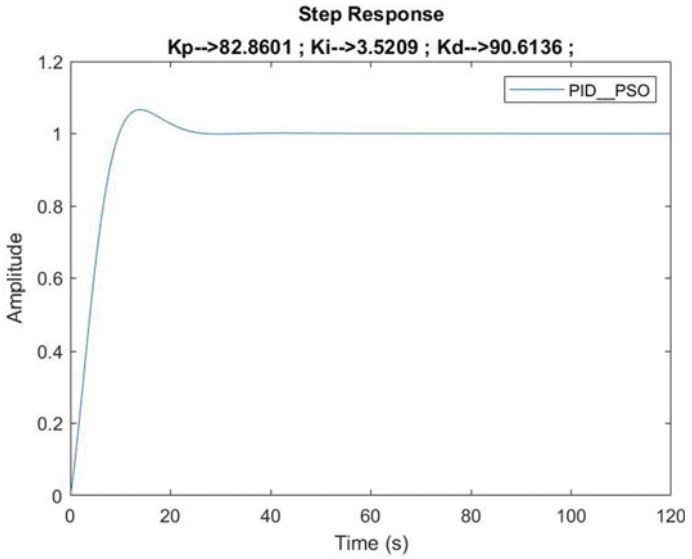

Fig. 5 Step output of PSO-based PID controller

7 Conclusion

The discussion inside the paper led to an important conclusion which revealed that FOPID-PSO and FOPID-TLBO are capable of giving very efficient and reliable results but the overshoot percentage of FOPID-PSO and the settling time are much higher than that of FOPID-TLBO (Fig. 9).

The comparative study of different factors in the previous section results as follows:

1. The rise time of all controllers' configurations which are based on FOPID is better.
2. The least settling time obtained for FOPID-TLBO along with minimum percentage of overshoot.
3. FOPID-TLBO and FOPID-PSO results with very minimum ISE.

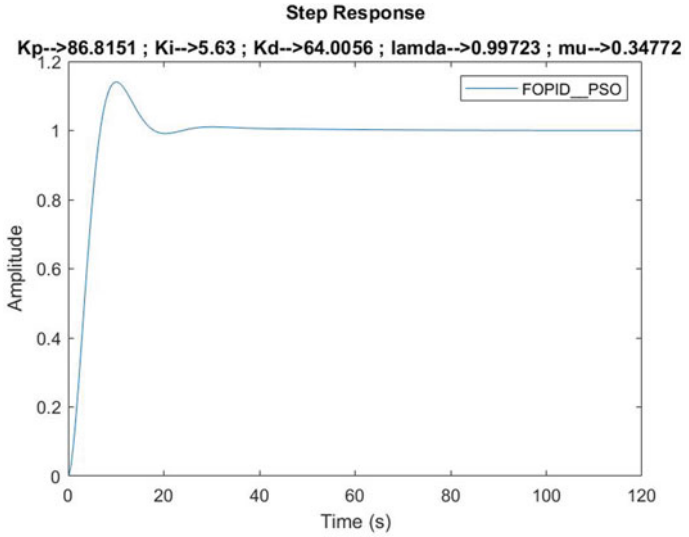

Fig. 6 Step output of PSO based on FOPID controller

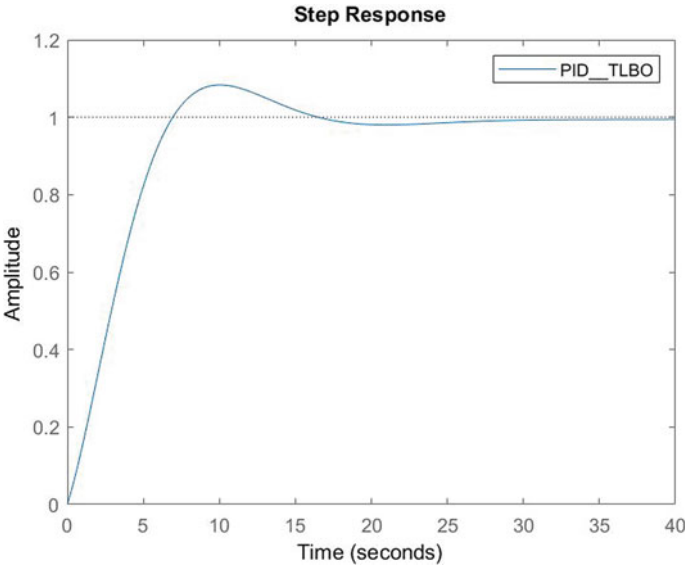

Fig. 7 Step response of TLBO based on PID controller

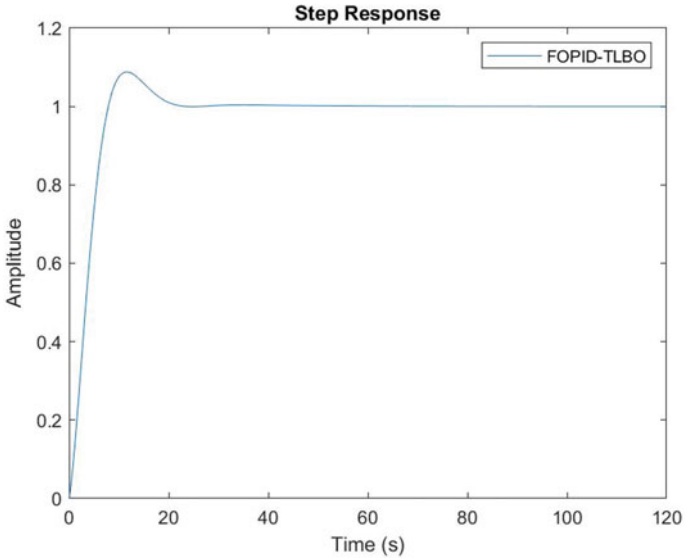

Fig. 8 Step response of TLBO based on FOPID controller

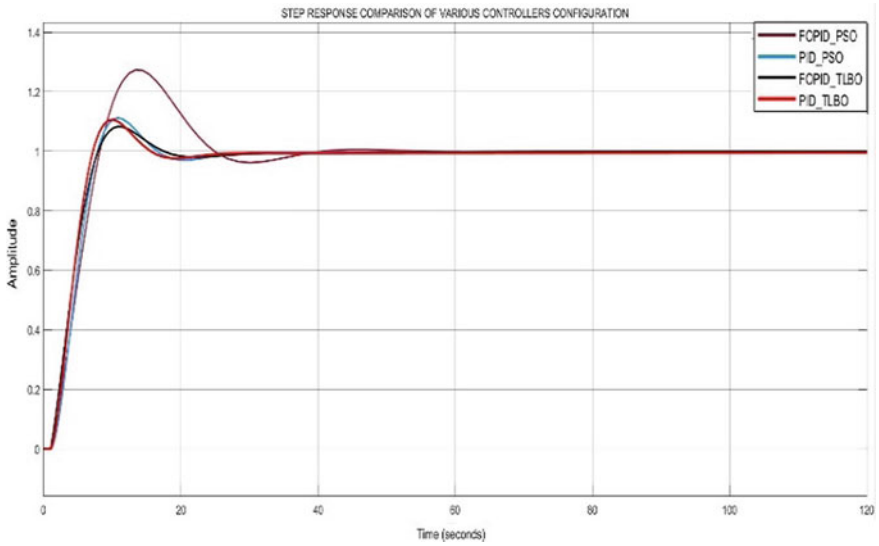

Fig. 9 Comparisons of step outputs for different controllers configurations

Therefore, after analyzing the results and simulations, we found that FOPID-TLBO is the most used configuration to control our system efficiently.

References

1. J.A. John, N.E. Jaffar, NagiBuaossa, Modelling and control of coupled tank liquid level system. Int. J. Eng. Res. Technol. (IJERT) **4**(06) (June-2015) ISSN: 2278-0181
2. T. Kealy, A. O' Dwyer, Comparison of open and closed loop process identification techniques in the time domain, in *Proceedings of the 3rd Wismarer Automatic Symposium*, (Wismar, Germany, Sept. 2001), pp. 3–4
3. A. Muntaser, N. Buaossa, Coupled tank non-linear system; modeling and level control using PID and fuzzy logic technique
4. K.J. Astrom, T. Hagglund, PID controllers: theory, design, and tuning, in *Instrument Society of America*, 2nd edn. (1995)
5. N. Khanduja, B. Bhushan, Optimal design of FOPID controller for the control of CSTR by using a novel hybrid metaheuristic algorithm, Sådhanå **46**:104, Indian Academy of Sciences (May 2021)
6. Y.C. Jun, L. Jin, G.C. Bing, Optimization of fractional order PID controllers based on genetic algorithms, in *Proceedings of the fourth international conference on machine learning and cybernetics*, (Guangzhou, 2005)
7. R.K. Sahu, S. Panda, U.K. Rout, D.K. Sahoo, Teaching learning based optimization algorithm for automatic generation control of power system using 2-DOF PID controller. Int. J. Electr. Power Energy Syst. **77**, 287–301 (May 2016)
8. M.P. Song, G.G. Chang, Research on particle swarm optimization: a review, in *Proceedings IEEE Conference of Machine Learning and Cybernetics* (2005)
9. M.M. Noel, A new gradient based particle swarm optimization algorithm for accurate computation of global minimum. Appl. Soft Comput. **12**, 353–359 (2012)
10. E.G. Gonzalo, J.L. Fernandez-Martinez, A brief historical review of particle swarm optimization (PSO). J. Bioinf. Intell. Control **1**, 13–16 (2012)
11. W. Nie, Z. Wu, C. Luo, S. Zhang, A tuning method for PID controller parameters based on particle swarm optimization (PSO), in *2020 Chinese Automation Congress (CAC)*
12. A. Rastogi, P. Tiwari, Advanced optimization by nature-inspired algorithms. Int. J. Soft Comput. Eng. (IJSCE) (May 2013)
13. R.V. Rao, V.J. Savsani, D.P. Vakharia, Teaching–learning-based optimization: a novel optimization method for continuous non-linear large-scale problems. Inform. Sci. **183**(1), 1–15 (2011)

A Novel White Shark Optimizer for Optimal Parameter Selection of Power System Oscillation Damper

Murali Krishna Gude and U. Salma

Abstract The higher voltage levels at long transmission lines are suggested for the efficient power network in the rapidly expanding power network scenario. These increased voltage levels lead to more stress on the stabilizers used for damping power oscillations. This paper proposes a novel approach to power system stabilizer (PSS) optimal parameter section using a white shark optimizer (WSO). The performance of the considered optimizer is compared with the recently proposed hybrid algorithm from the literature on a benchmark test power system. The oscillation damping performance obtained has been analyzed with the time-domain specifications for system parameters. The proposed WSO-based PSS provided promising results with faster setting time characteristics.

Keywords White shark optimizer · Power system stabilizer · Optimization

1 Introduction

In the present electrical power system regime, the electrical energy demand is growing rapidly, and the attempt to reduce the fossil fuel dependency is also trending. In this scenario, the concept of microgrids via regional renewable generation plants is in a great move. Even though these transitions result in solving various complex electrical energy generation constraints, they also introduce a challenging environment for the power system control operators. To this end, there is a need to have more study in improved power system modeling incorporating all system dynamics [1]. The required control action for finding a stable operating point after system perturbations significantly depends on the measurement of frequency oscillations in the system. For better system research on this problem, the researchers have proposed several test systems, of which the two-area-four-machine system is one of the recognized models. The most commonly used control technique for this problem is the loop frequency control (LFC) method [2]. This is also taken care of by fast-acting speed

M. K. Gude (✉) · U. Salma
Department of EECE, GITAM (Deemed to be University), GIT, Visakhapatnam 530045, India
e-mail: muralikrishnagude@gmail.com; 121860504002@gitam.in

© The Author(s), under exclusive license to Springer Nature Singapore Pte Ltd. 2023

K. Murari et al. (eds.), *Soft Computing Applications in Modern Power and Energy Systems*,
Lecture Notes in Electrical Engineering 975,
https://doi.org/10.1007/978-981-19-8353-5_15

governors employed for steam valve control of steam turbines [3]. Nevertheless, this may also lead to the oscillation of alternator, resulting in rotor angle stability.

The progressions in the hardware technologies of controller devices through the inventions of novel artificial intelligence methods result in sophisticated system design. With the transition of controller topologies across the complex engineering problems, the power system stability problem is significant and more research is recommended in possible directions [4]. The optimal controller parameter setting of power system stabilizers can be the most prominent solution in viewpoint of the traditional power system. In recent years, several metaheuristic algorithms have been proposed by various researchers with various inspirations, namely nature-inspired, swarm-based, etc. The algorithms are becoming more important due to their capability of fetching solutions for several complex engineering problems with more accuracy and probability of success [5]. A novel whale optimization algorithm-based PSS (WOAPSS) was developed and studied [6]. Eigenvalue analysis was done and tested for inter-connected three-machine nine-bus system.

This manuscript shows the analysis of rotor angle stability with the power system stabilizer (PSS) to damp out the oscillations produced during system uncertainties. A methodical derivation of alternator dynamic models and speed and voltage control subsystems is studied. These dynamic models are utilized to design the benchmark test system for the analysis considering different case studies. Conventional power system stabilizer (CPSS) consists of lead-lag filters with appropriate gain and time constants and provides superior control performance in damping power oscillations up to a certain operating point. But, the performance of CPSS degrades with change in operating point due to continuous load perturbation and heavy disturbances like three-phase faults. Various metaheuristic algorithms have been considered together for tuning the controller parameters of damping devices. This research proposes novel hybrid metaheuristic algorithms to obtain the controller parameter settings of power oscillation damping devices with quick damping features. The selection of controller parameters has been made to achieve the finest damping characteristics for the oscillations in the system. Hence, an objective function is framed for the quicker settling time characteristics during system oscillations. In past decades, supplementary excitation control signals provided from excitation systems via automatic voltage regulators (AVRs) have been used for sustaining terminal voltage to improve the steady-state and transient stability. But, the action of AVRs, negative damping torques, is introduced in the power system, affecting the stability [7]. Therefore, in order to avoid the counterproductive effect, PSS is used. PSS supplies stabilizing voltage signals to the exciter of the synchronous machine to damp power system oscillations. The conventional PSS (CPSS) is a lead-lag phase compensator that provides superior control performance in damping power oscillations up to a certain operating point. But, the performance of CPSS degrades with change in operating point due to continuous load perturbation, heavy disturbances like three-phase faults, etc. [8]. From the literature, the critical analysis of power system stabilizers can be summarized as follows:

In the beginning, CPSS was used as power system controller, which had some severe stability issues, making it unsuitable for robust and versatile conditions. Also, it lacked a self-tuning feature which made manual adjustment of parameters inevitable. In the later part, PID controller was used, which had somewhat overcome some of the demerits of CPSS. Later on, various control parameter calculating methods were incorporated, like root locus. The main problem with such methods is that although they are pretty simple to calculate, they become unusually complex with more machines connecting in the power system. In the meantime, some control topologies like $H\infty$, had been introduced for better performance of the PSS. The $H\infty$ loop controller suffered some serious issues with additive or multiplicative representation of the perturbations, which might lead to unstable zone of operation of the system. Some authors came up with the idea of decentralized controllers. This idea worked fair enough for a smaller sized power system network. But with larger networks, they suffered communication latency in the WAM scheme. So, the interconnected and fairly complex power system still posed a great challenge for power system engineers as finding the optimal parameter for such controllers became out of the human capacity with the conventional methods of optimizations.

With the advancement of optimization algorithms for solving quite complex and nonlinear problems, parameter tuning utilizing those methods became quite common. In earlier days, some of the classical standalone optimization methodologies were used like fuzzy neural networks, PSO, etc. The neural networks have a very long time requirement for their training. The number of iterative steps increases exponentially with the rise in the number of processing layers and neurons in each layer. Similarly, other standalone methods suffered some other similar drawbacks like trapping in local optima rather than global optima, long runtime, latency in appropriate response, impractically high or low parameter set, large deviational errors, etc. Nowadays, the drawbacks of one method of optimization are being covered by the merits of some other methods. Thus, in this way, better hybrid metaheuristic methods are being tested and employed in the power system for the proper and swifter tuning of parameters under varying operating conditions.

2 Test Power System with White Shark Optimizer (WSO)

Nowadays, most of the algorithms applied for them are metaheuristics, and they are a broad framework of higher versions of heuristic optimization algorithms. Therefore, a metaheuristic is developed to find a solution having high accuracy with less computing time. The reasons for the popularity of metaheuristic techniques are simplicity, flexibility, derivative-free, and stochastic.

The suggested WSO approach will tend to have both features of ideal stochastic approach for PSS parameter selection problem. These features include avoiding stuck in local optima and faster convergence to the optimal values. Hence, the suggested algorithm has more probability of having the best results for the oscillation damping problem in an electrical power system.

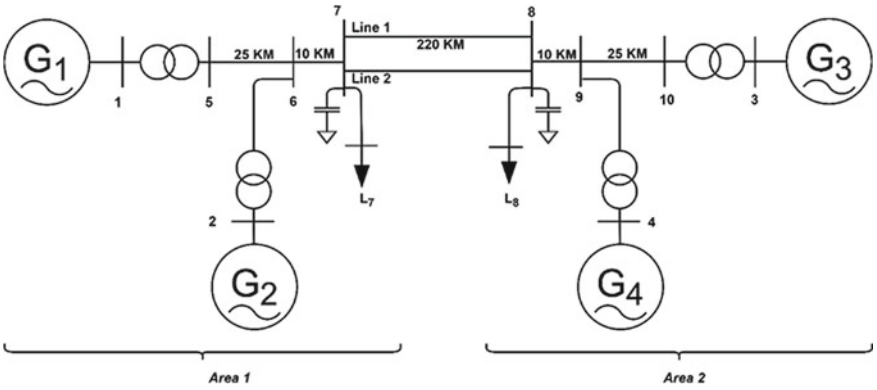

Fig. 1 Sample model for the system analysis

For the test system, the proposed research is shown in Fig. 1 as follows:

The power system stabilizer of each generator is effectively tuned with the suggested WSO algorithm in this paper and compared with other recently proposed algorithms and conventional power system stabilizer. The objective function and limits of controller parameters are considered the same with reference to the literature considered [9] for more transparency.

The optimal controller parameter settings of PSS of different generators with different standalone algorithms are given in Table 1. The system performance analysis under system uncertainties will be carried out with the achieved controller parameters of PSS to comment on different approaches. A transient condition of a self-clearing fault has been considered as system uncertainty, as explained before.

Table 1 Obtained tuned values

	Algorithms	K	$T1$	$T2$	$T3$	$T4$
Machine 1	GWO	50	0.0115	0.0205	0.9794	0.9976
	GWOSCA [9]	10.4246	0.5434	0.3118	0.4355	0.1702
	WSO	15.7334	0.543	0.702	0.6194	0.7793
Machine 2	GWO	3.1355	0.9584	0.9394	0.4422	0.3876
	GWOSCA [9]	11.2514	0.2523	0.1428	0.3799	0.5159
	WSO	18.4521	0.9756	1.2425	1.2455	0.3753
Machine 3	GWO	11.2345	0.0165	1	0.1875	0.1634
	GWOSCA [9]	18.1424	0.4748	0.3279	0.1463	0.2715
	WSO	14.7417	0.1252	1.3416	0.5437	0.0515
Machine 4	GWO	4.2449	0.9554	0.9867	0.2258	0.2655
	GWOSCA [9]	12.956	0.1586	0.1541	0.1255	0.4431
	WSO	0.7241	0.6253	0.3527	0.9435	0.5822

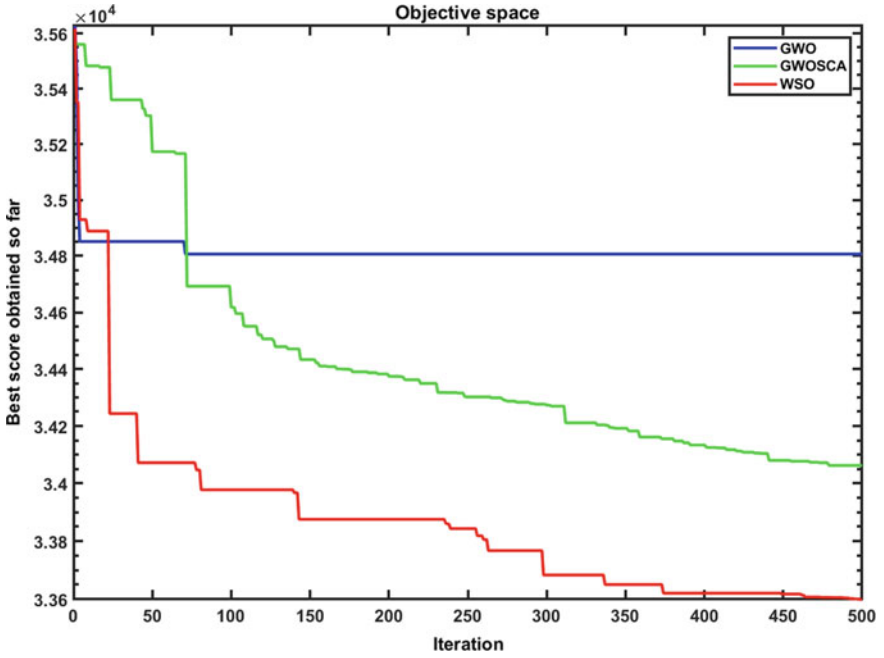

Fig. 2 Convergence characteristics

The listed parameters have been obtained with different algorithms by converging the considered objective function to the minimum value, as shown in Fig. 2. Here, the proposed WSO algorithm for the PSS controller parameter tuning is compared with GWO, GWOSCA. However, the balance between exploration and exploitation in the given number of iterations is not satisfactory in the literature. The speed of convergence for the GWO algorithm is fast for the considered research problem, but it is not converged to the smallest magnitude compared to the other algorithms.

3 Results and Discussion on the Test Power System

The characteristic of a mode designated to an eigenvalue λ_i which is time-dependent, is given by $e^{\lambda_i t}$. Hence, the system's stability is confirmed by eigenvalues as follows:

- A real-valued eigenvalue represents a non-oscillatory mode, i.e., mode with zero oscillations. A negative real-valued eigenvalue represents a decaying mode, i.e., oscillations with decreasing magnitude with respect to time. A positive real-valued eigenvalue represents monotonic instability which is aperiodic in nature, i.e., the magnitude of response will increase boundlessly, indicating a negative damping coefficient.

- Eigenvalues having imaginary parts and real parts, i.e., complex in nature, occur in complex conjugate pairs, and each pair represents a different oscillatory mode. The real part of the eigenvalues provides the damping and its coefficient, whereas the imaginary part signifies the oscillating frequency. The negative real component signifies a damped-oscillations, i.e., magnitude decreases with the passage of time, whereas a positive real component indicates oscillation with increasing amplitude as the time passes. Hence, for a complex conjugate pair of eigenvalues given by

$$\lambda = \sigma \pm j\omega \tag{1}$$

The frequency of oscillations (in units of Hz) is expressed as

$$f = \frac{\omega}{2\pi} \tag{2}$$

Similarly, the damping ratio is expressed as

$$\zeta = -\frac{\sigma}{\sqrt{\sigma^2 + \omega^2}} \tag{3}$$

The rate of decrement in the amplitude of oscillations is determined by ζ. The time constant of this amplitude decay is $\frac{1}{|\sigma|}$. It implies that amplitude decays to 37% of its initial value in $\frac{1}{|\sigma|}$ seconds or in $\left(\frac{1}{2\pi}\frac{\sqrt{1-\zeta^2}}{\zeta}\right)$ or $\left(\frac{f}{|\sigma|}\right)$ cycles of oscillations. The small-signal analysis program obtains the dynamic performance of the system by finding eigenvalues and their corresponding eigenvectors of the state matrix of the linearized model of the power system. It is desirable that all eigenvalues are stable, and all the electromechanical oscillations are damped out quickly (Table 2).

The low-frequency oscillations in a power system have to be damped in a timely manner to avoid adverse effects in the consolidated system. The system mathematical model and the corresponding tools for analyzing the performance characteristics can be utilized for the controller design in the system.

From Figs. 3, 4 and 5 show the variation in system parameters of different generators by considering the generator 1 torque angle as reference. The torque angle of generators 2, 3, and 4 shows a negative dip for the first machine cycle. After that, the oscillations decay with time. The time required to damp the oscillations for different generators with the different tuning approaches can be compared. The WSO approach resulted in faster damping of the oscillations. The overshoot values are also observed to be relatively lower than the controller parameters obtained from the WSO algorithm. The higher magnitudes of percentage overshoot (OS) for CPSS are significantly reduced with PSS parameters tuned using metaheuristics approaches for torque angle responses. The percentage OS of delta 2 with CPSS has been reduced to 44 from 77, delta 3 has been reduced to 64 from 142, and delta 4 has been reduced to 179 from 550 with the metaheuristic approach-based PSS. The settling time also quicker

Table 2 Obtained results are tabulated as follows

	Eigenvalues	Frequency (in hertz)	Damping ratio (ζ)		Eigenvalues	Frequency (in hertz)	Damping ratio (ζ)
CPSS	133.3701	0	−1	GWO	− 5.4578 − 10.02505j	1.59756	0.47428
	98.48533	0	−1		− 5.05441 + 9.87479j	1.57748	0.45425
	1.17526 + 67.9549j	10.81743	− 0.01531		− 3.67466 − 7.84559j	1.274	0.47587
	3.28549 + 26.4768j	4.20258	− 0.12465		− 2.4252 + 5.74459j	0.94482	0.35235
	0.08522	0	− 1		− 0.90417 + 3.34238j	0.54718	0.25444
	− 0.01454 + 0.0651j	0.00549	0.48728		− 1.88422 − 2.27823j	0.32493	0.63585
	0.03758	0	− 1		− 0.35313 − 0.54209j	0.07759	0.6148
	0.02251	0	− 1				
	0.01555	0	− 1				
GWOSCA	− 7.34282 − 12.8408j	2.04767	0.43542	WSO	− 4.5567 − 13.4274j	2.11454	0.31426
	− 8.39429 + 9.52401j	1.52249	0.65578		− 8.4152 + 11.2878j	1.75251	0.594474
	− 2.95869 − 6.5531j	1.03948	0.41327		− 2.1324 − 5.12121j	0.82262	0.33573
	− 2.36563 − 4.96523j	0.79053	0.43531		− 4.0872 + 4.29556j	0.68266	0.68545
	− 0.78421 − 3.84501j	0.61379	0.23087		− 1.26287 + 2.7036j	0.43277	0.4572
	− 1.03376 + 1.1538j	0.17676	0.68379		− 0.7938 − 0.0564j	0.00302	0.99788

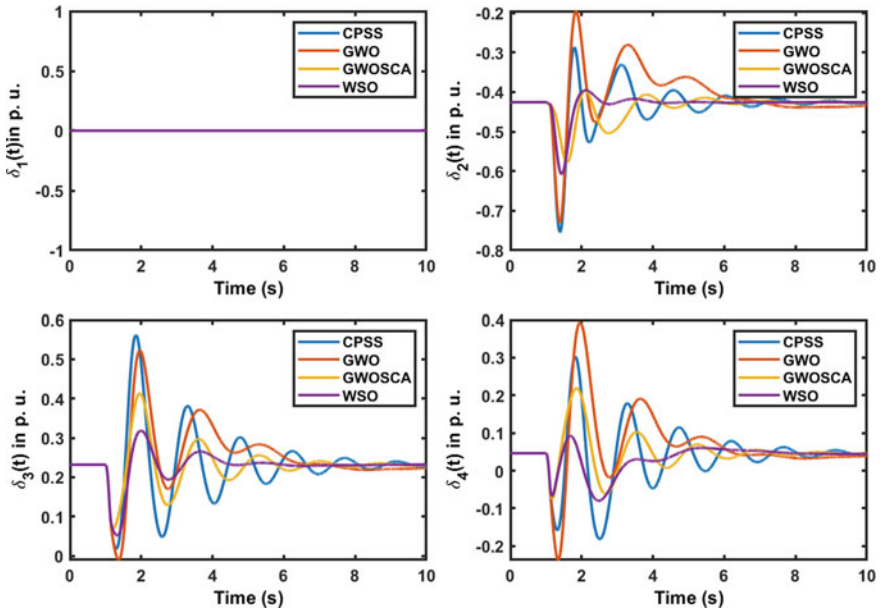

Fig. 3 Torque angle characteristics with considered approaches

with the suggested approaches compared to CPSS. Similarly, the improvement in system damping with the suggested algorithm can be observed.

4 Conclusion

In this paper, different approaches for damping power system oscillations have been proposed. Various population-based algorithms have been employed from literature, and their application to the considered research problem has been investigated. They have been framed by considering hallmark features of the individual algorithms that are handy for the considered research problem. A two-area four-machine benchmark model has been chosen to demonstrate the improvement in the damping nature during transient conditions with the tuned controller parameters obtained from the employed techniques. The time-domain specifications of system responses under the system uncertainties correspond to higher peak overshoots and larger setting times with the traditional CPSS. Where these values have been tremendously reduced to the lesser magnitudes with the PSS parameters extracted from the WSO-based PSS.

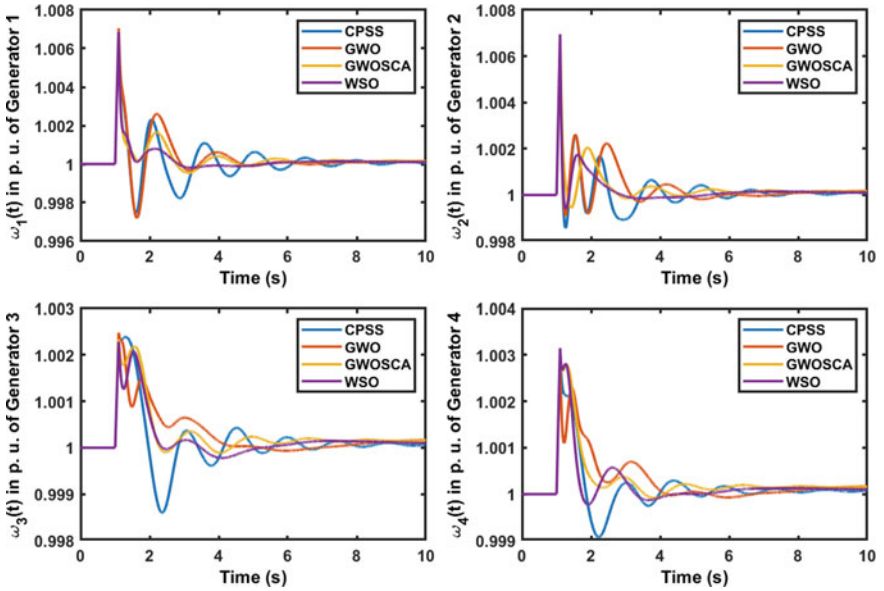

Fig. 4 Angular speed characteristics with considered approaches

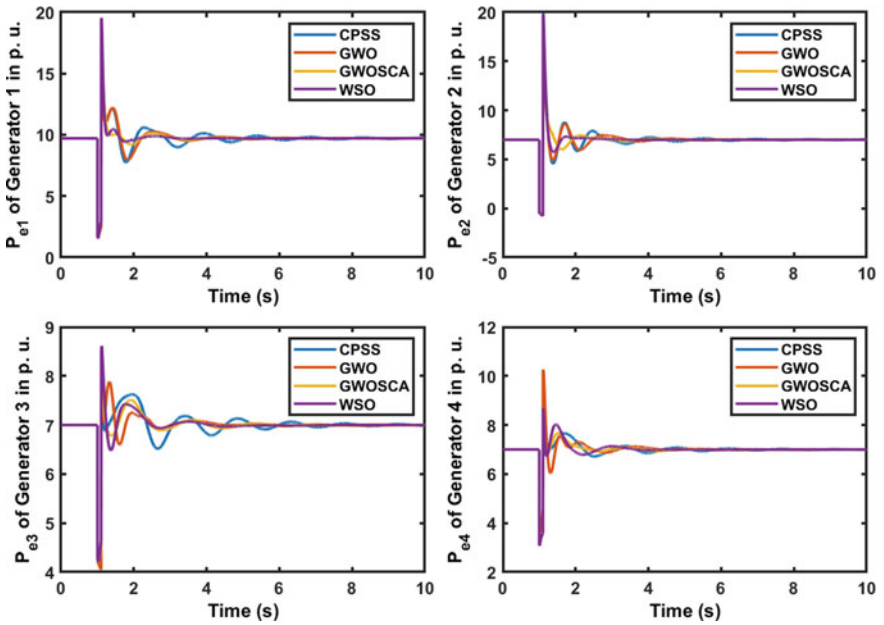

Fig. 5 Generator active power characteristics with considered approaches

References

1. R. Devarapalli, N.K. Sinha, F.P. García Márquez, A review on the computational methods of power system stabilizer for damping power network oscillations. Arch. Comput. Methods Eng. (Feb. 2022). https://doi.org/10.1007/s11831-022-09712-z
2. N.K. Sinha, R. Devarapalli, P.N. Rao, Novel approach for power system stability analysis and improvement: a case study based on UPFC application, in *Intelligent Data Analytics for Power and Energy Systems*, ed. By H. Malik, Md. W. Ahmad, D.P. Kothari, (Singapore, Springer, 2022), pp. 99–113. https://doi.org/10.1007/978-981-16-6081-8_6
3. A. Kannan, M. Nuschke, D. Strau-Mincu, LFC model for frequency stability analysis of prospective power systems with high shares of inverter based generation, in *2019 IEEE Milan PowerTech*, (Milan, Italy, Jun. 2019), pp. 1–6. https://doi.org/10.1109/PTC.2019.8810621
4. R. Devarapalli, V. Kumar, Power system oscillation damping controller design: a novel approach of integrated HHO-PSO algorithm. Arch. Control Sci. **31**(3) (2021). https://doi.org/10.24425/acs.2021.138692
5. R. Devarapalli, B. Bhattacharyya, Optimal controller parameter tuning of PSS using sine-cosine algorithm, in *Metaheuristic and Evolutionary Computation: Algorithms and Applications*, eds. By H. Malik, A. Iqbal, P. Joshi, S. Agrawal, F.I. Bakhsh (Singapore: Springer, 2021), pp. 337–360. https://doi.org/10.1007/978-981-15-7571-6_15
6. B. Dasu, M. Sivakumar, R. Srinivasarao, Interconnected multi-machine power system stabilizer design using whale optimization algorithm. Prot. Control Mod. Power Syst. **4**(1), 2 (2019). https://doi.org/10.1186/s41601-019-0116-6
7. F.P. Demello, C. Concordia, Concepts of synchronous machine stability as affected by excitation control. IEEE Trans. Power Apparatus Syst. **88**(4) 1969
8. S.R. Paital, P.K. Ray, A. Mohanty, Comprehensive review on enhancement of stability in multi-machine power system with conventional and distributed generations. IET Renew. Power Gener. **12**(16), 1854–1863 (2018). https://doi.org/10.1049/iet-rpg.2018.5401
9. R. Devarapalli, B. Bhattacharyya, A hybrid modified grey wolf optimization-sine cosine algorithm-based power system stabilizer parameter tuning in a multimachine power system. Optim. Control Appl. Meth. **41**(4), 1143–1159 (2020). https://doi.org/10.1002/oca.2591

Transient Analysis of a HOMER Designed Renewable Energy Sources (RES) Using MATLAB/Simulink

Jyotirmoy Hazarika and Om Prakash Roy

Abstract There are various methods for extracting electricity. There is a shift going on worldwide from conventional energy sources to renewable energy sources. Diminishing fossil fuels and its environmental aspects compels us to bend towards cleaner renewable resources. Various methods have been used for the useful combination of multiple renewable energy sources. In this paper, optimization of a community load in Deotola, North Lakhimpur District of India by HOMER software is analysed. As the location has a fair potential of solar and wind energy, extracting the resources efficiently to form a hybrid microgrid system cannot only resolve the existing power issues but also it can replace the old grid. Different cases in interlinking the energy sources as well as the transient behaviour of the systems in response to various faults are also analysed.

Keywords HOMERquickstart · Microgrid · Transient stability · Simulink

1 Introduction

Though there has been vast progress in technology, yet fossil fuels have been the prime source for generating electricity. According to the report of NITI Aayog, in India more than 70% of electricity is generated by burning fossil fuels. The dropping level of conventional sources and their adverse effect on the environment is putting a threat to the future generation [1]. The carbon emission because of the burning of fossil fuels is the key concern here, which speeds up the global warming problem [2]. In this circumstances, non-conventional energy sources can be the replacement of traditional sources in time ahead. Low running cost and its inexhaustible resource besides the eco-friendly nature gives always an edge to renewable energy sources. Microgrid technology using different energy sources in effective way

J. Hazarika (✉) · O. P. Roy
Department of Electrical Engineering, NERIST, Papum Pare, India
e-mail: jyotirmoyhazarika@ymail.com

O. P. Roy
e-mail: opr@nerist.ac.in

© The Author(s), under exclusive license to Springer Nature Singapore Pte Ltd. 2023

K. Murari et al. (eds.), *Soft Computing Applications in Modern Power and Energy Systems*,
Lecture Notes in Electrical Engineering 975,
https://doi.org/10.1007/978-981-19-8353-5_16

can bring sustainable growth of a country [3]. Some countries like Germany, UK, Denmark, and Australia are doing commendable progress in extracting electricity from renewable sources [4]. Intermittency nature of renewable sources is the only obstacle in total dependence on single renewable energy source. A hybrid system could eliminate this problem by using more than one such sources connecting them in a suitable combination [5, 6]. In considering the volatile and low penetrating nature of renewable sources, a storage system must be installed with the hybrid system [3]. To meet the ever growing power demand of populous countries like India, merging of different energy sources can be fruitful in supplying reliable and quality power to the consumer. The significance of renewable energy sources encourages to do the present work in a rural location of India where power failure is common. There are various approaches and tools for optimization of renewable sources in the hybrid system [7, 8] namely HOMER, iHOGA, etc., and this work uses a tool named HOMER to get an optimized system for a rural area named Deotola, Assam, India. Present work will concentrate on hybrid system of PV/wind/diesel/battery system combing with existing grid supply.

2 Methodology

Our aim is to design a reliable, cost effective system that can work on both online and offline operation of grid. There is variation of supply from renewable sources as renewable energy sources (RES) depends on weather condition of the location. To optimize such system thorough study of the climate condition of the respective location is required. Also, before designing the microgrid next step is to study the load demand of the location throughout the year. The mismatch of load estimation, i.e. lower load forecast can lead to unmet loads or higher load forecast can cause higher production for even storage of excessive energy. To sort out the technical problems and design a system which is economically justified, it is important to select the size of the RES [9].

Out of different optimization tools available, HOMERquickstart is used in this work. HOMERquickstart, the basic version of HOMER is handy for nonlinear analysis with a single objective as it simplifies the decision-making process by providing an ideal configuration of RES for the desired location. HOMER is also competent to test the technical, environmental, and economic aspect of the designed RES. This work discusses the options for hybrid renewable energy sources in a rural location, Deotola situated in North Lakhimpur, India (Fig. 1). The intermittency of RES makes it hard to predict them, so an optimization study will make it more reliable, cost effective.

The chosen location is at an altitude of 102 m from sea level and located at 27°01′23.9″ N latitude and 93°50′33.0″ E longitude and has an abundance of both solar and wind energy. The mean solar radiation of the location is 6.73 KWh/m2/day, whereas wind speed is 2.63 m/s. (solar and meteorological data from NASA). The clearance index is in between 57 (max) and 36 (min). The solar radiation, wind speed,

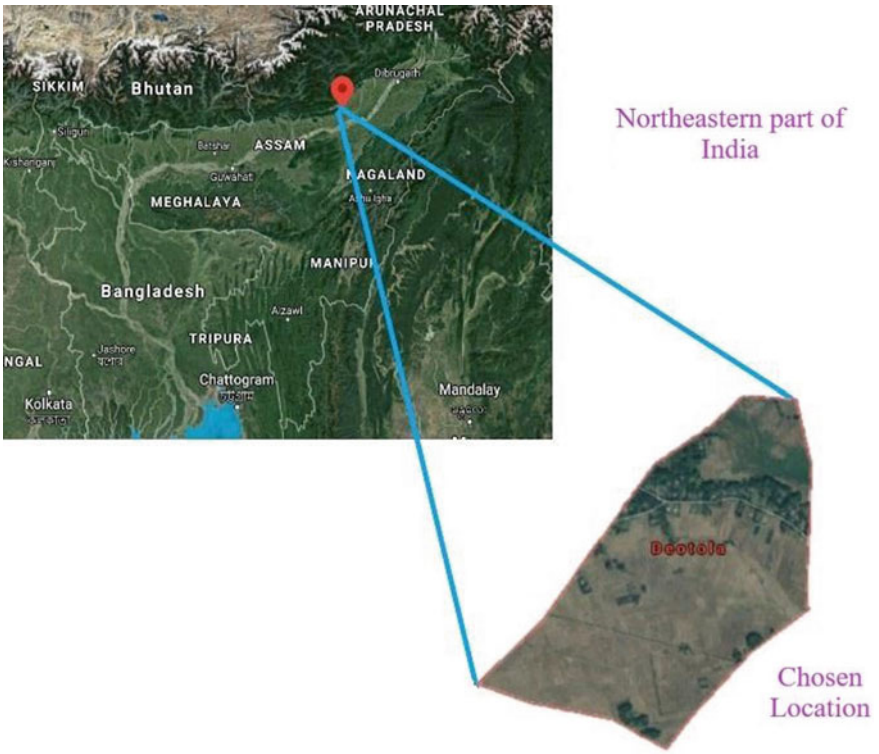

Fig. 1 Selected location, Deotola, India

and clearance index are plotted in Fig. 2. The bars represent the solar radiation and wind speed where the curve represents the clearance index.

The maximum insolation occurs in the month of May which is measured 8.56 KW-hr/m^2/day, and minimum solar radiation is measured in the month of Dec at about 4.55 KW-hr/m^2/day.

Taking a survey of load demand of the locality of 54 number of houses the average demand is found to be 216.8 KWh/day. In the proposed system, PV can supply the load combined with the grid. The peak load is provided by the wind farm. The peak load is 412 KW, so the load factor is 0.526. The community load pattern is shown in Fig. 3. The load increases gradually from morning 5.00 h a day to day activity starts. In evening time, load reaches peak value as all household lights are turned on at this time. This demand decreases gradually after 21.00 h.

HOMERquickstart takes the average insolation data along with ambient temperature to optimize the PV system. The optimized system model by HOMERquickstart is shown in Fig. 4. The output of the PV array can be depicted in Fig. 5. It is seen that the output power developed from PV array is maximum in the months of Nov and Dec due to high clearness index. The battery charging status can also be realized in Fig. 6. It is clear from that depicted plot that battery remains fully charged between

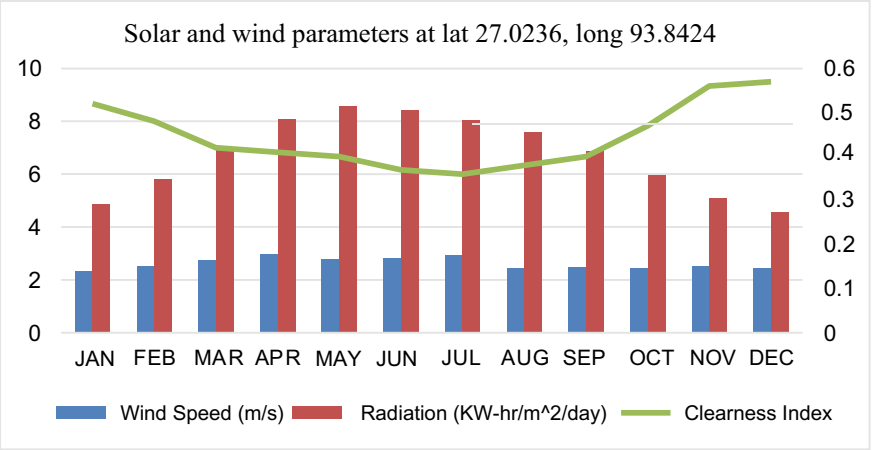

Fig. 2 Solar and wind energy parameters at Deotola

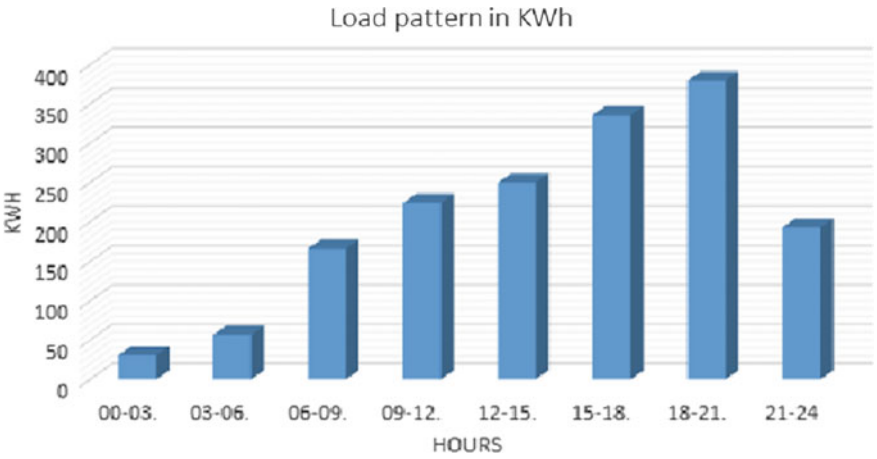

Fig. 3 Community load throughout the day

9.00 and 16.00 h as load demand is provided in this time is from available renewable sources.

3 Mathematical Formulation

For supplying reliable power, PV-wind hybrid system with battery and generator set is chosen in this work. Higher initial cost of the system will be justified with lower operating and fuel cost in the long run [10]. The optimized model obtained from

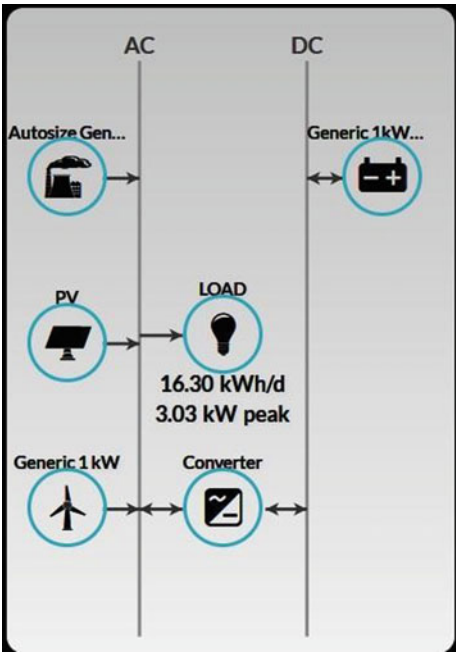

Fig. 4 System designed by HOMERquickstart

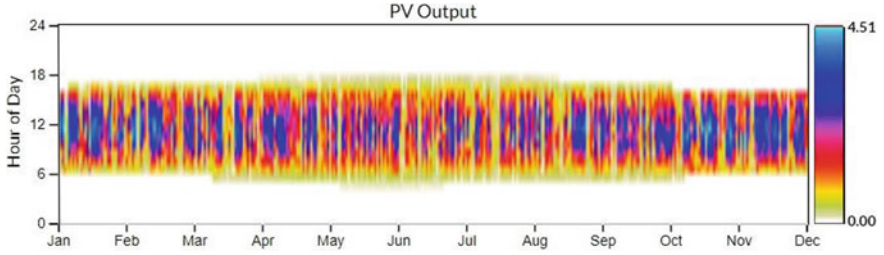

Fig. 5 PV output

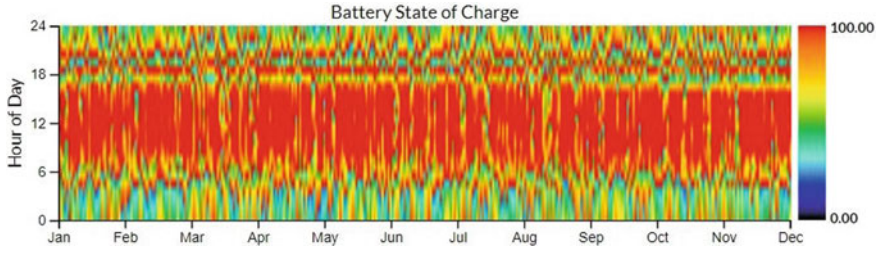

Fig. 6 Battery charging status

HOMERquickstart was designed in MATLAB Simulink, and transient stability of the system is tested by adding few conventional faults.

3.1 PV Modelling

A PV cell converts solar energy into electrical energy. Single diode solar cell is realized to make to make the array of solar cells in the panels. The generated current can be given by the equation [12].

$$I = I_{\text{ph}} - I_s\left[\mathrm{e}^{\frac{q(V+IR_s)}{NkT}} - 1\right] - \frac{V + IR_s}{R_{\text{sh}}} \tag{1}$$

where V is the voltage, I is generated current, and Iph is the photocurrent, Is the saturation current, K is the Boltzmann constant. Rs and Rsh are the series and shunt resistances, T is the temperature, and N is ideality factor of the diode.

3.2 Wind Farm Modelling

In designing the wind turbine, following equations are taken as reference [10, 13, 14].

$$T_{\Omega} = 0.5\frac{\rho V_{\omega}^3 RC_p}{\omega_r} \tag{2}$$

$$\lambda_i = \frac{RC_f}{\lambda} \tag{3}$$

$$C_p = 0.5(0.22\beta - \lambda_i - 2)\mathrm{e}^{\lambda_i} \tag{4}$$

T_{Ω} is wind turbine torque, ρ is air density, $V\omega$ is the wind velocity, R is the radius of the blade, Cp is the power coefficient, λ_i is the tip speed ratio, and β is the pitch angle. The designed model in Simulink with above references can be seen in Fig. 7. The system consists of PV system, wind farm, and generator set connected with grid.

3.3 Optimization

In optimizing, HOMER simulates altered system combinations and rejects the impractical one. The aim of optimizing process is to find the ideal system for each

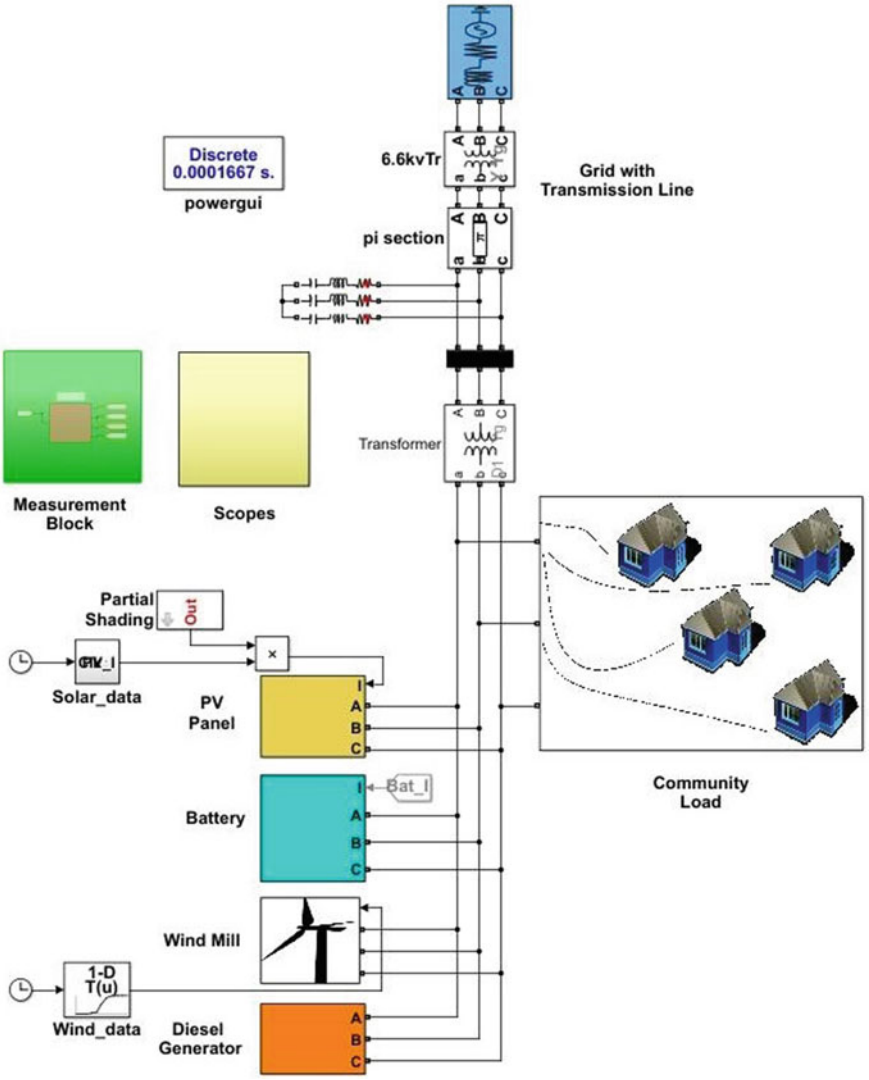

Fig. 7 Designed microgrid with PV and wind farm

decision variable [15]. The modeller sets different decision variable like the size of PV array, number of wind turbine, batteries, etc., with their respective parameters [11].

4 Result and Analysis

Based on the data received from meteorological department and load consumption data, the hybrid system is designed using MATLAB and HOMER. The transient response of the designed system (in Fig. 7) is tested by applying various faults. The system is analysed in some definite combinations exposing it to L-G, L-L, L-L-G, and L-L-L faults. The response of the system is analysed for a period of 0–600 ms. The behaviour of the generating units is also observed in details during that period.

4.1 First Combination: Generator with Wind

For this subsystem, PV subsystem is excluded from the microgrid, only generator is connected to the wind farm. The response of the system to the L-G, L-L-G, L-L, and L-L-L faults is observed at various points which is explained in details in the following cases. In every cases, fault is applied for the duration of 200–300 ms.

4.1.1 *Case 1:* Response to L-G Fault

Single phase to ground fault is applied to the load for the duration of 200–300 ms. The bus voltage is 0 throughout the fault, whereas there is harmonics in load voltage up to 0.7 p.u. is observed during the fault, and post fault voltage reaches more than 1 p.u though it stables very quickly (Fig. 8).

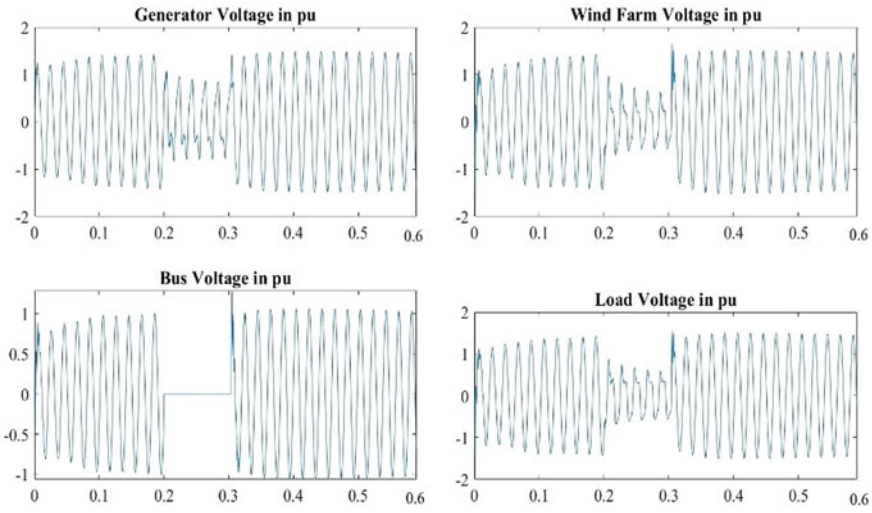

Fig. 8 Voltage of generator and wind system during L-G fault

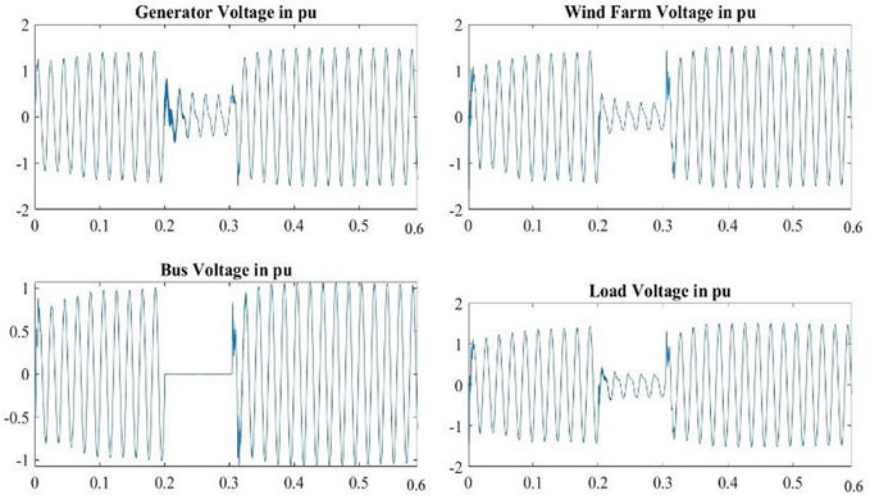

Fig. 9 Voltage of generator and wind during L-L-G fault

4.1.2 *Case 2:* Response to L-L-G Fault

The response of the wind generation combination to the double phase to ground fault is shown in Fig. 9. Here, harmonic distortion in load voltage is less than the previous L-G fault. Bus voltage is again 0 here during the fault. The distortion of the generator voltage and wind arm voltage is more than the previous case.

4.1.3 *Case 3:* Response to L-L Fault

The response of the system when double phase vault is applied is shown in Fig. 10. Bus voltage exceeds 1 p.u. unlike the previous two cases where the bus voltage was zero in both the cases. The load voltage is in the range of 1 p.u. during the fault which is much more than previous two cases. The generator and wind farm voltage profile is same like L-L-G fault.

4.1.4 *Case 4:* Response to L-L-L Fault

To the subsystem, a balanced three phase fault is applied and the plot of the voltage is shown in Fig. 11. During the fault time, both the bus and load voltage are zero. The distortion of the wind farm is very less (in the range of 3 p.u.).

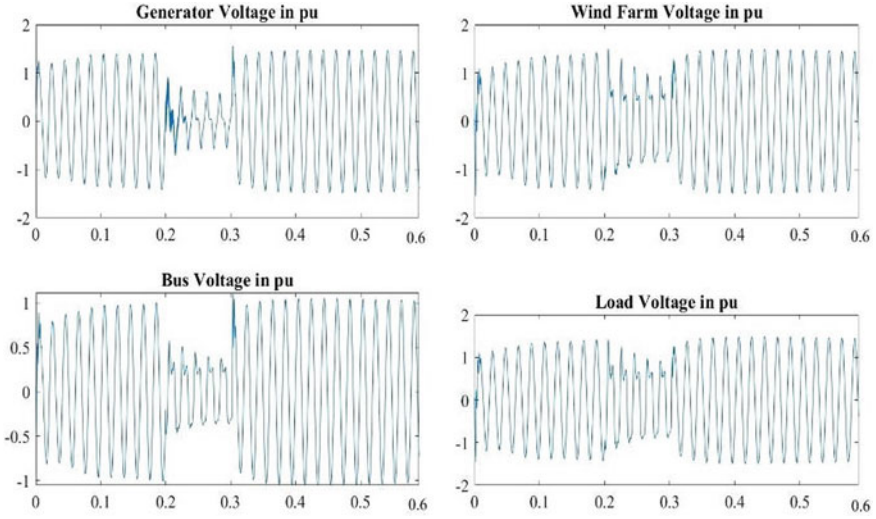

Fig. 10 Voltage of generator and wind during L-L fault

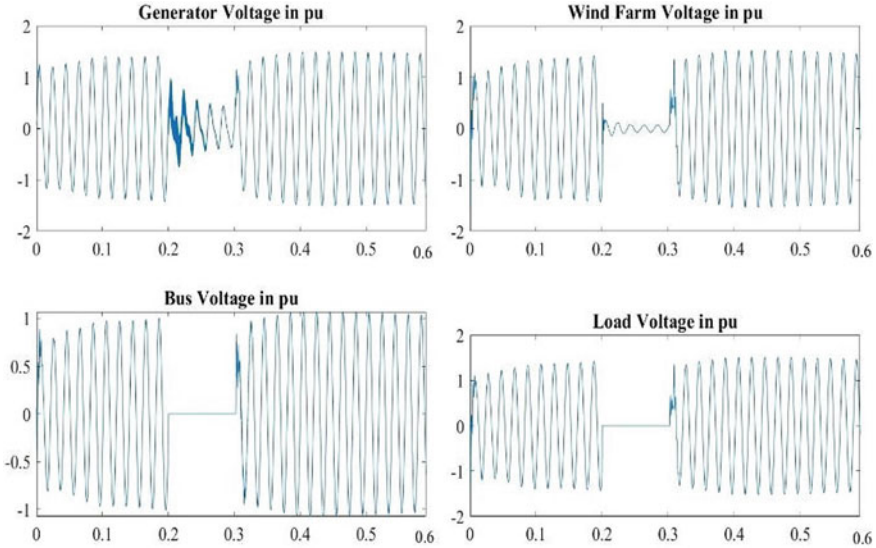

Fig. 11 Voltage of generator and wind during L-L-L fault

4.2 Second Combination: Generator with PV and Wind

In this case, both PV and wind are connected to the grid. Like previous combination here also various faults are applied to this subsystem and the responses of the system

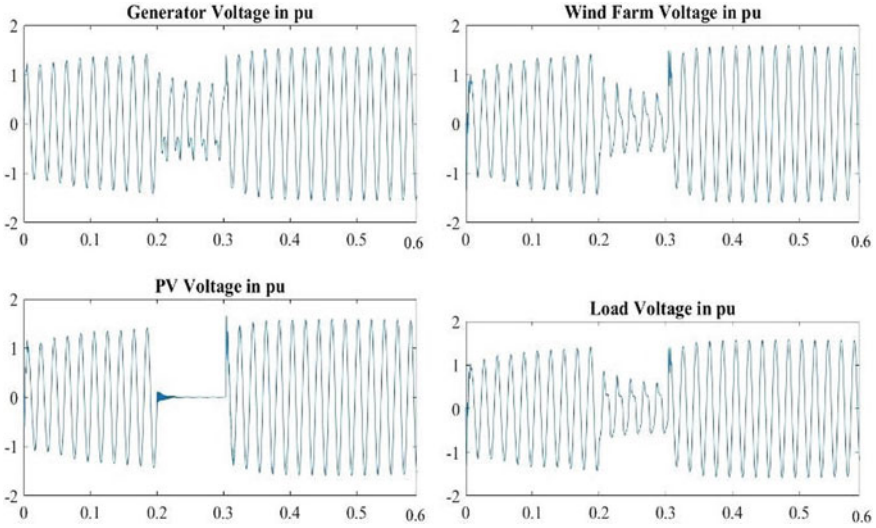

Fig. 12 Voltage of different point of system with PV and wind in L-G fault

before and after the fault are recorded. The fault is applied for the same duration 200–300 ms. The response of the system to the various faults is discussed as follows.

4.2.1 *Case 1:* Response to L-G Fault

Single phase to ground fault is applied to the load for the period of 200–300 ms. Voltages of generator, wind, PV, and load are plotted in the graph as shown in Fig. 12. It is seen that PV voltage is almost zero during the fault rises up to 1.8 p.u. immediately after the fault. Load voltage is in the range of 0.7 p.u. during the fault.

4.2.2 *Case 2:* Response to L-L-G Fault

When the system is exposed to double phase to ground fault, PV voltage distortion is more than L-G fault which is shown in Fig. 13. There is heavy distortion in the PV voltage graph is seen. Even wind farm harmonic reaches up to 1.8 p.u. after the fault before it comes to the normal.

4.2.3 *Case 3:* Response to L-L Fault

When the system is exposed to double phase fault, major distortion is seen in both the generator and PV voltage during the fault time. Wind farm voltage harmonic reaches 1.5 p.u. and also load voltage passes 1 p.u (Fig. 14).

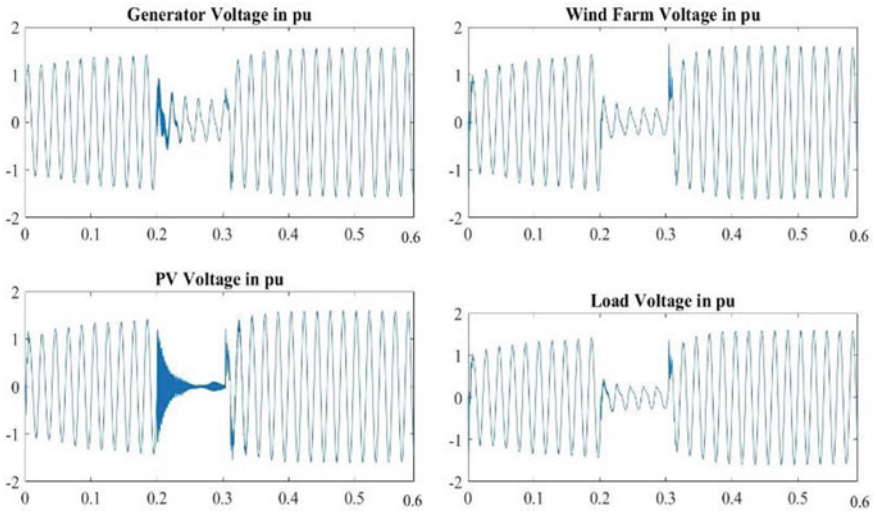

Fig. 13 Voltage of different point of system with PV and wind in L-L-G fault

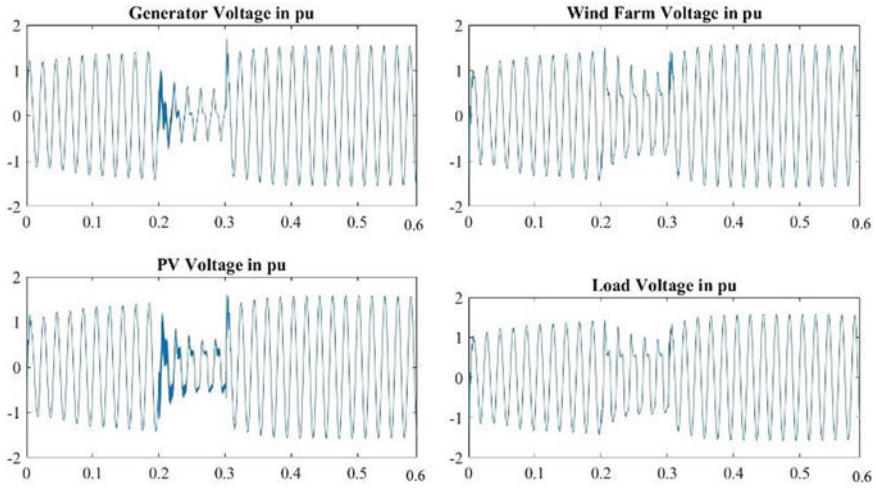

Fig. 14 Voltage of different point of system with PV and wind in L-L fault

4.2.4 *Case 4:* Response to L-L-L Fault

A balanced three phase fault is applied to the system, and the response of the system is plotted in the graph as shown in Fig. 15. Here, load harmonic is the lowest. It is 0 during the fault, and also post fault it does not passes 1 p.u. Though large harmonics is observed in generator and PV voltage

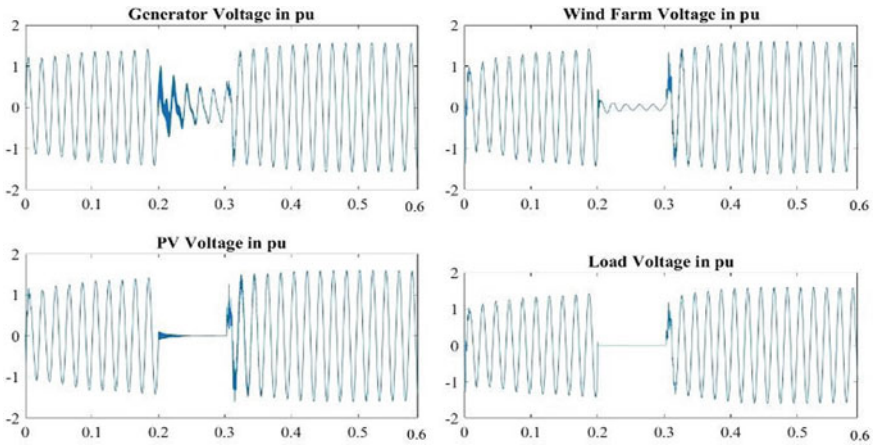

Fig. 15 Voltage of different point of system with PV and wind in L-L-L fault

5 Conclusion

The optimized model from the HOMERquickstart is designed in the Simulink to supply a load of 216.8 KW-hr/day to a rural location named Deotola, Assam. The various faults are applied to the system near the load, and response of the system can be seen in the above voltage plots. From the plots, it can be clearly seen that PV system combined with wind farm shows better transient behaviour than any PV or wind alone system with grid. In rural areas, where electricity supply is very unreliable, this system can be used as it will not only increase the reliability but it will also improve the transient stability of the system.

References

1. G.K. Suman, O.P. Roy, Microgrid system for a rural area—an analysis of HOMER optimised model using MATLAB, in *2019 3rd International Conference on Recent Developments in Control, Automation & Power Engineering (RDCAPE)*, (NOIDA, India, 2019), pp. 534–539. https://doi.org/10.1109/RDCAPE47089.2019.8979097
2. M. Mehrpooya, M. Mohammadi, E. Ahmadi, Techno-economic- environmental study of hybrid power supply system: a case study in Iran. Sustain. Energy Technol. Assess. **25**, 1–10 (2018)
3. J. Zhang, et al., Energy management of PV-diesel-battery hybrid power system for island stand-alone micro-grid. Energy Proc. **105**, 2201–2206 (2017)
4. A.K. Nag, S. Sarkar, Modeling of hybrid energy system for futuristic energy demand of an Indian rural area and their optimal and sensitivity analysis. Renew. Energy **118**, 477–488 (2018)
5. G.K. Suman, S. Yadav, O.P. Roy, HOMER based optimal sizing of a PV/diesel/battery hybrid system for a laboratory facility. in *2020 3rd International Conference on Energy, Power and Environment: Towards Clean Energy Technologies*, (IEEE, 2021)
6. O. Hafez, K. Bhattacharya, Optimal planning and design of a renewable energy based supply system for microgrids. Renew. Energy **45**, 7–15 (2012)

7. N. Saiprasad, A. Kalam, A. Zayegh, Comparative study of optimization of HRES using HOMER and iHOGA Software (2018)
8. T. Lambert, Micropower system modeling with homer, in *Integration of Alternative Sources of Energy*, eds. by F.A. Farret, M. Godoy Simoes (2006)
9. I. Strnad, R. Prenc, Optimal sizing of renewable sources and energy storage in low-carbon microgrid nodes. Electr. Eng. **100**(3), 1661–1674 (2018)
10. A. Acakpovi, E.B. Hagan, A wind turbine system model using a doubly-fed induction generator (DFIG). Int. J. Comput. Appl. **90**(15) (2014)
11. S.G. Malla, C.N. Bhende, Voltage control of stand-alone wind and solar energy system. Int. J. Electr. Power Energy Syst. **56**, 361–373 (2014)
12. H. Bellia, R. Youcef, M. Fatima, A detailed modeling of photo- voltaic module using MATLAB. NRIAG J. Astron. Geophys. **3**(1), 53–61 (2014)
13. R. Mahalakshmi, J. Viknesh, K.C. Sindhu Thampatty, Mathematical modelling of grid connected doubly fed induction generator based wind farm, in *2016 IEEE International Conference on Power Electronics, Drives and Energy Systems (PEDES)*, (IEEE, 2016)
14. F.A.R. Abbas, M.A. Abdulsada, Simulation of wind-turbine speed control by MATLAB. Int. J. Comput. Electr. Eng. **2**(5), 912–915 (2010)
15. K.M. Krishna, Optimization analysis of microgrid using HOMER—A case study. in *2011 Annual IEEE India Conference*, (IEEE, 2011)

Monitoring and Control of EV-to-Grid Load with REAL-TIME Data Communication by Using RSLINX-OPC Server Among MATLAB, PLC, and SCADA

Anand Kumar Maurya, Navdeep Singh, and A. K. Pandey

Abstract REAL-TIME control of the process is presented in this paper. Utilizing SCADA and MATHWORKS RSLINX-OPC Toolbox through programmable logic controllers. RSLinx Remote RSLINX-OPC server from Rockwell Automation works on servers that have a client architecture, and it uses an RSLINX-OPC DDE server. The Clients in this situation are SCADA and MATHWORKS. There is a three-phase design and implementation flow. Phase one involved designing PLC-based applications, followed by developing SCADA applications and integrating these with processes through the RSLINX-OPC server. Simultaneously accessing process data in real time is done with SIMULINK-MATHWORKS models in MATHWORKS. MATHWORKS and MicroLogix 1400B PLCs have been used to validate the realization of the test system. Test results and process control suggest that REAL-TIME data is exchanged among SCADA, PLC, and MATHWORKS in an efficient and reliable manner. Monitoring and control of EV-to-Grid Load utilization by using PLC and SCADA at real-time data acquisition are performed in this research. Using this technology, you may connect all operational systems to an OPC server and exchange data in a highly efficient manner. Simulink is used to simulate the SIMULINK model (.mat file), PLC used to control and interface other electronics systems to MATLAB mode, and SCADA used for operational purposes as a screen; all three systems are networked or interfaced on RSLINX OPC-SERVER.

Keywords PLC · SCADA · RSLINX-OPC server · MATHWORKS-Simulink-MATHWORKS · REAL-TIME Process control · Server–Client

A. K. Maurya (✉) · N. Singh · A. K. Pandey
Department of Electrical Engineering, Madan Mohan Malviya University and Technology, Gorakhpur, UP, India
e-mail: 2021038006@mmmut.ac.in

N. Singh
e-mail: nsee@mmmut.ac.in

© The Author(s), under exclusive license to Springer Nature Singapore Pte Ltd. 2023

K. Murari et al. (eds.), *Soft Computing Applications in Modern Power and Energy Systems*, Lecture Notes in Electrical Engineering 975,
https://doi.org/10.1007/978-981-19-8353-5_17

1 Introduction

A generic client–server interface standard using the COM/DCOM architecture, RSLINX-OPC technology provides a general mechanism for client–server data exchange and communication, as well as supporting network distributional application procedure communication and application procedure communication across different operating systems. The RSLINX-OPC standard enables integrating hardware and software from multiple vendors and provides a distant location REAL-TIME solution monitoring and control among process controllers and PCs. A powerful data calculation and graph plan function can be found in MATHWORKS by MathWorks Corporation [1]. Many useful toolboxes can be acquired from it in many domains. MATHWORKS and process devices can be remotely controlled through RSLINX-OPC toolbox so that REAL-TIME data can be obtained from the exterior and meaningful outputs can be obtained from the exterior. Specifically in this article, there is a REAL-TIME remote communication scheme among MATHWORKS and Micrologix 1400B products based on RSLINX-OPC technology.

1.1 Communication Principle

COM modules can be presented with both RSLINX-OPC custom interfaces and RSLINX-OPC automation interfaces, which are industry-standardization interfaces. RSLINX-OPC clients and RSLINX-OPC servers are connected via RSLINX-OPC interfaces through a "plug and play" process. The RSLINX-OPC Server component provides a standard interface to RSLINX-OPC objects; at the same time, the interface is used to manage RSLINX-OPC objects [1, 2]. In COM, the client can create and manage a server and access data objects in the server by calling the interface method. Objects in an RSLINX-OPC server are divided into three categories, which are server, group, and item objects. RSLINX-OPC servers include an RSLINX-OPC server object containing all the server's information, as well as its configuration. Objects in the RSLINX-OPC server include items, and items include group objects and item objects. Figure 1 depicts the RSLINX-OPC object hierarchical system [1].

Matrix laboratory® 7.0 and higher versions are capable of extending MATHWORKS's calculation environment with the RSLINX-OPC server Toolbox and function module. With Mathworks RSLINX-OPC data access standard, users can create object-oriented hierarchies, communicate with RSLINX-OPC servers, and read and write RSLINX-OPC data directly to RSLINX-OPC servers [3]. While we don't know the internal config of the RSLINX-OPC server, MATHWORKS and the RSLINX-OPC server may easily communicate using the RSLINX-OPC Toolbox software for constructing RSLINX-OPC customer equipment and programming to do uncooked analysis of data, measurement, and management.

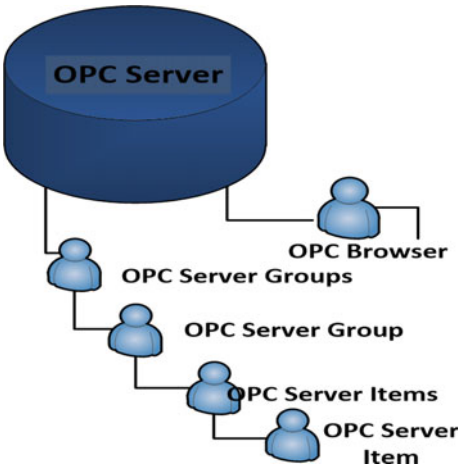

Fig. 1 The RSLINX-OPC object hierarchical system

Figure 2 depicts data access among the user's MATHWORKS application program and the method tool. Instead of direct access to the RSLINX-OPC server, user access to the MATHWORKS application program visits process data through the RSLINX-OPC server interaction and swap values with RSLINX-OPC server products. Consumer data can be organized using RSLINX-OPC product groups. An RSLINX-OPC object is the smallest logical unit for reading or writing data that is defined by an RSLINX-OPC server. It can provide a connection among the RSLINX-OPC-server and process data, i.e., each device is connected to a different process signal. RSLINX-OPC equipment provides RSLINX-OPC users with price, features, and timestamp and information on various signals, which is usually a guide to the registration process. All recording tools used by RSLINX-OPC users are made from its product object [3]. Because RSLINX-OPC products are not COM products and cannot provide user interfaces, users cannot work directly on the product, and access to RSLINX-OPC products must be completed by product category. Here are three ways to exchange data among the RSLINX-OPC client application program and the RSLINX-OPC server: synchronous method, asynchronous method, and registration method. When the exchange rate is low, the synchronized approach is utilized since it is a straightforward calculation. The asynchronous technique is more complicated and may interface with actual things directly.

When there are more customers and they effectively communicate, the asynchronous technique is more efficient. Using the registration method, the RSLINX-OPC-server will see received RSLINX-OPC Server client when the values changes. The application uses asynchronous methods to recognize communication data among the RSLINX-OPC client and the RSLINX-OPC-server.

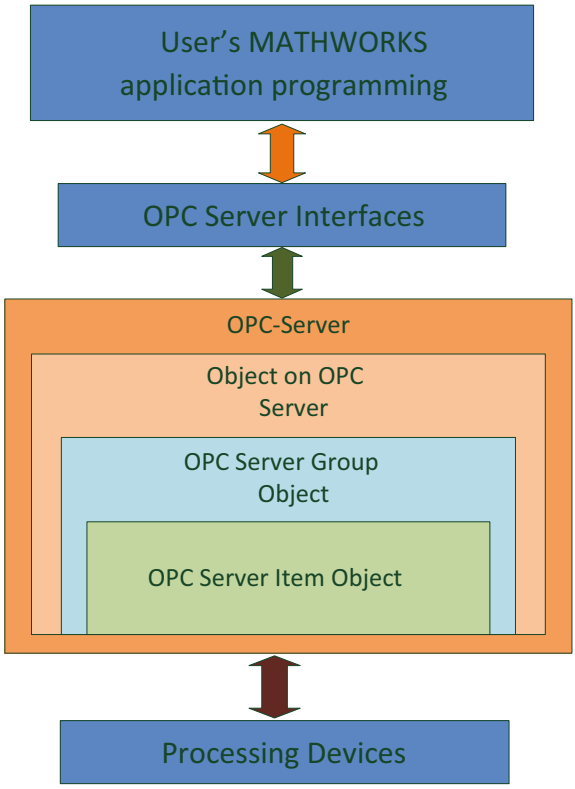

Fig. 2 Data accessible relationship among MATHWORKS applications programming and processing devices

1.2 Communication Latency

The term lag refers to communication delays over a network, also referred to as network latency. Generally data transfer, latency refers to the time it takes to capture, transmit, process across multiple devices, and finally receive at its destination and decode a packet of data [4].

By using fiber optics, data transfer latency will minimized, optical fiber connections, which make extensive use of laser technology, are critical enablers in today's information age. With the emergence of new technologies like IOT, big data, cloud-based services, VR technology, and machine intelligence, the demand for high-capacity transmitting data is rising, raising the bar for optical communication system technology [5, 6].

1.3 Test System Formation

Figure 3 depicts a schematic of the distant location REAL-TIME communication test setup among MATHWORKS and a PLC. The following are the basic hardware pieces in order: A personal computer (PC) with a standard network card installed; A Micrologix1400 CAT1766-L32BXB with a communication card (this card supports DF1, TCP/IP, and UDP, among other protocols). The RJ45 interface of the CPU1766 card is used to connect to industrial Ethernet, and it also has its own controller. It can deal with industry Ethernet data connection independently, has a single IP address, and can be put into operation immediately through the network); A CAT1762-IQ16 24 V DC digital input module; a CAT1762-OB16 24 V/0.5 A digital output module; a CAT1762-IF4 analog input module; and a CAT1762-IF4 analog output module; CAT1762-OB16 digital output module (24 V/0.5 A); CAT1762-IF4 analog input module; CAT1762-OF4 analog output module. A PC-Adapter is also included, which converts the PC's RS232 configure to the PLC's MPI/DP interface. With the PC-Adapter/Ethernet, the RSLinx Classic Logic and working Process may be downloaded to the PLC [1, 2, 7]. A power microgrid control system is the process system.

The Allen-Bradly basic software is shown as following: windows base operating system is needed (32/64 bit OS and it works on any version according to software version). RSLinx classic, RSLogix500 are use fore logic design and programed the PLC. For HMI design, FactoryTalk view Studio ME (Machine Edition) are used. For program the client PC need to install MATHWORKS 2018a.

MATHWORKS connects to RSLINX-OPC server through RSLINX-OPC interfaces and uses item object in RSLINX-OPC-server to access the data of Micrologix-1400 PLC devices register units. The Micrologix-1400 PLC exchanges data with the group object but not with the item object because the group object provides the interfaces to Micrologix-1400. The Ethernet/IP communication protocol is used by the

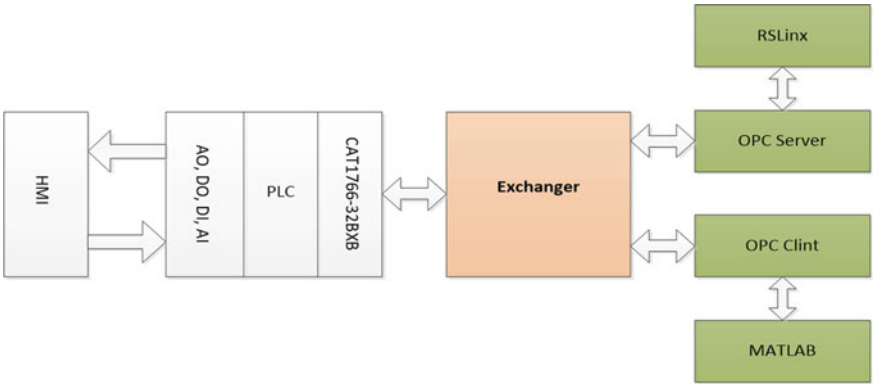

Fig. 3 MATHWORKS and PLC components are used for the remote real-time communication testing system

interfaces. The RSLINX-OPC connections can attach to the RSLINX-OPC-server after using RSLINX-OPC explorer to configure the RSLINX-OPC-server object, the group object, and the item object. The RSLINX-OPC server user application programming will visit the RSLINX-OPC-server and get access to the Micrologix-1400 PLC once the RSLINX-OPC interfaces are opened [8, 9]. After stabilizing the communication among PLC-MATHWORKS then communicate HMI with same RSLINX-OPC server, after communication design the HMI screen for supervise and data acquisition. The MATHWORKS and PLC components of the remote on-time communication test model shown in Fig. 3.

2 Communication Process

2.1 Steps of Configuration

The objective of implementing a connection is to connect the RSLINX-OPC-server and the user, and it entails the following particular considerations.

(1) Programming and Configuration with Hardware

There are two goals for configuring the Micrologix 1400 PLC hardware system. One is to configure the basic communication and location of the PLC and PC, which uses the RSLINX-OPC server; the other is to open the memory and data files that the computer needs to access and download. First, run the RSLinx Classic application program, and then complete the hardware PLC configuration of the micrologix 1400 PLC; after that, configure the PLC by using EtherNet/IP Driver. After that stabilize the communication among PLC-PC [1, 3]. When communication stabilize successfully then create RSLINX-OPC server by using RSLINX-OPC protocol. Second, select the communication point by setting the PC–PC interface to Ethernet, where the user selects the communicating device, adjusts the baud rate of PC-Adapter, the MPI address, the communication port address, and the communication path. Speed among both PC adapters. Finally, remove the configured hardware and PLC programming from the PLC CPU.

(a) *PLC Controller*

Programmable logic controllers (PLCs), microprocessor-based control systems, and microcontrollers are used in control systems instead of electronic control circuits, such as contactors, relays, and accessories such as timers. PLC is more desirable because of its ease of use and operation. In addition, PLC control processes provide solutions for complex control systems, especially PLC equipment designed for machine operation and so on.

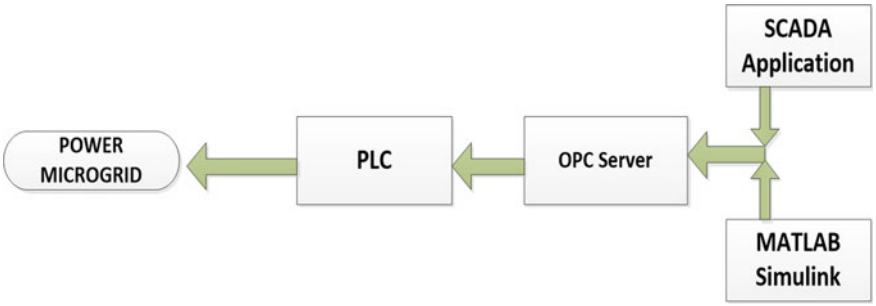

Fig. 4 Block diagram of the control unit

MicroLogix 1400B DC/DC series PLC is used to process and evaluate data from the system. A PLC with digital inputs and outputs and an 8192 byte data memory has 14 digital inputs, 10 digital outputs, and 2 analog inputs. A number of analog input channels were insufficient, so SM 123 analog module series was added to work with compatible PLCs. There are three analog input channels and two analog output channels. In analog channels, the digital-to-analog conversion has a resolution of 13 bits. The block diagram of the control unit is given in Fig. 4 [3].

(2) Configuration process of RSLINX-OPC Server

RSLINX-OPC server are programs that translate hardware communication protocols used by PLCs into RSLINX-OPC protocols. Typically, RSLINX-OPC clients are programs that connect to hardware, like an HMI. To receive data or to send commands to the hardware, the RSLINX-OPC client will communicate with the RSLINX-OPC server [10].

(a) *PLC DRIVER CONFIGURATION*

Choosing RS-232 DF1 devices and clicking on Add New brings us to this window. In Configure RS-232 DF1 devices, we have to name the PLC and then start configuring it. RSLinx can be allowed to make the selection of the optimal settings by using auto configure [10, 11].

(b) *CREATING NEW RSLINX-OPC TOPIC*

Creating an RSLINX-OPC topic and saving it for future reference is the next step. We have created a topic that will provide access to all the inputs and outputs of the PLC.

(c) *CREATING NEW RSLINX-OPC SERVER*

We open a new RSLINX-OPC server in the RSI-RSLINX-OPC test client. In order to prevent compatibility issues and limitations, we use RSLinx

Table 1 Data store address in PLC

Data type	PLC-address	Remarks
Input/output-REAL	I0, O:0	For real values
MEMORY FLOT	F8	For floating values

RSLINX-OPC Server, the proprietary software for Allen Bradley PLCs. Nonetheless, any RSLINX-OPC server can be used if that is what is needed.

(d) *CREATING A NEW GROUP*

Create a new group after creating the RSLINX-OPC server. The rest of the settings are left at their default settings.

(e) *CREATING ITEM/TAG*

Our next step is to add RSLINX-OPC tags, which are essentially input and output variables within the group. RSLinx requires the same name for the access path as the RSLINX-OPC Topic. A drop-down menu is available for choosing the data type of input/output variables based on the syntax of the PLC [3].

3 Configuration Variable

Configuration variables are used in the RSLINX-OPC connection among Micrologix 1400 PLC and RSLINX-OPC server. RSLinx remote server provides an RSLINX-OPC monitor application called RSLINX-OPC Scout. As part of RSLINX-OPC Scout, you can define an RSLINX-OPC connection group as well as variables for DB (Section memory (F8 and I0 in this case) sections corresponding to PLC. Creating item/tag-RSLinx requires the same name for the access path as the RSLINX-OPC Topic [12]. A drop-down menu is available for choosing the data type of input/output variables based on the syntax of the PLC. After configuring the new RSLINX-OPC server, we can use memory variables to exchange data from MATHWORKS to PLC or PLC to MATHWORKS. There are two types of data variables used one is real, and other is memory floating type which is mentioned in Table 1.

4 Designing and Implementation

The complete test system has been separated into three phases for ease of use.

(a) *Creating a process application based on a PLC*

Hardware and software components make up the design of a Power EV-to-grid. The physical components that make up a PLC-based system. Figure 5 [7] shows the PLC basic connections.

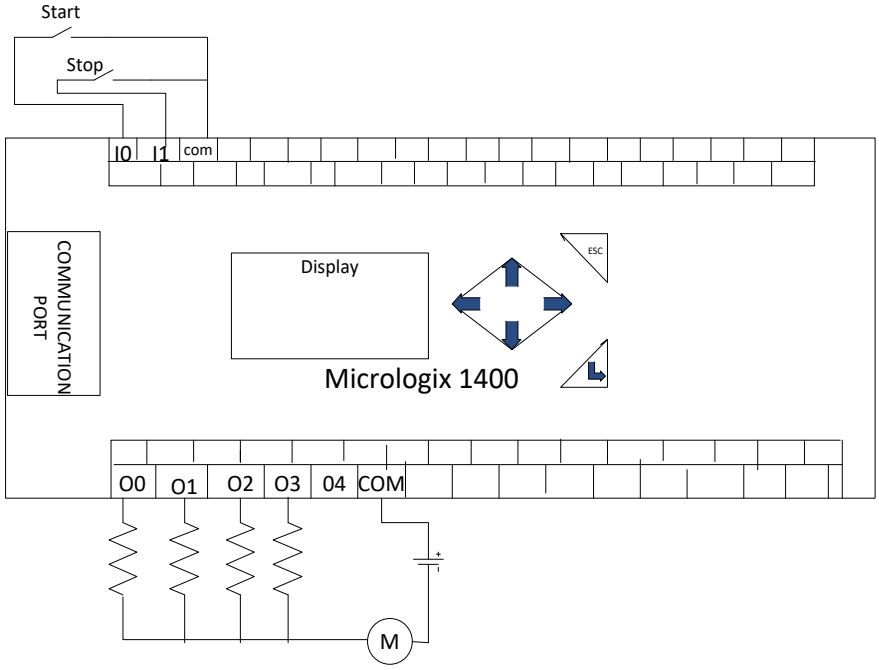

Fig. 5 Basic connections of PLC

(b) *Developing SCADA Application*

RSLinxRemote Server [11] is used to connect the MicroLogix 1400 PLC to Rockwell Automation's Citect SCADA HMI/SCADA software package. The factoryTalk view studio V11 HMI is designed for power grid machine relay control and data observation, and it can read and write REAL-TIME data in PLCs via an RSLINX-OPC DA server. A sample of a SCADA application for EV-to-grid load control is shown in Fig. 5.

RSLinxRemote Server [11] is used to connect the MicroLogix 1400 PLC to Rockwell Automation's Citect SCADA HMI/SCADA software package. The factoryTalk view studio V11 HMI is designed for power grid machine relay control and data observation, and it can read and write REAL-TIME data in PLCs via an RSLINX-OPC DA server. A snapshot of a SCADA application for EV-to-grid control is shown in Fig. 6.

The following are the steps involved in developing a SCADA-based application:

(i) Creating a new INPUT/OUTPUT device or server: The communication express wizard in the Citect project editor is used to establish a new INPUT/OUTPUT server that is coupled to the RSLinxRemote driver. The MicroLogix 1400 PLC driver is used to construct a new INPUT/OUTPUT device.

(ii) Creating variable tags and graphics: Variable tags are produced in the Citect project editor with particular tag names and data types. An INPUT/OUTPUT

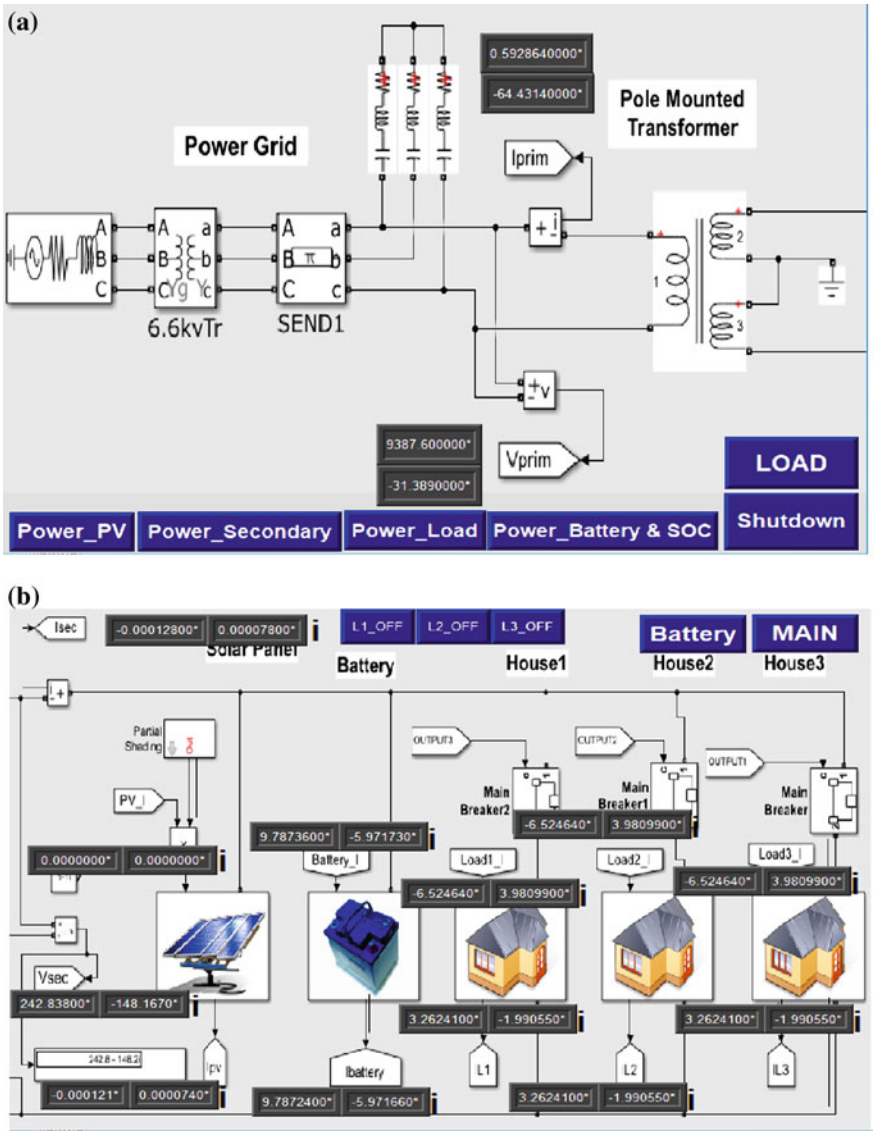

Fig. 6 Snapshot of a SCADA application for power EV-to-grid. **a** Main screen and **b** load control screen

device and an INPUT/OUTPUT server are connected to them. The variable tags are used to store REAL-TIME data from the PLC [13, 14].

(iii) The SCADA visual building platform is used to create required graphics. The necessary item's are chosen from the symbol-Factory or library and linked to PLC tags that have previously been established. Individual graphical objects'

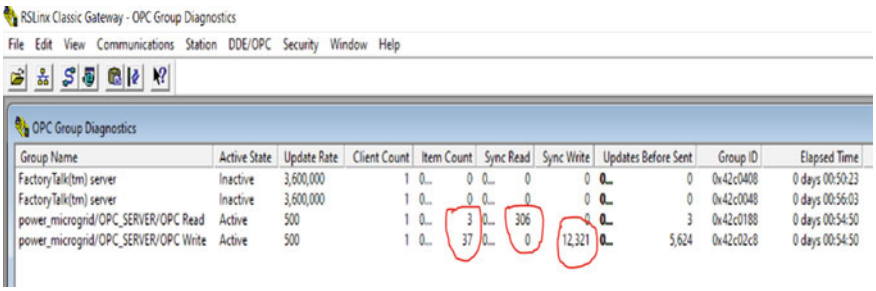

Fig. 7 Snapshot of the RSLINX-OPC quick client in RSLinx remote server

runtime behavior is controlled by modifying their properties. Provides data types and variable tags for a DC motor speed control application.

(iv) RSLinxRemote Server is an RSLINX-OPC server that connects SCADA clients to PLC-based applications. It provides REAL-TIME values to a SCADA client it purchased from PLC [13]. RSLinxRemote Server is set up, with proper data types for channel, device, groups, and tags. Figure 7 shows a snapshot of the RSLINX-OPC quick client in RSLinxRemote Server.

The fast client of RSLINX-OPC-server is used to read–write data, as well as run executable suites to evaluate server performance. Its exhaustive error reporting offers precise information about any RSLINX-OPC errors the server returns. It can help diagnose typical RSLINX-OPC-server client and server problems [12].

(c) *MATHWORKS-Simulink-MATHWORKS Model*

From inside the MATHWORKS, you may retrieve live and history RSLINX-OPC data using the MATHWORKS RSLINX-OPC Toolbox. RSLINX-OPC data may be read, written, and recorded by Remote devices linked through PLCs or other automated systems. There are two techniques in the MATHWORKS RSLINX-OPC Toolbox for attaching a MATHWORKS-Simulink-MATHWORKS client to a PLC through an RSLINX-OPC server [1]: one uses the MATHWORKS command prompt, and the other uses a simulation model.

According to this paper, create communication by using SIMULINK-MATHWORKS model. RSLINX-OPC toolbox available in SIMULINK-MATHWORKS library, directly pick the block from the library, and stabilized communication among PLC and MATHWORKS by using RSLinx RSLINX-OPC remote server. RSLINX-OPC toolbox block is shown below in figure. After establishing a connection among MATHWORKS and the RSLinxRemote RSLINX-OPC-server, the SIMULINK-MATHWORKS model is created using the RSLINX-OPC Toolbox. Figure 8 shows the Simulink-MATHWORKS model for the Power EV-to-Grid.

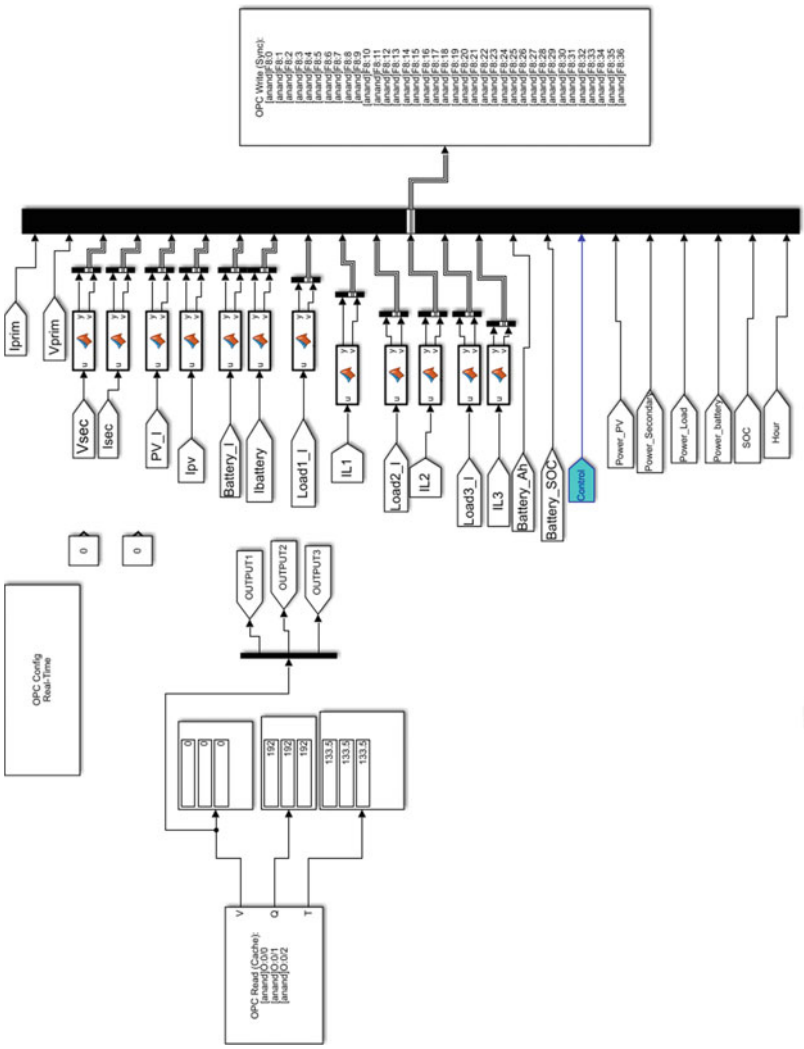

Fig. 8 Simulink-MATHWORKS model for the RSLINX-OPC server (read, wright RSLINX-OPC block)

RSLINX-OPC configuration, RSLINX-OPC read, and RSLINX-OPC write 3 RSLINX-OPC-server toolbox objects or blocks that are heavily used in this architecture. The RSLINX-OPC-server configuration block specifies the RSLINX-OPC Server clients that will be utilized in a model, as well as the model's pseudo-REAL-TIME action and action for RSLINX-OPC faults and alarm. The RSLINX-OPC server read block retrieves data on server from one or more RSLINX-OPC-server objects. The read operation might be synchronous (from the cache or from the device) or asynchronous (from the device) (from the device).

The RSLINX-OPC-server write block sends data to single or more RSLINX-OPC-server clients. A synchronous or asynchronous write operation is performed. Every element of the input array is written to the matching item in the RSLINX-OPC write block's Item ID list. Controlling EV-to-grid is quite difficult compared to manually doing the task and automating it. Figure 9 shows the differences in executions of the MATHWORKS model. According to the graph, L1, L2, and L3 are turned off. Changes in the graph can be easily detected.

5 Conclusion

The MATHWORKS RSLINX-OPC Toolbox provides a wealth of RSLINX-OPC tool capabilities, allowing the user to perform operations on RSLINX-OPC objects quickly and easily. They can make the development process easier and give a reliable way to achieve remote real-time connection among MATHWORKS and processing equipment. The approach of remote real-time communication among MATHWORKS and process equipment is typical and valuable to the research and use of REAL-TIME systems. Furthermore, MATHWORKS has a large number of control functions and complex control methods. On the behalf of this research, we may achieve sophisticated control of complex industrial processes in a network environment, therefore increasing control efficiency. We can control any electrical, industrial, or mechanical system using this principle. Fiber optics cable may be used for data transport to increase and reduce data loss. As an example, this article shows EV-to-Grid Load regulation and monitoring. On the basis of this notion, it is possible to control, supervise, and run complicated and larger operational systems in realtime from a remote location without requiring any human intervention in the plant, as well as avert catastrophic faults or losses.

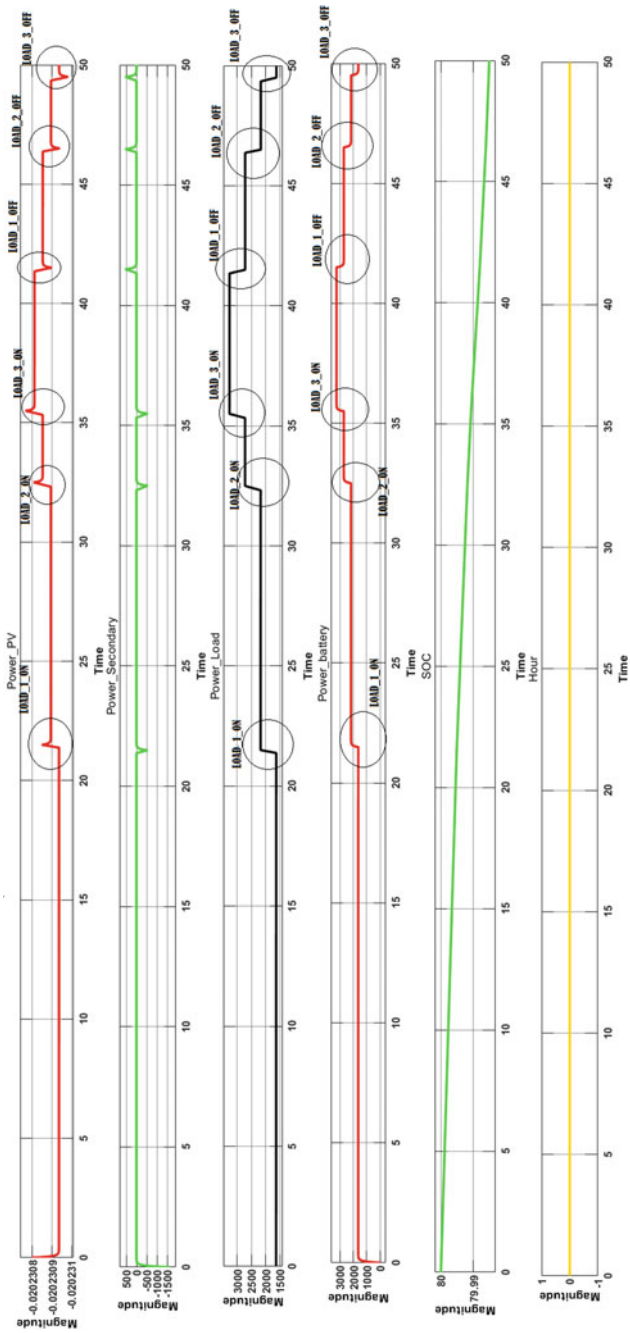

Fig. 9 Showing the change in graph along with load change

References

1. K.N. Bagal, C.B. Kadu, B.J. Parvat, P.S. Vikhe, PLC Based real time process control using SCADA and MATHWORKS. in *2018 Fourth International Conference on Computing Communication Control and Automation (ICCUBEA)*, (IEEE, 2018, August), pp. 1–5
2. Z. Lieping, Z. Aiqun, Z. Yunsheng, On remote REAL-TIME communication among MATHWORKS and PLC based on RSLINX-OPC technology. in *2007 Chinese Control Conference*, (IEEE, 2007, July), pp. 545–548
3. V.A.D.İ Seyfettin, Development of an RSLINX-OPC and PLC based remote-access laboratory: a synchronous motor control experiment. Int. J. Appl. Math. Electr. Comput. **3**(3), 172–177 (2015)
4. A. Chai, Y. Ma, Z. Yin, M. Li, Real-time communication model based on OPC UA wireless network for intelligent production line. IEEE Access **9**, 102312–102326 (2021)
5. S. Cavalieri, F. Chiacchio, Analysis of OPC UA performances. Comput. Stand. Interfaces **36**(1), 165–177 (2013)
6. N.K. Verma, T. Sharma, S. Maurya, D.J. Singh, A. Salour, Real-time monitoring of machines using open platform communication. in *2017 IEEE International Conference on Prognostics and Health Management (ICPHM)*, (IEEE, 2017, June), pp. 124–129
7. R. Bayindir, S. Vadi, Development of an RSLinx-OPC and Plc based remote access laboratory a synchronous motor control experiment. in *International Conference on Advanced Technology & Sciences (ICAT'14)* (2014)
8. S. Persin, B. Tovornik, N. Muskinja, RSLINX-OPC-driven data exchange among MATHWORKS and PLC-controlled system. Int. J. Eng. Educ. **19**(4), 586–592 (2003)
9. I.G. Pérez, A.J.C. Godoy, M.C. Godoy, Fuzzy control of a hybrid renewable power system based on REAL-TIME Mathworks-PLC Communication through RSLINX-OPC. ICINCO **1**, 15–21 (2012, July)
10. The Math Works Inc. RSLINX-OPC toolbox for use with MATHWORKS [P/OL]. 2004–10, http://www.mathworks.com/access /helpdesk/help/pdf_doc/RSLinx-OPC/RSLinx-OPC.pdf
11. X. Hong, W. Jianhua, Using standard components in automation industry: a study on RSLINX-OPC Specification. Comput. Stand. Interfaces **28**(4), 386–395 (2006)
12. L.L. Thanh, R. Caire, D. Thermoz-Liaudy, REAL-TIME communication among MATHWORKS and IEDs in electrical distribution systems using RSLINX-OPC Technology.in *IEEE conference, ICCE 2010-The Third International Conference on Communication and Electronic*, (2010, August)
13. U.D. Dahal, D. Cheten, Substation automation: mathworks and RSLINX-OPC driven substation monitoring system. in *2016 International Conference on Microelectronics, Computing and Communications (MicroCom)*, (IEEE. 2016 January), pp. 1–5
14. M.S. Mahmoud, M. Sabih, M. Elshafei, Using RSLINX-OPC technology to support the study of advanced process control. ISA Trans. **55**, 155–167 (2015)

Artificial Neural Network-Based Designing of Solar and Wind System with Modified Power Filter

Divyanshi Srivastava and Navdeep Singh

Abstract This paper includes the performance and designing of hybrid solar and wind with the modified power filter. Optimized maximum power of hybrid solar and wind energy systems has been achieved by radial basis function network (RBFN). A modified power filter mitigates the harmonics generated by nonlinear loads. A modified power filter comprises the series and shunt capacitor. This modified power filter consists of two switches and control by multiloop dynamic error using artificial neural network. This controlling of switching pattern is mainly governed by artificial neural network-based controller to minimize the harmonics contents in grid and source current. The comparative analysis of system performance has been discussed and analyzed for source and grid current in case of with and without modified power filter. The performance of multiloop dynamic error using artificial neural network-based controller has better result shown in simulation result.

Keywords Radial basis function network (RBFN) · Boost converter · Photovoltaic system · Wind energy system

D. Srivastava (✉) · N. Singh
Electrical Engineering Department, Madan Mohan Malaviya University of Technology, Gorakhpur, India
e-mail: divyanshisrivastava293@gmail.com

© The Author(s), under exclusive license to Springer Nature Singapore Pte Ltd. 2023

K. Murari et al. (eds.), *Soft Computing Applications in Modern Power and Energy Systems*, Lecture Notes in Electrical Engineering 975,
https://doi.org/10.1007/978-981-19-8353-5_18

1 Introduction

A renewable ever green energy generates power without any pollution, and it is interface with smart grid networks. A smart grid network will comprise the green renewable energy and distributed generation as well as FACTS stabilization, filtering devices for mitigate the problem of voltage instability and enhanced power factor by using FACTS (SFC)-based devices with dynamic systems for controlling are utilized [1]. A RBFN MPP tracking technique for hybrid system of renewable energy is designed for grid connected applications [2, 3]. As per requirement of load and higher demand of power, a hybrid renewable energy system has been developed and to obtain maximum power an adequate MPP tracking technique is used with DC–DC converter [4–6]. The power generated by hybrid energy system has been delivered to load and grid interface system and to enhanced performance of hybrid energy system the power electronics devices are mostly used. However, these are the main cause of harmonics injection in the power supply system and to reduce the effect of harmonics in power supply system a modified power filter (MPF) is used. A MPF concept is based off FACTS devices for increase the power quality, power factor correction, flicker control, and reduction in loss of electric energy. These are mostly opted for smart grid connections and renewable energy resources-based systems. Multiloop dynamic error controller (MDEC) has implemented for efficient working of renewable energy resources utilization scheme and multi stabilization purpose [7, 8]. Main contribution of this paper is the artificial neural network (ANN)-based multiloop dynamic controller is designed for the proper working of modified power filter (MPF). A MPF switches controlling has done by ANN-based MDEC. Hybrid system of PV and wind using the single RBFN-based MPPT to reduce the overall cost and the modified power filter reduced the power quality issues so performance of designed system is increased. A MPF is used to reduce the distortion in current, and it has good output performance as compared to without modified power filter-based system. In this paper, THD analysis of grid and source current in case of with and without MPF has shown.

2 PV and WE System with Modified Power Filter

A solitary MPP tracking approach is designed for both PV and WE system. Maximum power point (MPP) tracking techniques are categories in two parts as conventional and artificial-based techniques. The conventional MPP techniques are as P&O and INC, hill climbing techniques and artificial intelligence based as fuzzy logic, RFBN, genetic algorithm, etc. In general several MPP techniques, individual used for hybrid PV and WE system for attaining the MPP. A solitary RBFN-based technique has designed to operate for both power generation systems which reduced the overall cost of the system [3]. The $I\text{pv},w$ (current) and $V\text{pv},w$ (voltage) from PV and WE systems are work as an inputs for Radial basis function-based network (RBFN)-based

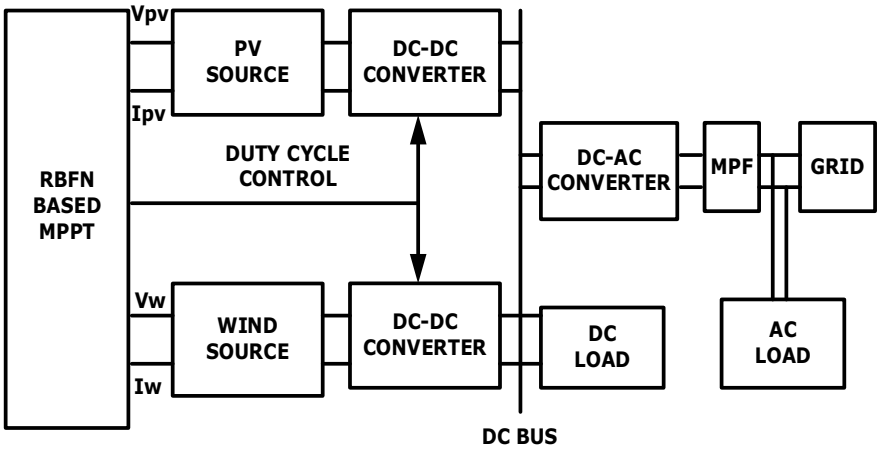

Fig. 1 Artificial neural network-based designing of solar and wind system with MPF

MPP controller, and MPP tracking technique is required to obtain peak power by changing the duty cycle of boost converter (DC–DC) [3].

ANN-based technique is easy to handle the nonlinearity problem and reduced the error by updating weights. All main process has done in hidden layer of feedforward network. Hidden layer comprises the different types of activation function as linear function, Gaussian function, and sigmoidal function, RBF. ANN-based techniques have accurate and good dynamic performance in compared to conventional techniques [9–15]. In this paper for good performance, RBF activation function is used to activate the artificial neurons when input is greater than or equal to the threshold value. RBFN method has used for PV and WE system to obtain peak power under the different environment conditions. The power generation from renewable resources supplied to the distribution network like electric grid, AC and DC load. The power generated by renewable energy resources contain harmonics due to the power electronics converter and AC loads [16], and to reduce the harmonics problem MPF is connected in series with the line, all connection of the system is given in block diagram Fig. 1.

3 Description of PV and Wind System Using RBFN Technique

Solar PV system required irradiance and temperature as an input. Solar cell is semiconductor device which is generating electron-hole pair after incident solar ray on it. Solar irradiance and heat converted into electrical energy by using photovoltaic array [17].

Wind energy (*WE)* is converted into the electrical power using the wind turbine system, and the cube of wind velocity (V_v) is proportional to the mechanical output power. The WE conversion using wind turbine system and generated power is transferred to grid [18].

Boost converter is used as power interfacing device in between renewable system and load. Two boost converters are designed for both PV and WE system. The RBFN-based MPPT is used to generate the duty cycle for boost converter [19].

Radial basis function (RBF)-based artificial technique involved the input, hidden and output layer for process. Radial function is used in hidden layer to deal with the complex nonlinear problem.

RBF-based ANN technique for PV and WE system is described, and simulation is provided in detail [12] (Table 1, 2 and 3).

Table 1 Parameters of PV module [12]

Voc (voltage at open-circuit)	64.2 V
ISC (current in short-circuit condition)	5.96 Amp
IMP (current at MPP)	5.58 Amp
VMP (voltage at MPP)	273.5 V
PMP (maximum power)	100 kW
Series connected module per string and parallel string	5.66
Solar irradiance/temperature	1000 W/m^2, 25 °C

Table 2 Parameters for 3.4 kW WE system [12]

Magnetizing flux	0.152 p.u
Armature inductance	6.35 mH
VM (rated wind speed)	12 m/s
Pairs of poles	2
Power (P)	3.4 kW
Resistance (Ra)	0.046 Ω

Table 3 Parameter specification for boost converter [12]

Vo(voltage at output side)	500 V
*V*pv (voltage at input side)	274.81 V
L(inductor)	5.1 mH
Two capacitor ($C1n = C2n$)	12000 μF
Switching frequency	5 kHz

4 Modified Power Filter

In this paper, the modified filter is used to mitigate the harmonics in power supply system. Modified filter comprises the two shunt capacitor and a single series capacitor. The shunt capacitor across the AC side of uncontrolled rectifier arm is connected. Hybrid of PV and WE system is interface with grid and grid consist different types of load which consume reactive power. To compensate the reactive power, MPF is used. Shunt capacitor is used to provide reactive power, and series capacitor is used increased the power transfer capability. When a series capacitor is added with the transmission line total reactance decreased and power transfer capability become increased. Working of modified filter is described in two cases. Case-1 if pulse P1 goes high, then circuit breaker 1 becomes closed. In this case, resistor and inductor will be disconnected and reactive power is totally supplied by the modified shunt filter. Series capacitor is connected permanently in the transmission line. Shunt capacitor used to provide reactive power and also act as the filter.Case-2 if pulse P1 goes low, then circuit breaker 2 becomes closed, and in this case, resistor and inductor connected with the circuit and it acts as the filter. In this case, shunt capacitor is charged through line and tuned element. P1 pulse is generated by modified error controller which is generating error, and this error is as an input for ANN technique using artificial neural network. A modified simulation diagram is shown in Fig. 5.

Multiloop dynamic error controller (MDEC) is designed to generate $e\,(A)$ and $e\,(B)$ as an output. Multiloop controller comprises the two main controller. Here, primary controller is used to regulate the dynamic tracking and it comprises the three loops. For tracking the reference voltage (Vg-ref), the initial loop operates as a voltage regulator. The second loop and third loop generally operate for dynamic tracking of current and power. The second block is used to reduce the ripple and on the basis of working it is known as minimal ripple regulator [1]. Simulation of MPF with ANN-based MDEC has shown in Figs. 6 and 7 provides the inside view of subsystem $e\,(A)$ of MDEC. The errors ($e\,(A)$ and $e\,(B)$) generated by MDEC are an input for artificial neural network which is denoted by $x\{1\}$. The input signal is passing through the layer 1. Layer 1 consists the weight and bias, activation function. Weight is update to minimize the error, activation function is used to activate the neurons to perform the task as per requirement. If input value is higher than the threshold value, then this signal is used to activate the neuron. In this paper, the activation function is sigmoidal and linear function, respectively, used in layer 1 and layer 2. $a\{1\}$ is output of layer 1 which work as a input for next layer and output of layer 2 is the $y\{1\}$ which is handled the switching of switch by providing pulse by P1. Figure 2 shows the two layers and inside view of layer1 for modified filter designing. Layer 2 designing is same as layer 1 (Table 4).

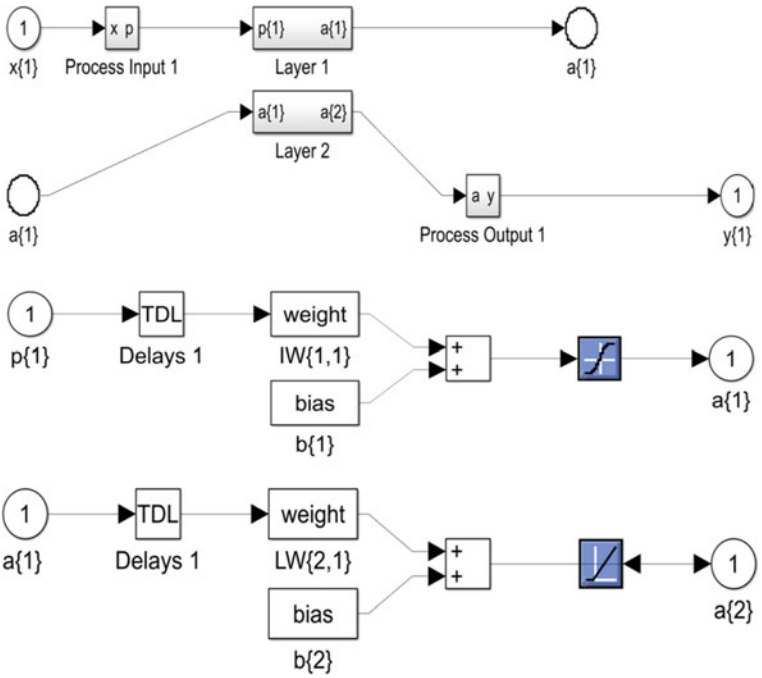

Fig. 2 ANN-based designing of MPF (layer construction and inside view of layer 1)

Table 4 Designed parameter for MPF

Transmission line voltage	25 kV
Subsystem–grid	120 kV
Dc bus voltage	500 V
Boost converter	5 kHz
Operating frequency	50 Hz
Shunt capacitor	500 μF
Series capacitor	1000 μF
Series inductor	1 H

5 Simulation and Results

The overall system connections and RBF-based neural network used to track MPP for hybrid system of PV and wind with MPF model exhibited in Fig. 3.

The designing of RBFN-based artificial neural network for PV and WE system shown in Fig. 4. The Ipv,w and Vpv,w from PV and WE system are selected as an inputs and pass to the RBFN block, and therefore, the radial function used in layer 1 and linear function is used in the layer 2. $P\{1\}$ and $a\{2\}$ are initial input and final output of artificial neural network, respectively.

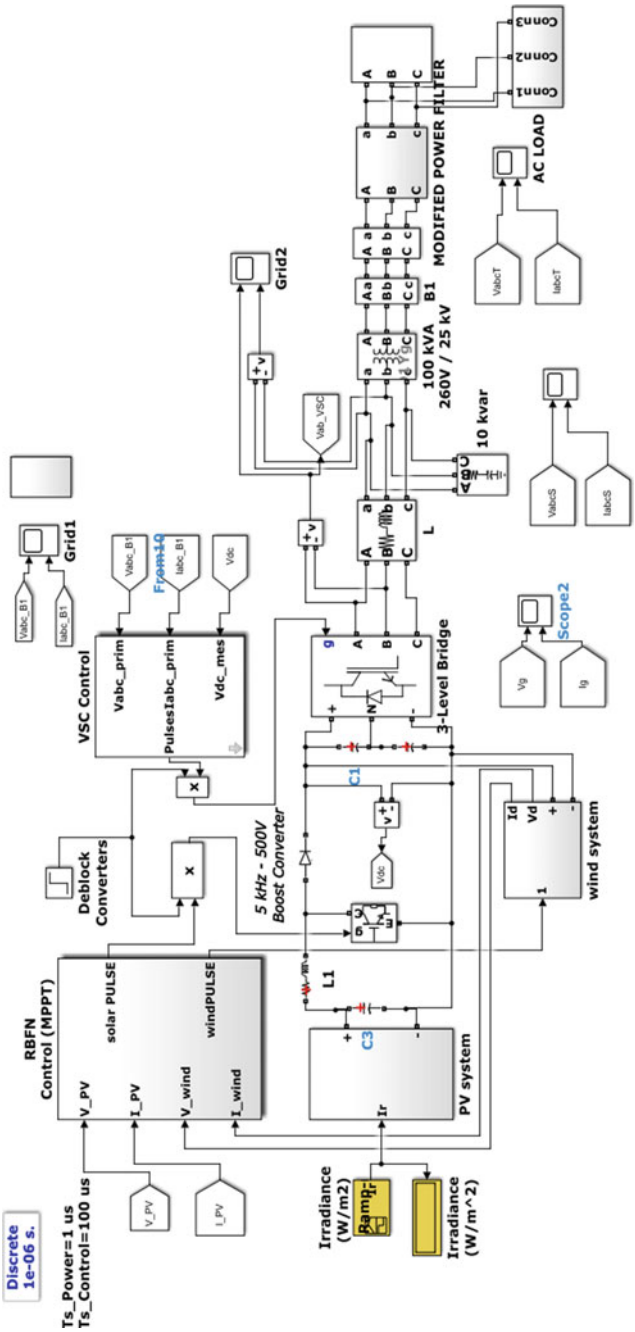

Fig. 3 Simulation model of artificial neural network-based designing of solar and wind system with modified power filter

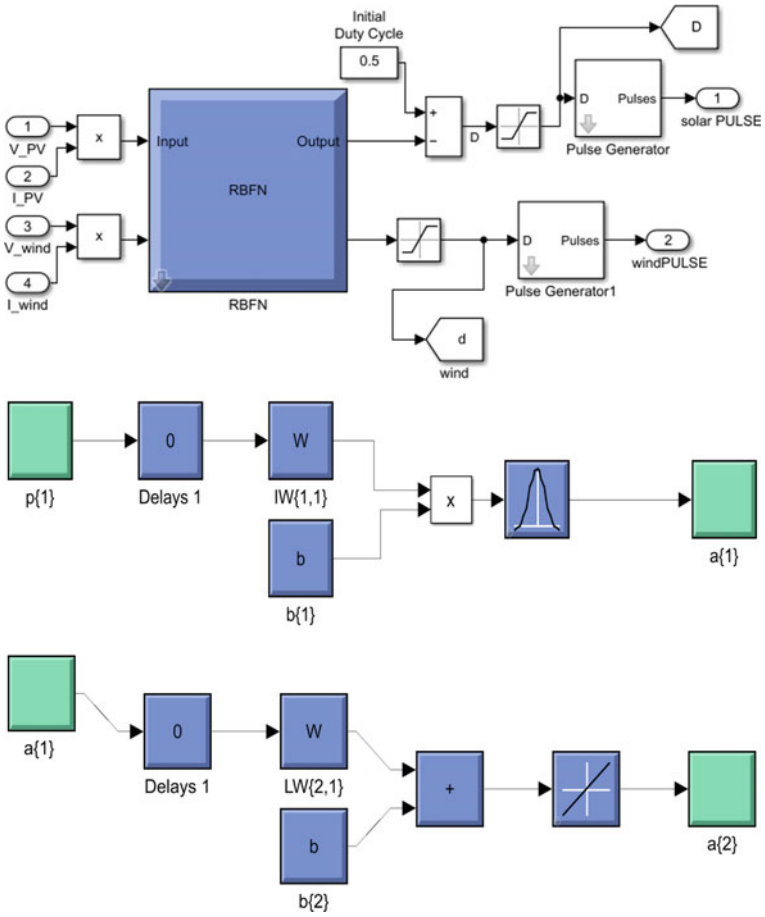

Fig. 4 Simulation design of radial basis function-based neural network with inside view of layer 1

The simulation of MPF is shown in Fig. 5, and therefore, a series and two shunt capacitor is connected which is used to minimized the harmonics and enhanced the power quality of the entire system. In Fig. 6, the simulation of multiloop dynamic error using artificial neural network has shown and *Vg* and *Ig*, *Pg* are used as an inputs for the MDEC and generate the error *e* (*A*), *e* (*B*). Subsystem *e* (*A*) inside view exhibited in Fig. 7. Error signal is passing through the neural network block which generates the pulse for P1 and control the switching operation of breaker.

The output power is generated by PV system is 82.3 and 102.6 kW at change in irradiance from 800 to 1000 W/m^2 exhibited in Fig. 8, and the generated power from the WE system is 3.1–3.48 kW at 8–12 m/sec shown in Fig. 9.

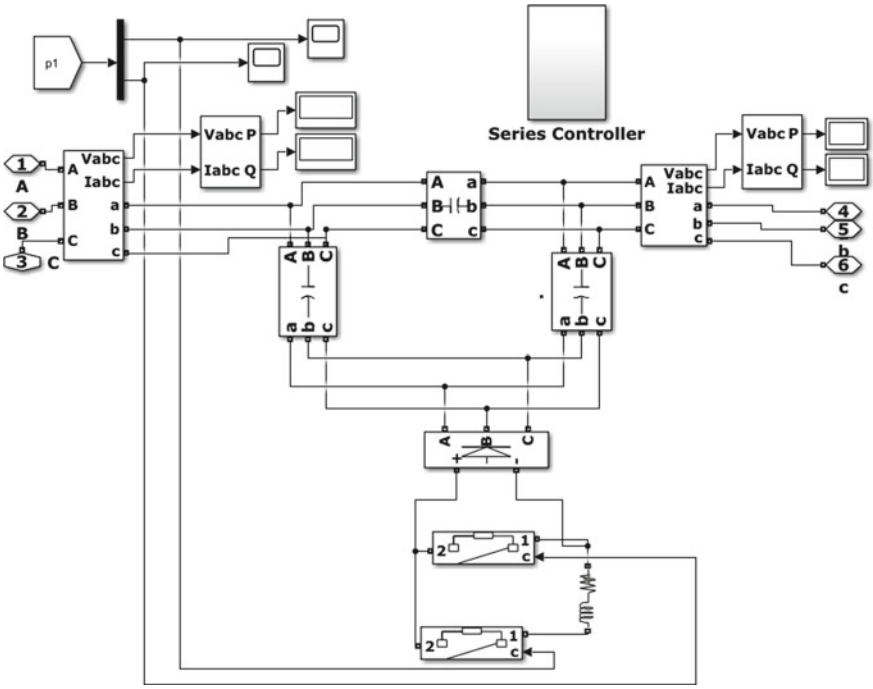

Fig. 5 Simulation of modified power filter

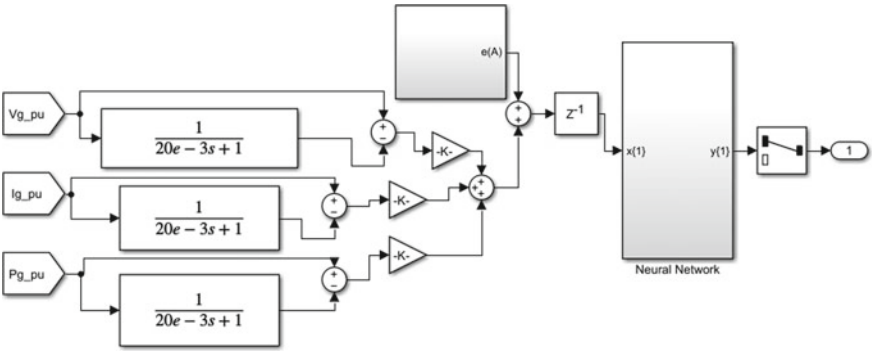

Fig. 6 Simulation model of ANN-based MDEC

The grid voltage and current in case of without MPF-based system shown in Fig. 10. The designed system without MPF has distortion in the grid current which increases the power quality issues, and the THD analysis of grid current is shown in Fig. 11 which is 23.39%.

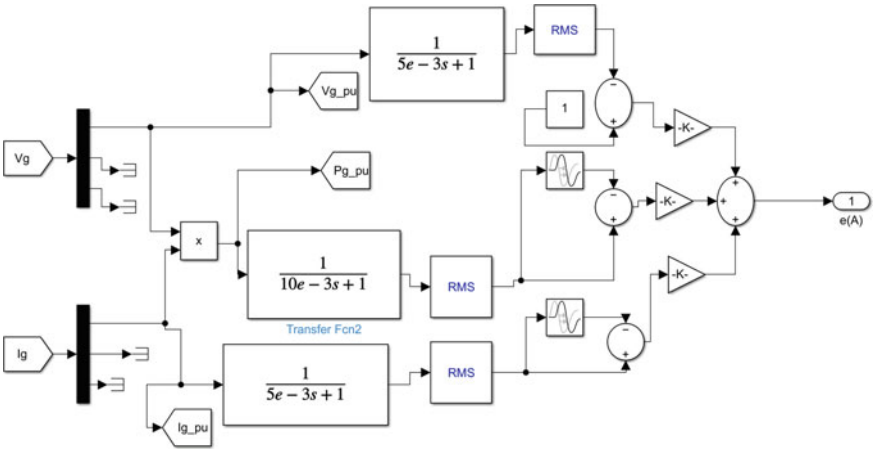

Fig. 7 Subsystem e (*A*) of MDEC

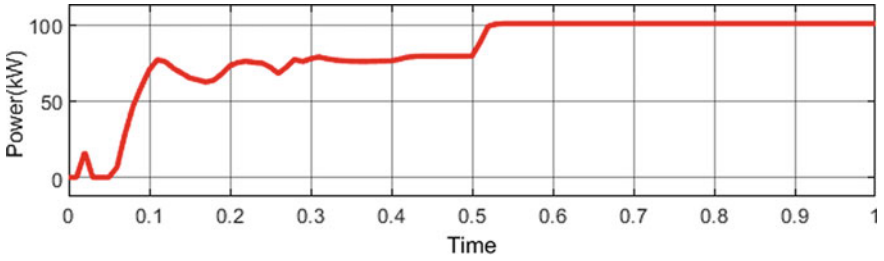

Fig. 8 Solar output power at irradiance change from 800 to 1000 W/m^2

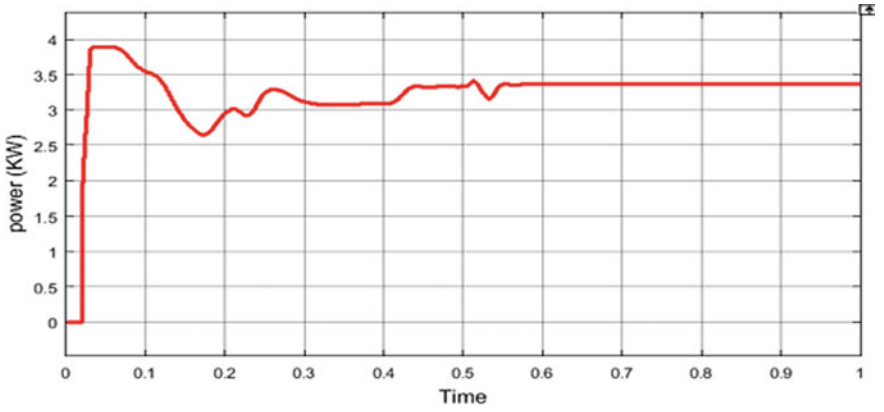

Fig. 9 Power generated by WE system

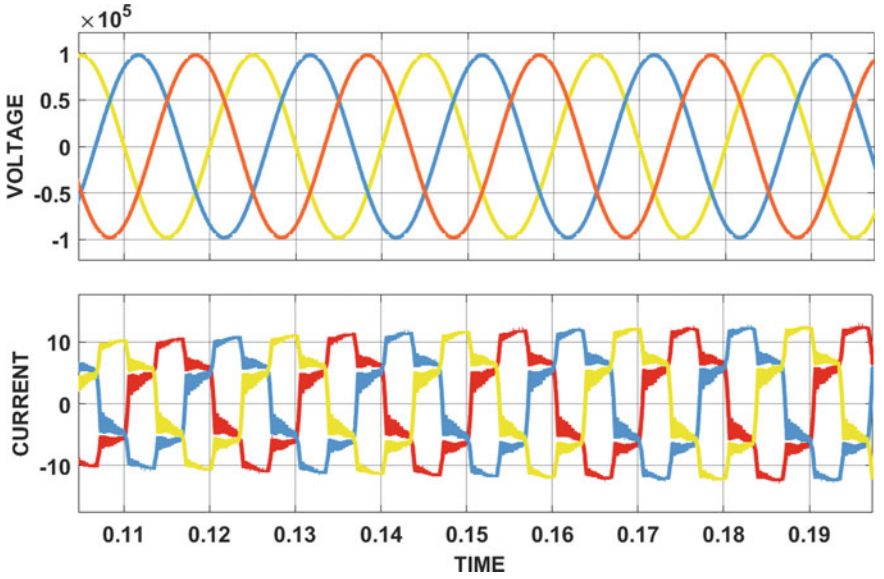

Fig. 10 Grid voltage and current without MPF

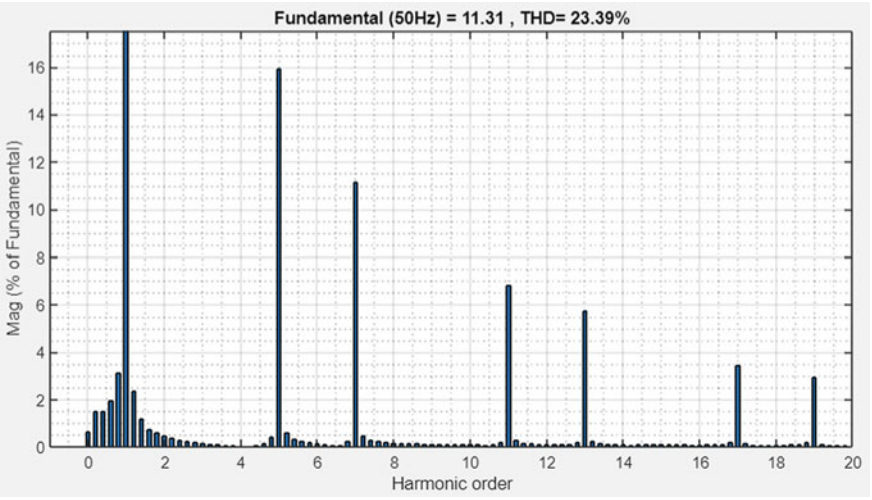

Fig. 11 THD analysis of grid current without MPF

Performance analysis of system without MPF is shown in this paper. Due the AC load and all converter causes voltage and current of source and grid is in distorted form and source current and voltage waveform shown in case of without MPF shown Fig. 12. In Fig. 13, the THD analysis of source current is 19.06%.

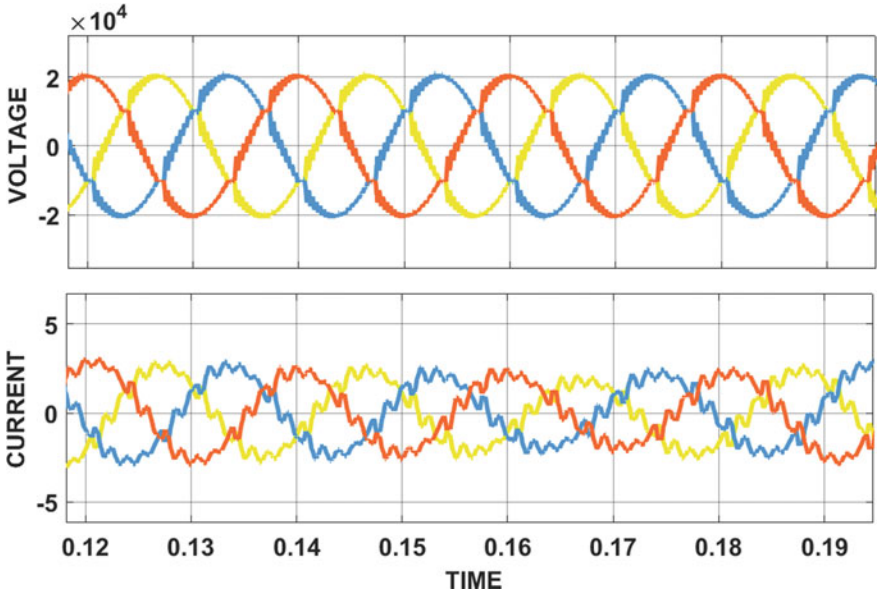

Fig. 12 Source voltage and current waveform in case of without MPF

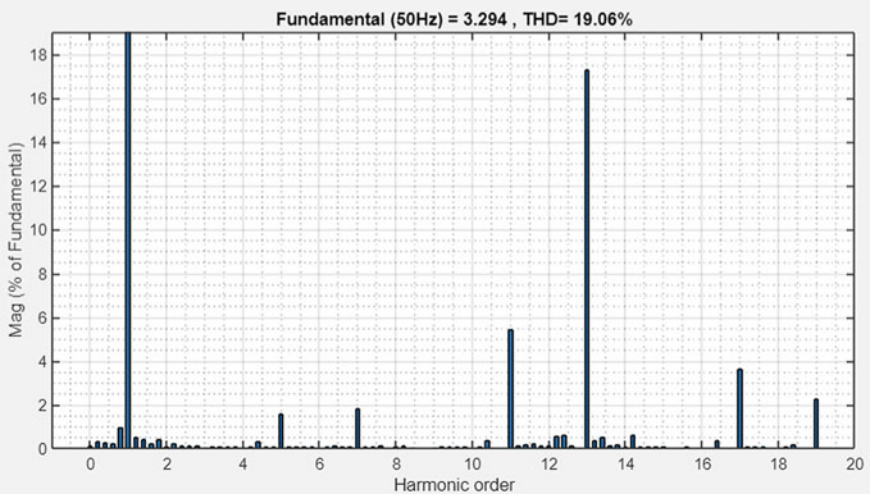

Fig. 13 THD analysis of source current in case of without MPF

The current and voltage waveform in case of MPF exhibited in Fig. 14 and the THD analysis in Fig. 15. THD analysis of grid current in this case is 1.66 %.

In Fig. 16, the source voltage and current is improved by using MPF and THD analysis of source current in this case shown in Fig. 17 and THD in this case is 1.45%.

Overall THD analysis of grid and source current in case of with and without MPF is shown in Table 5.

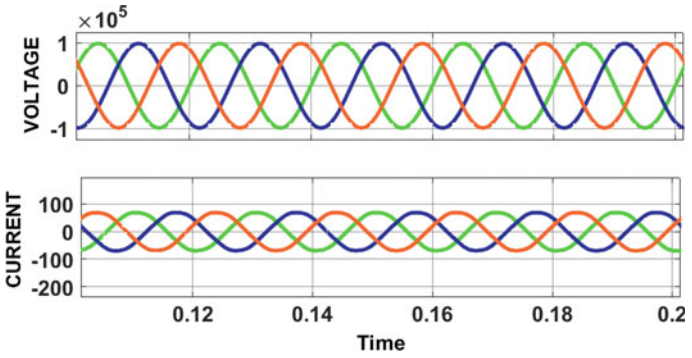

Fig. 14 Grid voltage and current in case of MPF

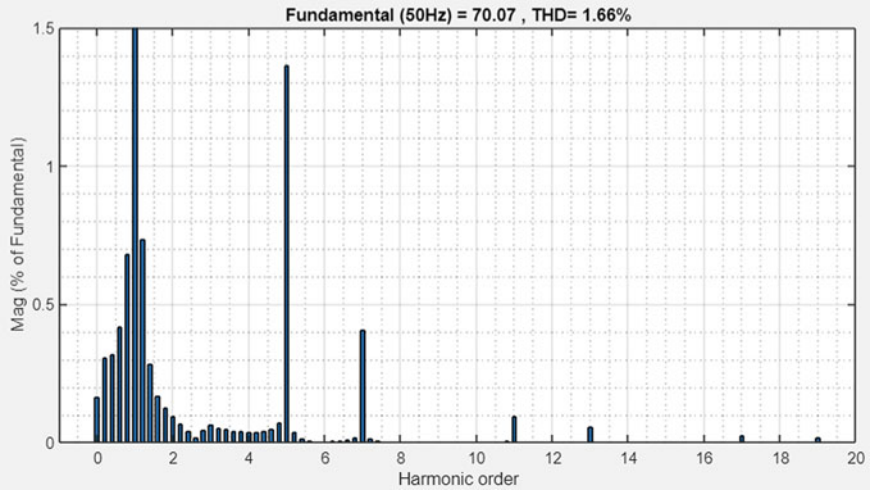

Fig. 15 Grid current THD analysis in case of MPF

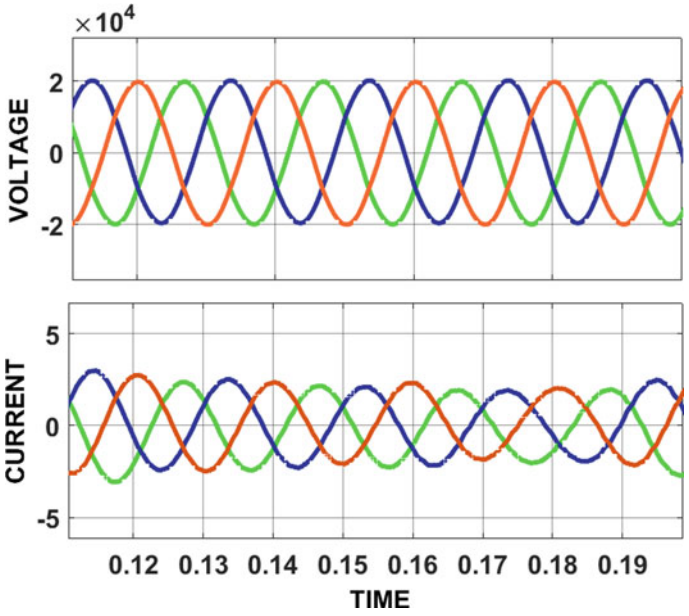

Fig. 16 Source voltage and current waveform in case of MPF

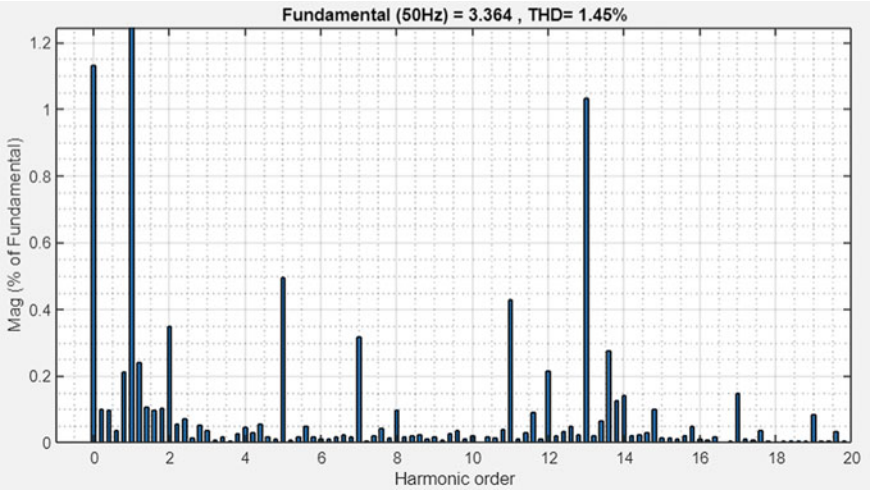

Fig. 17 Source current THD analysis in case of MPF

Table 5 THD analysis of grid and source current in case of with and without MPF

Harmonics order	Magnitude of harmonics in percentage in case of without MPF		Magnitude of harmonics in percentage in case of with MPF	
	Grid (%)	Source (%)	Grid (%)	Source (%)
5	16	1.5	1.38	0.5
7	11	2	0.4	0.3
11	7	5.5	0.1	0.44
THD in both cases	23.39	19.06	1.66	1.45

6 Conclusion

THD in case of with and without MPF, the grid current is 23.39% and 1.66%, respectively, and for source current is 19.06% and 1.45%. According to THD analysis, grid and source current are ensure that the reduction in harmonics and improve the power quality by introducing the MPF. Grid connected PV and wind system with modified filter has provided a desirable and fast response, also applicable for the application of smart grid for future research work.

References

1. N. Singh, V. Agarwal, A review on power quality enhanced converter of permanent magnet synchronous wind generator. Int. Rev. Electr. Eng. **8**(6), 1681–1693 (2013)
2. S. Saravanan, N. Ramesh Babu, RBFN based MPPT algorithm for PV system with high step up converter. Energy Conver. Manage. **122** 239–251 (2016)
3. K. Kumar, N. Ramesh Babu, K.R. Prabhu, Design and analysis of RBFN-based single MPPT controller for hybrid solar and wind energy system. IEEE Access **5** 15308–15317 (2017)
4. A.M. Hemeida, M.H. El-Ahmar, A.M. El-Sayed, H.M. Hasanien, S. Alkhalaf, M.F.C. Esmail, T. Senjyu, Optimum design of hybrid wind/PV energy system for remote area. Ain Shams Eng. J. **11**(1) 11–23 (2020)
5. N. Singh, A. Agarwal, V. Agarwal, Power control in centralized distributed AC load for Wind Energy System. AIP: J. Renew. Sustain. **9**(3) (2017)
6. J. Reddy, N. Sudhakar, Design and analysis of a hybrid PV-PEMFC system with MPPT controller for a three- phase grid-connected system. J. Green Eng. **8**(2) 151–176 (2018)
7. A.M. Sharaf, A.A. Abdelsalam, A novel switched filter compensation scheme for power quality enhancement and loss reduction. in *International Symposium on Innovations in Intelligent Systems and Applications*, (IEEE, 2011), pp. 398–403
8. A. Elgammal, A.M. Sharaf, Dynamic self adjusting FACTS-switched filter compensation schemes for wind-smart grid interface systems. Int. J. Renew. Energy Res. (IJRER) **2**(1) 103–111(2012)
9. S. Saravanan, N. Ramesh Babu, RBFN based MPPT algorithm for PV system with high step up converter. Energy Conver. Manage. **122**, 239–251 (2016)
10. S. Kumar, S. Yadav, N. Singh, P. Tiwari, Evaluation & analysis of MPPT controller for PV Systems, in *2018 International Conference on Computing, Power and Communication Technologies (GUCON)*, (2018), pp. 1161–1165

11. R. Akkaya, A.A. Kulaksız, Ö. Aydoğdu, DSP implementation of a PV system with GA-MLP-NN based MPPT controller supplying BLDC motor drive. Energy Convers. Manage. **48**(1), 210–218 (2007)
12. D. Srivastava, R.K. Rai, S.K. Srivastava, Performance analysis of single MPPT technique using RBFN for PV and wind hybrid system, in *2nd International Conference on Power Energy, Environment and Intelligent Control (PEEIC)*, (IEEE, 2019), pp. 88–93
13. S. Srinivasan, R. Tiwari, M. Krishnamurthy, M.P. Lalitha, K.K. Raj, Neural network based MPPT control with reconfigured quadratic boost converter for fuel cell application. Int. J. Hydrogen Energy **46**(9), 6709–6719 (2021)
14. R. Parabhane, S. Patil, N. Omase, Artificial neural networks based power management scheme with enhanced stability for a solar panel/wind turbine generator/fuel cell/battery/power supply designed for industrial loads, in *International Conference for Advancement in Technology (ICONAT)*, (IEEE, 2022), pp. 1–7
15. H. Tanuja, P. Usha, Multilayer artificial neural network based nano grid of hybrid PV/wind and energy storage. in *IEEE Mysore Sub Section International Conference (MysuruCon)*, (IEEE, 2021), pp. 824–830
16. C.P. Kumar, S. Pragaspathy, V. Karthikeyan, K.N.S. Durga Prakash, Power quality improvement for a hybrid renewable farm using UPQC. In *2021 International Conference on Artificial Intelligence and Smart Systems (ICAIS)*, (IEEE, 2021), pp. 1483–1488
17. M. Yadav, N. Singh, Small-signal modeling based hybrid optimized current and voltage controller for unbalanced DC microgrid. Int. Trans. Electr. Energy Syst. **31** (2021)
18. N. Singh, V. Agarwal, Single-stage AC–AC power conversion for WECS. Int. J. Electr. Power Energy Syst. **64**, 734–742 (2015)
19. R. Kumar, S. Kumar, N. Singh, V. Agrawal, SEPIC converter with 3-level NPC multi-level inverter for wind energy system (WES), in *2017 4th International Conference on Power, Control & Embedded Systems (ICPCES)*, (2017), pp. 1–6

Optimal Allocation of Capacitors for Loss Reduction in Distribution System

Manoj Kumar Kar, Uditanshu Mohanty, and Yashaskar Dash

Abstract In this work, a novel method is implemented to optimize the placement of capacitor bank in radial distribution systems (RDS) for reducing the system loss. It is a difficult task to select the best size and position of capacitors. This paper provides a two-stage method for determining the best capacitor positions and sizes in RDS. The loss minimization and costs of capacitors are considered as objectives of the work. For load flow calculations, the backward/forward sweep algorithm is used. A standard test system, such as 33-bus radial control systems is considered for case study. Numerical findings demonstrate that the proposed technique suggests the optimal position for a large reduction in overall cost while being more reliable and effective than other approaches in the literature, particularly when the delivery system sizing is increased the loss sensitivity analysis is used in the first stage to find the most candidate capacitor positions using loss sensitivity indices (LSIs). The particle swarm optimization (PSO) algorithm has been applied in the second stage to find the optimum positions and sizes of capacitors.

Keywords Distributed generator · Loss sensitivity · Optimal allocation · PSO · Real power loss

1 Introduction

The transmission of electrical power from generating stations to the consumers passes through different stages. During such type of energy transfer, power loss occurs with the impact of increase in the peak load [1]. Majority of losses occur in distribution side. The most effective strategy to compensate reactive power is the proper capacitor placement [2]. Minimization of reactive and actual power losses, appropriate voltage

M. K. Kar (✉)
EE Department, AISSMS College of Engineering, Pune, India
e-mail: manojkar132@gmail.com

EE Department, NIT Jamshedpur, Jamshedpur, Jharkhand, India

U. Mohanty · Y. Dash
EE Department, NIST Berhampur, Berhampur, Odisha, India

© The Author(s), under exclusive license to Springer Nature Singapore Pte Ltd. 2023

K. Murari et al. (eds.), *Soft Computing Applications in Modern Power and Energy Systems*,
Lecture Notes in Electrical Engineering 975,
https://doi.org/10.1007/978-981-19-8353-5_19

profile management, power factor improvement is some of the major advantages of the capacitor positioning in the distribution system [3]. Apart from these benefits, if the capacitor's measurements and location are not correct, the framework may be vulnerable and transform in strange traditions, and voltage increases may pass cut-off points, resulting in substandard power factors, parallel resonance problems, and bad configurations [4, 5]. The size and position of capacitor is chosen with an objective to minimize losses [6]. As a result, electrical power utilities have often prioritized optimal capacitor allocation in electrical delivery systems. The optimal capacitor allocation problem considers the position, type, and number of capacitors to be deployed in order to reduce cost while staying within the working constraints. Several solutions to this problem have been suggested, and they have been solved using a statistical approach. Nowadays, the placement of optical capacitor is the focus for most of the research work. Most of the papers on this topic has undertaken the issues with PSO, graph search algorithms, ant colony optimization, genetic algorithms, and fuzzy evolutionary programming [7]. Several promising methods are discussed for capacitor considering size and location [8–10]. The constraints are also taken in to consideration for selecting the location [11]. A nonlinear programming method was proposed for positioning of capacitor as well as reconfiguration in demand to attain the goal of radial distribution network service with the least amount of energy loss [12]. The improvement in voltage profile using integration of electric vehicle and renewable energy source was presented in [13]. From all possible nodes, the best node for a certain size of capacitor is chosen, and the capacitor is then assembled. In spite of faster solving capability, the analytical methods have a flaw in that they cannot get out of local optima. The shortcomings of computational methods are solved by evolutionary techniques were first used in the 1990s. Several researchers [14, 15] have published on evolutionary strategies such as virtual annealing, Tabu Quest, and GA. A general capacitor positioning problem formulation was proposed considering physical aspects of capacitors and, operating limitations at various load was solved.

2 Objective and Problem Formulation

The ultimate capacitor placement issue involves deciding the quantity, shape, and positioning of capacitors on a RDS for reducing losses and ensuring voltage stability at minimum cost of additional capacitors.

The load changes in the system over time are taken into account when measuring energy losses in the system. A piecewise linear equation is used to estimate the load length curve, and the time interval is separated using these assumptions. Based on these assumptions, the load length curve, and the time cycle is estimated.

$$\textbf{Minimize} \sum_{i=1}^{n} K_{ei} P_{Li} + \sum_{j=1}^{k} K_{cj} C_j \tag{1}$$

where K_{ei} = constant energy cost for load stage I

K_{cj} = the cost of a capacitor remains constant regardless of the form of capacitor used at the jth place.

P_{Li} = power loss at ith load stage.

C_j = kvar injected at the jth node.

n = number of load levels.

k = no. of locations.

PL = total losses in the system.

The limits of voltage amplitude are expressed in Eq. (2), and given below

$$V_{\min} \leq V_m \leq V_{\max} \tag{2}$$

3 Load Flow Analysis

3.1 Proposed Load Flow method

The direct backward forward sweep method (DBFSM) is a direct approach of load flow analysis. Additionally, it is more suitable for radial distribution system than the Newton Raphson method and Gauss–Seidel method, which are more useful in case of transmission systems. This is due to the characteristics of distribution network like radial construction, unbalanced load, lower time requirements, and a lower X/R (reactance/resistance) ratio.

3.2 Backward Forward Sweep Method

In this method, at first iteration of the backward sweep, the effective output power for each branch is estimated by taking into account the rated voltage at the source nodes, and the voltages are measured using the forward sweep (FS) process. Hence, the backward sweep (BS) begins at the end node and proceeds backward before it reaches the source node. Voltage calculated in backward sweep only at source node is used. The optimization technique stops if the voltage at the source node in BS is less than the convergence criterion; if the voltage is greater than the convergence point, the optimization process begins. Beginning with the feeder cluster head, the FS is used to establish the voltages at every node. The feeder substation voltage is set to the value obtained from a BS measurement. The successful branch current in each branch is held at the same amount as in the BS during the FS.

The load flow studies are essential in power system to analyze the system capability. The system's static output is obtained by the load flow. A power-flow analysis focuses on different types of AC power and typically uses simpler representation like one-line diagram, for example (i.e., voltages, real power, voltage angles, and reactive power). The transmission networks are classified as being in poor shape because of one or more of the following characteristics like weakly meshed networks, also known as radial networks, high R/X ratio of distribution system, unbalanced distributed load, inadequate length, multiphase, unbalanced process Generation at a distance, etc. The Newton Raphson and other transmission system algorithms have struggled with the distribution network as a result of these factors. Unlike NR techniques, this approach does not require a Jacobian matrix.

A. Output of Backward forward sweep method (without compensation)

The voltage profile of a 33-bus RDS without compensation method is shown in Fig. 1. It has been observed that the voltage profile is not good, and it has to be enhanced for efficient operation of power system. The minimum and maximum voltage magnitude without compensation is 0.94215 pu and 0.99421 pu, respectively. The active power loss is 216.0137 kW, and the annual cost is 36290.3061$.

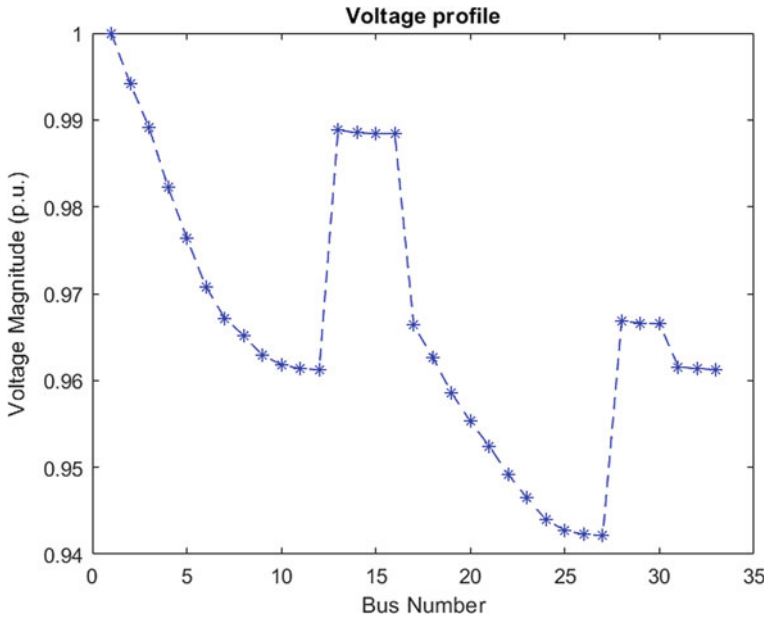

Fig. 1 Voltage magnitude of 33-bus system without compensation

4 Sensitivity Calculation

The primary goal of capacitor setting is to reduce losses. This goal can be achieved if the capacitor is mounted in a position that contributes the most for loss reduction, as not all positions have the same impact. Candidate destinations are chosen with buses having higher sensitivities. As a result, the search space will be reduced. A change in the system's active power loss as a result of a change in reactive power is expressed in Eq. (3), and is given by

$$\frac{\mathrm{d}P_l}{\mathrm{d}Q_i} = 2\sum_{j=1}^{n}(\alpha_{ij}Q_j + \beta_{ij}P_j) \tag{3}$$

where the values of α_{ij} and β_{ij} Eqs. (4) and (5), respectively

$$\alpha_{ij} = r_{ij}\mathrm{Cos}\left(\theta_i - \theta_j\right)/V_iV_j \tag{4}$$

$$\beta_{ij} = r_{ij}\mathrm{Sin}\left(\theta_i - \theta_j\right)/V_iV_j \tag{5}$$

P_j is the active and Q_j is the reactive power at bus j, respectively.
θ_i and θ_j represents the voltage angle at node i and j, respectively.
Equation is used to measure the sensitivity of all nodes. Candidate sites are selected from nodes with greater sensitivities.

5 Methodology

5.1 Particle Swarm Optimization

This method is used to improve the iterative process trying to find a candidate solution in terms of a mathematical validity parameter. It addresses the problem by generating a population of solutions (dubbed particles) and moving them around in the solution space to use a simple complex equation based on their velocity and position. The movement of each particle is dictated by its local best-known site, but it is often oriented toward the search space's best-known sites, which shift as other particles locate better places. As a result of this, the swarm is guided to the most favorable position. As a result, the swarm is expected to carry in the direction of the right solutions.

This approach can easily handle continuous state variables and efficiently explore the search space. The procedure, on the other hand, can be applied to both discrete and continuous variables. The PSO algorithm, like other evolutionary computational algorithms, manipulates individuals using evolutionary operators. This method is

chosen because of its simple concept, ease of implementation, better computational efficiency, and robustness to control parameters.

The particle swarm optimization principle contains each particle's velocity transition toward its distinct best (pbest) and global best (gbest) positions at each time level. A random term is used for weight acceleration, with different random numbers produced for acceleration toward the pbest and gbest positions.

The objective function can be formulated as

Minimalize $f(X)$

where in d-dimensional space, the ith particle is denoted by

$$x_{ii} = \{x_{i1}, x_{i2}, \ldots, x_{id}\}$$

The best previous location of the ith particle is verified and characterized as.

pbesti = {pbesti1, pbesti2,..., pbesti}

Between all the particles in the inhabitants, the directory of the finest particle is denoted as gbest. The proportion of the position change for ith particle is characterized as Si = {si1, si2,..., si}.

The updated velocity and location of an individual particle was considered from current velocity and the position after pbest to gbest, is stated as follows.

Velocity of the particle

$$v_i^{t+1} = w v_i^t + c_1 r_1 \left(P_i^t - x_i^t\right) + c_2 r_2 \left(G^t - x_i^t\right) \tag{6}$$

$$\text{Position of the particle} : x_i^{t+1} = x_i^t + v_i^{t+1} \tag{7}$$

where v = speed of particle, w = inertia weight,
c = acceleration factor, r = random variable,
P = personal best, G = global best,
x = position of particle, t = iteration number.

5.2 Selection of Inertia Weight:

$$w = w_{\max} - ((w_{\max} - w_{\min})/\text{iter}_{\max}) * \text{iter} \tag{8}$$

where w = inertia weight
$w_{\max} = 0.9$; $w_{\min} = 0.4$
iter = iteration number.
$\text{iter}_{\max}$ = maximum iteration.
The flowchart for implementing PSO algorithm is presented in Fig. 2.

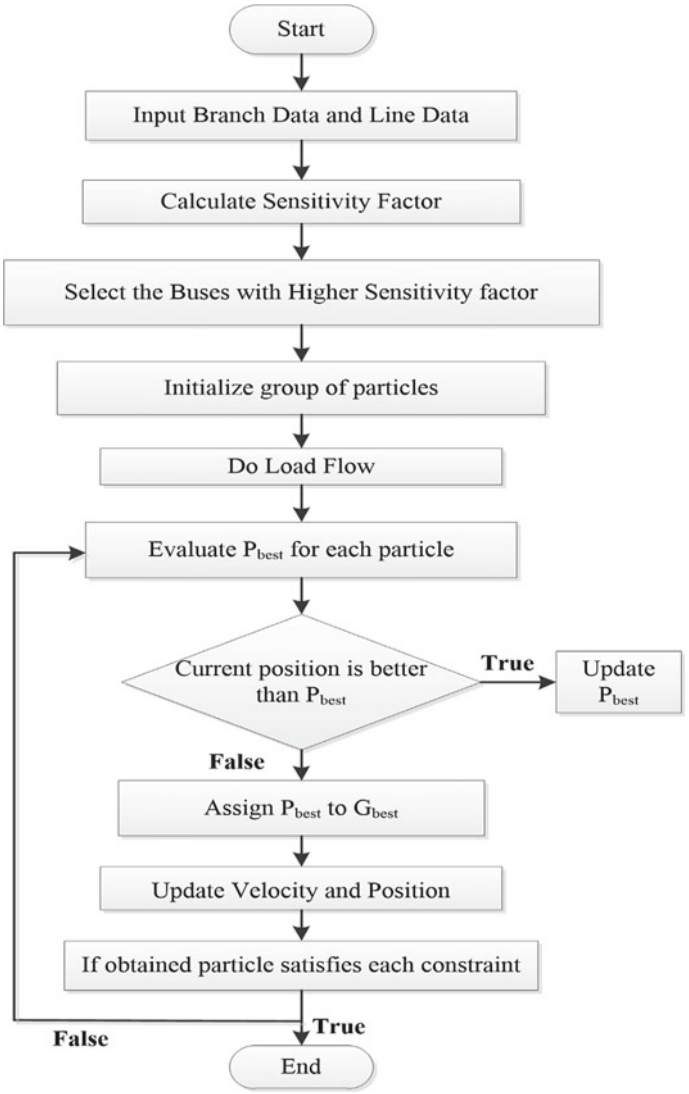

Fig. 2 Flowchart for PSO implementation

5.3 Selection of Capacitor

The capacitor which has to be installed has the same value as that of required reactive power of the bus when the required reactive power of the bus is same at all load points. A switchable capacitor having same reactive power demand at the highest load frequency is placed at a bus if the reactive power demand changes with load levels.

5.4 Choice of Number of Locations

The quantity of capacitor positions varies rendering to the downward order of their sensitivity factor to discover the optimum number of positions. The system losses after capacitor allocation have been noted, and it has been discovered that the system losses reduce as the number of capacitor installation locations increases. The decrease in actual power losses slows as the number of positions increases. The cost of installing capacitors rises with a greater number of capacitors. As a consequence, to increase savings, the number of positions should be optimized. This method is known as optimum capacitor distribution meanwhile the effect of capacitors located at earlier defined positions is not taken into consideration when deciding the next position. PSO algorithm is used to determine the best position for capacitor deployment.

6 Simulation Results

Two cases are considered for analysis. In the first case, three nodes are chosen for capacitor placement whereas in second case, four nodes are chosen for the placement of capacitor. Finally, a comparative analysis of voltage magnitude of a 33-bus system without compensation, with three capacitor placement, and with four capacitor placement is shown in Fig. 3. It has been seen that the voltage profile is remarkably enhanced with compensation. The minimum and maximum voltage magnitude in case-1 is found to be 0.95 pu and 0.99491 pu, respectively. In case-2, the minimum and maximum voltage magnitude is found to be 0.95022 pu and 0.99535 pu, respectively. Hence, it is confirmed that the voltage profile has been improved in case-2 with optimal placement of four capacitors.

Figure 4 presents the active power loss after compensation, and it is found to be reduced after capacitor placement. The active power loss without compensation was 216.0137 kW which was reduced to 164.2228 kW in case-1 and 157.1435 kW in case-2.

Comparative Analysis

A comparative analysis of active power loss, annual cost, the limits of voltage amplitude, and capacitor's size is presented in Table 1.

7 Conclusion

The performance of distribution system with the placement of capacitor is analyzed using IEEE 33-bus system. The power flow in each branch has been calculated using DBFS method. This method is suitable for the fast convergence characteristics and radial structure system. By using PSO, the optimal position of capacitors in a

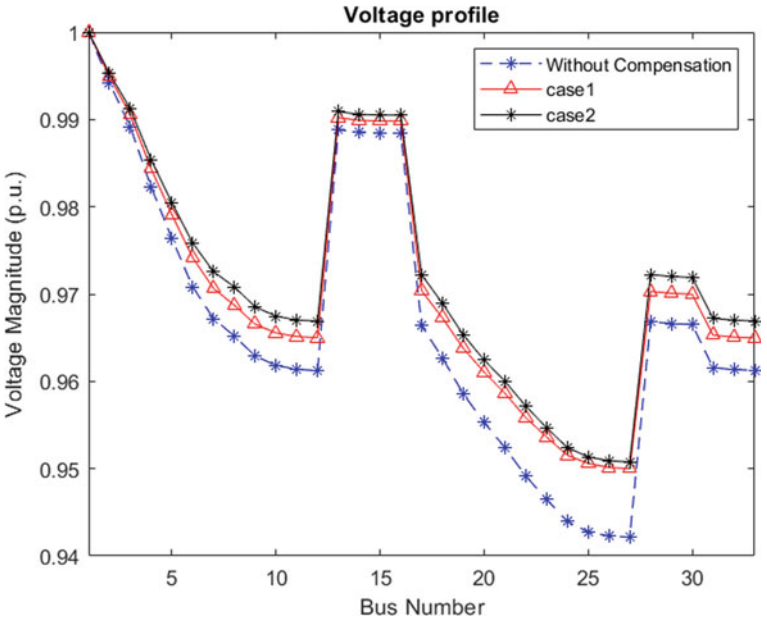

Fig. 3 Comparison of voltage magnitude of 33-bus system without and with compensation

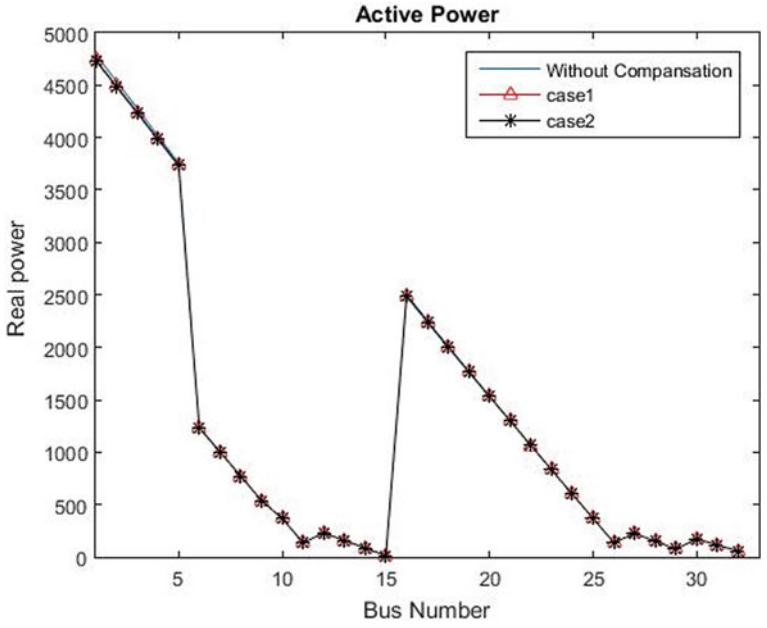

Fig. 4 Active power of a 33-bus system after compensation

Table 1 Comparative analysis of different parameters with and without compensation

Parameter	Without compensation	With compensation			
		Case-1		Case-2	
Active power loss (kW)	216.0137	164.2228		157.1435	
Annual cost ($)	36290.3061	27589.4339		26400.1029	
Minimum voltage (p.u.)	0.94215	0.95		0.95022	
Maximum voltage (p.u.)	0.99421	0.99491		0.99535	
Bus and capacitor size	Nil	Bus No.	Capacitor size (kVAR)	Bus No.	Capacitor size (kVAR)
		22	468.91	22	900
		25	933.33	4	450
		11	220.67	19	600
				9	750

33-bus system was found out. The effectiveness of capacitor placement has been analyzed using two cases. The significant reduction in loss and improvement in voltage profile has been observed. The placement of capacitors also reduces annual cost. It is observed that shunt capacitors efficiently minimize system power failure. Thus, it may be concluded that the use of shunt capacitors in distribution networks as reactive power compensators helps to reduce real power loss, overall cost, and savings.

References

1. H.N. Ng, M.M.A. Salama, A.Y. Chikhani, Classification of capacitor allocation techniques. IEEE Trans. Power Delivery **15**(2), 387–392 (2000)
2. N.M. Neagle, D.R. Samson, Loss reduction from capacitors installed on primary feeders. AIEE Trans. **75**, 950–959 (1956)
3. R.F. Cook, Optimizing the application of shunt capacitors for volt-ampere control and loss reduction. AIEE Trans. **80**, 430–444 (1961)
4. T.H. Fawzi, S.M. EI-Sobki, M.A. Abdel-Halium, A new approach for the application of shunt capacitors to the primary distribution feeders. IEEE Trans. Power Apparat Syst. PAS-**102**(1) 10–13 (1983)
5. M.E. Baran, F.F. Wu, Optimal sizing of capacitors placed on radial distribution system. IEEE Trans. Power Delivery **4**(1), 735–743 (1989)
6. R.A. Jabr, Optimal placement of capacitors in a radial network using conic and mixed integer linear programming. Electric. Power Syst. Res. **78**, 94–948 (2008)
7. W. de Oliveira Leonardo, J. Carneiro Sandoval, J. de Oliveira Edimar, J.L.R. Pereira, C. Silva Jr Ivo, S. Costa Jeferson, Optimal reconfiguration and capacitor allocation in radial distribution systems for energy losses minimization. Int. J. Electric. Power Energy Syst. **32**(8) 840–848 (2010)

8. M. Raju Ramalinga, K.V.S. Murthy Ramachandra, K. Ravindra, Direct search algorithm for capacitive compensation in radial distribution systems. Int. J. Electric. Power Energy Syst. **42**(1), 24–30 (2012)
9. P.V.R. Varma, M.K. Kar, A.K. Singh, Optimal sizing and location of DG for power loss reduction and voltage improvement of distribution system using IHSA algorithm. in *2021 IEEE 2nd International Conference on Applied Electromagnetics, Signal Processing, & Communication (AESPC)*, (2021), pp. 1–5. https://doi.org/10.1109/AESPC52704.2021.9708496
10. M. Montazeri, A. Askarzadeh, Capacitor placement in radial distribution networks based on identification of high potential busses. Int. Trans. Electric. Energy Syst. **29**(3), e2754 (2019)
11. A. Tripathy, M.K. Kar, Voltage profile enhancement of a 33 bus system integrated with renewable energy sources and electric vehicle, in *2021 8th International Conference on Signal Processing and Integrated Networks (SPIN)*, (2021), pp. 281–286. https://doi.org/10.1109/SPIN52536.2021.9566111
12. K. Mahmoud, M. Lehtonen, Simultaneous allocation of multi-type distributed generations and capacitors using generic analytical expressions. IEEE Access **7**, 182701–182710 (2019). https://doi.org/10.1109/ACCESS.2019.2960152
13. R. Rao Srinivasas, S.V.L. Narasimham, M. Ramalingaraju, Optimal capacitor placement in a radial distribution system using plant growth simulation algorithm. Int. J. Electric. Power Energy Syst. **33**(5), 1133–1139 (2011)
14. E.A. Almabsout, R.A. El-Sehiemy, O.N.U. An, O. Bayat, A hybrid local search-genetic algorithm for simultaneous placement of DG units and shunt capacitors in radial distribution systems. IEEE Access **8**, 54465–54481 (2020). https://doi.org/10.1109/ACCESS.2020.2981406
15. M.C. Suresh, J.B. Edward, A hybrid algorithm based optimal placement of DG units for loss reduction in the distribution system. Appl. Soft Comput. **1**(91), 106191 (2020)
16. L. Kumar, M.K. Kar, S. Kumar, Statistical analysis based reactive power optimization using improved differential evolutionary algorithm. Expert Systems, p.e13091 (2002)